NASA CR-54454
FPR-1

260-IN.-DIA MOTOR FEASIBILITY DEMONSTRATION PROGRAM

Volume 1: 260-SL Motor Aft-End Ignition System Development

Prepared for

NATIONAL AERONAUTICS AND SPACE ADMINISTRATION

CONTRACT NO. NAS3-6284

AEROJET GENERAL TIRE GENERAL

AEROJET-GENERAL CORPORATION

SACRAMENTO, CALIFORNIA

NASA CR-54454
FPR-1

FINAL PHASE REPORT

260-IN.-DIA MOTOR FEASIBILITY DEMONSTRATION PROGRAM

VOLUME I

260-SL MOTOR AFT-END IGNITION SYSTEM DEVELOPMENT

Prepared for

NATIONAL AERONAUTICS AND SPACE ADMINISTRATION

20 August 1962

CONTRACT NO. NAS3-6284

Technical Management
NASA Lewis Research Center
Cleveland, Ohio
James J. Kramer

AEROJET-GENERAL CORPORATION
A SUBSIDIARY OF THE GENERAL TIRE & RUBBER COMPANY

ABSTRACT

32258

The 260-SL motor ignition system development program was conducted to demonstrate the capability of an aft-end solid-propellant igniter to ignite the 260-SL motors. A mathematical model was derived to define the gas dynamics of aft-end ignition and to provide the parameters required for aft-end ignition system design. The test program demonstrated the ignition capability of the ignition system and provided sufficient data to verify the mathematical model and the criteria used for the design of the ignition system. The 44-in.-dia subscale motor ignition system development program further verified the 260-SL motor ignition system design criteria and provided preliminary data on the igniter ejection sequence. The aft-end ignition performance in three 44-SS motors showed predictable and reproducible performance. All objectives of the development program were achieved and the ignition capability of the 260-SL motor ignition system was fully demonstrated.

Author

TABLE OF CONTENTS

TABLE OF CONTENTS (cont.)

APPENDIXES

FIGURE LIST

FIGURE LIST (cont.)

FIGURE LIST (cont.)

FIGURE LIST (cont.)

FIGURE LIST (cont.)

I. SUMMARY

The 260-SL motor ignition system development program was conducted to demonstrate the capability of an aft-end solid-propellant igniter to ignite the 260-SL motors. The design of the 260-SL motor ignition system was based on parameters obtained from an analytical model derived to define the gas dynamics of aft-end ignition.

The 260-SL motor ignition system is composed of four subsystems: the ignition motor, booster, initiator, and safety-arming device. The ignition motor contains 1160 lb of ANP-2758 Mod 1 propellant, case bonded into a 30-in.-dia Ladish D-6ac steel chamber. The ignition motor booster is a modified Polaris B3 first-stage-motor igniter, containing a 1400-gm Alclo-iron main charge. The initiator is a small aluminum capsule containing boron and potassium nitrate pellets. The ignition motor booster and initiator are initiated by two squibs housed in the standardized Minuteman weapon system safety-arming device.

A test program was conducted to demonstrate the capability of the Mod 260 ignition motor assembly to ignite the 260-SL motors and to enable a critical evaluation of the ignition motor ballistic performance. Small-scale, cold-flow tests verified the equations and assumptions of the aft-end ignition analytical model. The ignitibility of 260-SL motor propellant was determined in arc-image furnace tests. The reproducibility of flame propagation from the squibs housed in the safety-arming device to the boron and potassium nitrate pellet initiator was demonstrated in a series of closed-chamber firings. The ballistic performance of the ignition motor booster was evaluated in three test firings. As a result of these tests, several changes were made in the ignition motor booster design. The tests demonstrated the performance of the ignition motor subsystems.

A subscale ignition program was conducted in conjunction with tests of the 44-in.-dia propellant demonstration motors. The objectives of the 44-SS motor ignition program were to verify the design criteria of the Mod 260 ignition motor and to obtain preliminary data on the ignition motor ejection sequence. The design

I, Summary (cont.)

criteria for the 44-SS ignition motor were identical to the criteria used in the design of the Mod 260 ignition motors. Three 44-SS free-volume simulator tests were conducted; the measured bore-pressure data correlated with the pressure values derived from the analytical model. Ejection of the 44-SS ignition motor was accomplished in the third free-volume simulator test. The design criteria and the ejection sequence of the Mod 260 ignition motor were verified by the successful ignition of three 44-SS motors.

The Mod 260 ignition motor ballistic performance was verified in a static open-air test. The capability of the Mod 260 ignition motor to ignite the 260-SL motors was fully demonstrated in two 260-SL free-volume simulator tests. The energy delivered to the simulator wall by the Mod 260 ignition motor was 40 to 50 times greater than the required threshold-ignition energy for 260-SL motor propellant and was sufficient to ignite patches of 260-SL motor propellant located along the simulator wall.

Two full-scale functional tests of the igniter retention-and-release system to be used for the 260-SL-1 motor test were conducted at the Aerojet-Dade Division. The igniter retention-and-release system is designed to retain the ignition motor in the 260-SL motor exit cone until motor ignition is accomplished, then to release and control the movement of the ignition motor through the 260-SL motor exit cone to a predetermined impact area away from the test facility. The igniter release-control unit is a solid-state electrical system designed to provide a command signal to the explosive bolts. The igniter release-control-unit logic is satisfied by either of two different signals: an analog input signal from the 260-SL motor fore-end pressure transducer or a preset time signal. When the explosive bolts are actuated by a signal from the igniter release-control unit, the ignition motor and support fixture move vertically up a track until the exit plane of the ignition motor is 31 ft above the 260-SL motor exit plane. The ignition motor and support fixture leave the track, and flight is controlled by four steel cables to the impact area. The tower is retracted out of the 260-SL motor exhaust after the ignition motor leaves the track.

I, Summary (cont.)

The retention-and-release system performed as designed in two functional tests. The electrical systems, explosive bolts, and tower hydraulic-retraction system functioned, and the ejected ignition motor impacted in the target area. The 260-SL free-volume simulator was installed to protect the Cast, Cure, and Test facility from the impinging igniter gases and to obtain free-volume-simulation pressure data. Excellent simulator exit cone and throat plane static pressure data were obtained during the test, so that the flow conditions during igniter ejection were further clarified.

The objectives of the 260-SL motor aft-end ignition system development program were achieved. The following conclusions are based on the results of the analytical studies performed and test data obtained during the program:

1. The capability of the Mod 260 ignition motor to ignite the 260-SL motors has been fully demonstrated.

2. The Aerojet-General aft-end-ignition analytical model has been verified as an effective method for defining design parameters.

3. Mod 260 ignition motor design criteria have been verified by the successful and reproducible ignition of the 44-SS motors.

4. The Mod 260 ignition motor meets all design objectives for ballistic performance and reproducibility.

5. The performance of the igniter release-control unit and the retention-and-release system meet design requirements, and operation of the system is not a hazard to the 260-SL motor.

II. INTRODUCTION

A. PURPOSE OF REPORT

This is the first in a series of final reports that will be issued as major phases of the 260-in.-dia motor feasibility demonstration program are completed. This series of reports, when completed, will constitute the major portion of the Final Report on this program.

This report describes the 260-SL motor aft-end ignition system development program.

B. SCOPE OF REPORT

This document summarizes in detail the 260-SL motor aft-end ignition system development program leading to the 260-SL motor test firing. The following phases of the program are included in this report:

1. Development of an analytical model to define the design parameters required for aft-end igniters.

2. Establishment of design crtieria for the 260-SL motor ignition system.

3. Description of the design of the 260-SL motor ignition system and the subscale 44-SS motor ignition system.

4. Completion of test program and analysis of the results.

5. Conclusions and final 260-SL-1 motor ignition performance prediction.

II, Introduction (cont.)

C. PROGRAM STATUS

The aft-end igniter development program has been completed and all data indicate that the Mod 260 ignition motor will satisfactorily ignite the 260-SL motors.

D. PROGRAM OBJECTIVES

The purpose of the development program was to demonstrate the capability of the aft-end ignition system to ignite the 260-SL motors. The test objectives were to evaluate the integrity and performance of each subsystem, demonstrate the ignition capability of the system, and demonstrate the validity of the analytical equations, assumptions, and criteria used in designing the 260-SL motor ignition system. Verification of the ignition system ballistic performance and of performance reproducibility were also program objectives.

E. APPROACH

A test plan was devised to provide sufficient data to enable critical evaluation of the ignition system performance and to confirm the adequacy of the ignition system design. Small-scale cold-flow tests were conducted to demonstrate the validity of the analytical model derived by Aerojet-General to describe the gas dynamics of aft-end ignition. Specimens of 260-SL motor propellant were subjected to arc-image furnace tests to determine the threshold ignition energy; the threshold ignition energy data were used later in the test program as one basis for evaluating ignition capability. The performance of the ignition system components were evaluated in a series of closed chamber and open-air tests. Subscale evaluation of the 260-SL motor ignition system design criteria was made during 44-SS free-volume simulator and 44-SS motor ignition tests. Two 260-SL free-volume simulator tests were made to demonstrate the ignition capability

II, E, Approach (cont.)

of the system. The final phase of the development program was the igniter retention-and-release tests. These tests were conducted to demonstrate, by actual operation of all electrical and mechanical subsystems, that the retention-and-release system would function in accordance with the design requirements.

F. PROGRAM SUMMARY

All of the program objectives were achieved. The capability of the ignition system to ignite the 260-SL motors was adequately demonstrated. The ignition performance data obtained in the 44-SS motor test firings indicated that the system met all of the design requirements and that the aft-end ignition system design criteria were satisfactory. The validity of the aft-end ignition analytical model was proven in the cold-flow tests and in the 44-SS and 260-SL motor free-volume simulator tests. The operation of the igniter retention-and-release system met all design requirements; the function of the retention system and the ejection of the ignition motor is not a hazard to the 260-SL motor or adjacent facilities.

III. DESIGN

A. AFT-END IGNITION ANALYTICAL MODEL

Before design of the 260-SL motor ignition system was started, an analytical model was developed by Aerojet to determine the design parameters required for aft-end ignition. Prior work on aft-end ignition of solid rocket motors had been accomplished by Aerojet during the 100-in.-dia large solid rocket program [1]* and by United Technology Center for the large rocket ignition study program [2]; however, a comprehensive analytical model defining the gas dynamics of aft-end ignition was not available.

The aft-end ignition analytical model developed by Aerojet-General is described in Appendix A. The model relates motor bore pressure and hot-gas penetration to igniter mass-flow rate and motor size. Thus, the design parameter, igniter mass-flow rate per unit area of motor throat ($\dot{w}/A_t$), can be calculated for any given motor configuration and any desired motor bore pressure or depth of hot-gas penetration.

B. 260-SL MOTOR IGNITION SYSTEM DESIGN CRITERIA

The criteria used in the design of the 260-SL motor ignition system were as follows:

1. Type of Ignition

The use of an aft-end solid-propellant ignition system for the 260-SL motor was specified in the 623A Program Work Statement[3].

*Superscript numbers indicate references shown in the Reference List, Section VIII.

III, B, 260-SL Motor Ignition System Design Criteria (cont.)

2. Depth of Hot-Gas Penetration

The parameter, $\dot{w}/A_t$, for the 260-SL motor ignition system was selected to obtain a hot-gas penetration of 70% of the motor bore length. The 70% penetration value was specified for the following reasons:

a. The relationship between fore-end motor bore pressure and percent of hot-gas penetration (Figure 1) showed that, at the higher penetration levels, a significant variation in motor bore pressure resulted in only a relatively small variation in the bore length penetrated. Conversely, at the lower penetration levels, significant variations in bore pressure resulted in significant variations in the bore length penetrated.

b. The heat flux required to raise the propellant surface temperature to ignition-threshold level is provided by radiation, forced convection, condensation, and hot-particle impingement of the igniter gases; of these, convective heat flux is the major heat-transfer mode. At the interface between the hot igniter gas and trapped cold air, the gas-flow rate is reduced to stagnation. The propellant surface forward of the stagnation zone is inaccessible to convective heat flux and is ignited by radiation at a much lower flux rate. As penetration increases, more propellant surface is directly exposed to convective heat transfer, and the capability of obtaining ignition reproducibility is gained.

c. Data from the United Technology Center aft-end ignition tests[2] showed that ignition can be accomplished at penetration levels as low as 30%. However, no data were available to show the minimum penetration necessary to achieve successful motor ignition. The 60 to 70% penetration provides a large margin of safety in the amount of propellant surface initially ignited.

III, B, 260-SL Motor Ignition System Design Criteria (cont.)

d. The following motors have been successfully ignited by aft-end igniters with mass-flow rates high enough to obtain 60 to 70 percent penetration:

(1) Aerojet-General Motors 40-ITM-1 and -2

(2) Aerojet-General Motor 100FW-4

(3) Aerojet-General Motors 44-SS-1, -2 and -3

(4) United Technology Center Motor TM-3A (20-in.-dia motor)

(5) Thiokol Motors 156-1 and 156-2C-1

3. Pressure

The 260-SL motor ignition system design pressures were as follows:

Nominal operating pressure, psia	1000
Maximum expected operating pressure, psia	1500
Hydrostatic test pressure, psig	2000
Hardware design pressure, psia	3000

The ignition motor mass-flow rate is controlled mainly by the internal operating pressure. As indicated in previous aft-end ignition programs, the ignition motor operating pressure should be as high as is practical to ensure high exit velocities and satisfactory penetration of the motor bore by the ignition motor gases. Selection of the practical operating pressure was based on the following considerations:

III, B, 260-SL Motor Ignition System Design Criteria (cont.)

a. At high motor operating pressures, the required nozzle throat area and grain free-flow area are small and consequently the ignition motor size is minimized.

b. At lower operating pressures, the design of pressure-vessel hardware and components is greatly simplified.

The selected 1000-psia operating pressure was a good compromise between ignition motor size and hardware design problems. The 2:1 design safety factor was more than adequate to ensure reliable performance of the pressure vessel.

4. Port-to-Throat Area Ratio

Propellant igniter performance in the Minuteman program indicated that overpressures occur most often in igniters with highly configurated propellant grains and port-to-throat area ratios of less than 2.0, so it was determined that the port-to-throat area ratio would be greater than 2.5 to minimize overpressures during ignition of the 260-SL motor ignition system.

5. Duration

Burning time of an aft-end solid-propellant igniter is not a critical factor, but the duration has to be long enough to ensure burning throughout the ignition phase. A nominal web-burning duration of 0.6 sec was selected for the 260-SL motor ignition system.

6. Prefiring and Handling Safety

The use of a qualified safety-arming device with remote disarm capability was specified in the 623A Program Work Statement.(3)

III, B, 260-SL Motor Ignition System Design Criteria (cont.)

7. Operating Temperature Range

A 60 to 100°F operating temperature range was specified in the Work Statement.

8. Ignition Pressure

A motor ignition pressure of not greater than MEOP was specified in the Work Statement.

9. Ignition System Position

The position of the aft-end ignition system in the 260-SL motor nozzle was controlled to prevent jet plume impingement on the 260 motor nozzle throat insert. One of the aft-end ignition analytical model assumptions was that all of the mass flow from the ignition system would enter the 260-SL motor bore, giving the desired bore pressure and penetration. The impingement of ignition motor jet plume on any portion of the 260-SL motor exit cone or throat insert before motor ignition occurred would result in a loss of efficiency. Jet plume impingement was also avoided to prevent any mechanical or thermal damage to the motor throat.

C. IGNITION SYSTEM DESCRIPTION

The ignition system for the 260-SL motors is shown in Figure 2. The Mod 260 ignition motor assembly consists of four major subassemblies: the main charge or ignition motor, the ignition motor booster, the initiator, and the safety-arming device.

III, C, Ignition System Description (cont.)

1. Ignition Motor

The ignition motor pressure-vessel components were fabricated of Ladish D-6ac steel forgings. The forgings were welded, rough machined, and heat-treated to a yield tensile strength of 200,000 to 217,000 psi. After machining to final dimensions, each pressure vessel was assembled and hydrostatically tested to 2000 psig.

The only ignition motor hardware fabrication problem was encountered during the vendor welding-procedure qualification. A tungsten-inert-gas (TIG) shielded, nonconsumable electrode procedure was specified for making the girth welds on the Ladish D-6ac components. The specified weld procedure emphasized the 650°F preheat and the 700 to 750°F postheat requirements. This welding procedure for Ladish D-6ac material was developed during the fabrication of second-stage Minuteman chambers and of segmented chambers for the 100-in.-dia motors. Radiographic inspection of the welded, heat-treated test plates revealed small cracks along the weld line. Weld procedure changes were made to obtain acceptable welds. Ladish Co. welding experience indicated that the specified pre- and postheats may have been too high relative to the thickness of the material being welded. The material being welded was 0.75 in. thick; the specified weld procedure was based on experience with material having a thickness of 0.5 in. or less. After several weld tests at different pre- and postheats, an acceptable set of test plates was produced. The preheat requirement was lowered from 650°F to 450 to 500°F, and this temperature was maintained during welding. The postheat was changed from 700° to 750°F to 450°F, and this temperature was held for 1 hr after welding. The first ignition motor chamber was then successfully welded, heat-treated, and hydrostatically tested. During the welding study, the possibility of changing the material and the fabrication methods was considered to eliminate the problem of welding the thick Ladish D-6ac steel. The ignition

III, C, Ignition System Description (cont.)

motor hardware fabricator placed an order with the Midvale-Heppenstall Co. of Philadelphia, Pennsylvania, for a forged cylindrical section, forward closure, and aft closure. Subsequently, the ignition motor hardware order was revised to include three welded units and one unit final machined from forgings, eliminating all welds.

The internal surfaces of the chamber and closures were insulated with GT&R Gen-Gard V-44 rubber, cured to a Shore A hardness ranging from 78 to 92. The throat insert was machined from pressure-molded rings of FM-5131 phenolic-impregnated silica cloth and bonded to the aft closure with Epon 913 prior to vulcanizing the rubber insulation.

The Mod 260 ignition motor grain configuration is a 30-point star with a 0.50 in. web; the configuration provides a slightly regressive burning curve, a 0.60- to 0.70-sec web-burning duration, and a 1.5-sec tailoff. The polyurethane propellant selected for the Mod 260 ignition motor is ANP-2758 Mod 1, which has a 0.8 in./sec burning rate at 1000 psia. This propellant was developed and fully qualified for use in the second-stage Wing II Minuteman ignition system. Required propellant properties are:

a. Maximum tensile strength at 77°F: 75 psi, minimum.
b. Elongation at Maximum tensile strength at 77°F: 25%, minimum.
c. Initial modulus at 77°F: 250 psi, minimum.
d. Cure hardness: 35 Shore A, minimum.
e. Liquid-strand burning rate: 0.99 to 1.11 in./sec at 1500 psia

Propellant installation is accomplished by a mold-casting, secondary-bonding technique. The propellant casting molds are 10 in. wide and 95 in. long, and are designed so that when the cured propellant slab is removed and bonded into the 30-in.-dia chamber, the propellant will have the required configuration. The propellant casting molds are dried and coated with RTV-60

III, C, Ignition System Description (cont.)

release agent prior to casting. The ANP-2758 Mod 1 propellant is mixed in 1800- to 2000-lb batch sizes and 112 to 116 lb are cast into each mold. A loaded propellant mold is shown in Figure 3. After cure, each loaded propellant mold is radiographically inspected for cracks and voids. Twelve to fourteen molds are loaded from each batch of propellant; 10 propellant slabs are required for each ignition motor. After radiographic inspection, approximately 0.02 to 0.05 in. of the exposed, cured propellant surface in the mold is removed. A rubber restrictor, (a 0.100-in.-thick sheet of Gen-Gard V-45) is bonded to the exposed surface with SD-850-2 liner and cured. Ten restricted propellant slabs are bonded to the inside of the chamber wall with Epon 948, as shown in Figure 4; the loaded ignition motor chamber is cured at +110°F for 24 hr before final assembly. During propellant installation, small samples of SD-850-2 liner, Epon 948 adhesive, ANP-2758 Mod 1 propellant, and Gen-Gard V-45 rubber are taken from each lot or batch of material used in the ignition motor. Liner bond tensile-strength tests of rubber-propellant samples are made of every batch of liner prepared. Adhesive peel-strength tests of Gen-Gard V-44 and V-45 rubber are also made of every batch of adhesive mixed. These tests are made to determine that the liner and adhesive materials have been properly mixed.

The Mod 260 ignition motor is designed to ensure maximum reuse of the hardware and insulation. After a test firing, the ignition motor is disassembled and visually inspected. If the firing has no adverse effect on the insulation and metal parts, the ignition motor is rehabilitated as follows:

a. All the exposed metal is cleaned.

b. The forward closure insulation char is removed by wire-brush and lightly sandblasted.

c. The 0.10-in.-thick Gen-Gard V-45 propellant slab restrictor, bonded to the chamber insulation during the propellant installation process, is machined out.

III, C, Ignition System Description (cont.)

d. The throat-insert is machined out and a new insert is bonded in. The gap between the aft-closure insulation and the new insert is filled with Gen-Gard V-61 potting insulation.

2. Booster System

The Polaris B3 first stage Alclo-grain igniter, shown in Figure 5, was selected as the Mod 260 ignition motor booster. The B3 igniter has a 1400-gm Alclo-iron, cylindrical, monoperforated grain, exhausting through four nozzle ports in the igniter chamber. The Polaris B3 igniter was selected as the booster because the main charge is adequate for fast ignition of the ignition motor propellant, detail component fabrication drawings and inspection and assembly procedures were available, and the design is similar to the fully qualified Polaris A3 first-stage motor igniter.

For use as the Mod 260 ignition motor booster, the B3 igniter design was modified as follows:

a. The K-ratio* was decreased to reduce the maximum operating pressure from 2400 to 1000 psia.

b. The number of nozzle ports was reduced from four to three, exhausting at 45 degrees from the igniter center line.

The K-ratio of the Polaris A3 and B3 igniters is the same (K-ratio = 22); however, the port-to-throat area ratio of the Polaris B3 igniter with a larger Alclo grain was considerably lower (1.4 for the Polaris A3 and 1.0 for the B3). Due to the lower port-to-throat area ratio and other ballistic phenomena not completely characterized, the peak operating pressure of the Polaris B3 igniter was 2400 psia, or approximately 900 to 1200 psi higher than the Polaris A3 igniter maximum operating pressure.

*K-ratio: Ratio of the main Alclo grain initial surface area to the igniter chamber throat area.

III, C, Ignition System Description (cont.)

The KR-80000-07 safety-arming device, which must withstand full booster chamber pressure, was proof tested to 3000 psig. To maintain a minimum safety factor of 2.0 between the booster MEOP and the safety-arming device proof pressure that is consistent with the structural design of the ignition motor hardware, the throat area of the booster chamber was sized to give a theoretical maximum operating pressure of 1000 $\pm$ 200 psia. Because of the larger throat size, only three nozzle ports were used to ensure the structural integrity of the aft end of the booster chamber. The energy correlation used to determine the required pyrotechnic charge weight for Alclo-type igniters is presented in Appendix B.

3. Initiator

The 2.0 gm 2A-BPN pellet initiator is a modification of the second-stage Minuteman Wing I and Wing II initiator systems. The BPN initiator is the connecting pyrotechnic link between the ES-003 squibs located in the safety-arming device and the Polaris B3 igniter.

4. Safety-Arming Device

The KR-80000-07 safety-arming device and the ES-003 squibs were fully tested and qualified for the Minuteman program.

D. 44-SS MOTOR IGNITION SYSTEM

The analytical model was used to determine the igniter mass flow rate required to achieve 70% hot-gas penetration into the 260-SL motor bore. The 44-SS motor ignition program was initiated to obtain subscale ignition data for verification of the Mod 260 ignition motor design criteria prior to the 260-SL-1 motor test. In addition, the subscale tests would provide data about

III, D, 44-SS Motor Ignition System (cont.)

the relationship between aft-end igniter position and motor overpressurization. No previous aft-end ignition test data with solid-propellant igniters at high penetration levels ($>$ 50%) were available, and the subscale tests would provide preliminary data measurements so that potential problem areas could be investigated.

To obtain useful and comparable data, the 44-SS ignition motor design criteria were identical to the criteria used in the design of the Mod 260 ignition motor, as shown in Figure 6. The 44-SS ignition motor design is shown in Figure 7.

The 44-SS ignition motor chamber and nozzle were standard, readily available components of the 10KS-2500 size motor. All the metal parts were hydrostatically tested to 1800 psig, which is the normal hydrostatic test pressure for 10KS-2500 motor hardware.

The propellant configuration was a case-bonded, internal-burning, cylindrical grain with a 0.5-in. web thickness. The ANP-2758 Mod 1 propellant was installed using the same mold-casting, secondary-bonding technique that was used for the Mod 260 ignition motor.

The 44-SS ignition motor booster was a standard 10KS-2500 altitude igniter, containing a solid 78-gm Alclo grain that was 1.5 in. in dia and 1.0 in. in length. The booster was initiated by an exploding bridgewire (EBW) squib and 2.0 gm of Alclo-iron pyrotechnic powder. The EBW squib, qualified in the Polaris program, was actuated by 2000 vdc discharged from a 0.5 microfarad capacitor.

E. STRUCTURAL ANALYSIS

The structural analysis demonstrated that the Mod 260 ignition motor assembly components meet the following design loads:

III, E, Structural Analysis (cont.)

1. Internal pressure:

MEOP (3 σ derivation at 100°F),	1500 psia
Design yield load (MEOP x a 2.0 safety factor),	3000 psia
Hydrostatic test pressure,	2000 psig

2. Thrust:

Limit,	267,000 lbf
Design	534,000 lbf

The minimum margins of safety were:

Component	Minimum Margin of Safety*
Forward head	0.06
Forward flange joint	0.12
Cylindrical section	0.15
Aft flange joint	0.09
Exit cone-aft closure flange joint	0.07

The Mod 260 ignition motor is based on a conservative design, proven materials, and maximum reuse of all components. The ignition motor materials and allowable yield stresses were:

Component	Material	Allowable Yield Stress, psi
Chamber and closures	Ladish D-6ac	175,000**
Exit cone	AISI-4130	100,000
Booster adapter	AISI-4340	142,000

* Margin of Safety = $\frac{\text{Allowable Stress}}{\text{Design Stress}} - 1.0$

Design Stress = Stress at MEOP x 2.0

**Allowable weld mismatch: 90% continuous membrane

III, E, Structural Analysis (cont.)

The ignition motor pressure-vessle was divided into different sections for more convenient analysis, as shown in Figure 8. The structural analysis is summarized in Figures 9 and 10.

F. RETENTION-AND-RELEASE SYSTEM

1. Design Criteria

The design criteria for the Mod 260 ignition motor retention-and-release system were based on a preliminary 260-SL motor ignition performance analysis, and on an analysis of the effect of the Mod 260 ignition motor on the structural integrity of the 260-SL motor nozzle and exit cone.

From the preliminary ignition performance prediction[4], an igniter-ejection actuation-command pressure of 275 psia was selected. The primary igniter-ejection actuation command was based on motor-bore pressure rather than on a predicted time to ensure that stable motor ignition was achieved before the igniter was ejected and to ensure that the igniter was completely free of the 260-SL motor exit cone before motor steady state operating pressure was achieved. Also, the bore-pressure measurement is a more positive method of monitoring the state of motor ignition, whereas a programed time-ejection command is only as reliable as the predicted ignition performance.

During normal motor-pressure rise, the static pressure on the motor nozzle and exit cone increases as the motor bore pressure increases. The presence of the igniter in the motor exit cone causes an increase in the exit static pressure. The static pressure on the 260-SL motor nozzle and exit cone was determined at various igniter locations in the exit cone at corresponding time intervals, assuming that the igniter-ejection sequence began when the motor bore pressure reached 275 psia. The method used to estimate the motor exit cone

III, F, Retention-and-Release System (cont.)

static pressures is presented in Appendix C; the results are shown in Figure 11, including static pressure under normal operating conditions and during igniter ejection. This was considered a worst-case estimate, as it was difficult to clearly define the transient flow field caused by interaction of the inlet jet plume and the motor exit gas stream.

The side load imparted to the 260-SL motor exit cone by the aft-end igniter was also considered. Since the motor exit cone was not designed for thrust-vector control, the side-load structural capability of the exit cone was limited (20,000 lb). The igniter had to be ejected vertically along the exit cone center line to a position above the motor exit plane where the flow from the igniter no longer affected the flow in the motor exit cone. This axial distance was determined by the bow shock displacement, and was a function of the jet-to-free stream total-pressure ratio, the body-to-jet dia ratio, and the inlet and exit gas stream Mach numbers. Studies of the effect of a blunt body in a high Mach number free stream[5] indicate that the shock displacement distance of the ignition motor inlet jet plume is 31.4 ft. Thus, the igniter must be ejected vertically for 31 ft to ensure no side-load effects on the motor nozzle. The structural analysis also showed that the igniter could not be canted more than 4.4 degrees in the exit cone to ensure a side force of less than 20,000 lb.

From these analyses and the igniter design criteria, the following retention-and-release system design criteria were established:

a. Location

The igniter is to be mounted on the 260-SL-1 motor center line, with the exit plane of the igniter located 29.50 $\pm$ 0.50 in. aft of the motor throat plane (ε^* = 1.21).

III, F, Retention-and-Release System (cont.)

The igniter thrust axis will be angularly aligned with the motor center line within ± 1.5 degrees and will not be displaced from the center of the motor throat more than 1 in.

b. Installation

The igniter will be attached to the retention-and-release structure at both the forward and aft igniter chamber mounting flanges.

Assembly of the igniter to the retention-and-release structure will be accomplished away from the 260-SL-1 motor.

The ignition motor or retention structure will not come in contact with any portion of the 260-SL-1 motor during installation and operation.

c. Ejection

The igniter-ejection sequence will be initiated by a pressure-sensing device located at the forward end of the 260-SL-1 motor. An electrical release command signal will be actuated when the 260-SL-1 motor bore pressure reaches 125 ± 5 psia.

If the pressure-sensing device fails to actuate the retention-and-release system, the impingement force generated on the igniter and retention structure by the exit gas stream plus the igniter thrust will be sufficient to cause mechanical failure of the retention system. The mechanical failure is to occur when the motor bore pressure is between 350 and 430 psia.

In addition to the preceding ejection methods, an automatic ejection command signal will be initiated at 0.525 ± 0.010 sec after fire switch.

III, F, Retention-and-Release System (cont.)

The movement of the ignition motor through the 260-SL-1 motor exit cone will be controlled and will not vary more than ± 1.5 degrees from the vertical until the igniter exit plane is at least 31 ft above the motor exit plane.

The time from electrical actuation of the retention-and-release system until the ignition motor exit plane clears the motor exit plane will not exceed 0.175 sec. The maximum acceleration of the igniter during ejection will not exceed 75 g.

d. Postejection Condition

No portion of the retention structure will remain in the 260-SL-1 motor exit gas stream longer than 2.0 sec after ejection of the ignition motor.

The igniter impact area will be no less than 100 yards from the test facility.

To determine the feasibility of the mechanical failure method of ejection, the drag forces on the ignition motor and retention structure were computed at various levels of motor bore pressure during the transient pressure rise. These calculations indicated that the mechanical failure method of ejection was not feasible.

Methods used to compute the drag forces are shown in Appendix D, and results are summarized in Figure 12. Although the approach used to estimate the drag forces shown in Appendix D was reasonable (as shown by the close agreement of the values computed by the two methods), the numerical value of the computed drag force was at best only ± 50% accurate. The inaccuracy in the calculation is due to high pressure gradients in the jet stream, nonuniform Mach

III, F, Retention-and-Release System (cont.)

numbers, and the complex impingement configuration with unpredictable flow-interference effects. Thus, to mechanically fail the retention system as specified, the following criteria had to be met:

The igniter must be retained under maximum load until the motor bore pressure reaches 275 psia. The ignition motor thrust (at 100°F) with the motor bore pressure at 275 psia is 300,000 lbf; the maximum drag force on the igniter and retention structure at 275 psia motor bore pressure is 462,000 lbf, as shown in Figure 12. Thus, the maximum calculated total force is 762,000 lbf.

The ignition motor must be released by mechanical failure of the retention system under minimum load before the motor bore pressure reaches 430 psia. The minimum drag force on the igniter and retention structure is 205,000 lbf. The igniter thrust (at 60°F) with the motor bore pressure at 430 psia is 200,000 lbf. The minimum total force is 405,000 lbf.

Therefore, the maximum force that must be withstood by the retention system at 275 psia (762,000 lbf) was greater than the minimum force required for mechanical failure at 430 psia (405,000 lbf), making the mechanical-failure method of igniter ejection unfeasible, and the requirement for this method of ejection was deleted.

2. Description

a. Mod 260 Ignition Motor Retention-and Release System

The Mod 260 ignition motor retention-and-release system consists of two main assemblies: the igniter release control unit and the retention structure.

III, F, Retention-and-Release System (cont.)

(1) Igniter Release Control Unit

The igniter release control unit is a solid-state electrical system designed to provide a discrete command signal to the retention-and-release system explosive bolts. A simplified circuit diagram of the igniter release control unit is shown in Figure 13. Two distinct input signals are used to actuate the control unit: an analog input signal and a preset time signal. Either input signal is capable of initiating an explosive bolt actuation command signal, provided that the igniter release control unit logic is satisfied.

The analog input is designed to operate from an analog signal source, specifically a strain gage transducer filtered through an amplifier. A Taber Model 206 pressure transducer, ranged from 0 to 750 psia, is mounted on the forward dome of the motor. The voltage output of the transducer is filtered through a 120 cycles/sec Kintel Model 114A amplifier to eliminate transient high-frequency pulses that might prematurely actuate the control unit. The analog actuation level is a + 1.5037 vdc output from the transducer, which corresponds to a 275 ± 2 psia motor bore pressure. (The transducer output was reduced later in the program to correspond to an actuation bore pressure of 200 ± 5 psia.) The analog switch operates a Schmitt trigger, which in turn provides a very fast rise time to operate a one-shot oscillator. The one-shot oscillator, which is set for a duration of 0.030 sec, is in the set or reset condition depending upon the condition of the Schmitt trigger. When the Schmitt trigger is turned on by receiving the proper analog actuation voltage at the input, the one-shot oscillator goes to the set condition. If, after an elapsed time of 0.030 sec, the Schmitt trigger is still turned on, the control logic will be satisfied when the oscillator returns to the reset state, providing the fire-switch signal is still turned on.

III, F, Retention-and-Release System (cont.)

Thus, three conditions are necessary to satisfy the control logic: the fire switch must be on; the Schmitt trigger must be on; and the oscillator must time out and reset. Once the control logic is satisfied, the explosive bolt actuation signal is sent. If the Schmitt trigger is turned on for less than 0.030 sec, the oscillator will be turned off by a reset pulse from the reset side of the Schmitt trigger and will not be allowed to time out. This is an added safety feature to eliminate the possibility of a short-duration pressure or voltage pulse causing a premature ignition release command. The oscillator is ready to start a new timing sequence on reaching the reset condition.

As a backup system to the pressure-sensing section of the igniter release control unit, a timer section is included. This section of the control unit is designed to provide a programed explosive bolt command signal 0.525 ± 0.010 sec after fire switch. The fire-switch input requires a 28 vdc step function at fire switch. The 28 vdc fire-switch signal is applied to the input terminal of the fire-switch Schmitt trigger. The fire-switch Schmitt trigger output is coupled to a 0.525 sec one-shot oscillator. When the oscillator times out and returns to the reset condition, an explosive bolt actuation signal is released.

(2) Retention Structure

To ignite the 260-SL motor, the ignition motor is mounted in the motor exit cone and is secured in that position until ignition of the main motor is accomplished. The ignition motor is then ejected from the motor exit cone and guided to a predetermined, remote impact area.

The overall retention structure for the Mod 260 ignition motor is shown in Figure 14. The retention structure consists of an igniter support fixture, a tower assembly, retaining cables, and explosive bolts.

III, F, Retention-and-Release System (cont.)

(a) Igniter Support Fixture

The igniter support fixture is shown in Figure 15. The Mod 260 ignition motor is bolted to two 24-in.-wide flanged beams. The support beams lay horizontally across the nozzle exit plane and are bolted to vertical A-frame supports on each side of the exit cone. Both vertical A-frame supports are installed on the two 36-in.-wide flanged beams that are part of the 260-SL motor antiflight structure. Aluminum wheels are installed on the tower end of the horizontal support beams. A 30-in.-dia by 204-in.-long pipe is welded to the horizontal support beams over the ignition motor mount. The upper end of the 30-in.-dia pipe has counterweights to offset the weight of the ignition motor, keeping the center of gravity near the physical center of the igniter support structure. Horizontal tubular struts with aluminum wheels are welded to the upper portion of the 30-in.-dia pipe. Additional struts are welded to the fixture to maintain a rigid structure.

The support fixture is designed to have a minimum of nonsymmetrical elements. The drag on the support fixture was computed using conventional drag coefficients with an estimate for drag interference. The drag is 11,190 lb at a velocity of 320 ft/sec. The center of pressure is located approximately 0.96 ft toward the wheel side of the support-fixture thrust center line.

An analysis of the support fixture at the top of the tower was made to determine the pitching moment when the upper wheels are off the track and the lower wheels are still on the track. The loads involved included misalignment, cable weight, friction of the wheels, and eccentricity of the thrust load. The analysis indicated an angular pitching moment of less than 0.5 degrees.

The design and size of the igniter support structure is controlled by the mounting flange configuration of the Mod 260 ignition motor chamber, the 0.175 sec maximum time for ejection of the igniter from the exit cone,

III, F, Retention-and-Release System (cont.)

the 75-g maximum acceleration requirement, ignition motor thrust, and the motor exit gas-stream impingement forces. Since the impingement force calculation was at best only ± 50% accurate, the following maximum and minimum values of impingement forces were used in the fixture design:

Motor Pressure	Maximum, lbf	Nominal, lbf	Minimum, lbf
275 psia	462,000	308,000	154,000
350 psia	540,000	360,000	180,000
430 psia	615,000	410,000	205,000

Also, the values of the impingement forces are assumed to decrease 1.25 %/ft of vertical movement. Based on these criteria, the limit weight of the igniter support structure is 17,200 lb. The calculated weight of the support fixture and cables was 18,800 lb. The weight increase was necessary to meet the structural loads imposed during the vertical ascent and flight. To compensate for the additional weight, the release control unit actuation pressure was reduced from 275 ± 2 psia to 200 ± 5 psia to ensure ignition motor ejection before the motor reached initial steady-state operating pressure.

The engineering analysis of the support fixture involved many types of loads that could be developed prior to and after release. The allowable misalignment given in the criteria is 3 degrees; however, the final requirement is 1 degree. The 3-degree misalignment imposed excessive loads on the top of the tower and on the tower retraction linkage.

(b) Tower Assembly

The tower assembly, shown in Figure 16, consists of two vertical channel-beam tracks and related structural support members. The four wheels on the igniter support fixture are guided into the channel track, and are lowered down the track until the horizontal support beams rest on the antiflight

III, F, Retention-and-Release System (cont.)

structure vertical A-frame supports. The tower assembly, after installation at the Cast, Cure, and Test Facility, is within 1 degree of vertical, so that the actual thrust misalignment is well within the 3-degree maximum limit. The tower assembly was designed to withstand winds of up to 80 mph and all forces generated by the movement of the igniter support fixture. The stress levels in the tower support members, pin connections at the base of the tower, and retraction linkage were computer to establish the force required to initiate tower retraction and the force needed to decelerate the tower before the end of travel. A force of 7000 lb is required to initiate tower retraction, and once the retraction linkage has moved past dead center, a force of 160,000 lb is required to decelerate the tower mass.

An MRL 1443 motion programmer, manufactured by Monterey Research Laboratory, Inc., was selected to control the tower movement. The installation of the tower retraction linkage, motion programmer, and hydraulic cylinder are shown in Figure 17. A schematic diagram of the motion programmer hydraulic system is shown in Figure 18. The motion programmer is a self-contained hydraulic system consisting of an actuating cylinder and the valves and accumulators necessary to maintain the required cylinder pressure. The energy needed to initiate tower motion is stored in the accumulators; the energy of the falling tower is absorbed by the throttling action of the three main relief valves. As shown in Figure 17, the hydraulic cylinder is attached to the tower retraction linkage, and the other components are packaged together in a cabinet and connected to the cylinder with flexible hoses. The system is put into operation by opening the solenoid valve (Figure 18). When the valve is opened, pressure is equalized throughout the hydraulic system and on both sides of the piston. Because the fluid pressure acts against unequal areas on opposite sides of the piston, the rod begins to extend. Fluid passes through the solenoid valve from the rod end of the cylinder, bypasses the three main relief valves through a check valve, and then flows into the blind end of the cylinder. The two large accumulators compensate for the volume of the rod. If the solenoid valve fails after motion of the system has been started, fluid flow will continue through the relief valve, which is in parallel with the solenoid valve.

III, F, Retention-and-Release System (cont.)

Before the rod reaches the end of its extension stroke, it is loaded in tension by the falling tower. Mechanical linkage reverses the load and the rod begins its retraction stroke. The decelerating pressure in the cylinder is held at a nearly constant level during the entire retraction stroke by three parallel main relief valves. Fluid then passes from these three main relief valves through the check valve in the upper branch and into the rod end of the cylinder to complete the cycle. The tower and retraction linkage at the end of the retraction cycle are shown in Figure 19.

(c) Cables

Four 2-1/8-in.-dia wire cables, each 326 ft long and weighing 9.1 lb/ft, are mounted to the igniter-support structure at equal distances from the center of gravity on the thrust axis. To reduce the cable weight horizontal force component on the igniter support structure at the top of the track, cable support towers were located 52 ft from the center line of the motor. The cable support towers were the same height as the tower assembly; when the igniter support assembly reaches the top of the tower assembly, the cable section between the cable support tower and the igniter support structure is a catenary, so that the horizontal force due to cable weight and drag is minimized.

The selection of the cables was based on the ultimate breaking strength required, with minimum weight per foot. The maximum load on the cables is the 788,000-lb centrifugal force generated by the flight of the ignition motor and support fixture through the 295-ft radius arc. The cables selected and the mass required to secure the cables are designed to this load. The ultimate strength of each cable is 220 tons.

As mentioned previously, two cable support poles were installed to reduce the loads on the tower. This was determined by establishing the catenary for the cables with one support and assuming that a percentage of the

III, F, Retention-and-Release System (cont.)

cable weight would be effective in producing a pitching moment on the ignition motor and support fixture. The cable support poles reduced the pitching moment from 24,200 to 1417 lb per cable.

(d) Explosive Bolts

Twenty-eight 5/8-18 UNF Holex explosive bolts are used to retain the igniter support structure. The minimum load capacity of each bolt, as specified by the manufacturer, is 20,000 lb.

(e) Supporting Equipment

The entire retention system is mounted on two 36-in.-wide beams that straddle the center of the caisson. These beams secure the antiflight equipment for the 260-SL motor and provide the required support for auxilliary equipment. Beam deflections due to the igniter and impingement thrust and dead load are a maximum of 0.3 in. from the unloaded condition. Natural frequency of the beams of 7 cycles/sec after release of the load causing the deflection. The maximum reaction on the system due to acceleration after releasing the load is approximately 3 g.

b. Retention-and-Release System for the 44-SS Ignition Motor

The retention-and-release system for the 44-SS ignition motors was actuated by the igniter release control unit previously described for the Mod 260 ignition motor retention system. As shown in Figure 20, the 44-SS ignition motor was bolted into a steel support cradle. Steel U brackets were welded to the base of the support cradle and the brackets were free to slide on the main H-beam track. The H-beam track was supported by a steel pipe structure mounted on the test-bay deck. The forward support cradle U brackets were retained

III, F, Retention-and-Release System (cont.)

by four 3/4-in.-dia Holex exploxive bolts designed to fail in shear when the actuation signal was received from the igniter release control unit. When the explosive bolts were actuated, the 44-SS ignition motor and support cradle moved along the H-beam track and were ejected clear of the 44-SS motor. The flight of the ignition motor and cradle support was retarded by two steel cables anchored approximately 50 ft aft of the 44-SS motor.

IV. TEST PROGRAM DESCRIPTION

The test program for the Mod 260 ignition motor assembly included the following phases:

a. Development of processing technology
b. Determination of motor propellant threshold-ignition energy
c. Cold-flow studies
d. Squib-to-initiator tests
e. Ignition motor booster open-air tests
f. Subscale ignition tests
   (1) Free-volume simulator tests
   (2) Firings of 44-SS motors
g. Mod 260 ignition motor assembly open air test
h. Mod 260 ignition motor assembly free-volume simulator tests
i. Mod 260 ignition motor assembly retention-and-release system demonstration tests

The specific objectives, special equipment, instrumentation and results for each test phase are discussed in detail below.

A. DEVELOPMENT OF PROCESSING TECHNOLOGY

1. Objectives

The objectives of the processing technology development phase of the Mod 260 ignition motor test program were to select the processing materials, evaluate their properties, and demonstrate the propellant installation technique. The materials to be selected were:

a. Liner for bonding the cured Gen-Gard V-45 rubber restrictor to cured ANP-2758 Mod 1 propellant.

IV, A, Development of Processing Technology (cont.)

b. Adhesive for bonding the Gen-Gard V-45 restrictor to cured Gen Gard V-44 rubber chamber insulation.

c. Release agent for use between the propellant and the wooden molds.

2. Results

a. Materials Selection

SD-850-2 PBAN liner was selected as the bonding material between the propellant and the Gen-Gard V-45 rubber restrictor. Double-plate tensile bonding tests showed that both SD-850-2 PBAN liner and Epon 948 epoxy adhesive have satisfactory bond strengths (145 to 149 psi) between cured ANP-2758 Mod 1 propellant and Gen-Gard rubber. The SD-850-2 liner material has better flow and application characteristics, longer pot life, and better propellant restricting properties than the Epon 948 epoxy adhesive.

The Epon 948 epoxy adhesive was selected as the bonding material between the Gen-Gard V-45 rubber propellant restrictor and the Gen-Gard V-44 rubber ignition motor chamber insulation. Selection was based on bond strength tests conducted as part of the 260-SL motor insulation development program.

General Electric RTV-60 silicone rubber was selected as the release agent between the wooden casting mold and the propellant.

b. Propellant Processing

Previous processing data for ANP-2758 Mod 1 propellant were limited to 60- and 150-lb batches used for the second-stage Minuteman igniters. As part of the processing technology development program, the propellant mixing

IV, A, Development of Processing Technology (cont.)

procedures were revised for scale-up to 1800-lb batches. An 1800-lb batch of ANP-2758 Mod 1 propellant was mixed and cast into the wooden molds. After cure, the exposed propellant surfaces were trimmed and the Gen-Gard V-45 rubber restrictors were bonded to the propellant with the SD-850-2 PBAN liner material. One of the molds was sectioned to check the propellant integrity. Every section examined was free of voids or cracks.

The propellant from two batches were tested for ballistic and mechanical properties. The results are shown in Figure 21. Ballistic data from all batches of ANP-2758 Mod 1 propellant processed for this program are included in Figure 21. The properties of both test batches met the design requirements, and the revised mixing procedures were incorporated into the ANP-2758 Mod 1 propellant process specification.

c. Propellant Installation

Three loaded propellant molds were reserved for the propellant installation demonstration. Epon 948 epoxy adhesive was applied to the Gen-Gard V-45 rubber chamber simulator insulation. Three propellant slabs were then installed into the 30-in.-dia tube as shown in Figure 22. Installation was readily accomplished without problems in handling, orienting, or aligning the propellant slabs. After being cured, the loaded tube was roughly handled, dropped, and vibrated without affecting the propellant or bond integrity. This propellant installation technique was completed satisfactorily, and a specification defining the process requirements for ignition motor propellant installation was released.

B. DETERMINATION OF MOTOR PROPELLANT THRESHOLD-IGNITION ENERGY

1. Objective

The objective of this phase of the program was to determine the threshold ignition energy of the 260-SL motor propellant, ANB-3105. The propellant

threshold-ignition energy data were used later in the free-volume simulator tests to evaluate the capability of the Mod 260 ignition motor to ignite the 260-SL motor propellant.

2. Procedure

Twenty 2-in. cubes of ANB-3105 propellant were supplied to Stanford Research Institute, Menlo Park, Calif., for testing. The chemical and physical properties of the propellant samples were representative of the propellant properties expected in the 260-SL-1 motor after casting. Ignitibility measurements were made with the SRI arc-image furnace. A schematic of the arc-image furnace is shown in Figure 23. Tests were conducted at flux levels of 70 and 100 cal/cm^2-sec, and at pressures of 1.5, 25, 50, 100, and 200 psig in a nitrogen atmosphere. Threshold-ignition energy was defined as the radiant energy required to ignite the propellant with a 50% probability, determined by visual observation of four consecutive no-fire and four consecutive fires with minimum separation of exposure times.

3. Results

The results of the threshold-ignition energy tests of samples of ANB-3105 propellant are shown in Figure 24. In Figure 25, the 260-SL motor propellant threshold-ignition energy requirements at various pressures are compared with the threshold-ignition energy requirements of polyurethane and polybutadiene propellants used in Polaris, Minuteman, Algol, and 100-in.-dia motors. These data showed that the ANB-3105 propellant, like the Minuteman polybutadiene ANB-3066 propellant, is insensitive to changes in ignition pressure and requires only slightly more ignition energy than the polyurethane propellants at the higher ignition pressures. ANB-3105 propellant has an ignition-threshold energy requirement of 2.6 to 2.8 cal/cm^2 at the expected 260-SL motor ignition pressures of 60 to 80 psia.

IV, Test Program Description (cont.)

C. COLD-FLOW STUDIES

1. Objectives

The objectives of the cold-flow studies were to verify the aft-end ignition analytical model, and to study the effect of aft-end igniter gas flow on motor throat blockage and chamber bore pressure.

2. Approach

To achieve the objectives, data relating igniter mass-flow rate, igniter pressure, motor port area, and motor throat area to motor-bore pressure were required. The analytical model assumptions and equations were applied to an igniter model flowing nitrogen into a motor-bore model. The analytical model equations were used to calculate the fore-end bore pressure and bore penetration in the motor-bore model as functions of igniter flow rate, motor port area and motor throat area for the nitrogen system, as shown in Figure 26.

Nitrogen at 530°R and 1000 psia was flowed through a calibrated nozzle into the motor-bore model, as shown in Figure 27. The independent parameters, $\dot{w}/A_t$ and A_p/A_t, were varied separately and together over a sufficient range to enable an accurate evaluation of the analytical model.

During the cold-flow tests, the position of the igniter exit plane with respect to the motor-bore model throat plane was also varied. The annular flow area around the igniter exit plane, referred to as ϵ^*, was 1.3, 1.5, and 1.8 for three test runs.

An additional test was made to study the effect of motor-bore model throat blockage caused by the incoming igniter jet plume on the motor-bore model pressure. To simulate the counter-flow condition, air at 530°R was flowed through the motor-bore model while nitrogen was flowed from the igniter. The

IV, C, Cold-Flow Studies (cont.)

effect of aft-end igniter jet plume on motor-bore model pressure was determined by measuring differences in motor-bore model pressure at various igniter flow rates, motor-bore flow rates, and igniter positions.

3. Test Apparatus

The igniter model consisted of a long steel tube connected to a regulated supply of dry nitrogen. A nozzle was mounted on the end of the tube by a bolted flange. Three nozzles, with throat diameters of 0.739, 0.64, and 0.522 in., were fabricated. In this way, three igniter flow rates were simulated at any given operating pressure. The igniter nozzle was moved axially by adding or removing shims at the flange joint, and the annular flow area around the igniter nozzle exit plane, ε *, was varied.

The motor-bore model was a large diameter tube, lined with wooden inserts to simulate motor bore and nozzle configurations. Two wooden inserts were fabricated; both inserts had a 3.09-in. throat diameter and a 17.5-degree exit cone half-angle. The inserts had different cylindrical port diameters to give port-to-throat area ratios of 3.0 and 1.3, which correspond closely to those of the short- and full-length 260-in.-dia motors.

4. Instrumentation

Taber transducers were mounted on both the motor-bore and igniter models to obtain the required pressure data. Since significant variations in pressure due to temperature change could occur, a series of chromel-alumel thermocouples were installed to monitor the inlet and outlet gas temperatures. The measured bore pressures were corrected for temperature variations.

5. Results

The basic cold-flow test data are presented in Figure 28. The data shown in Figures 29 through 34 present the comparison between the measured

IV, C, Cold-Flow Studies (cont.)

pressures and pressures predicted by the analytical model. The solid lines are the pressures predicted from the analytical model; the cold-flow test data are plotted on the graphs for comparison. Composite graphs of all cold-flow pressure data plotted as a function of igniter flow rate, for an igniter model position of $\epsilon^* = 1.3$ and for motor-bore model port-to-throat area ratios of 1.3 and 3.0, are shown in Figures 35 and 36, respectively. The data show that changes in igniter operating pressure do not significantly affect the correlation between the measured and calculated pressure.

Data showing the effect of motor-model throat blockage caused by the incoming igniter jet plume on the motor-model bore pressure are shown in Figure 37. During the counterflow test, the igniter model was supplied with a constant 700 psia nitrogen supply and the motor model counter air flow was varied over the range available. The measured motor model bore pressure was 14 to 20% higher than the predicted pressure. Apparently the actual jet plume blockage of the motor model throat was higher than the blockage calculated from the analytical model.

D. SQUIB-TO-INITIATOR TESTS

1. Objectives

The 2.0-gm 2A boron-potassium nitrate initiator is the connecting pyrotechnic link between the safety-arming device and the Polaris B3 first-stage igniter and had not been previously tested in the configuration used in the Mod 260 ignition motor. Therefore, a series of tests were made to verify the reproducibility of flame propagation from the ES-003 squibs through the 2A-BPN initiator to the 2.0-gm Alclo-boron barium chromate (BBC) booster initiator.

2. Test Apparatus

The Mod 260 ignition motor booster-initiator flame propagation was verified by firing the pyrotechnic train into a closed pressure vessel and

IV, D, Squib-to-Initiator Tests (cont.)

measuring the pressure output. A test fixture was designed to simulate the initiator pyrotechnic train configuration. The squib-to-initiator test configuration is shown in Figure 38.

Installation of the 2.0-gm 2A-BPN initiator assembly capsule and the safety-arming device was identical to that in the Mod 260 ignition motor booster. Installation of the 2.0-gm Alclo-BBC powder booster initiator was slightly modified to enable easy assembly and disassembly during this test series. The 2.0-gm Alclo-BBC booster initiator was loaded into a threaded insert. The 2.0-gm Alclo-BBC booster-initiator insert assembly was then installed in the test fixture adapter as shown in Figure 38. After each test, the insert assembly was easily removed and replaced with a new unit. In the Mod 260 ignition motor booster, the 2.0 gm of Alclo-BBC powder will be loaded directly into the initiator cavity in the booster adapter.

A firing train test fixture (FTTF) was used in place of the KR-80000-07 safety-arming device in ten of the twelve tests to reduce cost. The FTTF configuration is identical to that of the safety-arming device, but is less expensive due to the elimination of switches and the electric motor.

The test chamber volume was 50 cu in., which is close to the free volume in the Mod 260 booster. The 50 cu in. test volume is also the standard test volume used for the second-stage Minuteman initiator qualification tests. Three 3/8-18 NPT taps were provided in the chamber wall for instrumentation and pressure relief.

3. Instrumentation

The squib-to-initiator tests were conducted at the Bulova Research and Development Laboratories in Woodside, New York. All of the instrumentation was furnished by Bulova. Two Kistler P2-14 transducers were installed in the test chamber for pressure measurement. The Kistler pressure data were recorded on

IV, D, Squib-to-Initiator Tests (cont.)

Kodak Linagraph direct print paper by a Mod 1108 Visicorder, operated at 80 in./sec. Each squib was actuated by 4.0 amp from a 28 vdc supply. A Dumont scope camera (Polaroid) was used to photograph an oscilloscope trace of each test firing.

4. Test Sequence

The test sequence was as follows:

Run No.	Configuration	Objective
1 through 6	An FTTF was mounted on the test fixture with both initiators installed	Flame propagation reproducibility
7	An FTTF was mounted on the test fixture with the 2.0-gm BPN pellet initiator installed. The 2.0-gm Alclo-BBC booster initiator was omitted	Off-design test to determine if flame propagation will occur with a portion of the initiator train omitted
8 and 9	A KR-80000-07 safety-arming device was mounted on the test fixture with both initiators installed	Flame propagation reproducibility
10	An FTTF was mounted on the test fixture with both initiators installed; 4.0 amp was applied to the upper squib only	Off-design test to determine if flame propagation will occur with only upper squib actuated

IV, D, Squib-to-Initiator Tests (cont.)

Run No.	Configuration	Objective
11	An FTTF was mounted on the test fixture with both initiators installed; 4.0 amp was applied to the lower squib only	Off-design test to determine if flame propagation will occur with only lower squib actuated
12	An FTTF was mounted on the test fixture with the 2.0-gm Alclo-BBC booster initiator. The 2.0 gm of BPN pellets was omitted	Off-design test to determine if flame propagation will occur with a portion of the initiator train omitted.

5. Results

A summary of the squib-to-initiator test data is shown in Figure 39. A typical Visicorder trace of the pressure-vs-time data is shown in Figure 40. The standard deviation of the measured pressures (not including the off-design tests where a portion of the pyrotechnic train was deliberately omitted) was 20.5 psi. The variation in the time between fire-switch and peak pressure was only $\pm$ 0.004 sec.

The instrumentation was calibrated for a 40 psig/in. deflection on Run No. 1; however, the pressure went off scale at about 175 psia. For all subsequent runs, the instrumentation was calibrated to give approximately 80 psig/in. deflection on the Visicorder.

The hardware was visually examined after each test. The residue in the test chamber and on the hardware was dark, with no evidence of unburned Alclo. The hardware showed no evidence of erosion, and there was no visual evidence to indicate incomplete combustion, excessive pressure in the initiator containers, or misalignment between components.

IV, D, Squib-to-Initiator Tests (cont.)

During the tests, a 20- to 50-psi deviation was noted in the pressure data between the Kistler pressure transducers. Both transducers had been calibrated on 17 March 1964, and had not been used prior to this test series. Several attempts were made to check the calibration of both the transducers and the Visicorder, but the cause of the pressure variation could not be found. The purpose of this test series was to evaluate performance reproducibility, and recording the absolute pressure value was secondary. Therefore, both pressure values were reported, and an average pressure value was used to evaluate the performance reproducibility.

This test series verified the performance reproducibility of the pyrotechnic link from the ES-003 squibs in the KR-80000-07 safety-arming device to the ignition motor booster. The test series showed that flame propagation will occur in the event one of the ES-003 squibs fails to function and with only a portion of the initiator installed, though the propagation will be slower and at a lower pressure.

E. MOD 260 IGNITION MOTOR BOOSTER OPEN-AIR TESTS

1. Objectives

The booster open air tests were conducted to determine the K-ratio required to obtain a 1000 $\pm$ 200 psia booster operating pressure, to verify the flame propagation of the pyrotechnic train, and to demonstrate the hardware integrity.

2. Test Apparatus

A test fixture was designed and fabricated for mounting the Mod 260 ignition motor booster to the test bay deck in a nozzle-up position, as shown in Figure 41. A firing train test fixture was used in place of the KR-80000-07 safety arming device.

IV, E, Mod 260 Ignition Motor Booster Open-Air Tests (cont.)

3. Instrumentation

Internal booster chamber pressure was measured by a Taber transducer through a pressure tap in the booster adapter.

4. Results

The data from the three Mod 260 ignition motor booster open-air tests are summarized in Figure 42 and shown graphically in Figure 43.

a. Test No. 1

The throat area of the first Mod 260 booster was 7.65 sq in. (K-ratio = 13), as determined by the theoretical design calculations to achieve a 1000-psia operation pressure. The pressure-vs-time data are presented in Figure 43. A postfiring photograph of the booster chamber nozzle ports is shown in Figure 44. Overall erosion was not very severe, except in the narrow metal area between the ports, as shown in Figure 44. The burnthrough in this area probably occurred late in the firing or near tailoff, since the hemispherical contour of the chamber was not deformed. The chamber burnthrough, though not a critical failure, caused concern, since the Polaris B3 igniter showed no erosion around or between the four nozzle ports. The Mod 260 igniter booster chamber and the Polaris B3 igniter chamber design, materials and fabrication were identical, except for the size and location of the nozzle ports.

The pressure level of the first booster was lower than had been expected. The erosive-burning correction factor for Alclo-grain igniters was apparently not accurate at port-to-throat ratios of less than 1.0. The erosive-burning data were derived from test firings at higher port-to-throat area ratios, and were extrapolated to include lower port-to-throat area ratios.

IV, E, Mod 260 Ignition Motor Booster Open-Air Tests (cont.)

b. Test No. 2

The throat area of the second booster was 6.12 sq in. (K-ratio = 16). The K-ratio was selected to achieve a booster operating pressure of 1000 psia. Previous Polaris B3 igniter test firing data were as follows:

K-Ratio	Throat Area, sq in.	Pressure, psia
22.8	4.24	2350
21.1	4.58	2150
18	5.38	1860

These data and the first booster test data are plotted on the K-ratio-vs-chamber pressure chart shown in Figure 45. The theoretical K-ratio data for iron-Alclo is also shown in Figure 45 for reference. Evaluation of the available data indicated that a K-ratio of 16 was the best value to achieve the desired 1000 psia operating pressure. This value was determined by drawing a line between the K-ratio 13 data point from the first open-air test and an average K-ratio data point for the Polaris B3 igniter tests, as shown in Figure 45.

The peak pressure in the second booster test was 1428 psig, or about 400 psi higher than predicted. Also, severe Alclo-grain breakage was evident from the ballistic firing curve. Recent Polaris B3 test firings indicated that grain breakage occurred at high K-ratios. X-ray movies taken during the Polaris B3 igniter test firings indicated the following:

(1) Breakage occurred shortly after ignition of the main igniter grain.

(2) The grain broke radially near the middle and not along a bond line.

IV, E, Mod 260 Ignition Motor Booster Open-Air Tests (cont.)

(3) The peak pressure did not seem to be greatly influenced by moderate amounts of grain breakage; only the shape of the pressure curve was affected.

(4) The use of wider grain supports, called I bars, held the grain in place during the firing and prevented grain breakage at high K-ratios in the igniters tested.

A check of Polaris A3 igniter test data also indicated a variation in peak operating pressure. The pressure variation was attributed to Alclo buring rate variation, grain breakage, and unknown factors, However, the reproducibility of motor ignition was not significantly influenced by variations in the Polaris A3 igniter operating pressure, but was more sensitive to the surface condition of the motor propellant.

The nozzle end of the booster chamber had completely failed, as shown in Figure 46. The structural failure was attributed to overheating of the narrow metal area between the nozzle ports and eventual fracture due to the high pressure. An investigation of several methods of reducing the heat transfer into the metal around the nozzle port was initiated.

Unexpectedly long delays from fire switch, to initial initiator rise, and to peak initiator pressure also occurred. Data from the squib-to-initiator test series indicated the flame propagation from the squibs to the initiator took only 0.020 to 0.030 sec. The poor squib-to-initiator flame propagation reproducibility in the two booster tests was due to an excessive amount of squib and initiator gas exhausting out of the adapter leak-check hole.* This was evident in the motion-picture coverage; evidence of the gas flow is shown in the postfiring photograph (Figure 47). The time to initial pressure rise was

*The leak-check hole in the booster adapter was used to enable checking of the O-ring seal between the adapter and the safety-arming device.

IV, E, Mod 260 Ignition Motor Booster Open-Air Tests (cont.)

the same in both tests, although the initiator reached peak pressure 0.025 sec sooner in the second test. The gas path from the squibs and initiator to the leak check hole is a labyrinth, and the flow area depends on the tolerance buildup between the adapter and the safety-arming device mating surfaces. Thus, the amount of gas exhausting through the leak-check hole will vary with the flow area available.

c. Test No. 3

The third booster had a throat area of 6.75 sq in. (K-ratio = 14.5) and the leak-check hole was plugged by inserting and welding a 0.172-in.-dia by 0.50-in.-long steel press-fit pin.

The extensive review of the Polaris ignition data indicated that good motor ignition was achieved over wide ranges of igniter operating pressure. Better ignition performance reproducibility could also be achieved at lower operating pressures where main Alclo-grain breakage did not occur. The 14.5 K-ratio was selected for the third open-air test to achieve as high a pressure as possible without fracturing the Alclo grain.

The 380-psia average operating pressure in the third booster test was lower than expected, with only a 45-psi pressure increase above the 13 K-ratio igniter operating pressure. The small pressure increase indicated that choked flow occurred inside the booster chamber, apparently due to the low port-to-throat area ratio. Thus, any further adjustments in the nozzle throat size would have little effect on the booster chamber operating pressure at the lower K-ratios. The shape and duration of the booster pressure-vs-time curves for both the 13 and 14.5 K-ratios were similar, indicating reproducible performance was achieved when the main Alclo grain remained intact.

The effect of plugging the leak-check hole in the adapter was clearly indicated, as the time from fire switch to first pressurization and the time to reach full initiator pressure was significantly reduced.

IV, E, Mod 260 Ignition Motor Booster Open-Air Tests (cont.)

The booster chamber burned through at the narrow section between the nozzle ports. However, as in the first open-air test, the contour of the chamber was not affected. The location and degree of chamber burn-through indicated that the uninsulated metal around the nozzle ports was being exposed to the extreme temperature of the Alclo-gas (7000°F), and the narrow metal section between the nozzle ports was structurally weakened. About 0.25 in. of the external Gen-Gard V-44 insulation around the nozzle ports was machined away during fabrication to enable welding of the closure to the chamber; as a result, approximately 0.25 in. of the chamber metal around each nozzle was exposed. The structural failure probably occurred during the latter phase of booster operation, since the internal chamber pressure was too low to cause deformation in the first and third tests. In the second booster firing the internal pressure was sufficient to cause deformation. To minimize exposure of the chamber metal area around the nozzle ports to the Alclo gas, trowelable U. S. Polymeric NRL-1795 insulation was installed around the nozzle ports (Figure 48). Increasing the internal insulation around the nozzle ports appeared unnecessary because visual inspection of all the chambers tested showed that the internal insulation around the nozzle ports was intact and the internal metal surfaces were not exposed.

5. Summary

Based on the results of the booster open-air tests, the following design changes were incorporated prior to the open-air static test of the Mod 260 ignition motor assembly:

a. The leak-check hole in the booster adapter was plugged.

b. Trowelable NRL-1795 insulation was installed around the nozzle ports in the booster chamber.

c. The diameter of the nozzle ports in the booster chamber was changed to 1.725 in. to correspond to a K ratio of 14.5. At the 14.5 K ratio, a pressure range of 300 to 600 psia was expected.

IV, Test Program Description (cont.)

F. SUBSCALE IGNITION TESTS, 44-SS MOTORS

1. Free-Volume Simulator Tests

a. Objectives

Details pertaining to the 44-SS ignition motor free-volume test series were as follows:

(1) Test No. 1

The objective of the first test was to evaluate the ballistic performance of the 44-SS ignition motor and to obtain free-volume chamber pressure data. Standard bolts were substituted for the explosive bolts in the retention system, and no attempt was made to eject the ignition motor.

(2) Test No. 2

The objective of the second free-volume test was also to obtain ballistic data, but the test was primarily intended to demonstrate the retention-and-release system. The explosive bolt ejection command was programed to actuate at 0.600 $\pm$ .010 sec after fire switch.

Due to a malfunction during Test No. 2, a third test was added to the program. The objectives of the third test were the same as those of the second test.

b. Test Apparatus

The throat size, port area, and volume of the 44-SS free-volume simulator were identical to those of the 44-SS motor. Threaded bosses

IV, F, Subscale Ignition Tests, 44-SS Motors (cont.)

were welded into the chamber wall at various stations for pressure transducer installation. Installation of the free-volume chamber and the 44-SS ignition motor is shown in Figure 49.

c. Instrumentation

The instrumentation consisted of Taber pressure transducers located on the free-volume chamber 20, 59, and 98 in. from the throat plane and at the forward head. Another pressure transducer was located at the throat to measure the static pressure at the throat plane. For the third test, a Pitot tube was installed through the pressure tap in the throat plane to measure the total pressure of the exit gas stream. A pressure transducer was mounted on the booster adapter to measure the internal operating pressure of the 44-SS ignition motor.

The free-volume simulator bore pressure was measured with Taber Model 206 pressure transducers ranged from 0 to 100 psig, close-coupled to the chamber wall. The output of these transducers was recorded on a 36-channel Consolidated Electrodynamics Corp. oscillograph and on an Ampex 501 tape transport. The ignition motor pressure was measured by a Taber transducer ranged from 0 to 1500 psig and recorded as described above. Vibration and shock at the forward head of the free-volume simulator were measured by an Endevco Model 2208 crystal accelerometer and were recorded on Ampex tape. The oscillograph data were recorded at 40 in./sec; the Ampex tape data were recorded at 60 in./sec.

d. Results

The ballistic firing curves for all the 44-SS ignition motors tested, including the motor firing tests, are shown in Figure 50; the ballistic performance data are summarized in Figure 51. The 44-SS ignition motor propellant properties are shown in Figure 21.

IV, F, Subscale Ignition Tests, 44-SS Motors (cont.)

The measured 44-SS free-volume simulator pressures for all three tests are summarized in Figure 52. The measured free-volume simulator throat plane static and total pressures and the forward-end bore pressures are shown in Figure 53.

(1) Test No. 1

The first free-volume test was conducted on 5 May 1964. This was a ballistic test only, and no attempt was made to eject the ignition motor.

The actual web average pressure of 844 psia was lower than the 1000 psia design pressure. The lower pressure was apparently due to small differences between the actual and the design propellant burning rate, burning surface area, throat area, and initial propellant temperature.

The oscillograph recording of the free-volume chamber pressure revealed high-frequency (2500 to 3000 cycles/sec) pressure oscillations, with amplitudes of approximately 80% of the steady-state pressure level. Because of the overlapping of the galvanometer traces as a result of severe oscillation, data could not be reduced from the oscillograph record. The Ampex tape data were played back through 150 cycles/sec low-pass filters and were recorded on a Minneapolis-Honeywell Visicorder to obtain readable data.

Curves of the measured bore pressure and the measured static pressure at the throat plane, shown in Figure 53, were similar to the type of pressure curves obtained in the cold-flow test program. When gas began to flow into the free-volume chamber, the static pressure tap recorded less than atmospheric pressures. However, when the bow shock from the inlet jet plume penetrated the throat plane, the pressure increased sharply to the steady-state value.

IV, F, Subscale Ignition Tests, 44-SS Motors (cont.)

(2) Test No. 2

The second free-volume test was conducted on 12 May 1964. The test setup was identical to that of the first test, except that an ignition motor ejection command was programed to actuate the explosive bolts at 0.600 ± 0.010 sec after fire switch.

Several instrumentation modifications were made for the second test to determine if the 2500 to 3000 cycles/sec pressure oscillations actually existed, or if the oscillations were simply the result of mechanical chamber vibrations that excited the sensitive axis of the Taber transducers. The Taber transducers located 20 and 59 in. from the throat plane were isolated from the chamber by 12-in. flexible tubing and were mounted on a support stand remote from the free-volume chamber. A high-frequency Statham Model PG 285 transducer was substituted for the Taber transducer at the station located 98 in. from the throat plane. The output of the Taber transducers located at the throat plane and at the forward end of the chamber was filtered to 120 cycles/sec at the amplifier to enable immediate data reduction.

The ballistic performance of ignition motor 44-SS-IM-02 met the design requirements. The 880-psia web average pressure was slightly higher than the 844 psia pressure recorded for the first ignition motor tested. As shown in Figure 21, a slight increase in burning rate at pressures of less than 1000 psia could be expected, since the greater amount of propellant in the second ignition motor had the same burning rate at 1000 psia but exhibited a lower burning-rate exponent. The initial grain temperature of the second ignition motor was 80°F, which also tended to raise the web average pressure.

The free-volume chamber pressure data from the second test showed that the 2500 to 3000 cycles/sec pressure oscillations were induced by a mechanical dynamic input to the transducers. The two isolated Taber pressure transducers showed pressure oscillations at the same frequency as those that had

IV, F, Subscale Ignition Tests, 44-SS Motors (cont.)

occurred in the first test. However, the amplitude was reduced from approximately 80 to 20% of the steady-state pressure level using the isolated mounting technique. The high-frequency Statham transducer produced a pressure curve similar to the pressure curve of the close-coupled Tabers, even though the natural frequency of the Statham is greater than 10,000 cycles/sec. The manufacturer's data showed that both transducers have a dynamic acceleration response of 0.02 to 0.04% of full scale per g. Assuming that the measured dynamic response ($\pm$1000 g at 2500 to 3000 cycles/sec) of the forward chamber head was transmitted to the pressure transducer, calculations indicated that the pressure oscillations were a function of mechanical vibrations at a harmonic frequency of the resonant frequency of the chamber and were not actual pressure fluctuations within the free-volume chamber. All of the free-volume pressure data reported were reduced from a signal filtered at the amplifier prior to being recorded on the oscillograph or from a filtered playback of the Ampex tape record. Both methods were effective in eliminating the exaggerated dynamic response.

The attempt to eject the ignition motor at 0.600 sec after fire switch failed. The oscillograph record of the explosive bolt firing circuit indicated a proper ejection command signal was given at 0.580 sec after fire switch. Postfiring inspection revealed that three of the four explosive bolts retaining the ignition motor had functioned, but the fourth bolt had failed to actuate. The malfunction resulted from damage to the lead wires due to exhaust gas impingement or from disconnection of the lead wires during the functioning of the other three bolts.

The malfunction revealed that better environmental protection of critical circuits was required, and the entire 44-SS ignition motor retention-and-release system design was re-evaluated. The ignition motor-support cradle assembly was being retained by four explosive bolts, two bolts on each side of the main assembly stand, but the stress analysis indicated that only one of the 3/4-in.-dia Holex bolts was required to retain the

IV, F, Subscale Ignition Tests, 44-SS Motors (cont.)

ignition motor-support cradel assembly. The design also called for a 0.906-in.-dia by 0.25 in. counterbore at the shear plane of each bolt. The retention-and-release system used in the second free-volume test did not have these counter bore areas. Since the system used in the second test was not fabricated to print, it is questionable whether ejection would have been successful even if the fourth bolt had functioned properly.

The following action was taken:

(a) A third free-volume test was added to the test program to demonstrate the retention-and-release system.

(b) The number of explosive bolts retaining the ignition motor-support cradle assembly was reduced from four to two.

(c) The design of the flange interface was changed, so that each bolt would fail in tension rather than in shear.

(d) A metal pipe was used to shield the critical firing circuits.

(3) Test No. 3

The third free-volume test was conducted on 25 May 1964, using the redesigned retention-and-release system. A Pitot tube was installed into the free-volume chamber throat-plane pressure tap to measure the total pressure of the exit gas stream.

The web average pressure was 928 psia, compared with the 1000-psia predicted value. Figure 21 shows that a higher pressure could be expected for ignition motors 44-SS-IM-03 and-04, because the liquid-strand burning rate data indicated a high burning rate for batch No. 64-769.

IV, F, Subscale Ignition Tests, 44-SS Motors (cont.)

Ejection of the ignition motor occurred as planned. The explosive bolt actuation signal was initiated 0.612 sec after fire switch. The ignition motor moved out of the free-volume simulator exit cone and impacted on the test bay deck about 80 ft away. The chamber pressure trace (Figure 53) shows that a pressure peak occurred 0.697 sec after fire switch, or 0.085 sec after the explosive bolts were actuated. The 10- to 20-psi pressure surge was caused by the bow shock, which is formed between the exit gas stream and the inlet jet plume, passing through the chamber throat plane. The location or velocity of the ignition motor when the bow shock passed through the throat plane could not be determined from the instrumentation.

The total pressure data correlated with the previous static pressure data.

2. Motor Firings

a. Objectives

The objective of the 44-SS motor test firing, related specifically to the 260-SL motor ignition system development program, was to obtain subscale ignition data to evaluate the Mod 260 ignition motor design criteria.

b. Test Firing Setup

The 44-SS ignition motor was installed into the exit cone of the 44-SS motor so that the exit plane of the ignition motor was 6.75 in. aft of the motor throat plane ($\varepsilon^* = 1.21$). The igniter release control unit was set to actuate the retention system explosive bolts when the motor chamber pressure reached 230 $\pm$ 2 psia. As a back-up actuation system, the release control unit timer was set to actuate the explosive bolts at 0.600 $\pm$ .010 sec after fire switch. An overall 44-SS motor test setup is shown in Figure 54.

IV, F, Subscale Ignition Tests, 44-SS Motors (cont.)

c. Instrumentation

The instrumentation for the ignition phase of the test firing included an ignition motor chamber pressure measurement, a fire-switch trace, and an explosive bolt actuation trace. Motor chamber pressure was measured by two Taber transducers mounted on the forward head of the motor; the igniter release control unit was actuated by the output from one of the forward-head transducers. The transducer output was amplified by a Kintel Model 114 amplifier, which has a frequency response of 120 cycles/sec and will not pass or amplify input above this value. The amplifier was used to eliminate the exaggerated high-frequency mechanical oscillations that occurred during the 44-SS free-volume simulator tests. Although the high-frequencey oscillations would be greatly reduced in a fully loaded motor, compared with those in an empty free-volume chamber, the Kintel amplifiers were used to ensure satisfactory actuation of the igniter release control unit.

d. Results

The ignition details for motors 44-SS-1, -2 and -3 are shown in Figure 55. The ballistic performance curves for the 44-SS ignition motors used in the motor tests are shown in Figure 42, which includes the performance of all the 44-SS igniter motors. The ignition and ejection sequences for the three 44-SS motors are shown in Figure 56.

(1) Motor 44-SS-1

The initial attempt to fire motor 44-SS-1 was unsuccessful and resulted in a no-fire, which was attributed to either a defective EBW squib or a malfunction in the fire-switch circuitry. During the initial firing attempt, the 2000 vdc capacitor discharge appeared normal as indicated by the control-room visual meter. However, when the programed fire switch was

IV, F, Subscale Ignition Tests, 44-SS Motors (cont.)

actuated, the characteristic dip in the high voltage discharge did not occur. Since the retention system explosive bolts were automatically actuated 0.600 sec after fire switch and all the motion picture cameras were actuated at fire switch, a second attempt was not made to fire the suspect EBW squib. The booster was removed from ignition motor 44-SS-IM-04 and was replaced. The second firing attempt was successful.

Prior to the initial attempt to fire motor 44-SS-1, the fire-switch circuitry was verified by firing a simulated squib during normal prefire checkout. Approximately 12 simulated firings were performed prior to the actual firing attempt; the last check was made 30 min before firing. The suspect EBW squib passed all tests and measurements made. The squib was actuated and fired normally.

A series of unsuccessful attempts were made to duplicate the original malfunction. The high-voltage console was also checked and no discrepancies were found. The only suspect phase of the fire circuitry was the 2000-v dc capacitor discharge-relay actuation. This relay is actuated by 28 v dc minimum at fire switch; if the actuation voltage is too low, the relay may fail to actuate. For all subsequent tests, the relay actuation voltage was increased to 32 v dc.

Ignition of motor 44-SS-1 was accomplished as predicted. The performance of the retention-and-release system met all of the design requirements. Ignition motor ballistic performance was normal.

(2) Motor 44-SS-2

Ignition of motor 44-SS-2 was successfully accomplished. The ignition motor pressure transducer cable was damaged before the end of the firing so that internal chamber pressure data were lost 0.186 sec after fire switch. However, the ballistic performance of ignition motor 44-SS-IM-05 was normal during the 0.186 sec measured.

IV, F, Subscale Ignition Tests, 44-SS Motors (cont.)

The retention-and release system again performed satisfactorily. To obtain more complete data related to the ejection sequence and the time delay of the igniter release control unit, additional instrumentation had been included for the 44-SS-2 motor test to determine the following:

(a) Time of oscillator actuation
(b) Time of final relay closure to explosive bolts
(c) Time of first motion of the ignition motor during ejection
(d) Time when the ignition motor leaves the support stand during ejection

The additional instrumentation enabled evaluation of the ejection sequence and indicated that the estimated ejection sequence reports for motor 44-SS-1 was accurate.

(3) Motor 44-SS-3

Ignition of motor 44-SS-3 was normal. Once again the ignition motor pressure transducer cable was damaged prematurely so that internal pressure was lost 0.17 sec after fire switch. The ballistic performance of ignition motor 44-SS-IM-06 was normal during the 0.17 sec measured.

Ejection of the 44-SS ignition motor was accomplished as designed. A signal comparator was used to initiate ignition motor ejection because the igniter release control unit is now installed in the test facility control room at the Aerojet-Dade Division. The function of the signal comparator is similar to the igniter release control unit, except that the analog voltage (pressure sensing) and timer sections are controlled by one circuit in the signal comparator. The analog voltage and timer sections in the igniter release control unit are independent of each other.

IV, Test Program Description (cont.)

G. MOD 260 IGNITION MOTOR OPEN-AIR TEST

1. Objectives

The objectives of the open-air test were to verify the ballistic performance, the propagation of the pyrotechnic train, and the structural integrity of the Mod 260 ignition motor hardware.

2. Test Apparatus

The ignition motor test equipment, shown in Figure 57, consisted of two steel support saddles and an aft end retention support. This test equipment was designed for the open-air test and for use in the subsequent free-volume simulator tests.

3. Instrumentation

The Mod 260 ignition motor chamber pressure was measured by two Taber Model 260 transducers ranged from 0 to 1500 psia. Booster chamber pressure was measured by a Taber transducer, also ranged from 0 to 1500 psia. Ignition motor thrust was measured with a Baldwin-Lima Hamilton, Type U-1, 250,000-lb load cell. The outputs of the load cell and pressure transducers were recorded on a Consolidated Electrodynamics Corp. oscillograph and on Ampex tape. The oscillograph data were recorded at 40 in./sec; the Ampex tape data were recorded at 60 in./sec.

4. Results

The ballistic firing data for the Mod 260 ignition motor are presented in Figures 58 and 42. The actual and predicted ignition motor performance data are shown in Figure 59.

IV, G, Mod 260 Ignition Motor Open-Air Test (cont.)

The performance of the ignition motor met all the design requirements and was close to the predicted performance. Predicted performance data were obtained from a computer program using a 0.80 in./sec (at 1000 psia) propellant burning rate. Earlier 260-SL motor ignition motor performance predictions were based on propellant burning rates of 0.85 and 0.83 in./sec. However, as shown in Figure 21, the actual burning rates that occurred in motor firings were lower than those indicated by liquid-strand tests. Since the liquid-strand burning rate for propellant batch No. 4-MM1-3 was lower than that of the other batches used in the 44-SS ignition motors, an effective burning rate in the full-scale ignition motor of 0.80 in./sec was used for the performance prediction.

Postfiring inspection of the ignition motor showed that the throat insert and insulation had minimal erosion, and the metal parts were undamaged. The ignition motor hardware was refurbished and reprocessed.

The 1040-psia ignition motor booster pressure was higher than the expected 300 to 600 psia pressure range. The booster performance curve is shown in Figure 60. During the booster open-air test series, the booster chamber throat area was revised twice in an attempt to achieve a 1000-psia operating pressure. Based on the firing data obtained in the three open-air booster tests, a K-ratio of 14.5 was selected, with an expected pressure range of 300 to 600 psia. The higher pressure in booster 260-IMB-04 was apparently due to grain breakage, which also occurred during the test firing of booster 260-IMB-02. Since grain fracture did not occur during the test firings of boosters 260-IMB-01 and -03, the 14.5 K ratio was assumed to be small enough to prevent grain fracture. Due to the higher booster operating pressure and resulting higher energy delivery rate, ignition of the Mod 260 ignition motor was approximately 50 millisec faster than predicted. Also, the actual rate of ignition motor pressure rise of 7700 psi/sec was higher than the 6000 psi/sec predicted rise rate. Grain fracture appears to be inherent in this type of igniter design, particularly at low port-to-throat area ratios. However, Polaris program ignition data indicate that motor ignition time is not significantly affected by wide ranges of igniter operating pressure.

IV, G, Mod 260 Ignition Motor Open-Air Test (cont.)

The condition of the booster chamber after the test firing was excellent. External chamber insulation was only slightly charred and the narrow metal area between the nozzle ports was intact. The NRL-1795 insulation, installed over the exposed metal around the nozzle ports, was severely eroded in the area between the nozzle ports. However, the NRL-1795 insulation around three quarters of the nozzle port diameter was in good condition and prevented a burnthrough in the narrow metal area between the nozzle ports, even at the higher operating pressure.

H. MOD 260 IGNITION MOTOR FREE-VOLUME SIMULATOR TESTS

1. Objectives

The 260-SL free-volume simulator test series was conducted primarily to demonstrate the ignition capability of the Mod 260 ignition motor. The test objectives were to measure the simulator bore pressure, the heat energy distribution along the simulator wall, and the time required to ignite patches of motor propellant located at various stations along the chamber wall. The secondary objectives were to obtain additional Mod 260 ignition motor ballistic performance data and to further evaluate the aft-end ignition analytical model developed by Aerojet-General.

The Mod 260 ignition motor was fired into the aft end of a chamber simulating the 260-SL motor free-volume, throat area, and exit cone configuration. The pressure in the free-volume simulator was measured at stations along the length of the chamber. Patches of 260-SL motor propellant and calorimeters were also located along the simulator wall to measure ignition time and total heat flux distribution. Accelerometers were mounted on the forward dome and exit cone of the simulator to measure the dynamic response of the system.

IV, H, Mod 260 Ignition Motor Free-Volume Simulator Tests (cont.)

2. Test Apparatus

The free-volume simulator was installed in the test stand as shown in Figure 61. The cylindrical section of the simulator was fabricated in two segments of 0.50-in.-thick ASTM-A7 steel plate, rolled and welded to an internal diameter of 126 in. The forward segment of the simulator consisted of a cylindrical section, forward dome, and flange. The forward dome was a 126-in.-dia ASTM-201 steel elliptical dished head welded to the cylindrical section. The 135.75-in.-dia flange was fabricated from ASTM-A7 steel plate and welded to the cylindrical section. The aft segment of the simulator consisted of the cylindrical section, aft head, exit cone, and flange. The aft head was a 126-in.-dia ASTM-201 steel having a 90-degree included angle conical dished head welded to the cylindrical section. The conical rolled-and-welded exit cone was welded to the aft head after a hole was cut in the aft head to simulate the 260-SL motor throat size. The overall length of the free-volume simulator was 755.0 in. The design pressure of the simulator was 125 psia. The free volume, throat area, and exit-cone half-angle were identical to those of the 260-SL motor configuration.

The Mod 260 ignition motor was retained by two steel saddles as shown in Figure 61. This same retention equipment was previously used for the open-air test.

3. Installation

The Mod 260 ignition motor was mounted along the free-volume simulator center line, with the exit plane of the ignition motor located 29 in. downstream of the simulator throat plane. The thrust axis of the ignition motor did not deviate more than 3 degrees from horizontal.

IV, H, Mod 260 Ignition Motor Free-Volume Simulator Tests (cont.)

4. Instrumentation

Fifty-eight channels of data were recorded from measurements on the free-volume simulator and the Mod 260 ignition motor. The location of instrumentation is shown in Figure 62; a list of all the instrumentation, including designation, location, range, and description, is presented in Figure 63.

a. Free-Volume Simulator Pressure

Taber Model 217 pressure transducers, ranged from 0 to 100 psig, were used to measure the free-volume-simulator bore pressure. The transducer outputs were recorded primarily by the Beckman 210 analog-to-digital converter (ADC) system. The Beckman system has a basic sampling rate of 2500 samples/sec and the transducer output is recorded on magnetic tape. Eleven channels of simulator bore pressure data, Pvc-2, -3, -4, -5, -7, -8, -9, -11, -12, -13, and -15, were also recorded on Consolidated Electrodynamics Corp. Model 5-119 (CEC) oscillographs. The output of these 11 transducers was amplified by Kintel Model 114A amplifiers, which have a maximum frequency response of 120 cycles/sec and will not pass or amplify input above this value. The use of these amplifiers eliminates the false high-frequency oscillations resulting from mechanical vibration of the free-volume simulator during the test. The output from the other four transducers, Pvc-1, -6, -10, and -14, were recorded on Ampex Model 501 tape. The Ampex system has a frequency respond to 10,000 cycles/sec and the data were filtered to 120 cycles/sec during playback on the Visicorder record to facilitate data reduction.

Pressure measurements were also taken on the simulator exit cone and at the simulator throat plane. Three Statham Model PG285 transducers ranged from 0 to 50 psig were used to measure static pressure at two locations on the exit cone and at the nozzle throat. These static pressure measurements were filtered to 120 cycles/sec through the 114A amplifier and were recorded on the ADC and CEC systems.

IV, H, Mod 260 Ignition Motor Free-Volume Simulator Tests (cont.)

The total pressure of the exit gas stream at the simulator throat plane was measured by three Pitot tubes installed around the throat, extending 3.0, 6.0, and 9.0 in. into the simulator throat section, as shown in Figure 64. The output from the Taber transducers was recorded on the ADC system and the Ampex 501 tape.

b. Mod 260 Ignition Motor Pressure and Thrust

The Mod 260 ignition motor chamber pressure was measured by two Taber transducers, ranged 0 to 1500 psig, installed on the ignition motor booster adapter. A third 0- to 1500-psig Taber transducer was installed on the adapter to measure the ignition motor booster chamber pressure. These measurements were recorded on the ADC system, the CEC oscillograph, and the Ampex 501 tape.

Ignition motor thrust was measured by a Baldwin-Lima-Hamilton, Type U-1, 250,000-lbf load cell and was recorded as previously described.

c. Heat Flux Measurement

Fourteen Hy-Cal Model C-1092-A-TTT calorimeters were installed along the simulator wall, flush with the interior surface. These calorimeters measured the thermal energy absorbed by an exposed metallic disk; the temperature rise of the disk was measured by an imbedded thermocouple. The calorimeters were calibrated by the manufacturer using a black-body reference.

d. Instrumented Propellant Patch

The propellant patch assembly is shown in Figure 65. A BIM microminiature thermocouple was installed in the propellant patch holder. ANB-3015 propellant was cast into the cavity surrounding the thermocouple. After ignition of the ANB-3015 propellant, the thermocouple burns through, resulting in an open circuit and a discontinuity in the CEC oscillograph trace.

IV, H, Mod 260 Ignition Motor Free-Volume Simulator Tests (cont.)

e. Accelerometers

Two Endevco Model 2240 accelerometers, ranged ± 1000 g, were mounted on the simulator, one on the forward dome and one at the throat plane, to measure the dynamic response of the system. The data were recorded on the Ampex 501 tape.

5. Results

a. Free-Volume Simulator Data

A summary of data obtained at each station along the free-volume chamber is presented in Figure 66. The blowback effect of the hot exhaust gases from the free-volume simulator were more severe than expected. Although all instrumentation cables had been protected from heat and turbulence, the cables and transducers nearest the exit cone were not sufficiently insulated, and data were not obtained for exit cone or nozzle pressures during the first test. The test indicated that instrumentation cables and transducers near the aft end of the simulator require better protection against the exhaust gases. For the second test, all instrumentation near the aft-end of the free-volume simulator was protected with metal conduit and the transducers were enclosed or protected by blast shields, as shown in Figures 67 and 68. Similar protection was given to the instrumentation on the ignition motor, as shown in Figure 69.

The data obtained during the free-volume tests are described in detail as follows:

(1) Bore Pressure

The free-volume simulator bore pressure data are summarized in Figure 70. Data recorded from Pvc-2, -4, -7, -9, -12, and -15 are shown in Figure 71.

IV, H, Mod 260 Ignition Motor Free-Volume Simulator Tests (cont.)

The maximum measured bore pressure was 88.3 psia for the first test measured at Pvc-14 at 0.25 sec after fire switch, and 86.5 psia for the second test, measured at Pvc-13 at 0.5 sec. The ignition parameters for ignition motors 260-IM-02 and -03 were 0.31 and 0.28, respectively. Using the aft-end ignition analytical model (Figure 72), the predicted bore pressures were 81 and 78 psia, respectively. Assuming no error in the measurement, the actual bore pressures were from 7 to 8 psi higher than predicted. This 10% deviation was not unexpected because several of the assumptions made in the development of the one-dimensional aft-end ignition analytical model were not completely valid.

(2) Exit Cone and Throat Plane Pressure

As previously indicated; no throat plane total pressure and static pressure data were obtained during the first test, and one of the transducer cables on the exit cone (Pvn-A) was blown off. For the second test, the total-pressure Pitot tubes were reinforced and the transducers on the outside of the simulator were protected by a welded metal closure. The exit cone static pressure measurement (Pvn-B) and the throat plane static-pressure measurement (Pvn-01) were invalid for the second test due to a malfunction in the amplifier. However, at approximately 0.50 sec, the amplifier for the throat plane static-pressure measurement (Pvn-01) recovered and the data appear to be valid for the remainder of the firing.

The exit cone static pressure data are shown in Figures 73 and 74. The calculated static pressures, which are included for comparison, were determined from the measured bore pressure data for each test. The measured static pressure curves were plotted directly from the ADC print-out. Although there was oscillation in the data, the measured static pressure correlates closely with the calculated values.

IV, H, Mod 260 Ignition Motor Free-Volume Simulator Tests (cont.)

The total pressures of the exit gas stream at the throat plane are shown in Figures 75, 76, and 77. The Pitot tubes lasted from 0.3 to 0.5 sec under severe flow conditions. The maximum total pressure, measured at the time the Pitot tubes were lost, were as follows:

68 psia @ 0.50 sec, Pvn-02
74 psia @ 0.32 sec, Pvn-03
72 psia @ 0.41 sec, Pvn-04

The maximum measured static pressure was 43 psia at 0.6 sec (Pvn-01).

The nozzle pressure data correlated with the measured bore pressure and with the pressure ratio at choked flow. An increase in total pressure measured by the 9.0-in.-long Pitot tube (Pvn-04) occurred at approximately 0.24 sec. During the initial time of bore pressurization, 0.13 to 0.25 sec, the 9.0-in.-long tube was immersed in the ignition motor jet plume. At approximately 0.24 sec, the throat plane static pressure increased to about 30 psia, and the jet plume boundary contracted. At this time, the 9.0-in.-long tube was clear of the jet plume and began recording exit stream total pressure.

(3) Heat-Flux Measurement and Propellant Patch Ignition

All 14 propellant patches were ignited during each test. The propellant patch ignition times are shown in Figure 66. The total heat flux values measured by the calorimeters located along the free-volume simulator wall are shown in Figures 66, 78, and 79. The measured heat-flux rates are shown in Figure 66.

The total energy delivered to the simulator wall by the Mod 260 ignition motor ranged from 131 cal/cm^2 at the aft end to 10 cal/cm^2 at the forward end. The area of maximum heat transfer was readily apparent, and occurred

IV, H, Mod 260 Ignition Motor Free-Volume Simulator Tests (cont.)

approximately 140 in. upstream of the simulator throat plane (Station 3). The heat flux recorded by the forward calorimeters apparently was due to radiant energy reflected from the forward dome. The delivered energy to the area of maximum heat transfer (130 cal/cm^2) was approximately 40 times greater than the threshold ignitibility requirements of ANB-3015 propellant.

The propellant patch ignition time (Figure 80) was difficult to determine because the temperature rise recorded by the embedded thermocouple is affected by its location relative to the propellant surface. To obtain accurate data the end of the thermocouple must be located just below the propellant surface. Apparently some of the thermocouples were exposed or were embedded too far beneath the surface. As a result, the temperature rise was significantly different than the normal trace and was difficult to interpret.

The general pattern of propellant patch ignition was as expected, with the patches nearest the zone of maximum heat transfer being ignited first. Although all 14 patches ignited, the time required to ignite the patches located forward of Stations 10 (65% penetration) was slightly longer. This data indicated that there was low heat-flux forward of the stagnation zone, so that the forward patches were ignited by residual radiant heat.

(4) Accelerometer Data

The measured dynamic response of the forward dome was 350 to 400 cycles/sec, with an amplitude of 500 g. The response of the simulator exit cone was approximately 4000 cycles/sec, with a 700 to 800 g amplitude. There was no significant acoustical resonance recorded.

The acceleration levels appear to be normal for an empty free-volume chamber. The calculated resonant frequency of the 260-SL motor free-volume simulator is about 400 cycles/sec. Thus, the measured dynamic response of

IV, H, Mod 260 Ignition Motor Free-Volume Simulator Tests (cont.)

the forward dome appears to be the resonant frequency of the simulator. The dynamic response of a loaded motor during aft-end ignition is expected to be negligible.

b. Mod 260 Ignition Motor Assembly Performance

Ballistic performance data for the Mod 260 ignition motors tested are presented in Figures 81 and 82. Performance data are shown in Figure 42. The ballistic performance of the Mod 260 ignition motors met all design requirements. A postfiring view of ignition motor 260-IM-02 is shown in Figure 83. Both ignition motors were disassembled and visually inspected. The insulation and throat inserts showed only minimal erosion, and the metal parts were intact and undamaged. The refurbished ignition motor, 260-IM-03, was in good condition, indicating that the refurbishing procedure is adequate. These ignition motors were refurbished, reprocessed, and used in the 260-SL motor ignition system demonstration tests conducted at the Aerojet-Dade Division.

Only partial ignition motor ballistic data were obtained in the first test due to various measurement malfunctions. One of the transducers for the ignition motor pressure measurements did not function during the prefiring instrumentation checkout. This transducer was not replaced, since removal of a pressure transducer would necessitate another leak check. The other transducer also failed to respond during the test. The ignition motor booster pressure transducer output was invalid about 0.110 sec after fire switch. This condition was attributed to an overloaded amplifier. The ignition motor pressure data were calculated from the thrust data; however, the thrust data were lost at 0.390 sec because the cable to the load cell was burned off by the exhaust blowback. The performance of ignition motor 260-IM-02 for the initial 0.390 sec was normal, and the measured free-volume simulator bore pressure indicated the performance of the ignition motor from 0.390 sec to tailoff was also normal.

IV, H, Mod 260 Ignition Motor Free-Volume Simulator Tests (cont.)

The pressure level of ignition motor 260-IM-03 was approximately 100 psi lower than the two first ignition motors tested. Properties of ANB-2758 Mod 1 propellant formulated for the Mod 260 ignition motors are shown in Figure 21. Ignition motor 260-IM-03 was processed with six slabs of batch 4-MMI-6 and four slabs of batch 4-MMI-4. The lower pressure was due to the lower burning rate of batch 4-MMI-6.

The performance of the ignition motor boosters, shown in Figure 60, met all the design requirements. The booster performance reproducibility in the three ignition motor firings to date was better than expected. Postfiring inspection showed the booster chambers were intact and in good condition, indicating that the minor design changes made after the booster open-air test series were effective.

I. MOD 260 IGNITION MOTOR ASSEMBLY RETENTION-AND-RELEASE SYSTEM DEMONSTRATION TESTS

1. Objectives

a. To demonstrate, by actual operation of all electrical and mechanical subsystems, the performance of the Mod 260 ignition motor retention-and-release system.

b. To verify that the operation of the retention-and-release system was not a hazard to the 260-SL motor or adjacent facilities.

c. To provide a final checkout of the tooling, facilities, and controls associated with the retention-and-release system prior to the 260-SL-1 motor test.

IV, I, Mod 260 Ignition Motor Assembly Retention-and-Release System Demonstration Tests (cont.)

2. Test Sequence

The 260-in.-dia free-volume chamber was installed nozzle up in the Cast, Cure, and Test facility. The Mod 260 ignition motor support fixture was positioned on the beams above the chamber with the aid of transits, in accordance with the alignment requirements. When the fixture was secured, the hydraulic actuator and its associated piping and controls were installed. The tower retraction cycle was functionally checked with the same remote command signal that was used during the actual test.

The support fixture mounting plate was bolted to the aft flange of the ignition motor. The ignition motor and support fixture were placed on the A frames and were secured to the A frames with nonexplosive bolts during subsequent alignment and assembly operations. When the alignment and positioning requirements were met, the tower assembly was raised to the vertical position. The four wheels connecting the support fixture to the track were then installed.

The 10-amp minimum firing command to the KR-80000-07 safety-arming device on the 260-SL ignition motor was manually actuated. The ignition motor explosive bolt actuation command was remotely triggered by a signal received from the igniter release control unit. The pressure-sensing feature of this unit was to be used in the first test. Explosive bolt actuation pressure was 60 psig, as measured at the forward head of the free-volume chamber and filtered to 120 cycles/sec maximum, with the 0.600-sec timer as a backup. A 0.600-sec delay from initial fire-switch actuation was to be used for the second test explosive bolt actuation command, with the pressure-sensing system locked out.

IV, I, Mod 260 Ignition Motor Assembly Retention-and-Release System Demonstration Tests (cont.)

3. Instrumentation

Twenty-seven channels of data were recorded from measurements on the Mod 260 ignition motor free-volume simulator and retention equipment. A list of all instrumentation for the retention-and-release system demonstration tests is shown in Figure 84.

The instruments used in the retention tests were the same as the instruments used for the 260-SL free-volume tests previously described. The output of all the pressure transducers was amplified by Kintel Model 114 A amplifiers. All data were recorded on CEC Model 5-119 oscillographs. Six cameras, five Fastax and one sequencing, were used to record the flight and impact of the ejected ignition motor.

4. Results

a. Test No. 1

The first retention-and-release system demonstration test was conducted at the Aerojet-Dade Division on 29 October 1964. An overall view of the prefiring test setup is shown in Figure 85. When the igniter release control logic was satisfied at 0.590 sec, the ignition motor and support fixture moved up the track, were restrained by the cables, and flew in a controlled arc (Figure 86) until the unit impacted in a water-filled trench about 650 ft from the Cast, Cure, and Test facility. The ignition motor rotated around its center-of-gravity approximately 450 degrees during its flight before impact. The cables became slack after pulling the ignition motor off the initial vertical trajectory and remained slack until the unit was near impact. The cables became tight again at about 30 degrees from horizontal during the descending portion of the flight. At this point in the flight, the cable attachment brackets that were welded to the igniter support fixture failed and impacted in the trench just prior to the impact of the ignition motor and support fixture assembly.

IV, I, Mod 260 Ignition Motor Assembly Retention-and-Release System Demonstration Tests (cont.)

The Mod 260 ignition motor ballistic performance curve is shown in Figure 87. A summary of the free-volume simulator bore, throat plane, and exit cone pressure data is shown in Figure 88. Included in Figure 88 are the times of significant events that were measured during the test. A summary of the pressure and flow conditions in the free-volume simulator exit cone and throat is presented in Figure 89.

The igniter release control unit logic was satisfied by the 0.600 ± 0.010 sec backup oscillator, and not by the pressure-sensing system as originally intended. The pressure-sensing Schmitt trigger was set to actuate when the simulator bore pressure reached 75 psia. This pressure value was selected after reviewing the fore-end bore pressure data from the two free-volume simulator tests. The maximum measured fore-end bore pressure in the test was 82.5 psia, and the pressure remained above 75 psia until 0.70 sec. However, the oscillation in the pressure measurement was approximately $\pm$ 10 psia, which was caused by resonant vibration of the free-volume simulator and was transferred to the pressure transducers. Each time the analog voltage from the transducers dropped below the 75 psia level, the pressure-sensing Schmitt trigger was turned off and the oscillator was reset. The pressure oscillation was significantly higher in this test than the oscillations recorded in the free-volume tests conducted at Aerojet-General, Sacramento. This condition was due to the difference in the method of mounting the free-volume simulator. For the free-volume tests, the simulator was firmly mounted on the test bay deck by two large saddles at each end of the chamber; for the retention test, the simulator was welded to six supports or legs at the forward head, and the aft end of the simulator was retained by four cables at the throat plane. Therefore, the mounting of the free-volume simulator in the Cast, Cure, and Test facility was not as rigid, and the chamber was capable of transferring a higher dynamic excitation to the pressure transducers. The Taber transducers used on the simulator will respond 0.04% of full-scale output to a 1-g input.

IV, I, Mod 260 Ignition Motor Assembly Retention-and-Release System Demonstration Tests (cont.)

The performance of ignition motor 260-IM-05 and booster 260-IMB-10 are shown in Figures 87 and 90. The ballistic data are summarized in Figure 42. The operating pressure of the ignition motor was lower than measured in previous tests; the grain temperature of ignition motor 260-IM-05 was 68 to 72°F at fire switch, compared with the 80°F temperature in previous tests.

Ignition of the propellant patches located 68.5 and 137.0 in. upstream of the simulator throat plane occurred at 0.355 sec, which is approximately 60 to 130 millisec longer than the ignition times measured in the free-volume tests. The propellant patches were installed in the free-volume simulator at T-2 hr on 27 October 1964. Because of rain prior to the test, the surface of the propellant patches was wet, and a longer delay was expected.

After the igniter was released, the cables pulled the ignition motor away from its initial vertical course, and the unit began to rotate about its center of gravity. When the ignition motor and support fixture were approaching the end of the arc, the cables were again pulled taut. The load on the cable attachment brackets caused the brackets to fail at the welds and in the parent metal. However, the load imparted at this time was in the opposite direction from the design load, as shown in Figure 91. This failure mode was verified by the postfiring condition of the brackets shown in Figures 92 and 93. The failure angle of both the upper and lower brackets was 90 degrees opposite the angle that would be expected if the brackets had failed under the design load.

The accelerometer on the igniter support fixture indicated that the ignition motor received a maximum shock of 43 g when the simulator throat pressure reached 65 psia. The shock subsided to a 10-g amplitude high-frequency vibration during steady-state operation. When the explosive bolts were actuated, the measured acceleration increased to 25 g until the instrumentation cable was broken. The measured accelerations were well below the specified 75 g maximum acceleration.

IV, I, Mod 260 Ignition Motor Assembly Retention-and-Release System Demonstration Tests (cont.)

Postfiring inspection indicated that the retraction of the tower was successful. The electrical signal to retract the tower was initiated at 1.123 sec when the uppermost break-wire circuit on the tower was opened by the ignition motor. Hydraulic pressure was measured in the retract section of the actuator at 1.137 sec, and the tower was fully retracted within 5.0 sec after command. The thermocouples on the tower during the firing indicated that only small temperature rises occurred, except as measured by a thermocouple at the 39-ft level. The majority of the temperatures rose to a maximum of between 150 and 180°F after 2.0 sec. The temperature recorded at the 39-ft level was approximately 1200°F at 0.9 sec. Apparently this thermocouple had become unbonded. Examination of the tower revealed no damage that could be attributed to excessive heat.

The accelerometers on the tower recorded maximum vibration in the Z axis near the top of the tower. High-frequency accelerations of up to 40 g were recorded during initial ignition motor operation and during ignition motor vertical movement at these locations. Vibration measurements in the X axis were negligible except for the accelerometer located at the 27-ft level, where a 12 g reading was recorded at the start of ignition motor ejection.

Changes of temperature in the metal parts adjacent to the pit (quench hardware and controller box) were not significant. The thermocouples around the circumference of the pit indicated temperatures ranging from 210 to 230°F after 3 sec in the downwind quadrant and ambient temperatures in the upwind quadrant. The temperature-sensitive paint panels indicated that temperatures around the concrete pad were less than 100°F.

Values for the acceleration and velocity during the vertical movement of the ignition motor and support fixture were determined from the break-wire data. The calculated and actual values for distance, velocity, and acceleration vs time are presented in Figure 94. The calculated values were determined from

IV, I, Mod 260 Ignition Motor Assembly Retention-and-Release System Demonstration Tests (cont.)

ignition motor thrust, weight of ignition motor and support fixture, cable weight, and cable drag; impingement forces on the supported fixture from the exit gas stream were not included. By correcting the calculated thrust and weight values to obtain measured values, the impingement force required to obtain the measured velocity acceleration and distance was 40,000 to 50,000 lb. Using the methods for estimating impingement force shown in Appendix D, and the measured simulator exit gas stream pressures, the calculated impingement force is 120,000 lb. The calculated impingement values presented in Appendix D for the 260-SL motor firing apparently were very conservative. Impingement forces were not used as an ejection method because of the difficulty of ensuring accurate calculations.

b. Test No. 2

The second Mod 260 ignition motor retention-and-release system demonstration test was conducted at the Aerojet-Dade Division on 17 February 1965. Based on the results of the first retention test, the following changes had been made:

(1) The igniter release-control unit actuation pressure was reduced from 60 to 35 psig to ensure that the pressure oscillation will not reset the Schmitt trigger.

(2) Additional breakwires were installed on the tower assembly to obtain better resolution of the velocity and acceleration of the ignition motor and support fixture during the vertical ascent.

(3) A microswitch was installed to indicate first motion of the tower retraction linkage.

IV, I, Mod 260 Ignition Motor Assembly Retention-and-Release System Demonstration Tests (cont.)

(4) A secondary timer circuit, which is independent of the igniter release-control unit, was incorporated to improve the reliability of obtaining explosive bolt actuation in the required time.

(5) The cable attachment brackets on the igniter support fixture were strengthened.

(6) Additional guy wires were installed on the cable support poles. If any of the poles break due to the whip effect of the cables, the guy wires will prevent pieces from falling on the 260-SL motor or adjacent facilities.

A prefiring view of the second retention test setup and of the impact target area is shown in Figure 95.

As shown in Figure 96, a 260-SL motor nozzle weather seal was installed into the free-volume-simulator nozzle. The 6.0-in.-thick Styrofoam weather seal will be used as a support for a plastic, water-tight liner to be installed in the 260-SL-1 motor nozzle during final test firing preparations. The seal and liner will prevent water from reaching the internal surface of the motor bore and nozzle. The weather seal was used in the second retention test to determine its effect on the ignition sequence.

The 10-amp minimum firing command to the KR-80000-07 safety-arming device on the 260-SL ignition motor was manually actuated. The ignition motor explosive bolt actuation command was remotely triggered by a signal received from the igniter release control unit. When the igniter release control unit logic was satisfied at 0.205 sec, the ignition motor and support fixture moved up the track, were restrained by the cables, and flew in a controlled arc until the unit impacted in a water-filled trench about 581 ft from the Cast, Cure, and Test facility. Once again, the welded cable attachment brackets came off prior to impact of the assembly.

IV, I, Mod 260 Ignition Motor Assembly Retention-and-Release System Demonstration Tests (cont.)

The Mod 260 ignition motor ballistic performance curve is presented in Figure 97. A summary of the free-volume simulator bore, throat plane, and exit-cone pressure data is shown in Figure 98; the times of significant events that were measured during the test are included.

The igniter release control unit was actuated at 0.175 sec by an analog signal from the fore-end pressure transducer. The measured fore-end bore pressure at 0.175 sec was 53 psia. When the oscillator timed-out 0.03 sec after actuation, the igniter release control unit logic was satisfied and the explosive bolt actuation command was given at 0.205 sec. The pressure-sensing feature of this unit was to have been used in the first test; however, pressure oscillations in the free-volume chamber in excess of $\pm$ 10 psi occurred and the output of the fore-end Taber transducer dropped below the preset level of 75 psia. Therefore, the igniter release control unit (Schmitt trigger and one-shot oscillator) was continuously turned off and reset. As a result, the explosive bolts in the first test were actuated by the 0.600-sec release control timer. For the second demonstration test, explosive bolt actuation pressure was 50 $\pm$ 2 psia, as measured at the forward head of the free-volume simulator and filtered to 120 cycles/sec, maximum, with the 0.600-sec timer as a backup. The secondary independent timer was set to actuate the explosive bolts at 0.300 sec.

The trajectory of the ignition motor and support fixture was similar to that of the first test. The unit flew in a nearly perfect arc for approximately 110 to 120 degrees. At this point the cables became taut, and one of the attachment brackets came off. The unit began to rotate and roll about its center of gravity until it impacted nozzle-down in the trench. A postfiring photograph of one of the cable attachment brackets is shown in Figure 99. Postfiring inspection of the ignition motor showed that the hardware was undamaged, except for the exit cone. The failure of the cable attachment brackets was identical to the failure that occurred during the first demonstration test. However, the

IV, I, Mod 260 Ignition Motor Assembly Retention-and-Release System Demonstration Tests (cont.)

cables and attachment brackets met the design requirements of being structurally capable of retaining the ignition motor during ascent and of directing the flight of the unit to the target area.

Ballistic performances of the ignition motor and ignition motor booster were normal, as shown in Figures 42 and 97.

The postfiring condition of the ignition motor booster, shown in Figure 100, is further evidence that the insulation installed around the nozzle ports was effective in controlling the metal erosion.

Values for the actual acceleration and velocity during the ascent of the ignition motor and support fixture were determined from the break-wire data. The calculated and actual values for distance, velocity, and acceleration-vs-time are presented in Figure 94. The calculated values were determined from ignition thrust, weight of ignition motor and support fixture, cable weight, and cable drag. Impingement forces on the supported fixture from the exit gas stream were not included. By correcting the calculated thrust and weight values to obtain measured values, the impingement force required to obtain the measured velocity acceleration and distance was 40,000 to 50,000 lb.

The flow conditions in the free-volume simulator nozzle during igniter ejection were identical to the flow conditions measured in the first retention test, but the sequence of events was faster. Subsonic exit gas flow existed in the simulator nozzle until 0.18 sec. At this time the simulator bore pressure was high enough to give separated choked flow of the sonic exit gas stream. At 0.25 sec, equilibrium simulator bore pressure was attained, and steady-state flow conditions existed between the inlet and exit gas streams until the explosive bolts were actuated. When the ignition motor moved away from the simulator throat plane, the inlet jet plume boundary expanded as the pressure ratio

IV, I, Mod 260 Ignition Motor Assembly Retention-and-Release System Demonstration Tests (cont.)

increased. As shown in Figure 98, the static pressure in the free-volume simulator nozzle increased 20 to 30 psi at 0.4 sec, while the bore pressure showed no increase. Thus, during this time interval, the exit gas stream was choked in the simulator exit cone by the expanding inlet jet plume and subsonic gas spillage from the inlet stream. At 0.6 sec, the bow shock formed by the interaction of the inlet and exit gas streams passed through the simulator throat plane. The passage of the bow shock through the throat plane was indicated by the increase in the bore, throat, and exit cone static pressures.

The accelerometer on the igniter support fixture indicated that the ignition motor received a maximum shock of 33 g due to impingement of the reflected shock wave and exhaust gases from the simulator. This coincided with the actuation of the explosive bolts that caused an overriding high frequency (approximately 1500 cycles/sec) response, probably resulting from localized resonance of the fixture, with random acceleration peaks to 38 g. Vibration loads on the ignition motor continually decreased as the motor and support fixture ascended the track, with 10 g at 800 cycles/sec recorded just prior to instrumentation cable breakage at 0.58 sec. The measured vibration and shock loads were all below the specified 75-g maximum acceleration.

Postfiring inspection, recorded data, and motion pictures indicate that the tower retraction operation was successful. The electrical signal to retract the tower was initiated at 0.437 sec, when the uppermost break-wire circuit on the tower was opened. Since the ignition motor had traveled only about 8 ft at this time, this premature actuation of the tower retraction control break-wire apparently was caused when a piece of the ejected nozzle weather seal or the instrumentation cable struck the break-wire.

Visual examination of the tower revealed no damage due to heat. Accelerometers on the tower recorded maximum vibration in the Z axis at the upper locations. High-frequency accelerations (600 to 800 cycles/sec) up to 70 g

IV, I, Mod 260 Ignition Motor Assembly Retention-and-Release System Demonstration Tests (cont.)

were recorded at these locations during ignition motor operation and during initial ignition motor ascent. Accelerations in the X axis were generally minor, except for the accelerometer located at the 27-ft level, where a 20-g reading was recorded at the start of ignition motor ejection. At the relatively high frequencies when the maximum g loads were recorded, the actual displacements were very small (less than 0.002 in.) and are not a hazard to the successful operation of the retention-and-release system.

The temperatures of the metal parts adjacent to the caisson (quench hardware and controller box) showed very little change during or after the firing. Temperatures on the quench-boom bearings did not increase over 20°F during the test. A successful postfiring functional check of the quench-boom unit was performed immediately after the test.

V. ANALYSIS OF TEST RESULTS

A. DESIGN CRITERIA

The Mod 260 ignition motor design criteria were verified by the ignition performance of the 44-SS motors. The 44-SS motor subscale ignition program was initiated to verify all phases of the Mod 260 ignition motor design criteria. However, the major purpose of the subscale ignition tests was to determine the effects of high bore penetration and igniter position on motor ignition.

1. Bore Penetration

Most of the previous aft-end ignition performance data were obtained in tests of motors ignited by solid-propellant igniters at lower bore penetration depths, ranging from 25 to 50%.[2] Ignition data at high penetration depths were available from only two motor tests: United Technology Center motor, TM-3A, three-segment, Test No. 1387[2] and Aerojet motor 100 FW-4.[1][7] The ignition parameter for the TM-3A motor igniter was 0.2, giving a theoretical bore-penetration depth of 60 to 63%. The 100 FW-4 aft-end Alclojet igniter produced hot-gas bore penetration ranging between 55 to 65%. The ignition parameter for the 44-SS ignition motors was 0.3, giving a theoretical bore-penetration depth of 70%. The 70% bore-penetration depth was verified indirectly in the 44-SS free-volume simulator tests by measuring the actual fore-end bore pressure and calculating a corresponding bore-penetration depth.

The ignition intervals for the three 44-SS motors tested were 0.160, 0.165 and 0.162 sec, indicating that satisfactory ignition was achieved with high bore penetration. The ignition performance of the 44-SS motors and motors TM-3A and 100 FW-4 showed no perturbations in the motor pressure rise or ignition overpressures.

2. Igniter Position

The position of the aft-end igniter relative to the motor throat plane appeared to affect the motor ignition transient. Tests conducted by United

V, A, Design Criteria (cont.)

Technology Center showed that as the exit plane of the igniter was moved farther away from the motor throat plane (ε^* increased from 1.1 to 1.8), the motor ignition interval was significantly increased. Cold-flow test data also showed that the measured fore-end bore pressure decreased slightly as ε^* was increased. The increase in ignition interval was attributed to:

a. Impingement of the igniter jet plume on the motor exit cone and throat, causing gas spillage and reduced efficiency.

b. A decrease in bore penetration depth, causing a slower pressure rise rate.

Besides affecting the ignition interval, the igniter position also can affect the motor ignition pressure. United Technology Center motor ignition tests showed that a motor ignition overpressure occurred when the igniter exit plane was close to the motor throat plane (ε^* = 1.0 and 0.8). The counterflow tests in the cold-flow test program showed that overpressures occurred when the igniter was located at an ε^* of 1.3. Small-scale aft-end ignition tests conducted by the Air Force[8] showed that overpressurization occurred when the igniter was located at an ε^* of 1.2, but no overpressurization occurred at an ε^* of 2.0. In the AFRPL tests, the igniter was fired into the aft end of a motor that had been ignited by a conventional fore-end igniter, so that motor steady-state operating pressure was achieved before the aft-end igniter was fired.

The causes of overpressurization in a solid-rocket motor during aft-end ignition are:

a. Blockage of a portion of the motor throat by the inlet igniter jet plume.

b. Choking of the motor exit gas stream around the igniter, usually at the area between the exit cone of the motor and the exit plane of the igniter.

V, A, Design Criteria (cont.)

Motor overpressurization during aft-end ignition can be prevented by:

a. Ejecting the aft-end igniter so that inlet jet plume penetration of the motor throat plane is terminated before attaining motor steady-state operating pressure.

b. Positioning the aft-end igniter exit plane far enough away from the motor throat plane to prevent choking of the motor exit gas stream around the igniter exit plane.

Ejection of the aft-end igniter is the method to be used in the 260-SL-1 motor tests. The ejection sequence of the ignition motor was successfully demonstrated in the 44-SS motor firings and in the Mod 260 ignition motor retention-and-release system tests.

B. ANALYTICAL MODEL

Another objective of the 260-SL motor ignition system development program was to verify the analytical model assumptions and equations. Data were obtained from the cold-flow, 44-SS free-volume simulator, and 260-SL free-volume simulator tests. In addition, data from aft-end ignition tests conducted by the United Technology Center,[2] the Air Force,[8] and Thiokol[12] were used to verify the analytical model. The results from all these tests are summarized in Figure 101, and the measured fore-end bore pressures are compared with the fore-end bore pressures calculated by the Aerojet-General analytical model. Assuming no error in the pressure measurements, the measured fore-end bore pressures were from 5 to 10 psi higher than the pressures calculated from the analytical model. This 8 to 10% variation between the measured and calculated bore pressures was not unexpected; several of the assumptions used in the development of the analytical model were only partially true and were made to simplify the analysis.

V, B, Analytical Model (cont.)

The most significant variation between the measured and calculated fore-end bore pressure is introduced in the determination of the portion of the motor throat area that is blocked by the igniter inlet jet plume. The effective motor throat area is expressed as:

$$A_t \text{ effective} = A_t - A_i$$

For the condition of choked exit gas flow:

$$P_s = \left(\frac{2}{\gamma + 1}\right)^{\frac{\gamma}{\gamma + 1}} P_t \qquad \text{(Appendix A, Equation 8)}$$

The flow area of the igniter inlet jet plume A_i, when expanded to the static pressure in the motor throat, is expressed in the following equation:

$$\frac{A_i}{A_{ign}} = \frac{\left(\frac{2}{\gamma + 1}\right)^{\frac{\gamma + 1}{2(\gamma - 1)}}}{\left(\frac{P_s}{P_{ign}}\right)^{\frac{1}{\gamma}} \sqrt{\left(\frac{2}{\gamma + 1}\right)\left[1 - \left(\frac{P_s}{P_{ign}}\right)^{\frac{\gamma - 1}{\gamma}}\right]}} \qquad \text{(Appendix A, Equation 7)}$$

The calculation of A_i in the analytical model is based on the one-dimensional flow-area ratio, although in reality the flow is three-dimensional. Using a method of characteristics flow analysis instead of the one-dimensional area ratio, the inlet jet plume size can be computed as a function of external pressure and includes the correct plume shape and pressure variation across the jet stream. The one-dimensional area ratio assumes a constant pressure across the jet stream. To show the error introduced by the one-dimensional flow analysis, the following sample calculation is presented:

V, B, Analytical Model (cont.)

Using sample igniter design parameters,

$\dot{w}/A_t$ = 0.32 lb/sec-in.^{2}

P_{ign} = 1000 psia

A_p/A_t = 3.13

the values of static pressure at the motor throat plane (P_s), total pressure at the motor throat plane (P_t), inlet jet plume area expanded to the static throat plane pressure (A_i), and the motor fore-end bore pressure (P_2) were computed by the one-dimensional equations derived in Appendix A and by the three-dimensional method of characteristics. The results are shown below:

	Method	
	One-Dimensional Flow Analysis	Three-Dimensional Flow Analysis
P_s	34.8	39.7
P_t	61.8	70.5
A_i	774	1240
P_2	83.2	92.3

Thus, using the three-dimensional method of characteristics flow analysis, the computed fore-end bore pressure (P_2) is approximately 10% higher than the value computed by the one-dimensional flow analysis. This is the same percentage increase recorded in the measured free-volume simulator fore-end bore pressures, as shown in Figure 101.

The three-dimensional method of characteristics flow analysis is more accurate in computing the igniter flow parameters; however, the method is complex and requires a special computer program input for every flow condition analyzed. The one-dimensional analytical model equations are readily programed in the computer for predicting the entire ignition transient as described in Appendix E. Also, the

V, B, Analytical Model (cont.)

additional accuracy that is possible with the three-dimensional flow analysis is not necessary for the application of aft-end ignition. Therefore, the analytical model as derived in Appendix A is correct and becomes an effective tool to define the design parameters required for aft-end ignition systems. An 8 to 10% increase over the calculated fore-end bore pressure is then expected during actual operation; however, this produces only a 1 to 2% variation in the igniter gas penetration depth.

C. IGNITION CHARACTERISTICS

The heat-flux data were used to evaluate the ignition characteristics of the Mod 260 and 44-SS ignition motors. The ignitibility of solid propellant is both pressure and energy dependent, as proven by arc-image furnace tests of many types of propellants. As described previously propellant samples under a fixed pressure were exposed to a radiant energy source to determine the time required for ignition. The pressure parameter was varied so that the resulting propellant ignitibility data were a curve at constant heat-flux in terms of pressure and ignition time.

The igniter-induced heat-flux at the aft surface of the free-volume simulator wall or propellant surface was analytically determined by defining convective heat flux in terms of a heat transmission coefficient and a temperature drop between the gas stream and the surface of the wall:[6]

$$\bar{q} = h\,(Tg - Ts)$$

and

$$h = 0.0296\,\frac{\gamma Q}{T_o}\left(\frac{\mu_g}{x}\right)^{0.2}\left(\frac{\dot{w}_i}{A_p/144}\right)^{0.8}$$

$$\therefore q = 0.0296(Tg - Ts)\frac{\gamma Q}{T_o}\left(\frac{\mu g}{x}\right)^{0.2}\left(\frac{\dot{w}_i}{A_p/144}\right)^{0.8}$$

To simplify the convective heat-flux expression, the following assumptions were made:

V, C, Ignition Characteristics (cont.)

1. The propellant surface temperature is negligible in relation to the ignition motor exhaust gas temperature, so that $T_s \approx 0$.

2. Generally, values for the ratio of $\frac{T_g}{T_o}$ range from 0.8 to 0.9, thus, $\gamma(\frac{T_g}{T_o}) \approx 1.0$.

3. Since the area of maximum heat transfer between the inlet igniter gas and the motor propellant occurs at the initial impingement point, the term $\frac{H_g}{X}$ can be dropped from the expression, since X would be zero. Thus, the calculated induced heat-flux from the Mod 260 ignition motor was determined:

$$\bar{q} = 0.0296\, Q \left(\frac{\dot{w}_i}{A_p/144}\right)^{0.8}$$

where
Q = 2160 Btu/lb for ANP-2758 propellant
A_p = 12,250 sq. in.
$\dot{w}_i$ = 1200 lb/sec
$\bar{q}$ = 526 Btu/ft^2-sec = 143 cal/cm^2-sec

The maximum measured heat-flux rates near the aft-end of the free-volume simulator were 125 cal/cm^2-sec in the first test and 138 cal/cm^2-sec in the second test. Thus, at Station 3, the Mod 260 ignition motor induced a minimum heat-flux of approximately 120 cal/cm^2-sec to the surface of the simulator wall.

The next step in evaluating the ignition characteristics is to determine the igniter-induced motor bore pressure required to satisfy the heat-flux requirements of the propellant. The igniter-induced bore pressure can be calculated from Equation 14 of Appendix A or measured bore pressures can be used. The measured igniter-induced bore pressure from the Mod 260 ignition free-volume test is plotted in Figure 102; the ignition motor performance curve is included in Figure 102. To more nearly simulate the pressure conditions that existed during arc-image furnace tests, time-averaged, igniter-induced bore pressures are used instead of instantaneous pressures. The time-averaged, igniter-induced bore pressure is determined by the expression,

V, C, Ignition Characteristics (cont.)

$$\bar{P}_c = \frac{\int_o^t P_2 dt}{t}$$

and is plotted in Figure 102.

The arc-image furnace data for ANB-3105 propellant is then superimposed on the plot of time-averaged, igniter-induced bore pressure, as shown in Figure 102, assuming that zero time in the arc-image tests corresponds to the time the maximum igniter-induced heat flux reaches the free-volume simulator wall near Station 3. In the Mod 260 ignition motor free-volume tests, this time occurs approximately 8 to 10 millisec after the ignition motor attained full operating pressure. Thus, the pressure and heat-flux conditions required for ignition of ANB-3105 propellant are satisfied between 0.190 and 0.210 sec after fire switch in the free-volume tests. The measured propellant patch ignition times were as follows:

Theoretical	0.19 - 0.21 sec
Free-volume test No. 1	0.23 sec
Free-volume test No. 2	0.29 sec
Retention test No. 1	0.36 sec (wet propellant)
Retention test No. 2	Data invalid

A similar analysis was made to evaluate the ignition characteristics of the 44-SS igniter. In this case, actual motor ignition data were available instead of propellant patch data. The determination of the effective heat-flux for the 44-SS ignition motor was more arbitrary, since the 44-SS ignition motor performance was progressive, while the Mod 260 ignition performance was neutral to slightly regressive. To obtain a realistic value, an average induced heat-flux rate was computed as follows:

$$\bar{q} = 0.0296\, Q \left(\frac{\dot{w}_i}{A_p/144} \right)^{0.8}$$

$$Q = 2160 \text{ Btu/lb}$$

$$A_p = 316 \text{ sq. in.} = 2.47 \text{ sq. ft}$$

$$\therefore \bar{q} = 17.3 \left(\frac{\dot{w}_i}{2.47} \right)^{0.8} \text{ cal/cm}^2\text{-sec}$$

V,C , Ignition Characteristics (cont.)

P_{ign}	$\dot{w}_i$	$\dot{w}_i/2.47$	$(\dot{w}_i/2.47)^{0.8}$	$\bar{q}$
100	4.2	1.7	1.5	26
300	12.5	5.1	3.7	64
500	20.8	8.4	5.5	95
700	29.1	11.8	7.2	124
900	37.4	15.1	8.8	152

The average $\bar{q}$ was 77 cal/cm^2-sec for ignition motor 44-SS-IM-03. As indicated in Figure 51, the ballistic performance of igniter 44-SS-IM-03, test fired in the third 44-SS free-volume test, was close to that of igniter 44-SS-IM-04, which was used to ignite motor 44-SS-1, and the induced bore pressure and heat-flux for both igniters were comparable. The 44-SS-IM-03 igniter chamber pressure, P_{ign}, and the measured free-volume simulator bore pressure, P_2, are plotted in Figure 103. The time-averaged induced bore pressure, $\bar{P}_c$, was computed and plotted in Figure 103. The arc-image furnace data, measured at the 70 cal/cm^2-sec heat-flux rate for ANB-3105 propellant, was then superimposed in Figure 103, assuming that zero time in the arc-image tests corresponds to the time of initial bore pressurization. This is a reasonable assumption, since an average heat-flux value was used instead of a maximum steady-state heat-flux rate. The pressure and heat-flux conditions required for ignition of ANB-3105 propellant in the 44-SS motors are met between 0.090 and 0.100 sec after fire switch, or 0.055 to 0.065 sec after capacitor discharge to the EBW squib. The initial propellant ignition times in the 4-SS motors were as follows:

Motor	Time to First Propellant Ignition, sec	Time of Capacitor Discharge, sec	Time to First Propellant Ignition After Capacitor Discharge, sec
Theoretical	-	-	0.055 to 0.065
44-SS-1	0.090	0.035	0.055
44-SS-2	0.070	0.016	0.054
44-SS-3	0.075	0.012	0.063

V, C, Ignition Characteristics (cont.)

There was a closer correlation between the theoretical and observed first propellant ignition times for the 44-SS motor propellant than for the 260-SL free-volume simulator propellant patches. This was expected because the installation of the propellant patch in the simulator wall was significant; the patch must be installed flush with the inside surface of the chamber wall. Also, the actual ignition time as determined from the thermocouple trace had an accuracy of $\pm$ 0.05 sec. Conversely, the time of first propellant ignition in the 44-SS motors was readily determined; the correlation was good enough in both instances to verify the ignition capability of the Mod 260 ignition motor and the analytic method derived[6] to define the ignition characteristics.

D. FLOW CONDITIONS DURING IGNITION MOTOR EJECTION

The free-volume simulator pressures recorded during the retention-and-release system tests provided sufficient data to analyze the inlet and exit gas flow conditions during ignition motor ejection. As shown in Figures 88 and 104, for the first retention test, subsonic exit gas flow existed initially throughout the simulator bore, throat, and exit cone. At approximately 0.175 sec, the pressure in the simulator bore was high enough to achieve separated choked flow of the sonic exit gas stream, as shown in Figure 104. At 0.250 sec, the equilibrium bore pressure of 82 psia was achieved. The steady-state flow condition shown in Figure 104 existed until the explosive bolts were actuated and the ignition motor started its vertical movement out of the simulator exit cone. As the ignition motor moved away from the simulator throat plane, the inlet jet plume boundary expanded as the pressure ratio increased. As shown in Figure 88, the static pressure in the simulator throat and exit cone increased 20 to 30 psi at 0.78 sec, while the simulator bore pressure showed no increase. Thus, the exit gas stream was choked in the exit cone by the expanding inlet jet plume and subsonic gas spillage from the inlet stream, as shown in Figure 104. At 0.95 sec, the bow shock formed at the intersection of the inlet jet plume and the exit gas stream passed through the simulator throat, as shown in Figure 104. The passage of the bow shock through the throat was shown by an increase in the bore, throat, and

V, D, Flow Conditions During Ignition Motor Ejection (cont.)

exit cone pressures. The pressure effect of the bow shock also occurred during ejection of the 44-SS ignition motors.

The ignition motor had moved vertically 15 to 17 ft when the bow shock passed through the simulator throat. The approximate vertical distance traveled was measured by break-wires on the tower assembly. Since the 260-SL motor exit cone is 14 ft long, the ignition motor jet plume bow shock will be clear of the 260-SL motor exit plane when the ignition motor has traveled vertically 29 to 31 ft. Therefore, the estimated 31-ft vertical clearance specified for the Mod 260 ignition motor retention-and-release system appears to be valid.

E. IGNITION MOTOR PERFORMANCE

The Mod 260 ignition motor assembly met all requirements for performance and reproducibility. A composite of all the ignition motor performance curves is presented in Figure 105. The quality of ignition motor hardware fabrication, propellant installation technique, and postfiring refurbishing procedure was demonstrated in the test program. The reproducibility of flame propagation from the safety-and-arming device, initiator, and booster to the ignition motor was also demonstrated.

F. FINAL 260-SL-1 MOTOR IGNITION PERFORMANCE PREDICTION

The final 260-SL-1 motor ignition performance prediction is presented in Figure 106. A computer program was developed at Aerojet-General to predict the ignition transient of solid rocket motors ignited by aft-end igniters. The program is presented in Appendix E. The program combines the equations from the aft-end ignition model (Appendix A) and a semiempirical method[9] of predicting motor pressure rise transients. The program also includes variations in motor pressure rise generated during aft-end igniter ejection.

V, F, Final 260-SL-1 Motor Ignition Performance Prediction (cont.)

This program was used to predict the ignition transients of motors 44-SS-2 and 120-SS-1. Ignition of motor 120-SS-1 was accomplished by a conventional fore-end igniter, but the basic computer program is capable of predicting ignition transients for either fore- or aft-end igniters. The actual and predicted ignition transients for these two motors are shown in Figures 107 and 108. To further test the computer program, an ignition performance prediction was made for the United Technology Center three-segment motor, TM-3A[2] and the data were compared with the actual performance, as shown in Figure 109. The correlation between the actual and predicted performance was good; calculated ignition times were within 3 to 10 millisec of the actual ignition times.

VI. CONCLUSIONS

The objectives of the 260-SL motor aft-end ignition system development program were achieved. The results of previous aft-end igniter programs, Nike-Zeus booster aft-end igniter, development of ignition system for large solid-propellant motors[2], and the 100 FW-4 motor aft-end ignition system[1][7] development, provided the background data necessary to establish the objectives and approach to the current program. Based on the results of analytical studies performed and test data obtained during the program, the following conclusions have been reached:

1. The capability of the Mod 260 ignition motor assembly to ignite the 260-SL motors was clearly demonstrated. This ignition capability was shown as follows:

a. The energy delivered to the 260-SL free-volume simulator wall by the Mod 260 ignition motor was 30 to 40 times greater than the measured threshold-ignition energy of 260-SL motor propellant.

b. The energy delivered by the Mod 260 ignition motor was sufficient to ignite small patches of 260-SL motor propellant installed along the 260-SL free-volume simulator wall.

c. The correlation between the observed initial propellant ignition times of the propellant patches and 44-SS motor propellant, and the ignition times theoretically determined from propellant arc-image furnace ignition data as related to igniter induced pressure and heat-flux were within the expected analytical variation.

2. The analytical model, as derived in Appendix A, was verified as an effective design tool for obtaining aft-end igniter mass-flow-rate requirements, motor-bore pressurization, and degree of bore penetration as functions of motor size.

VI, Conclusions (cont.)

3. The Mod 260 ignition motor design criteria were verified by the reproducible ignition performance of the 44-SS motors.

4. Desirable ignition was achieved with high igniter hot-gas bore penetration, as demonstrated by the ignition performance achieved in the 44-SS motor tests.

5. The Mod 260 ignition motor assembly met all the design objectives for ballistic performance and reproducibility.

6. The design criteria for the Mod 260 ignition motor retention-and-release system were verified in the tests conducted at the Aerojet-Dade Division.

7. The performance of all the Mod 260 ignition motor retention-and-release system electrical and mechanical subsystems was demonstrated by operation in the tests conducted at the Aerojet-Dade Division. The ejected ignition motors impacted in the target area; consequently, the operation of the system is not a hazard to the 260-SL motors or adjacent facilities.

8. The performance of the igniter release control unit was demonstrated in the 44-SS motor firings and in the retention-and-release system functional tests.

9. The flow conditions during ignition motor ejection are not a hazard to the structural integrity of the 260-SL motor exit cone or throat section, provided the inlet jet plume blockage of the motor throat plane is terminated before steady-state operating pressure is achieved.

10. The selected mold-casting secondary-bonding process proved to be a fast, reliable method for ignition motor propellant installation.

11. Based on the results of the 260-SL motor ignition system test program, an outline for the design of an aft-end ignition system is presented in Appendix F.

VII. LIST OF REFERENCES

1. Aerojet-General Corp. Report No. SSD-TDR-62-103, Final Report, Phase II Larger Solid Rocket Program, Aft-End Ignition, dtd October 1962.

2. United Technology Center, Final Report, Technical Documentary Report No. RTD-TDR-63-10, Theoretical and Experimental Investigations of Ignition Systems for Very Large Solid-Propellant Motors, dtd May 1963 (UTC Report 2012-FR-2).

3. Statement of Work, 260-in.-Dia Motor Demonstration, Exhibit "A" to Contract No. AF 04(695)-350.

4. Aerojet-General Corp. Report RPL-TDR-64-4, 260-in.-Dia Motor Program, Technical Note, Contract No. AF 04(695)-350, 1 October through 31 December 1963, dtd 30 January 1964.

5. National Aeronautics and Space Administration Technical Note D-1605, Exploratory Investigation of the Effect of a Forward Facing Jet on the Bow Shock of a Blunt Body in a Mach Number 6 Free Stream.

6. Aerojet-General Corp. Technical Memorandum 249-SRP, Wing VI Minuteman Ignition Study Final Report, Letter Contract No. AF 04(694)-258, dtd April 1964.

7. Aerojet-General Corp. Report 0606-01TD-T4, 100FW-4 Test Data Report, Large Solid Rocket Programs, Contract No. AF 04(611)-8012, Program No. 623A, dtd 15 April 1963.

8. Bretting, M. M. Major, USAF, and Niessen, W. R. 1/Lt., USAF, The Study of an Ignition Technique for Large Solid Rocket Motors, Air Force Rocket Propulsion Laboratory, Edwards Air Force Base, California.

VII, List of References (cont.)

9. Aerojet-General Corp. Technical Memorandum 233 SRP, A Semi-Empirical Study of the Ignition Transient of Large Solid Rocket Motors, dtd 25 September 1963.

10. Thiokol Chemical Corp. Technical Memorandum I. Subj: An Investigation of the Loads on the 156-Inch Motor Nozzle Caused by the Pyrogen Igniter, F. W. Martin, dtd 2 July 1964.

11. Thiokol Chemical Corp., Supporting Data, Calculation of Pressure Distribution in Space Booster Nozzle with Pyrogen Restricting the Flow.

12. Thiokol Chemical Corp., Wastach Division, Brigham City, Utah, Quick Look Report, Motor 156-1 (TU-412.01) Static Test, Contract AF 04(695)-363, dtd 21 December 1964.

VIII. NOMENCLATURE

A_e - sonic flow area of gas leaving motor chamber, sq in.

A_i - flow area of igniter-gas, inlet-jet plume when expanded to the static pressure in the motor throat plane, sq in.

A_b - burning surface area of ignited propellant in the motor chamber, sq in.

A_{ign} - igniter throat area, sq in.

A_f - annular flow area between the igniter exit plane and the motor exit cone, sq in.

A_p - motor port or free-volume area, sq in.

A_t - motor throat area, sq in.

A_{h1} - motor bore area hidden from igniter gases due to grain configuration (fins, slots, segment faces, etc.), sq in.

A_{h2} - motor bore area hidden from igniter gases due to trapped, compressed, cool air, sq in.

a* - sonic velocity of igniter gas, ft/sec

C_d - drag coefficient

C_w - mass flow coefficient, $\left(\frac{2}{\gamma + 1}\right)^{\frac{\gamma+1}{2(\gamma-1)}} \frac{\gamma g}{RT}$, sec^{-1}

c - propellant burning rate constant

F - force (thrust), lbf

g - earth surface gravitational acceleration, ft/sec^2

h - heat transfer coefficient, $Btu/ft^2\text{-}sec - °F$

K - total initial motor propellant surface area, sq in.

L_1 - length of hidden area A_{h1}, in.

L_2 - length of hidden area A_{h2}, in.

M_i - Mach number of igniter inlet jet plume at velocity v_i

M_o - Mach number of exit gas stream at velocity v_o

VIII, Nomenclature (cont.)

$\dot{m}$ - igniter mass flow rate, slugs/sec

n - propellant burning rate pressure exponent

$\overline{P}_c$ - time-averaged, igniter-induced motor bore pressure, psia

P_{equi} - motor initial steady-state operating pressure, psia

P_{ex} - motor bore pressure when the igniter release control unit logic is satisfied

P_1 - initial ambient pressure in motor bore, psia

P_2 - fore-end, motor-bore pressure, psia

P_o - pressure of exit gas stream at velocity v_o

P_a - ambient pressure, psia

P_{ign} - igniter total pressure, psia

$\frac{P_{ign}}{\sqrt{T}}$ - igniter flow rate parameter used as the abscissa to report cold-flow test data, $\frac{\dot{w}_i}{A_{ign}\, C_w \sqrt{T}}$

P_s - static pressure in motor throat, psia

P_t - total pressure of exit-gas stream, psia

$\int PdA$ - integrated pressure-area force of gas in the motor bore on the converging portion of motor exhaust nozzle, lbf

q - dynamic pressure, $1/2 \rho\, v^2$

$\bar{q}$ - igniter induced heat flux in motor bore, $Btu/ft^2\text{-sec}$

Q - igniter propellant heat of explosion, Btu/lb

R - universal gas constant, ft/°R

T - igniter gas total temperature, °R

T_g - temperature of motor bore gas, °F

VIII, Nomenclature (cont.)

T_s - temperature of motor bore surface, °F

T_m - motor propellant combustion temperature, °R

T_o - isochric flame temperature (closed bomb), °F

V^* - fraction of propellant gas in motor bore which is at the stagnation pressure, cu ft

V_1 - motor bore free volume, cu ft

V_2 - volume occupied by trapped cold air after compression by inlet igniter gas, cu ft

v_e - velocity of the exit gas stream at the motor throat, ft/sec

v_i - velocity of igniter inlet-jet plume when expanded to the static pressure in motor throat, ft/sec

v_o - velocity of exit-gas stream at the entering plane of the motor nozzle converging section, ft/sec

$\dot{w}_i$ - igniter flow rate, lb/sec

$\dot{w}_e$ - flow rate of exit-gas stream, lb/sec

W_c - mass of propellant gas in motor bore, lb

$\dot{w}/A_t$ - aft-end igniter design parameter, lb/sec-in.^{2}

X - distance downstream (or upstream in aft-end ignition) of gas impingement point, ft

t - time, sec

Δt - time interval used by computer program in integrating equations, sec

t_b - time measured from the time of first motor propellant ignition t_1, sec

t_{ex} - time required to eject the igniter from the motor exit cone after explosive bolt actuation, sec

t_{ign} - igniter web burning duration, sec

t_1 - time of first motor propellant ignition, sec

VIII, Nomenclature (cont.)

ε^* - ratio of minimum annular flow area between the igniter exit plane and the motor exit cone, A_f, to the motor throat area, A_t

ϕ - heat flux, cal/cm^2-sec

μ - dynamic viscosity of igniter propellant exhaust gas, lb/ft-sec

ρ - propellant density, lb/cu ft

τ - time constant, sec

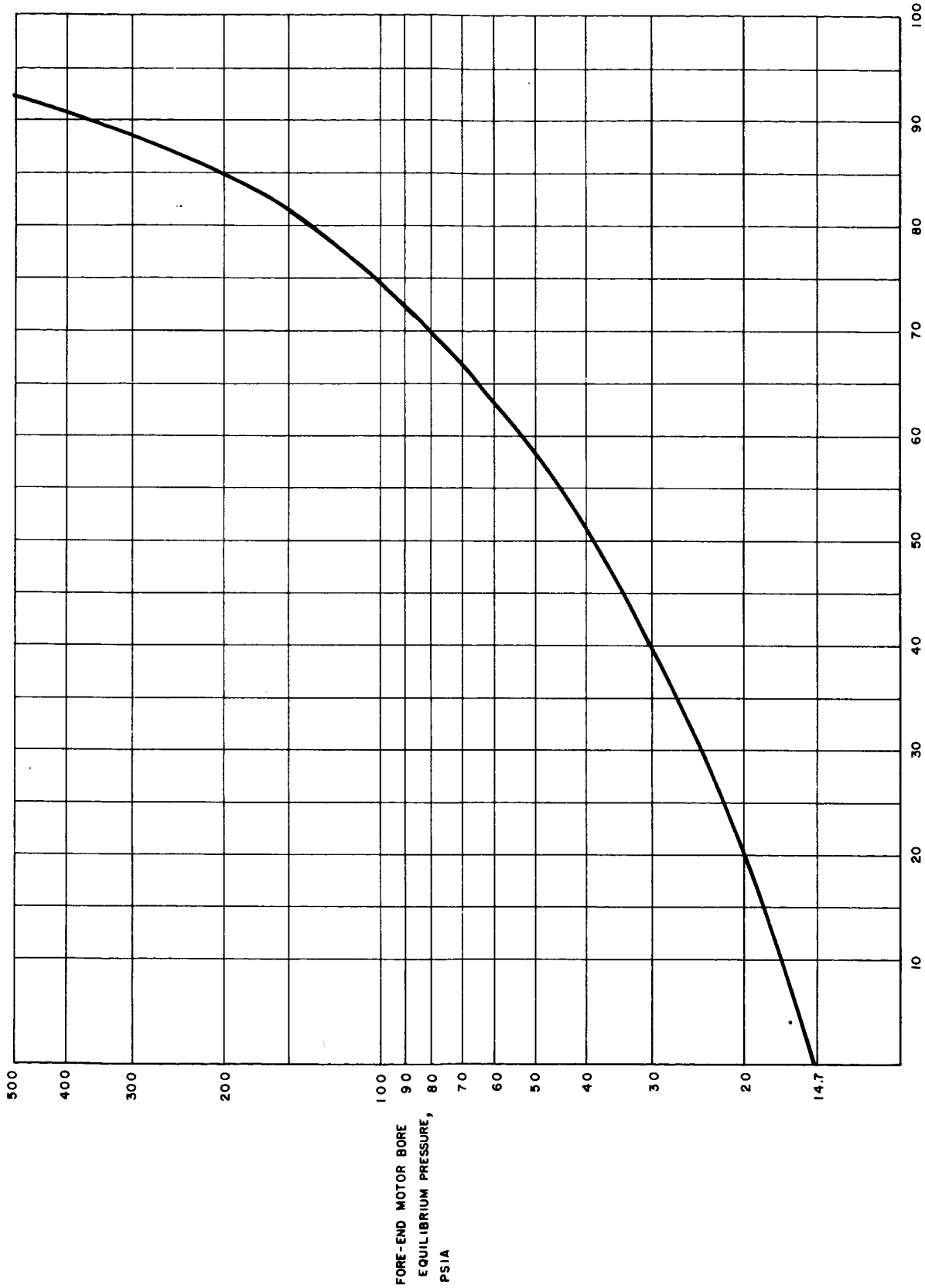

Aft-End Igniter Hot-Gas Penetration as a Function of Motor Bore Pressure

Figure 1

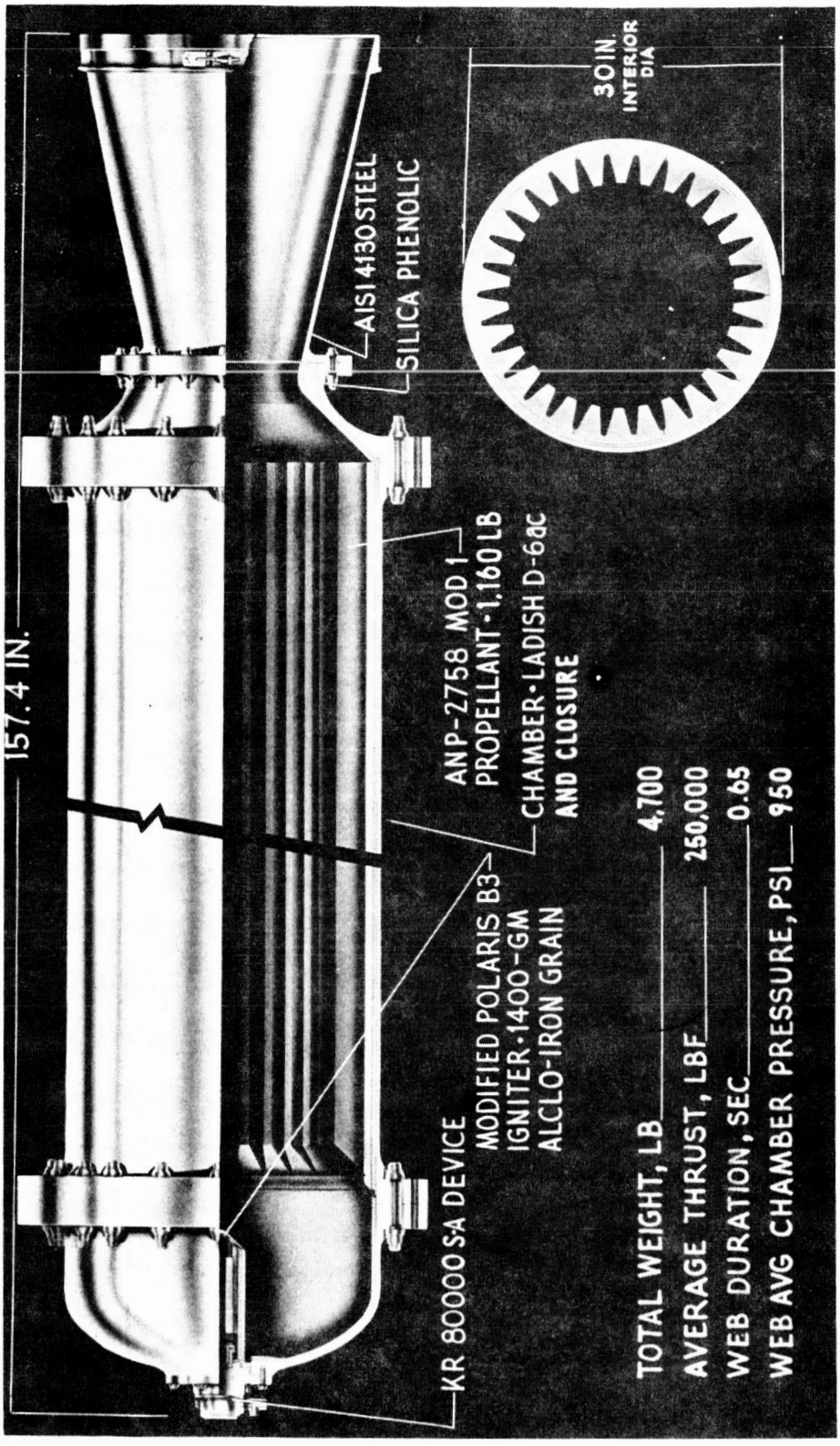

Ignition System for 260-SL Motors

Figure 2

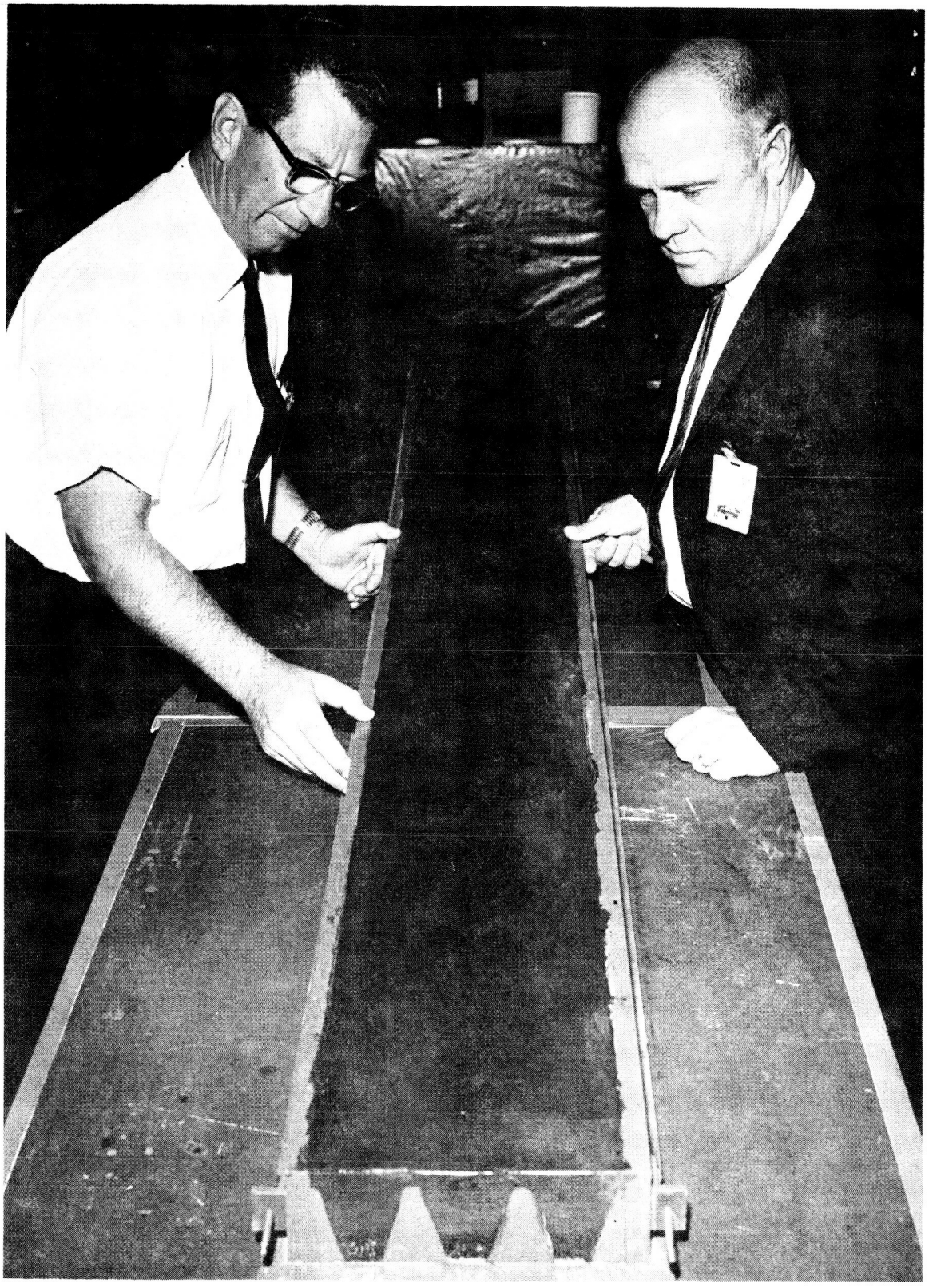

Loaded Propellant Mold for 260-SL Motor Ignition Motor

Figure 3

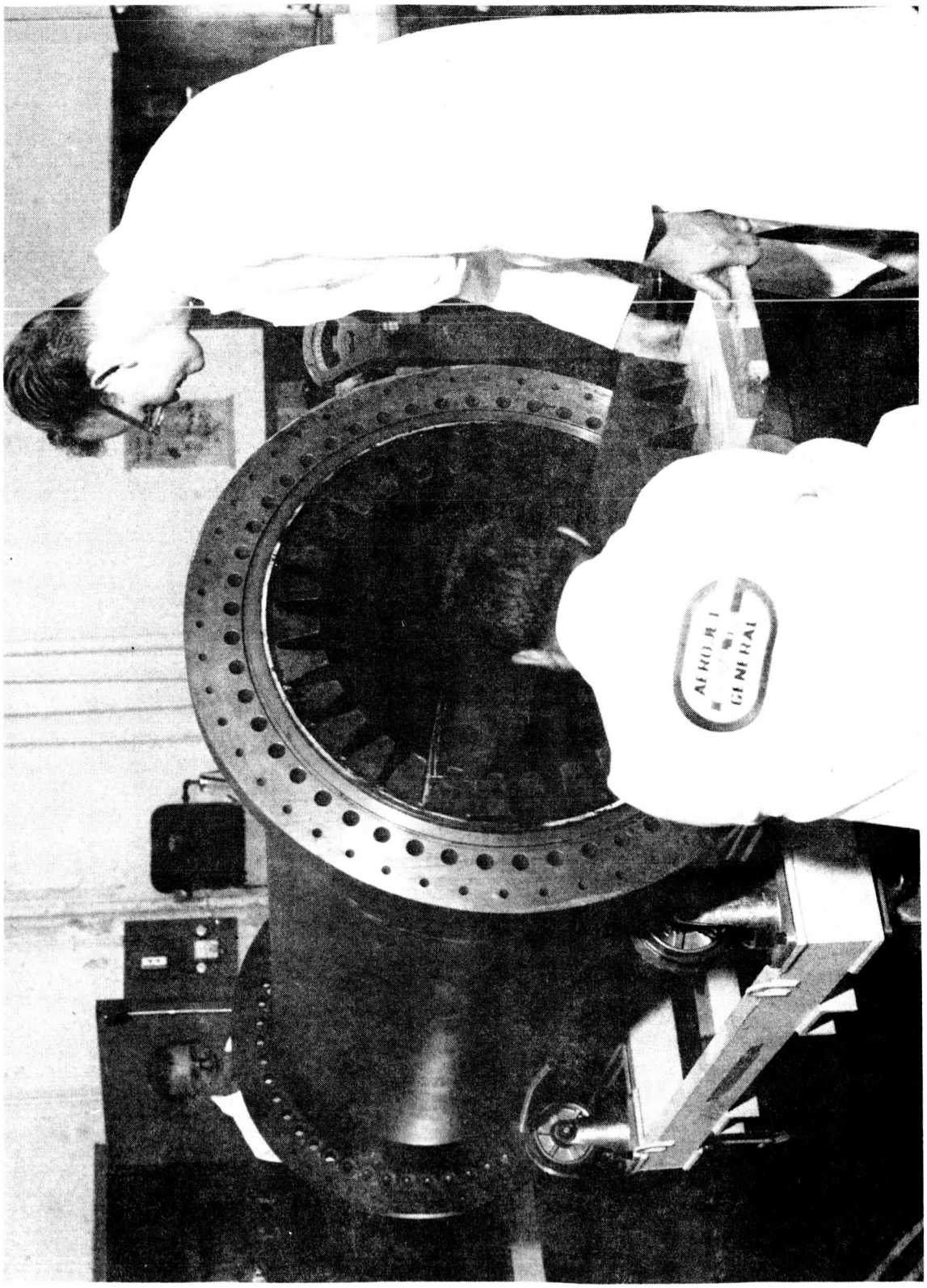

Cured and Restricted Propellant Slab Being Installed into
a Mod 260 Ignition Motor Chamber

Figure 4

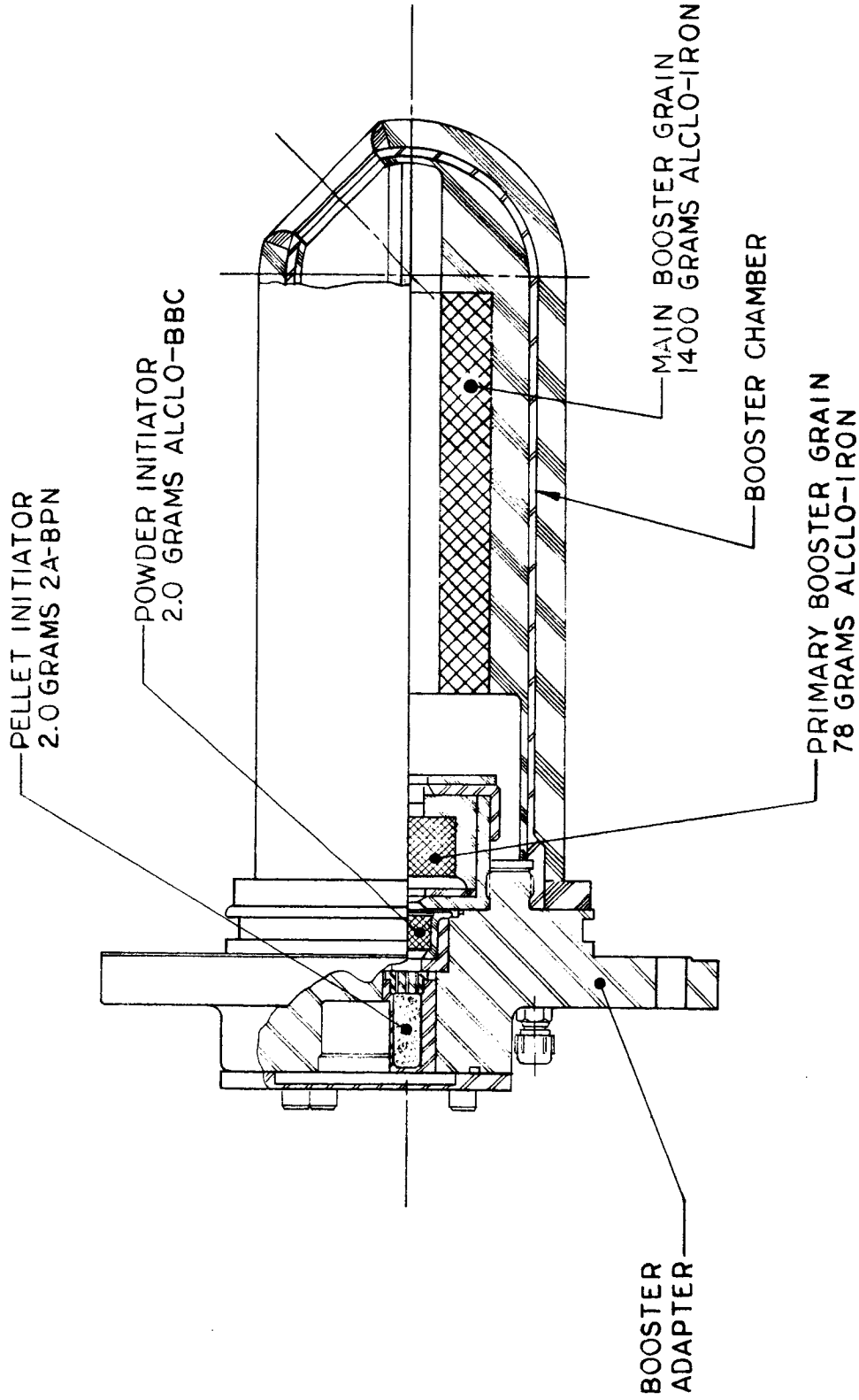

Mod 260 Ignition Motor Booster

Figure 5

	260-SL Ignition Motor	44-SS Ignition Motor
Penetration, %	70	70
Web Average Pressure, psia	1000	1000
Nozzle Expansion Ratio	4	4
Nozzle Half Angle, degrees	12.5	12.5
Igniter Position, ε^*	1.21	1.21
Ignition Parameter, $\dot{w}/A_t$	0.3	0.3

Motor Parameters	260-SL	44-SS
Throat Area, $in.^2$	3960	135
Port-To-Throat Ratio	3.13	2.65

Comparison of 44-SS and 260-SL Ignition Motor Design Criteria

Figure 6

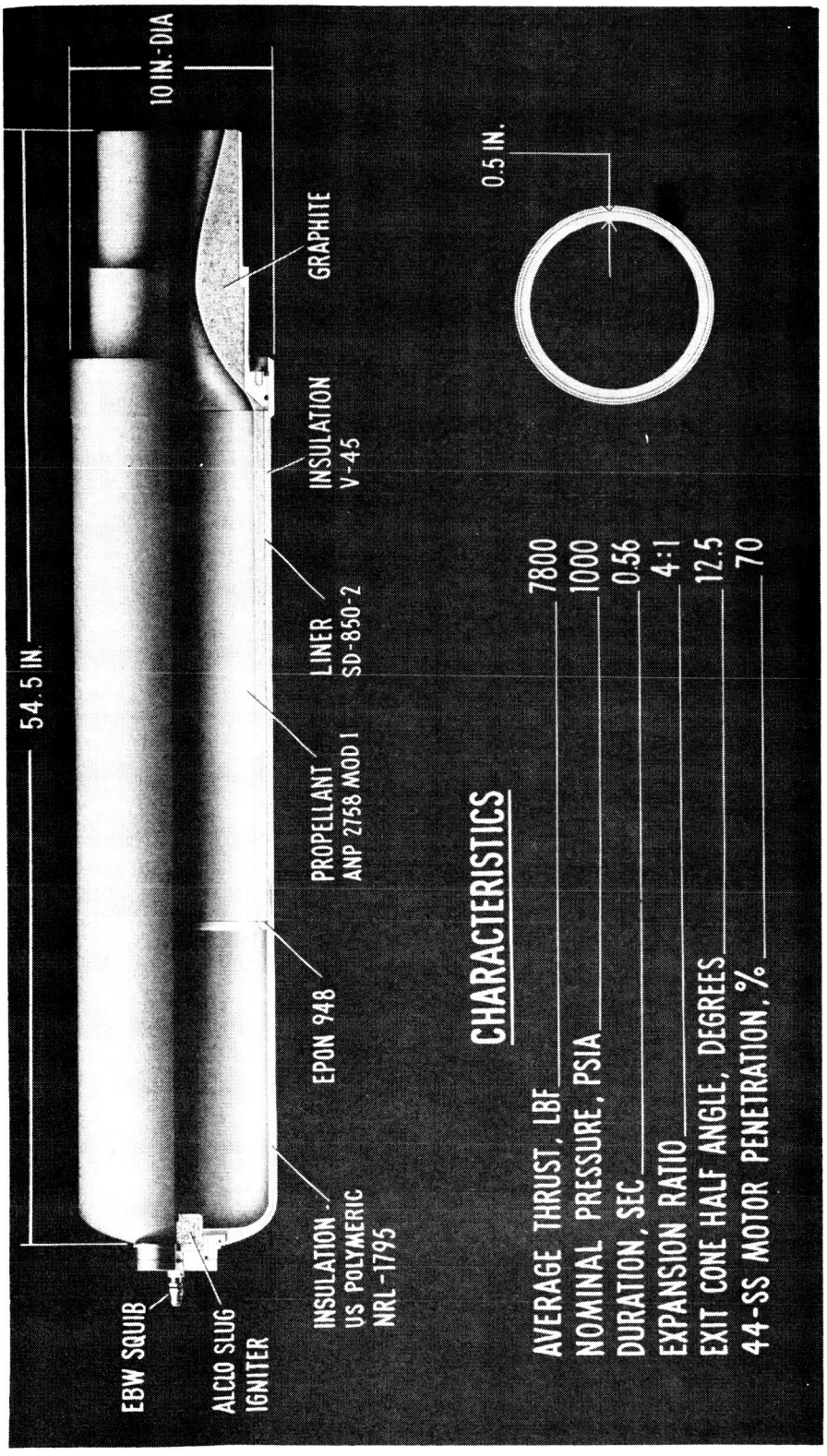

44-SS Motor Aft-End Ignition Motor

Figure 7

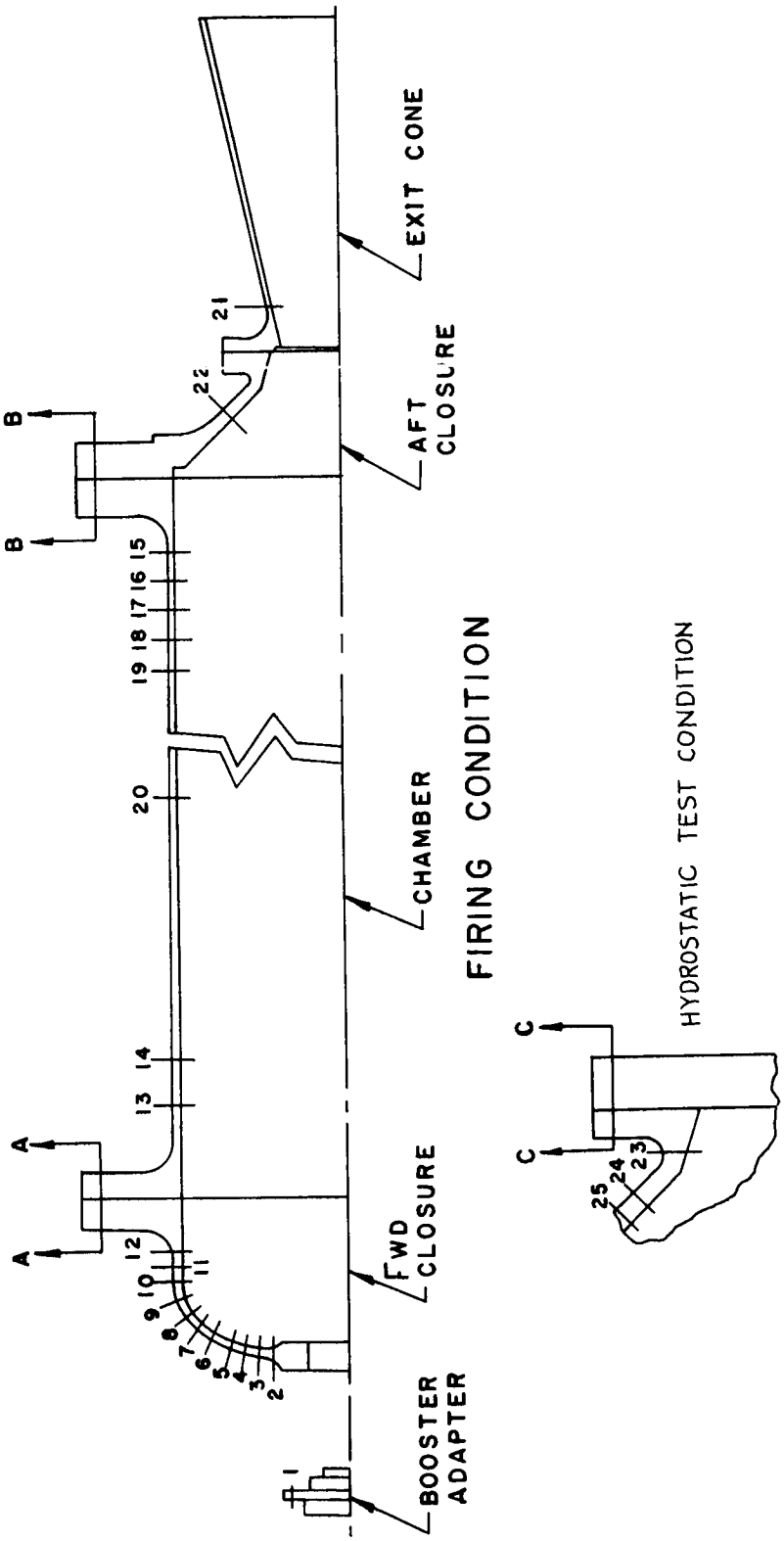

Location of Mod 260 Ignition Motor Structural Elements

Figure 8

Element Location [1]	Membrane Thickness	Maximum Stresses, psi [2]	Maximum Stresses, psi [3]	Stress Type	Allowable Stress, psi	Margin of Safety
1	0.860	127,700		Bending in Flange	142,000	0.111
2	0.550	93,900	91,700	Meridional-Outer	175,000	0.86
3	0.370	142,700	117,400	Meridional-Outer	175,000	0.23
4	0.370	133,600	120,300	Meridional-Outer	175,000	0.31
5	0.370	117,700	115,000	Meridional-Outer	175,000	0.49
6	0.370	94,300	96,400	Meridional-Outer	175,000	0.81
7	0.370	132,800	133,100	Meridional-Inner	175,000	0.31
8	0.370	128,100	129,500	Meridional-Inner	175,000	0.35
9	0.370	119,700	116,800	Meridional-Outer	175,000	0.46
10	0.370	154,500	151,400	Meridional-Outer	175,000	0.13
11	0.370	155,800	154,900	Meridional-Outer	175,000	0.12
12	0.370	134,800	140,900	Meridional-Outer	175,000	0.24
13	0.300	153,900	154,100	Hoop-Outer	175,000	0.14
14	0.300	151,600	151,700	Hoop-Outer	175,000	0.15
Sect. A-A	5.00	103,000		Bending in Flange	175,000	0.70
15	0.300	84,600	69,600	Hoop-Outer	175,000	1.07
16	0.300	135,700	127,500	Hoop-Outer	175,000	0.29
17	0.300	157,300	154,900	Hoop-Outer	175,000	0.11

1 Element location shown in Figure 8.

2 Assuming joint has full shear-transfer capacity

3 Assuming joint has no shear-transfer capacity

Structural Analysis Summary, Mod 260 Ignition Motor Pressure Vessel

Element Location [1]	Membrane Thickness	Maximum Stresses, psi 2	Maximum Stresses, psi 3	Stress Type	Allowable Stress, psi	Margin of Safety
18	0.300	157,300	154,900	Hoop-Outer	175,000	0.11
19	0.300	153,800	154,200	Hoop-Inner	175,000	0.14
20	0.300	151,700	151,700	Hoop-Inner	175,000	0.15;
Sect. B-B	5.00	106,600		Bending in Flange		0.64
21	0.300	53,900	64,100	Meridional-Inner	100,000	0.56
22	0.500	70,500	82,000	Hoop-Inner	175,000	1.13
		72,000 [4]	82,600 [4]	Hoop-Outer	175,000	1.12
23	0.700	85,900 [4]	88,300 [4]	Hoop-Outer	175,000	0.98
24	0.500	41,800 [4]	43,800 [4]	Meridional	175,000	2.39
Sect. C-C	1.75	163,400 [4]		Bending in Flange	175,000	0.07

1 Element location shown in Figure 8.

2 Assuming joint has full shear transfer capacity.

3 Assuming joint has no shear transfer capacity.

4 Hydrotest condition.

Tructural Analysis Summary, Mod 260 Ignition Motor Pressure Vessel

1. Booster Adapter - Forward Closure Joint

   Bolt Type: EWB22-8-12

   Total Bolt Load: 14,693 lb/bolt

   Recommended Torque Preload: 19,600 lb/bolt

   Margin of Safety: 0.06

2. Forward Closure - Chamber Joint

   Chamber - Aft Closure Joint

   Bolt Type: LWB22-16A-76 (FN22-1614 Nut)

   Total Bolt Load: 96,651 lb/bolt

   Recommended Torque Preload: 97,625 lb/bolt

   Margin of Safety: 0.39

3. Aft Closure - Exit Cone Joint

   A. Hydrostatic Test Condition

      Bolt Type: LWB22-12-50 (FN22-1216 Nut)

      Total Bolt Load: 51,677 lb/bolt

      Recommended Torque Preload: 52,595 lb/bolt

      Margin of Safety: 0.42

   B. Firing Condition

      Bolt Type: LWB22-12-32 (FN22-1216 Nut)

      Recommended Torque Preload: 45,000 lb/bolt

      Margin of Safety: High

Structural Analysis Summary, Mod 260 Ignition Motor Pressure Vessel Bolt Preload

Figure 10

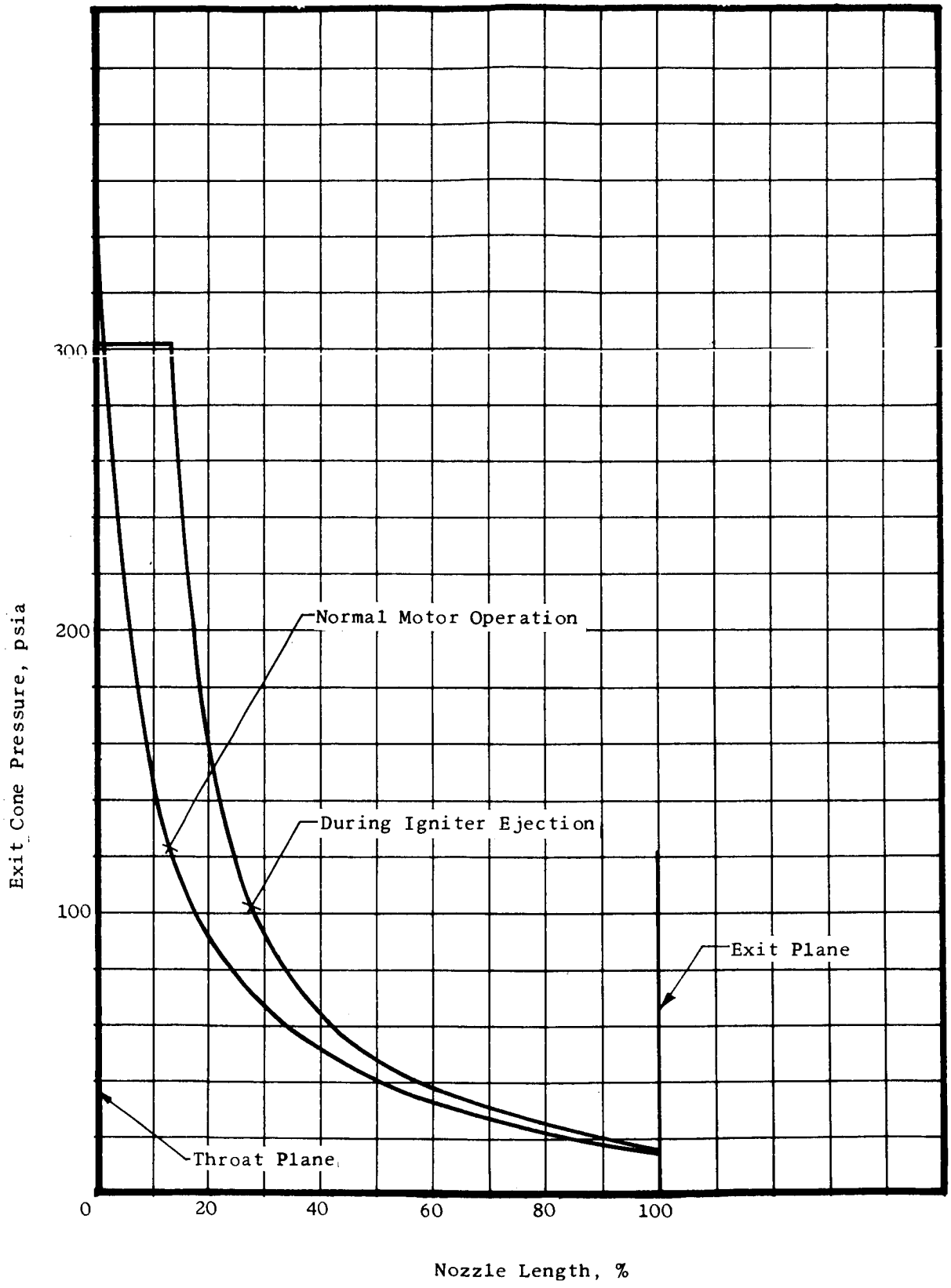

Estimated 260-SL Motor Exit Cone Pressure During Ignition Motor Ejection

Figure 11

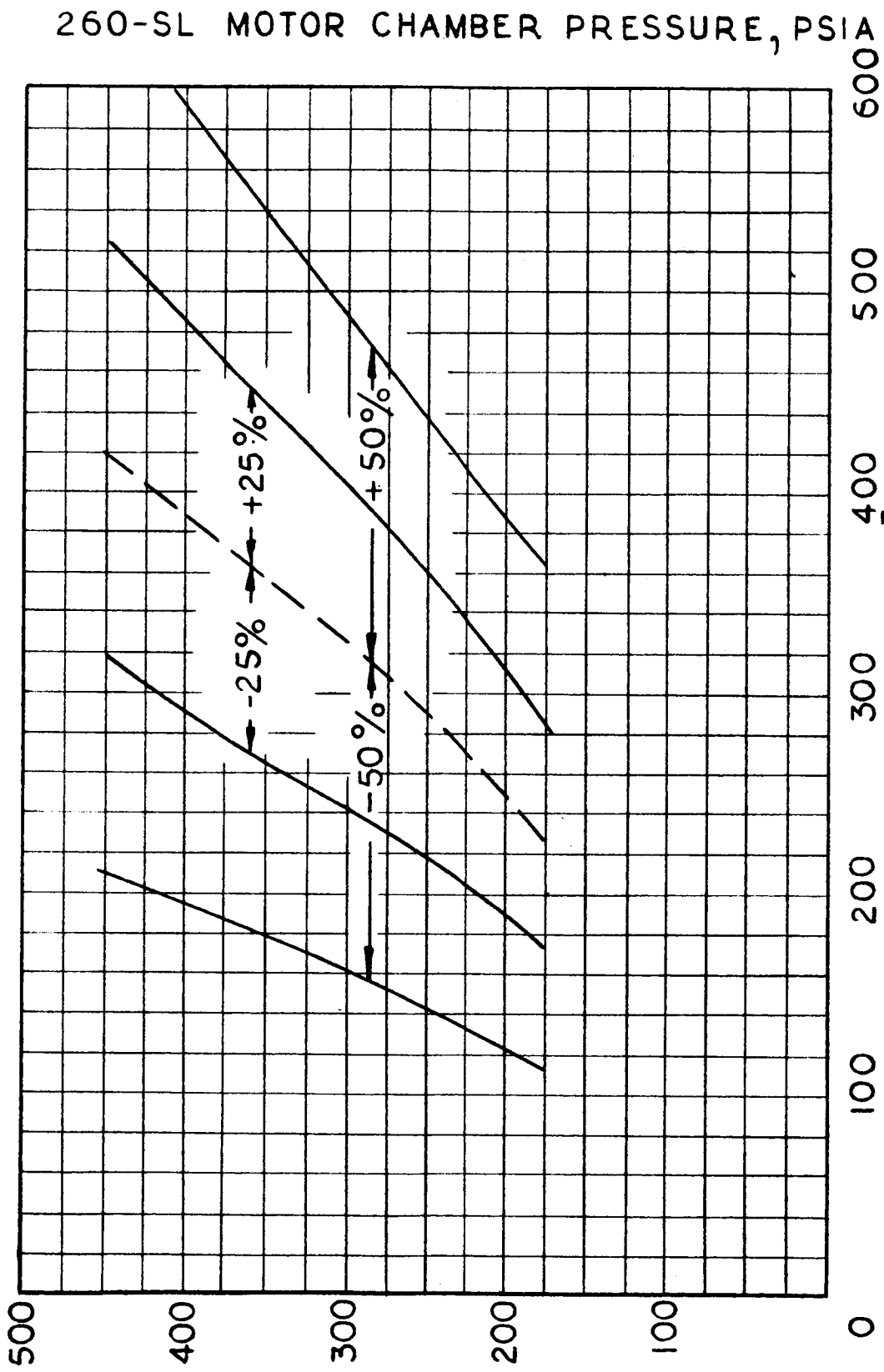

Estimate of the Drag Force on the Mod 260 Ignition Motor Assembly and Retention Equipment vs Motor Chamber Pressure

Figure 12

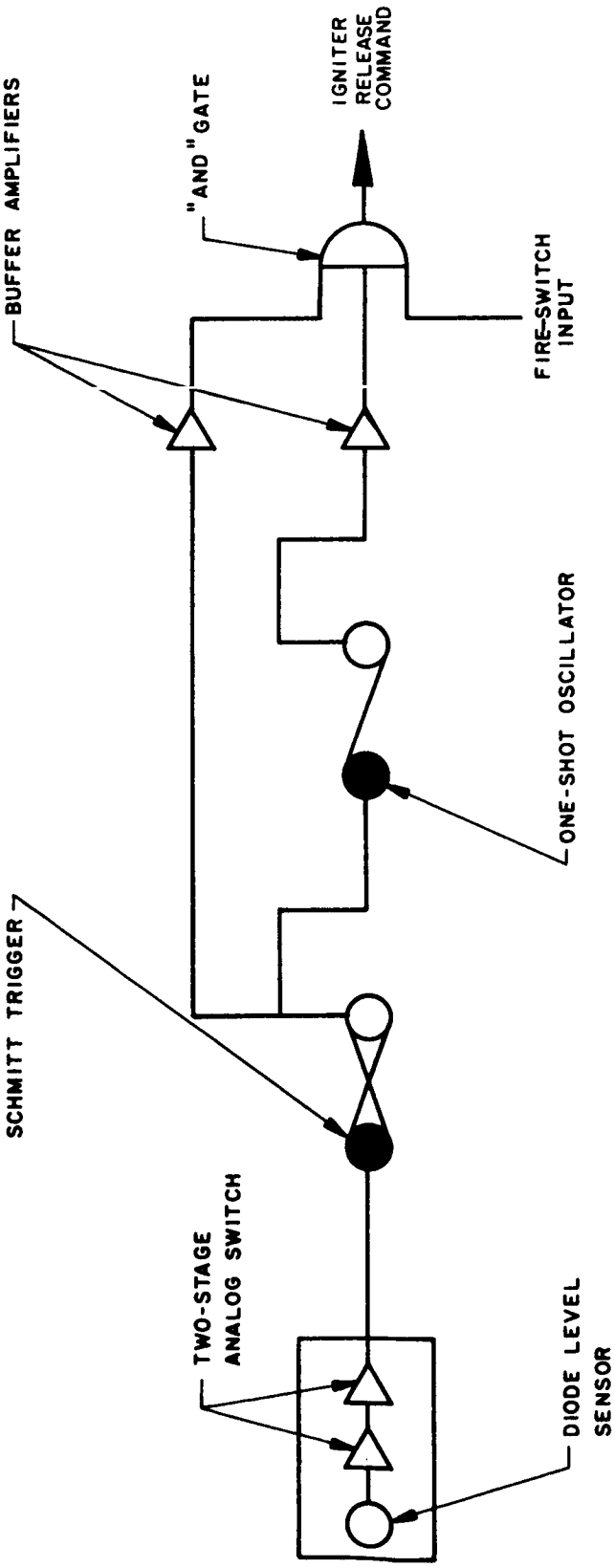

Simplified Block Diagram of the Igniter Release Control Unit Analog Section

Figure 13

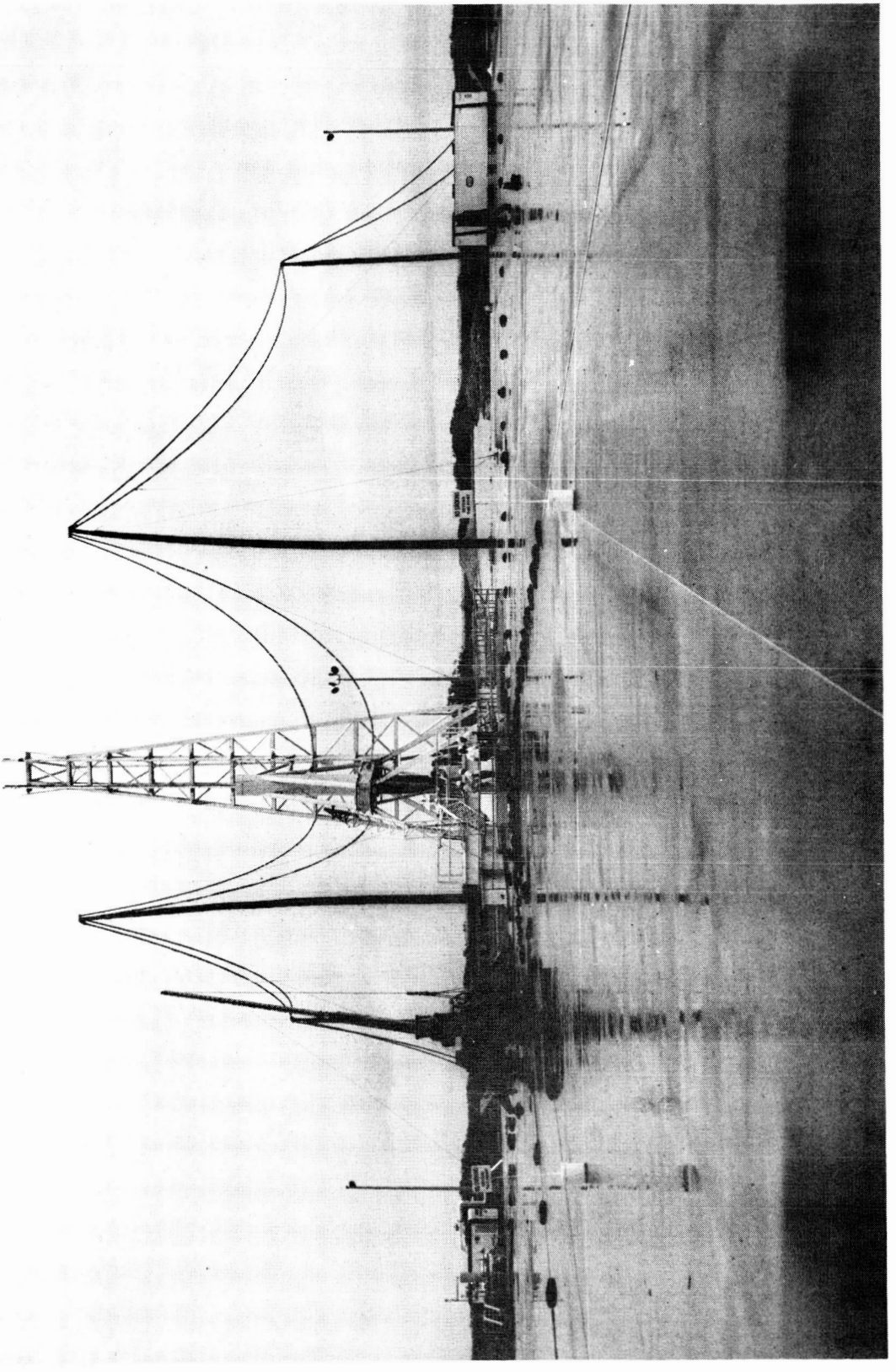

Mod 260 Ignition Motor Retention-and-Release System

Figure 14

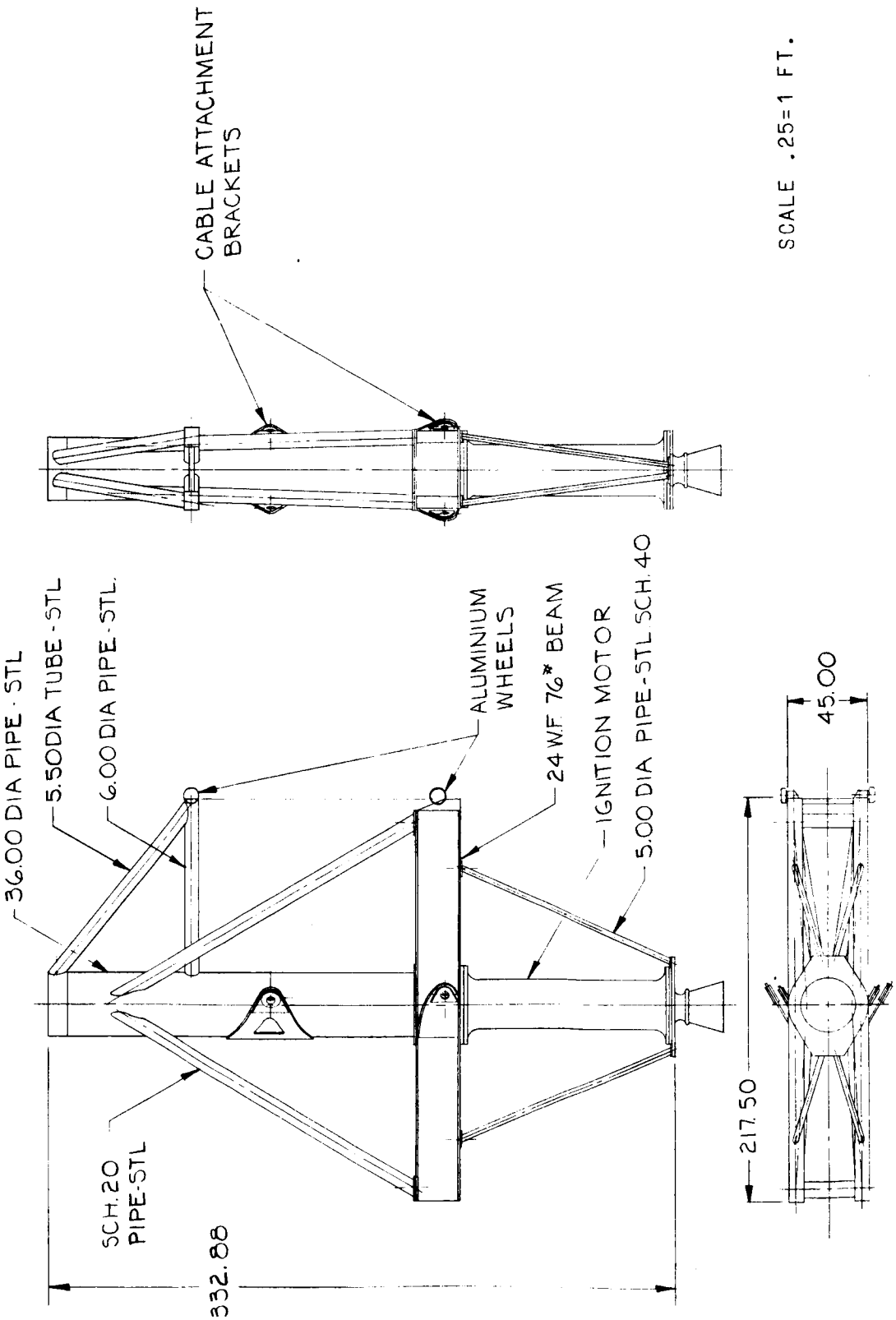

Mod 260 Ignition Motor and Support Fixture Assembly

Figure 15

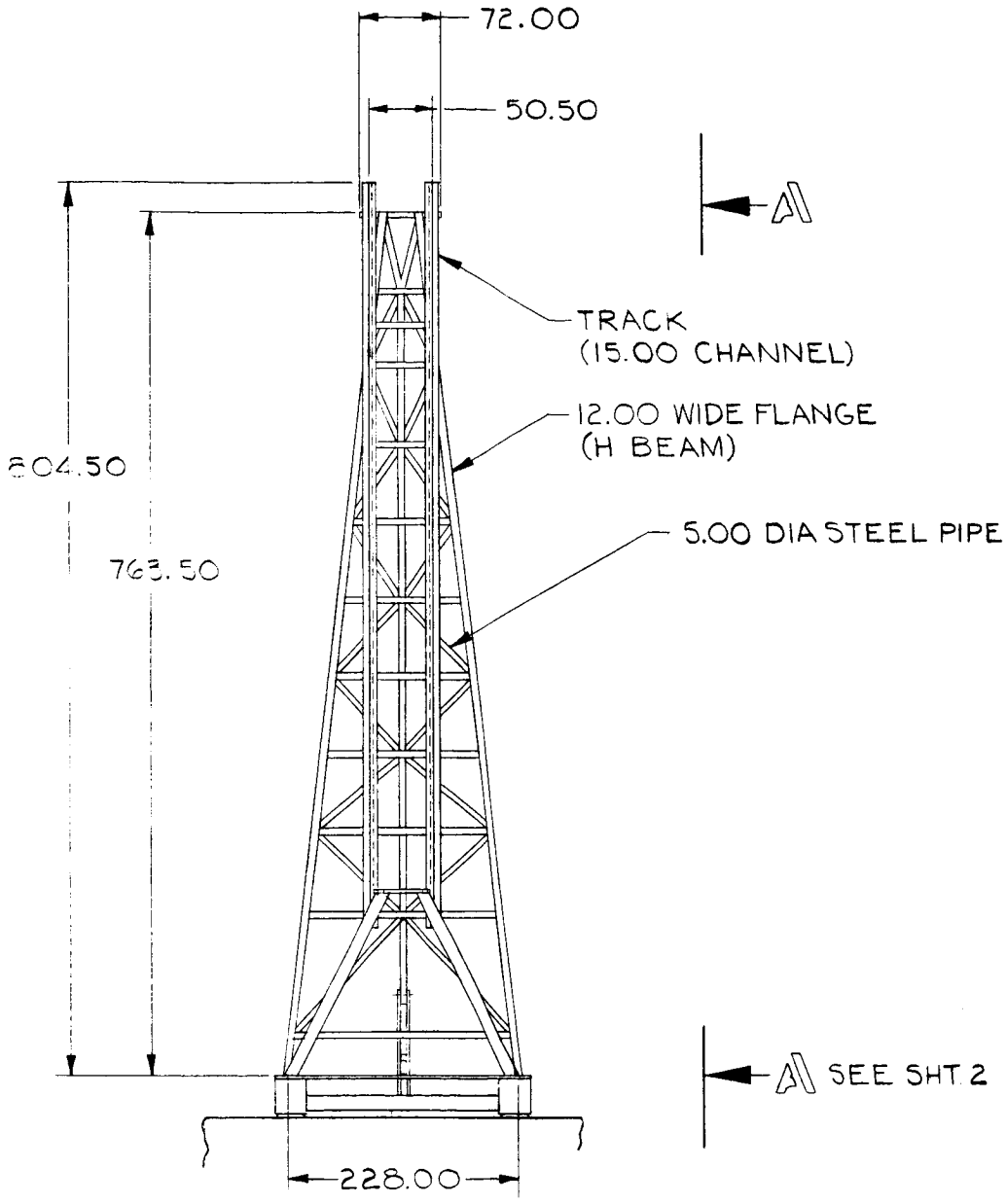

SCALE. 12=1 FT. SHT. 1

Mod 260 Ignition Motor Retention-and-Release System Tower Assembly

Figure 16, Sheet 1 of 2

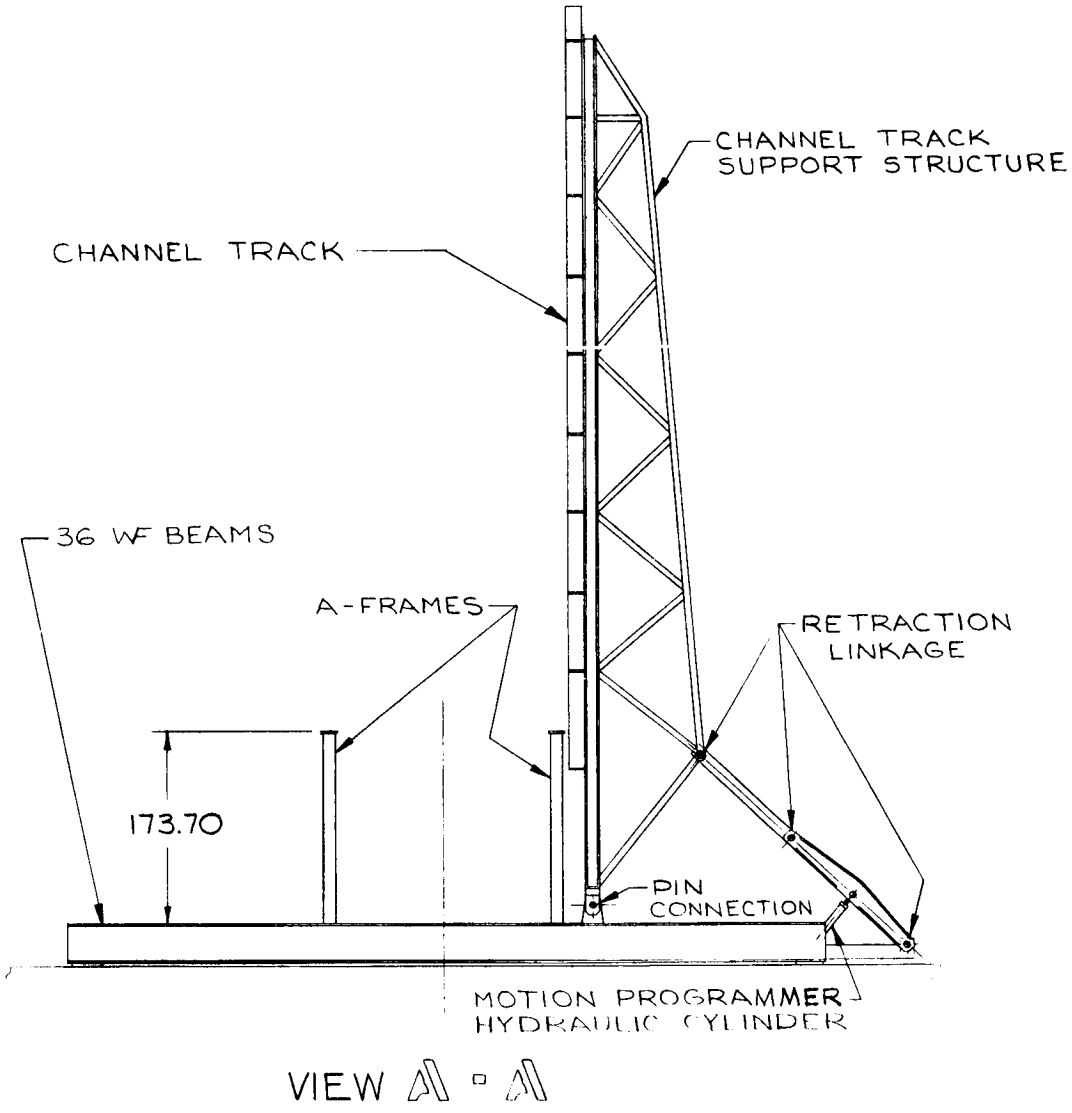

SCALE.12=1 FT. SHT. 2

Mod 260 Ignition Motor Retention-and-Release System Tower Assembly

Figure 16, Sheet 2 of 2

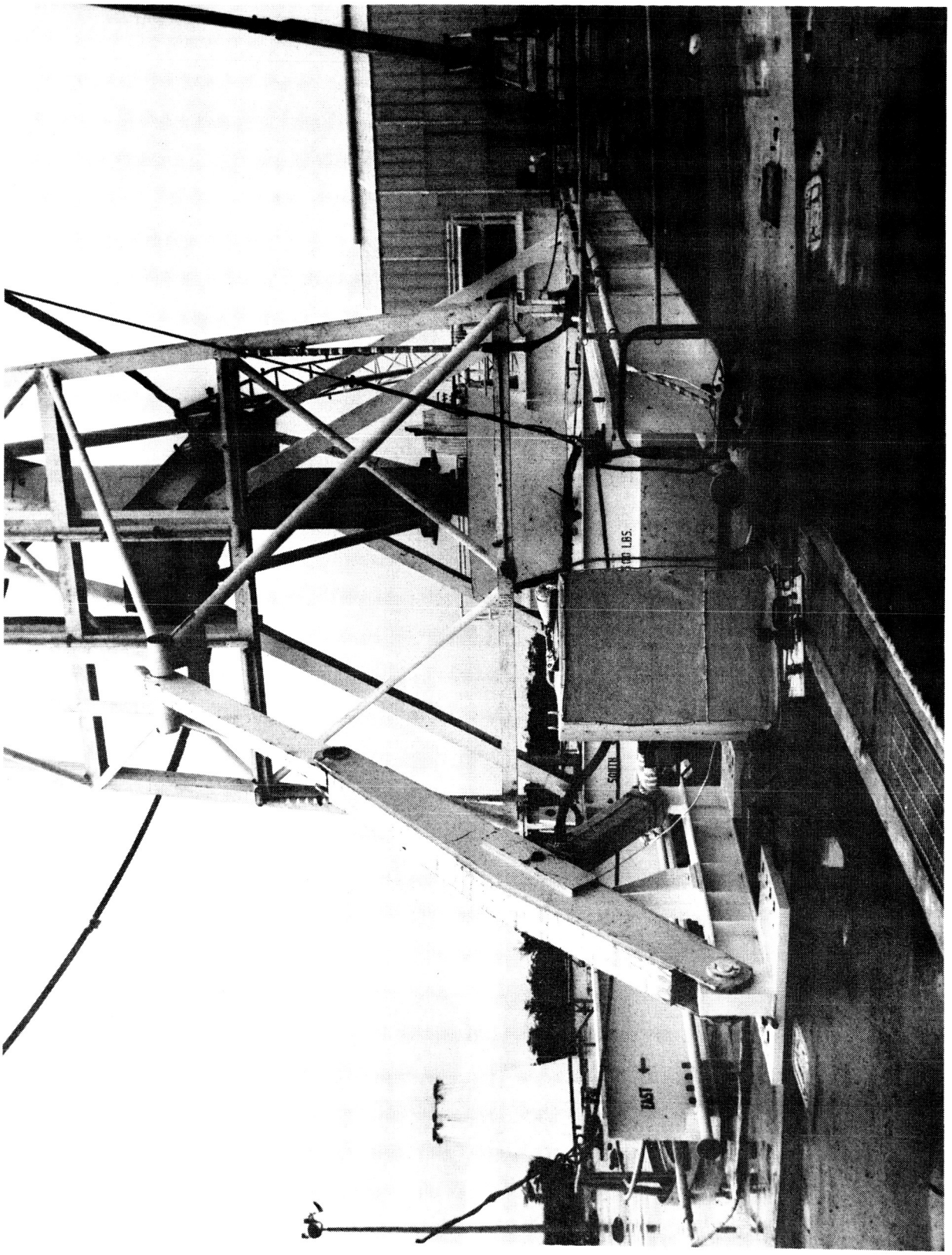

Mod 260 Ignition Motor Retention-and-Release System Tower Assembly
Retraction Linkage and Motion Programmer

Figure 17

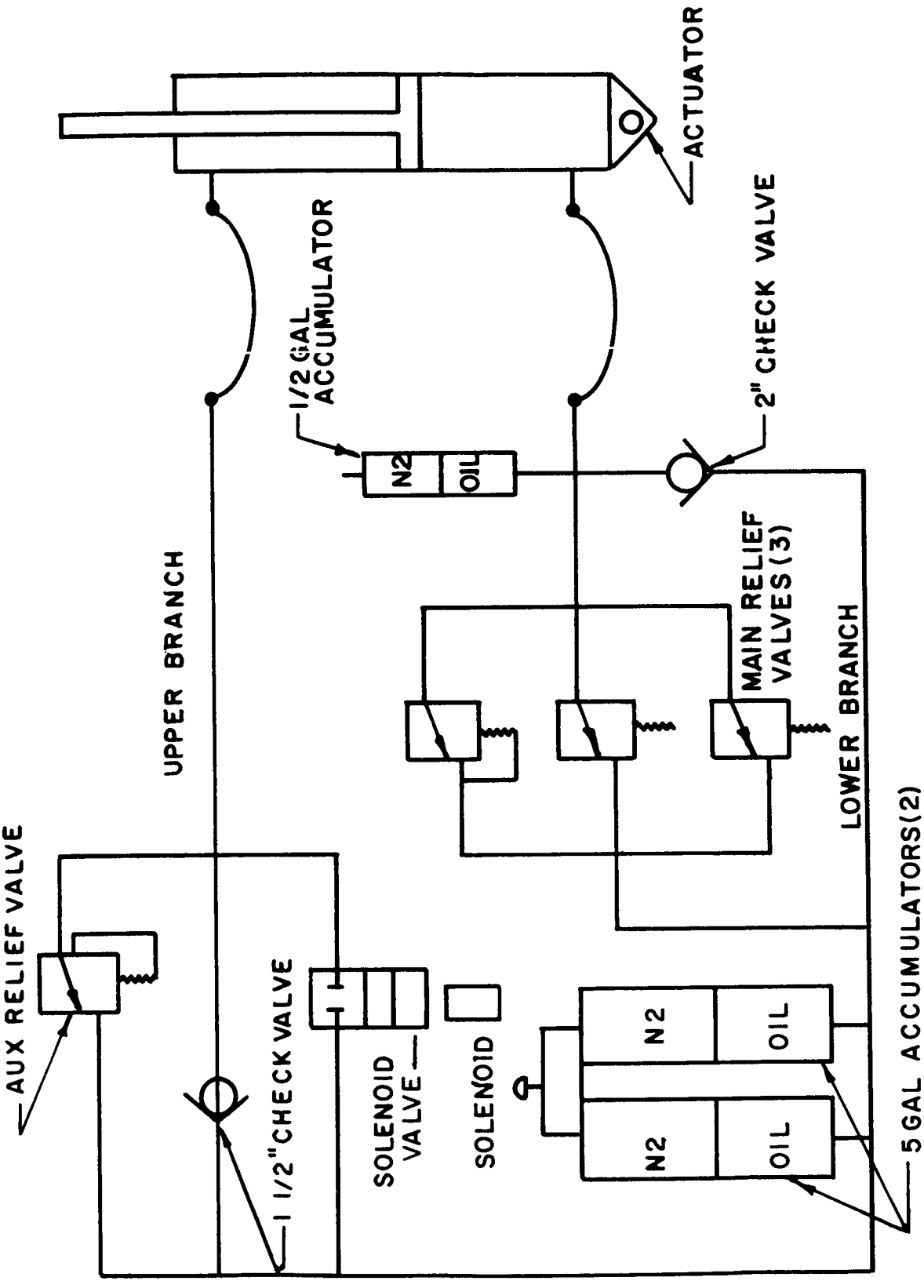

Tower Assembly Retraction Motion Programmer Hydraulic Circuit

Figure 18

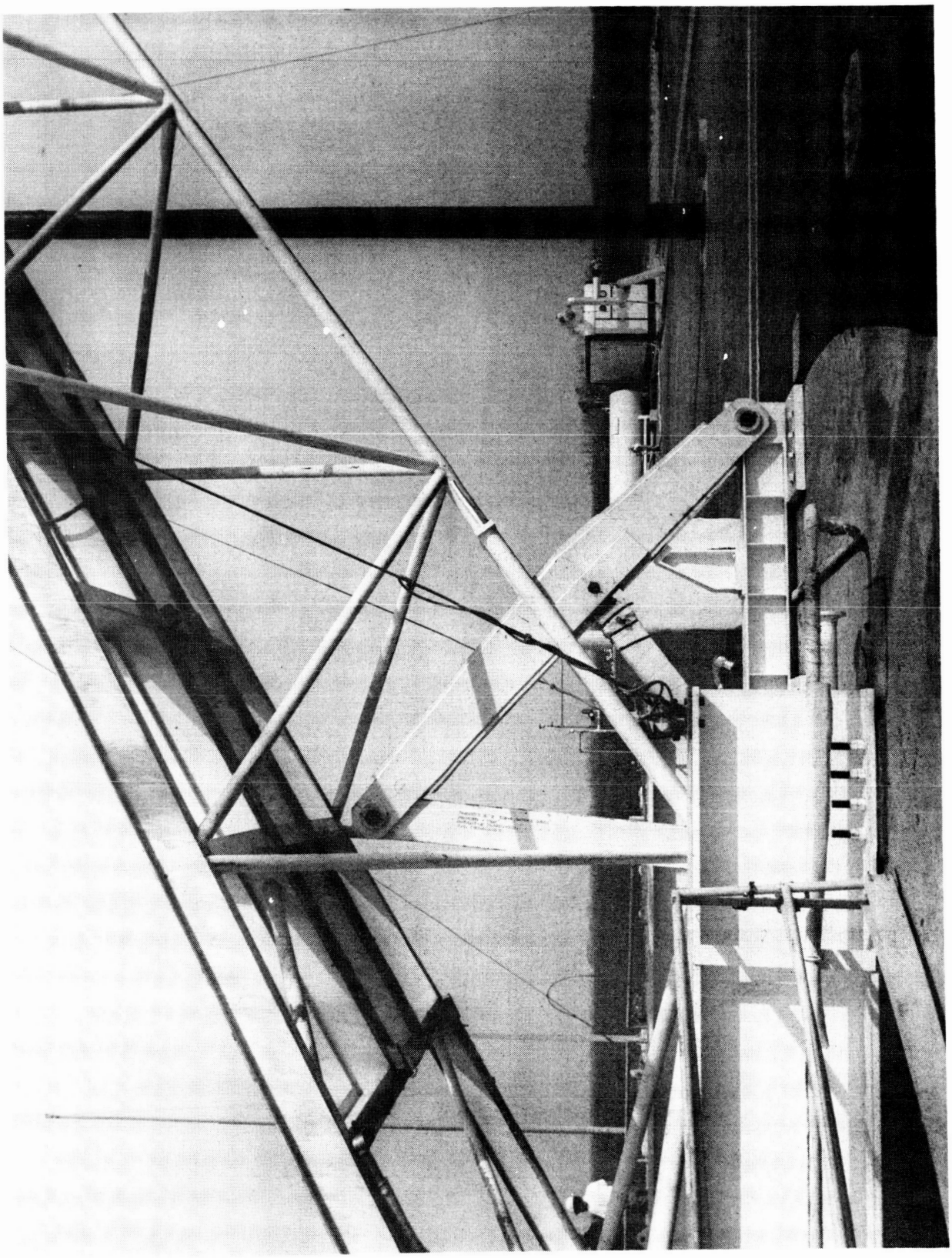

Position of Retention-and-Release System Tower Assembly at End of Retraction Cycle

Figure 19

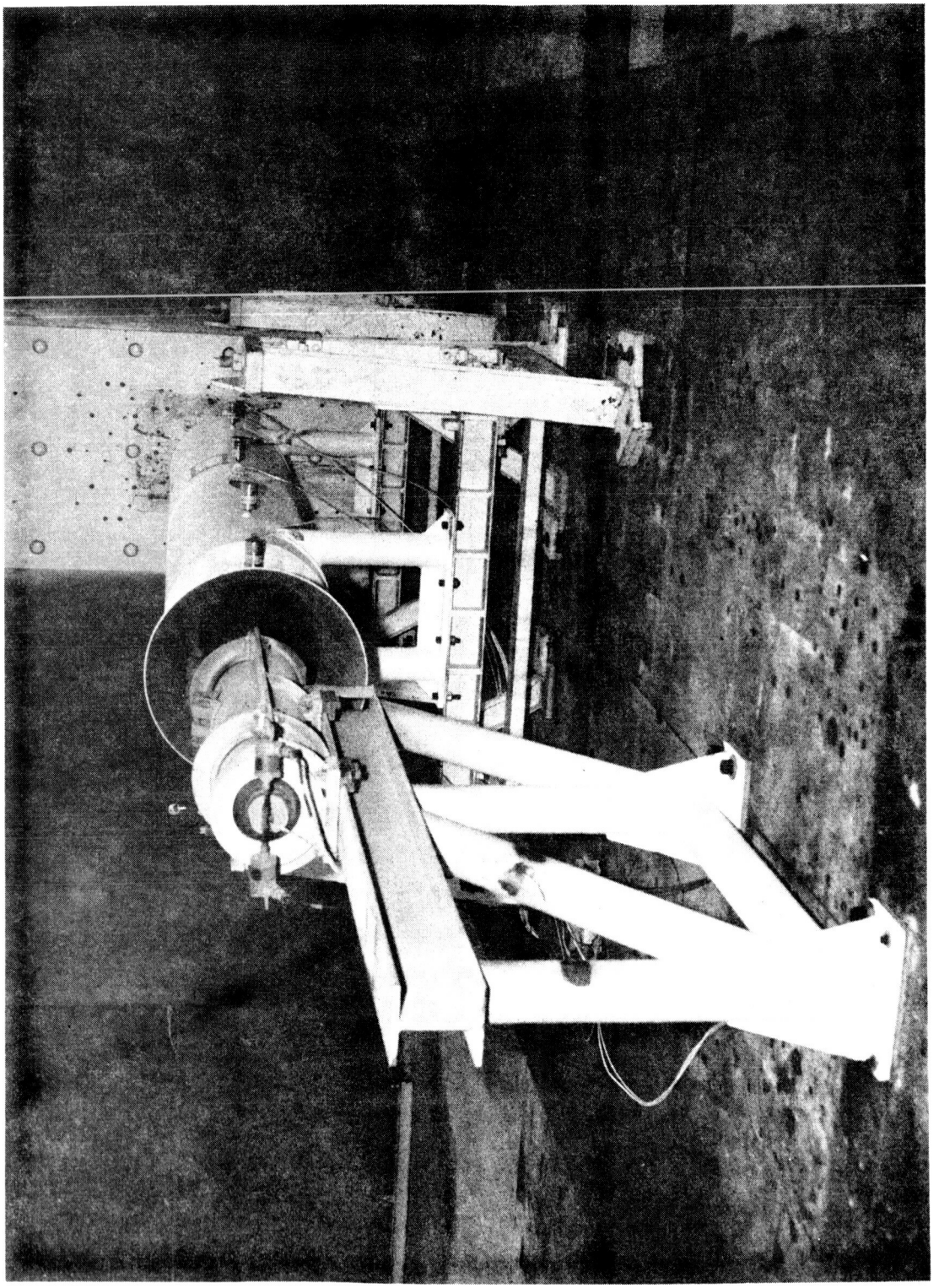

44-SS Ignition Motor Retention-and-Release System

Figure 20

Propellant Batch No.	Max. Tensile Strength psi	Elong. at Max. Tensile Strength %	Initial Modulus psi	Liquid Strand Burning Rate @1000 psia, in./sec	@1500 psia, in./sec n	3KS-500 Burning Rate Data @ 1000 psia, in./sec	n	Batch Size	Used in Ignition Motor
4-MM1-3	111	56	323	0.85	1.04 0.48	0.80*	----	1800	260-IM-01
4-MM1-4	97	52	304	0.86	1.04 0.49	----	----	1800	260-IM-02 & 03
4-MM1-5	Batch rejected, failed to cure to the minimum required 35 Shore "A" hardness							1800	----
4-MM1-6	124	42	441	0.83	1.02 0.49	0.71*	----	1800	260-IM-03
4-MM1-7	Batch rejected, failed to cure to the minimum required 35 Shore "A" hardness							1800	----
4-MM1-8	97	44	330	0.84	1.03 0.49	----	----	1800	260-IM-04 & 05
4-MM1-9	Batch rejected, failed to cure to the minimum required 35 Shore "A" hardness							1800	----
4-MM1-10	Batch rejected, failed to cure to the minimum required 35 Shore "A" hardness							1800	----
4-MM1-11	169	35	672	0.85	1.04 0.49	----	----	1800	260-IM-04 & 05
				Test Batches					
4-MM1-1	156	38	590	0.83	1.01 0.49	0.81	0.33	1800	----
4-MM1-2	46	53	166	0.86	1.03 0.48	0.81	0.36	1800	----
				Batches Used in 44-SS Ignition Motors					
64-636	95	50	272	0.85	1.03 0.48	0.81**	----	60	44SS-IM-01 & 02
64-666	174	33	699	0.85	1.06 0.48	0.82**	----	60	44SS-IM-01 thru 06
64-734	151	36	623	0.86	1.05 0.48	----	----	60	44SS-IM-05 & 06
64-769	131	34	529	0.87	1.06 0.49	0.83**	----	60	44SS-IM-03 & 04

* These are the observed burning rates of the propellant from the 260-SL ignition motor tests.

** These are the observed burning rates of the propellant from the 44-SS ignition motor tests.

Properties of ANP-2758 Mod 1 Propellant

Figure 21

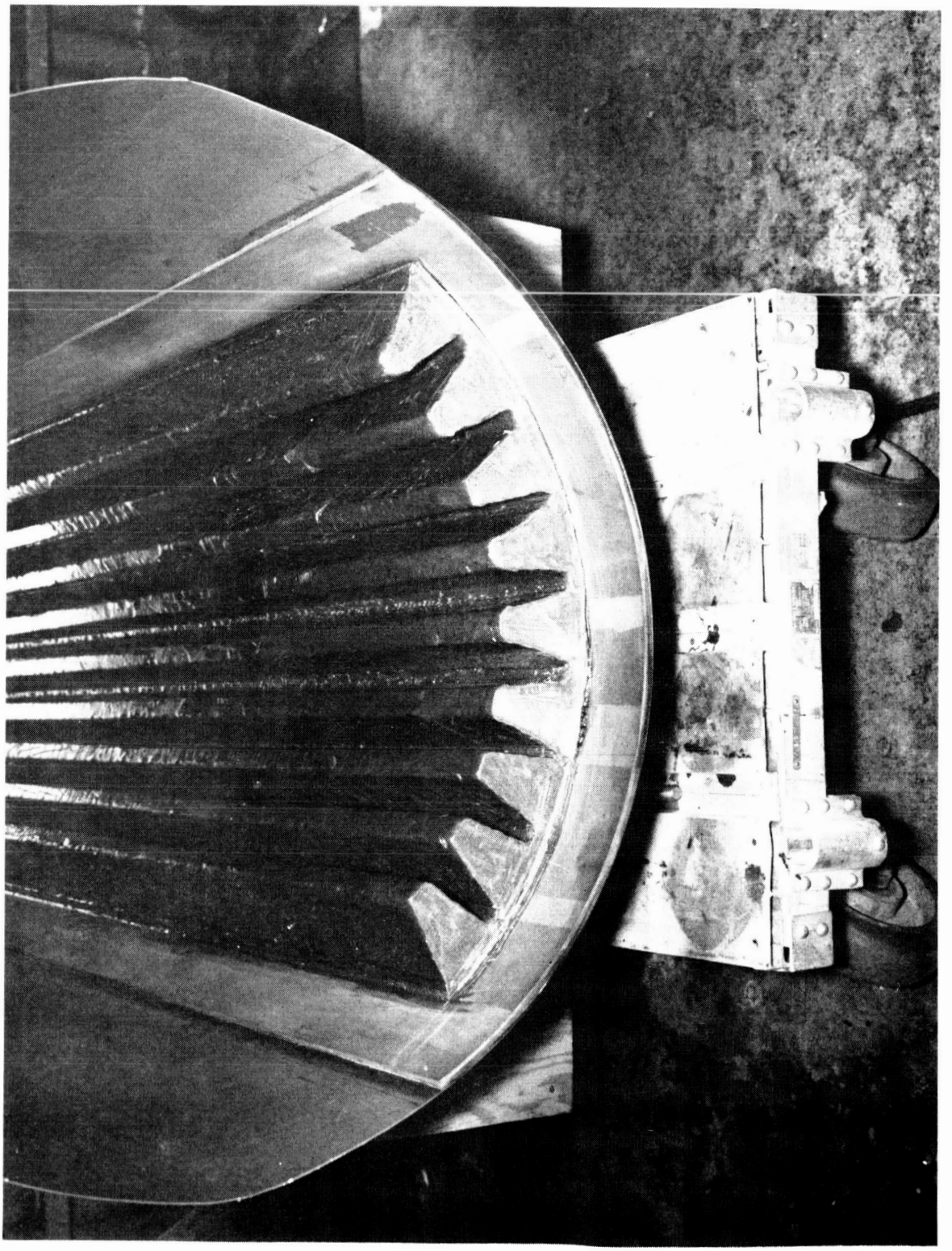

Molded Slabs of ANP-2758 Mod 1 Propellant Installed in Simulated Igniter Chamber

Figure 22

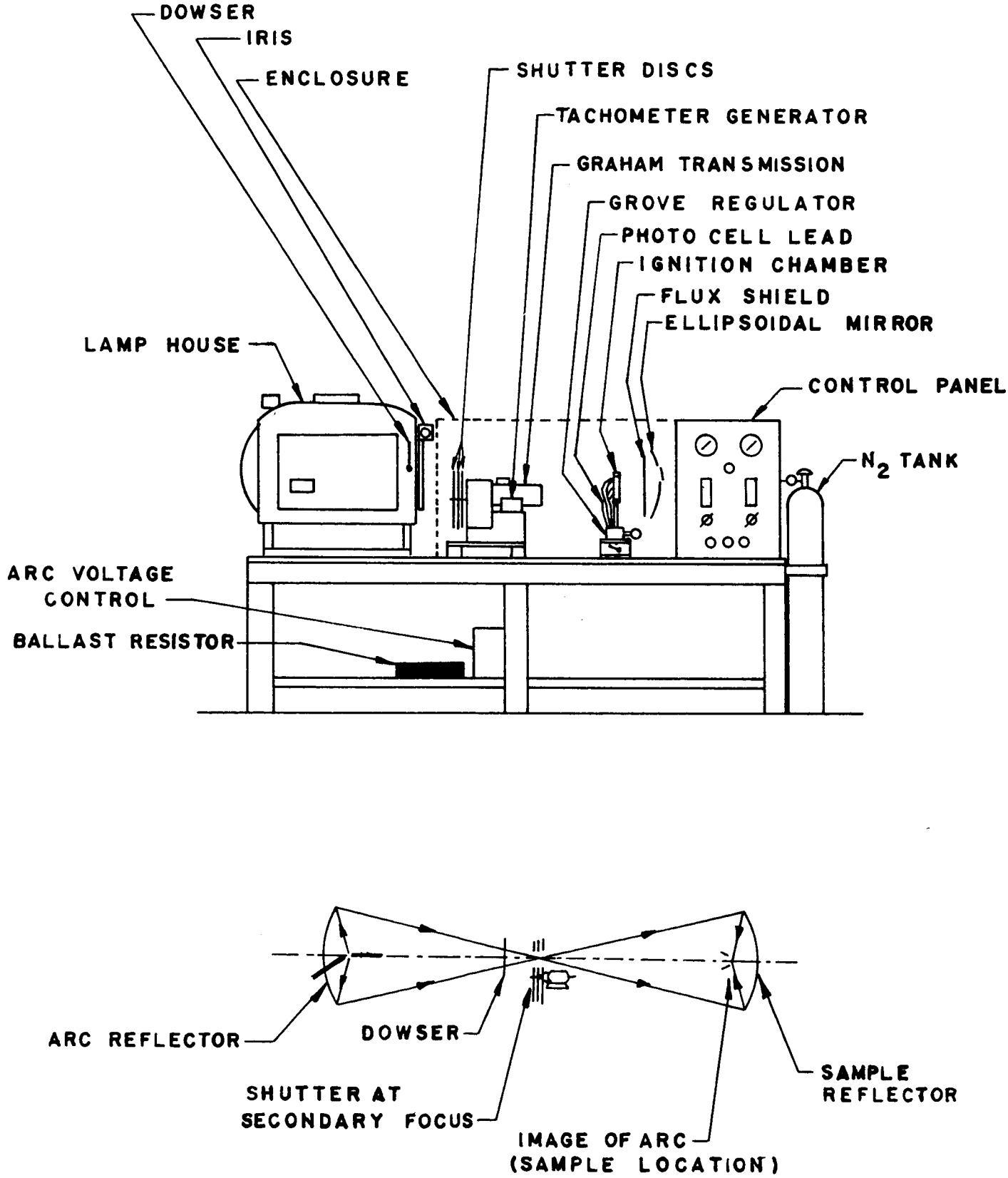

Schematic Diagram of Arc-Image Furnace

Figure 23

Propellant Sample Pressure, psig	Time to Propellant Ignition, sec	Threshold Ignition Energy, cal/cm^2
	FLUX RATE, 70 CAL/CM^2-SEC	
1.5	0.056 ± 0.004	3.9 ± 0.3
25	0.049 ± 0.003	3.4 ± 0.2
50	0.042 ± 0.002	2.95 ± 0.15
100	0.0355 ± 0.0015	2.5 ± 0.1
200	0.0355 ± 0.0015	2.5 ± 0.1
	FLUX RATE, 100 CAL/CM^2-SEC	
1.5	0.033 ± 0.001	3.3 ± 0.1
25	0.0275 ± 0.0008	2.75 ± 0.08
50	0.024 ± 0.001	2.4 ± 0.1
100	0.0213 ± 0.0005	2.13 ± 0.05
200	0.0192 ± 0.0008	1.92 ± 0.08

Threshold Ignition Energy for ANB-3105 Propellant

Figure 24

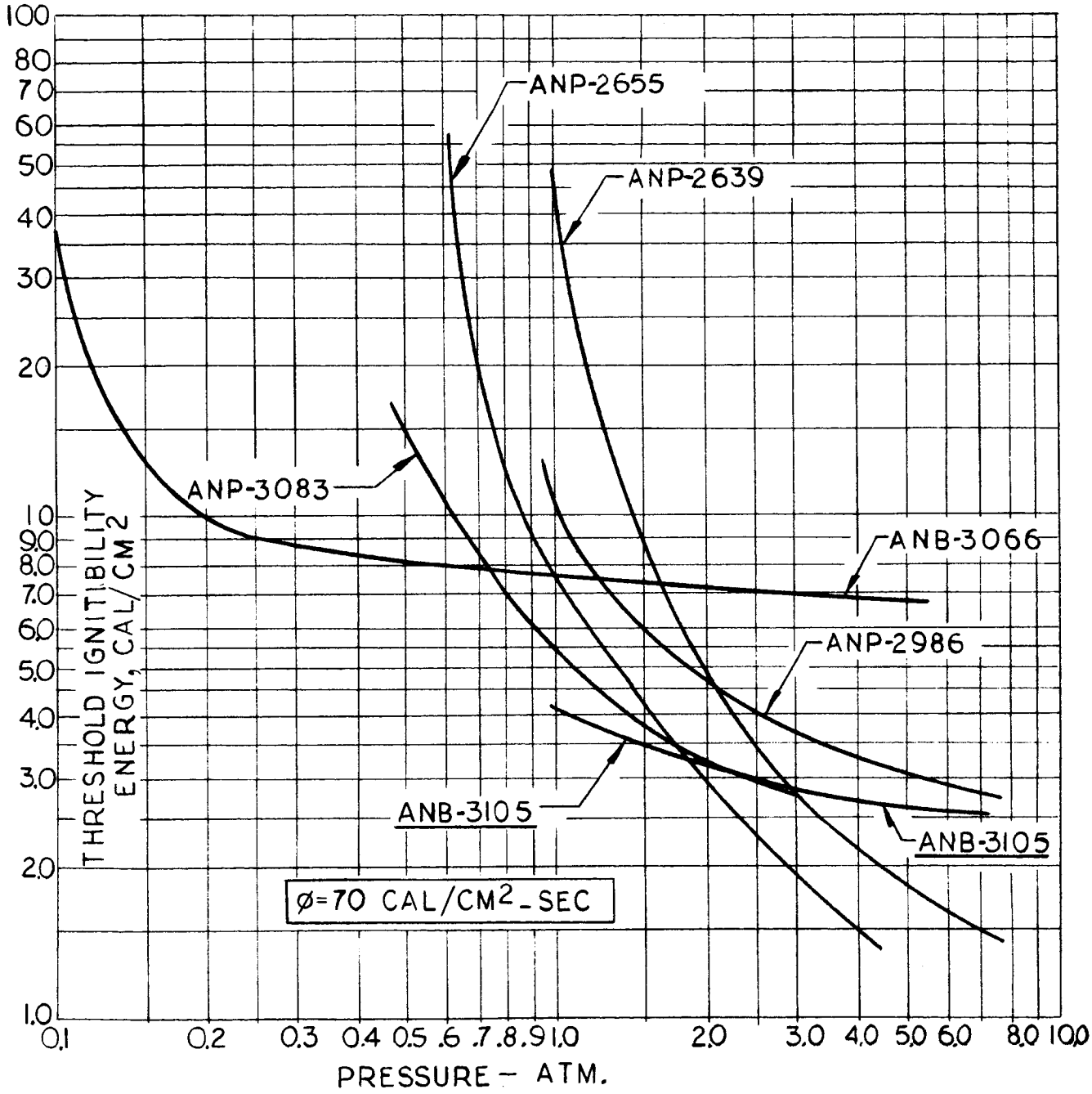

260-SL Motor Propellant, ANB-3105, Arc-Image Furnace Ignitability Date

Figure 25

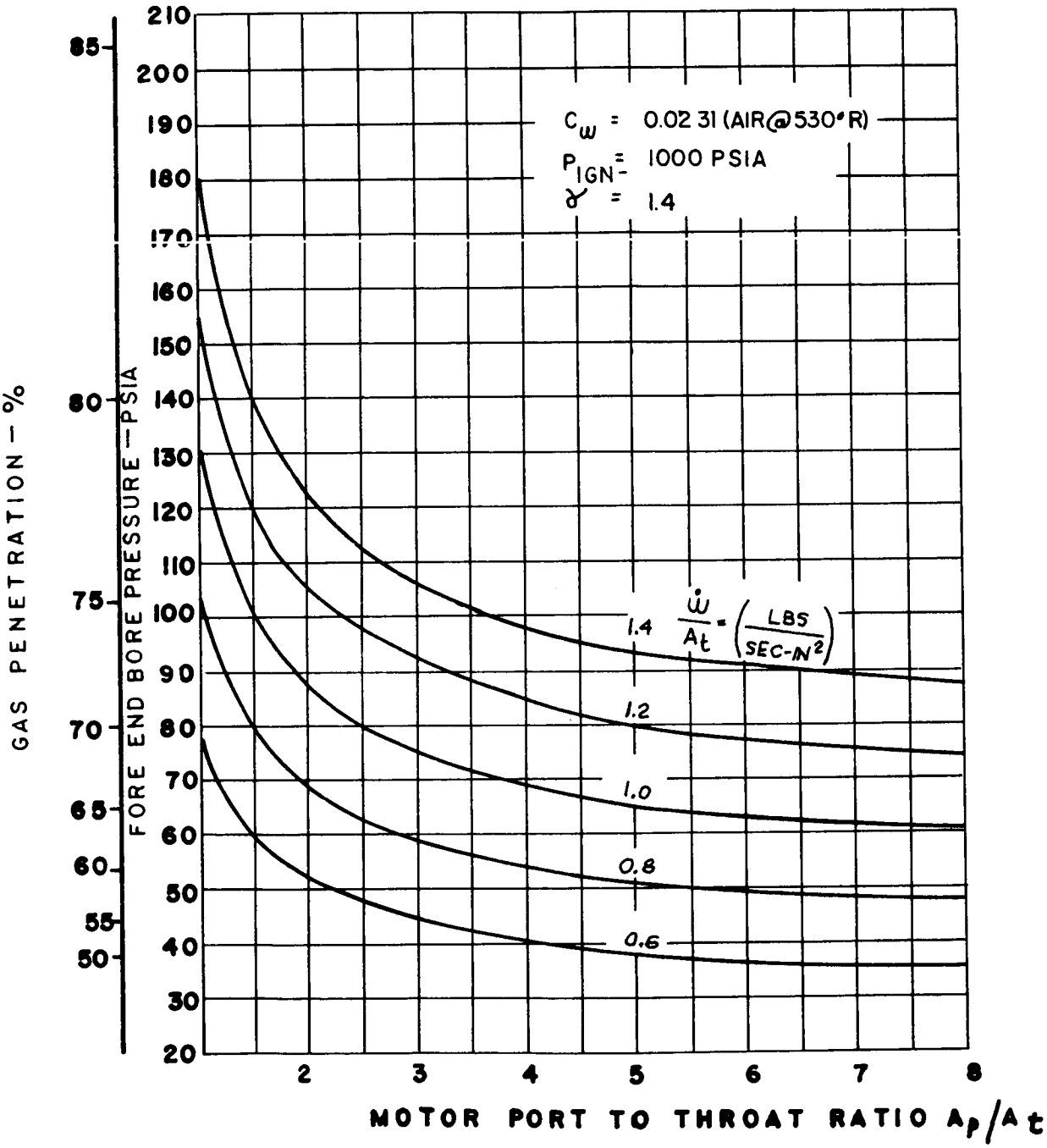

Motor Bore Pressure and Gas Penetration Plotted as Functions of Igniter Mass Flow and Motor Size for the Nitrogen-Air System

Figure 26

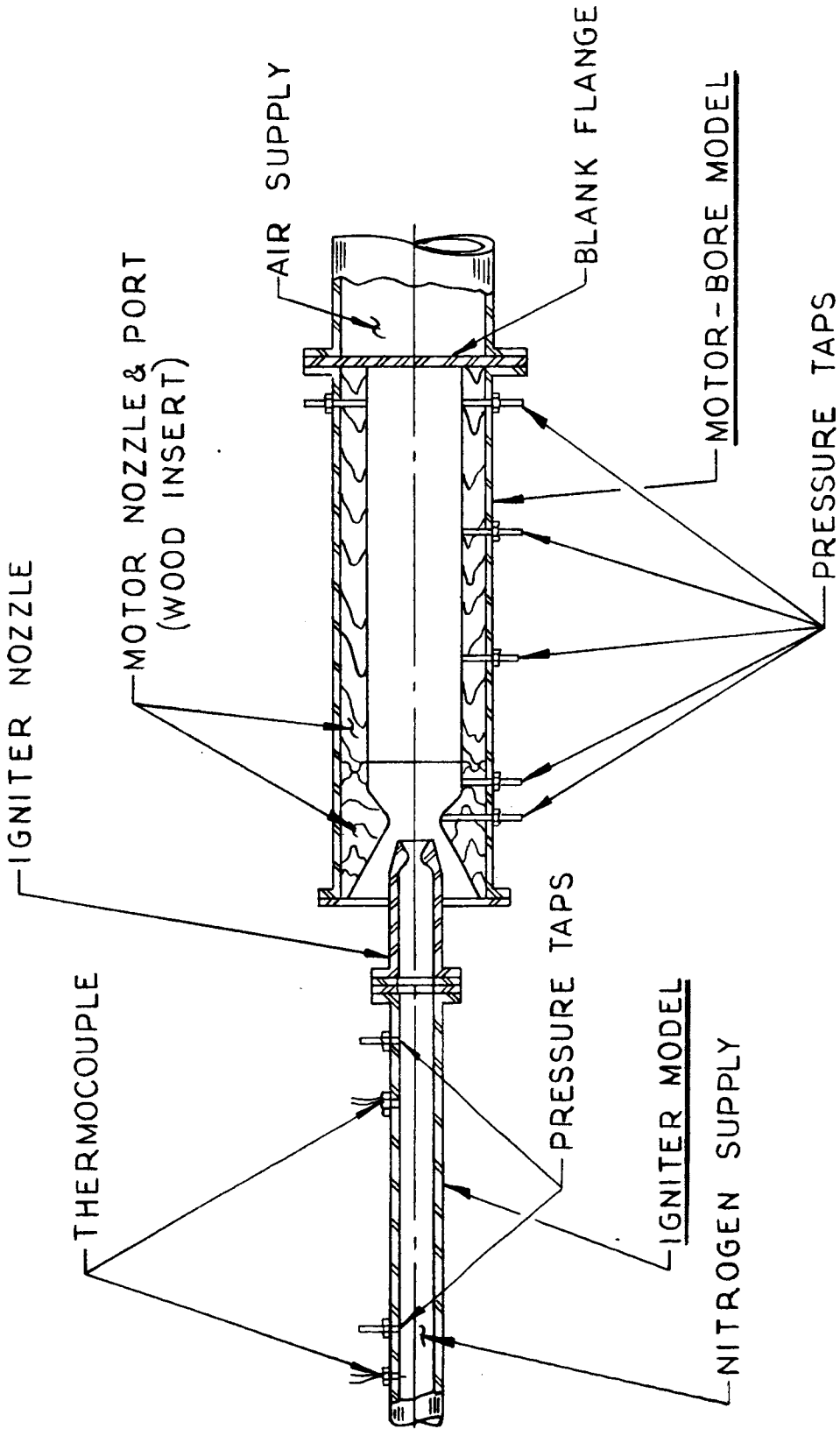

Schematic Diagram of Cold-Flow Test Equipment

Figure 27

Run No.	$\frac{A_p}{A_t}$	Igniter Nozzle Diameter, in.	*	Throat Pressure, psi	Throat Entrance Pressure, psi	Chamber Pressure, (1) psi	Chamber Pressure, (2) psi	Fore End Chamber Pressure, psi	Igniter Pressure, (avg of 2) psi	Nitrogen Total Temperature, °R
1	3	0.739	1.3	38	51	57	57	58	488	494
2	3	0.739	1.3	38	58	64	64	65	572	496
3	3	0.739	1.3	40	68	76	74	76	676	499
4	3	0.739	1.3	45	77	86	84	85	770	500
5	3	0.739	1.3	53	86	97	95	96	865	504
6	3	0.739	1.3	61	98	110	108	109	983	508
7	3	0.739	1.55	39	50	55	54	55	495	496
8	3	0.739	1.55	40	57	63	63	63	585	498
9	3	0.739	1.55	45	68	75	72	74	676	500
10	3	0.739	1.55	49	78	85	84	84	782	504
11	3	0.739	1.55	58	90	98	96	97	877	507
12	3	0.739	1.55	65	100	110	108	108	985	511
13	3	0.739	1.8	45	53	56	56	57	531	486
14	3	0.739	1.8	45	60	64	64	65	633	494
15	3	0.739	1.8	51	71	74	74	75	728	496
16	3	0.739	1.8	61	85	88	88	89	837	504
17	3	0.739	1.8	72	98	100	100	101	946	513
18	3	0.64	1.3	38	53	59	58	58	680	498
19	3	0.64	1.3	41	67	75	73	75	884	503
20	3	0.64	1.3	38	44	48	47	48	492	496
21	3	0.64	1.3	38	48	53	52	53	585	506
22	3	0.64	1.3	37	59	66	65	66	781	503
23	3	0.64	1.3	45	73	82	81	82	983	509
24	3	0.64	1.55	41	47	49	49	50	575	487
25	3	0.64	1.55	40	52	55	56	57	690	490

(1) Pressure tap located 16 in. from fore-end pressure tap.

(2) Pressure tap located 8 in. from fore-end pressure tap.

Cold-Flow Test Data

Figure 28, Sheet 1 of 4

Run No.	$\frac{A_p}{A_t}$	Igniter Nozzle Diameter, in.	*	Throat Pressure, psi	Throat Entrance Pressure, psi	Chamber Pressure, (1) psi	Chamber Pressure, (2) psi	Fore End Chamber Pressure, psi	Igniter Pressure, (avg of 2) psi	Nitrogen Total Temperature, °R
26	3	0.64	1.55	41	59	62	62	64	790	493
27	3	0.64	1.55	46	67	70	70	72	877	497
28	3	0.64	1.55	51	76	80	80	81	990	500
29	3	0.64	1.8	45	49	52	51	53	581	498
30	3	0.64	1.8	41	56	60	60	59	772	504
31	3	0.64	1.8	52	74	78	77	79	983	512
32	3	0.522	1.3	36	42	45	45	46	695	497
33	3	0.522	1.3	37	45	48	49	49	800	500
34	3	0.522	1.3	37	47	51	51	53	904	502
35	3	0.522	1.3	33	50	55	56	57	1020	505
36	3	0.522	1.55	46	48	48	58	49	705	494
37	3	0.522	1.55	42	45	47	47	49	800	497
38	3	0.522	1.55	37	48	49	50	50	900	499
39	3	0.522	1.55	36	49	53	53	54	1010	502
40	3	0.522	1.8	45	46	47	47	48	708	501
41	3	0.522	1.8	47	48	49	49	50	791	503
42	3	0.522	1.8	46	50	57	57	53	902	505
43	3	0.522	1.8	45	52	55	55	56	1026	508
44	1.3	0.739	1.3	31	(3)	64	64	66	496	495
45	1.3	0.739	1.3	32	(3)	73	72	75	569	493
46	1.3	0.739	1.3	35	(3)	86	86	88	677	501
47	1.3	0.739	1.3	38	(3)	95	94	96	740	505
48	1.3	0.739	1.3	45	(3)	113	112	116	891	511
49	1.3	0.739	1.3	48	(3)	123	122	123	969	517
50	1.3	0.739	1.55	36	57	64	64	66	526	494

(1) Pressure tap located 16 in. from fore-end pressure tap.

(2) Pressure tap located 8 in. from fore-end pressure tap.

(3) Polarity was reversed on the oscillograph and data were not recorded.

Cold-Flow Test Data

Figure 28, Sheet 2 of 4

Run No.	$\frac{A_p}{A_t}$	Igniter Nozzle Diameter, in.	*	Throat Pressure, psi	Throat Entrance Pressure, psi	Chamber Pressure,(1) psi	Chamber Pressure,(2) psi	Fore End Chamber Pressure, psi	Igniter Pressure, (avg of 2) psi	Nitrogen Total Temperature, °R
51	1.3	0.739	1.55	36	65	75	74	77	617	492
52	1.3	0.739	1.55	42	77	86	86	88	715	498
53	1.3	0.739	1.55	46	86	97	97	99	805	505
54	1.3	0.739	1.55	54	98	109	108	112	906	513
55	1.3	0.739	1.8	39	56	60	59	61	520	492
56	1.3	0.739	1.8	38	64	70	69	71	626	495
57	1.3	0.739	1.8	43	77	80	80	83	715	497
58	1.3	0.739	1.8	49	87	91	91	93	805	500
59	1.3	0.739	1.8	58	98	102	101	104	890	504
60	1.3	0.64	1.3	35	43	47	47	48	415	498
61	1.3	0.64	1.3	35	45	53	53	54	520	500
62	1.3	0.64	1.3	32	48	60	59	61	610	500
63	1.3	0.64	1.3	32	54	68	68	59	715	502
64	1.3	0.64	1.3	35	60	78	77	79	805	504
65	1.3	0.64	1.3	38	68	88	88	89	910	508
66	1.3	0.64	1.3	42	77	98	97	99	1017	510
67	1.3	0.64	1.55	36	48	54	54	55	580	498
68	1.3	0.64	1.55	34	54	64	64	65	710	501
69	1.3	0.64	1.55	38	66	76	76	77	836	504
70	1.3	0.64	1.55	36	60	69	69	71	775	502
71	1.3	0.64	1.55	39	69	80	79	81	872	504
72	1.3	0.64	1.55	42	79	89	89	91	993	508
73	1.3	0.64	1.8	48	53	55	54	56	590	498
74	1.3	0.64	1.8	39	54	59	59	60	686	501
75	1.3	0.64	1.8	39	60	66	66	68	785	505

(1) Pressure tap located 16 in. from fore-end pressure tap.

(2) Pressure tap located 8 in. from fore-end pressure tap.

Cold-Flow Test Data

Figure 28, Sheet 3 of 4

Run No.	$\frac{A_p}{A_t}$	Igniter Nozzle Diameter, in.	*	Throat Pressure, psi	Throat Entrance Pressure, psi	Chamber Pressure,(1) psi	Chamber Pressure,(2) psi	Fore End Chamber Pressure, psi	Igniter Pressure, (avg of 2) psi	Nitrogen Total Temperature, °R
76	1.3	0.64	1.8	47	79	85	85	86	995	513
77	1.3	0.64	1.8	41	69	77	76	77	892	515
78	1.3	0.522	1.3	33	42	46	45	57	616	501
79	1.3	0.522	1.3	35	45	50	50	51	715	503
80	1.3	0.522	1.3	31	45	56	56	57	822	506
81	1.3	0.522	1.3	28	49	64	63	65	974	510
82	1.3	0.522	1.55	43	45	48	48	49	626	503
83	1.3	0.522	1.55	42	48	51	51	52	730	504
84	1.3	0.522	1.55	33	47	54	54	55	850	507
85	1.3	0.522	1.55	31	49	59	58	59	937	509
86	1.3	0.522	1.8	44	46	47	47	48	635	505
87	1.3	0.522	1.8	46	49	51	50	51	740	508
88	1.3	0.522	1.8	45	51	54	54	55	840	510
89	1.3	0.522	1.8	42	53	58	57	59	936	510

(1) Pressure tap located 16 in. from fore-end pressure tap.

(2) Pressure tap located 8 in. from fore-end pressure tap.

Cold-Flow Test Data

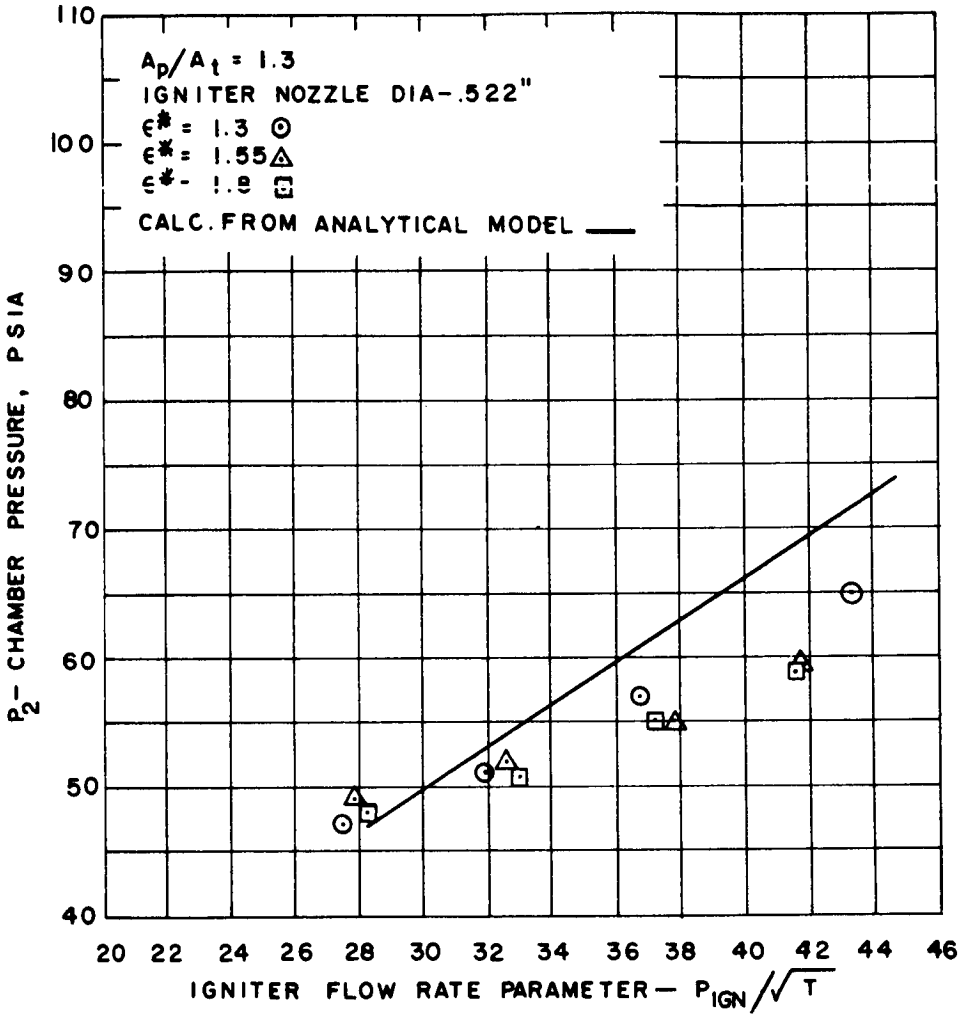

Aft-End Ignition Cold-Flow Test Data for Igniter Model:Throat Diameter of 0.522 in. and Motor-Bore Model Port-to-Throat Ratio of 1.3

Figure 29

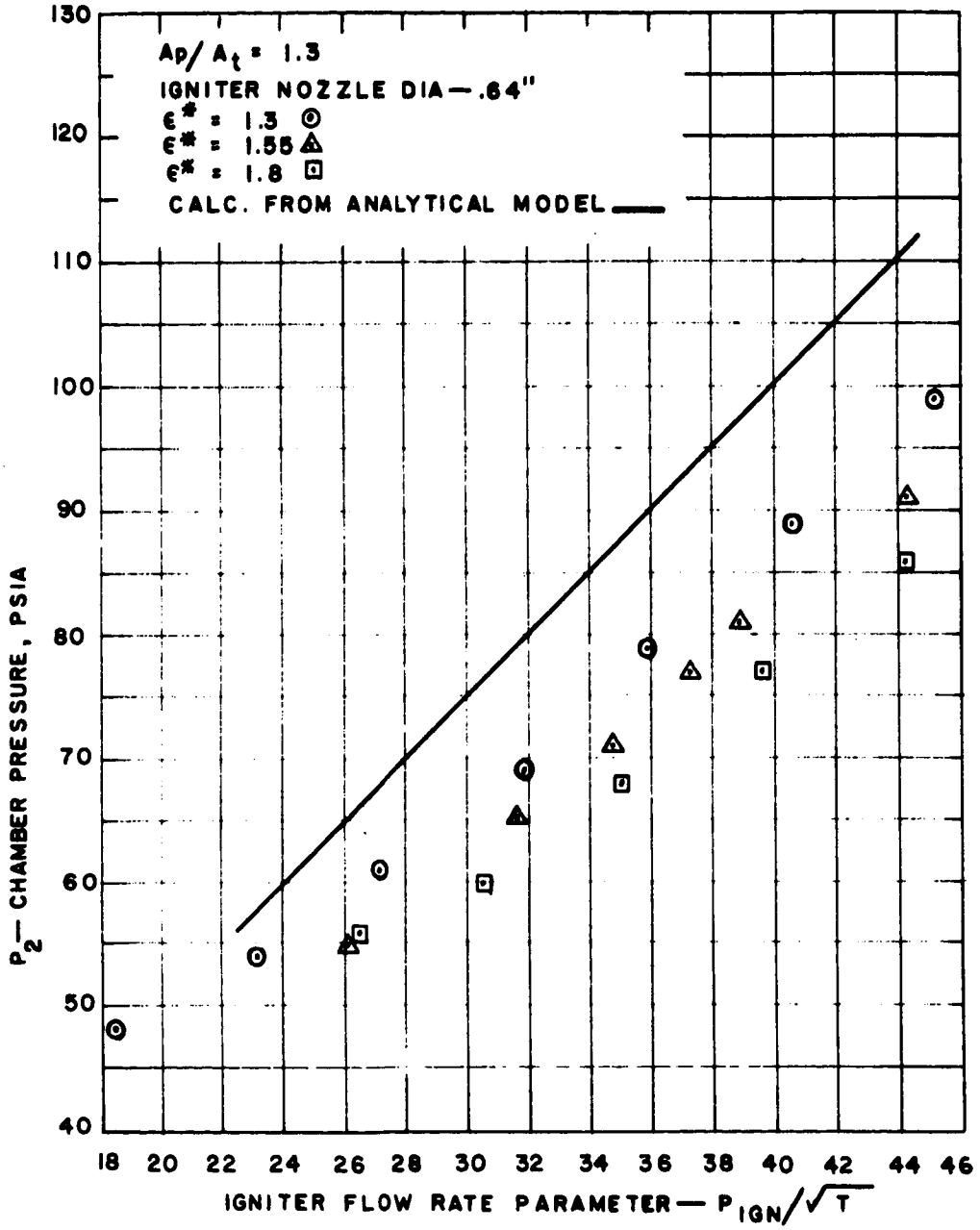

Aft-End Ignition Cold-Flow Test Data for Igniter Model:Throat Diameter of 0.64 in. and Motor-Bore Model Port-to-Throat Ratio of 1.3

Figure 30

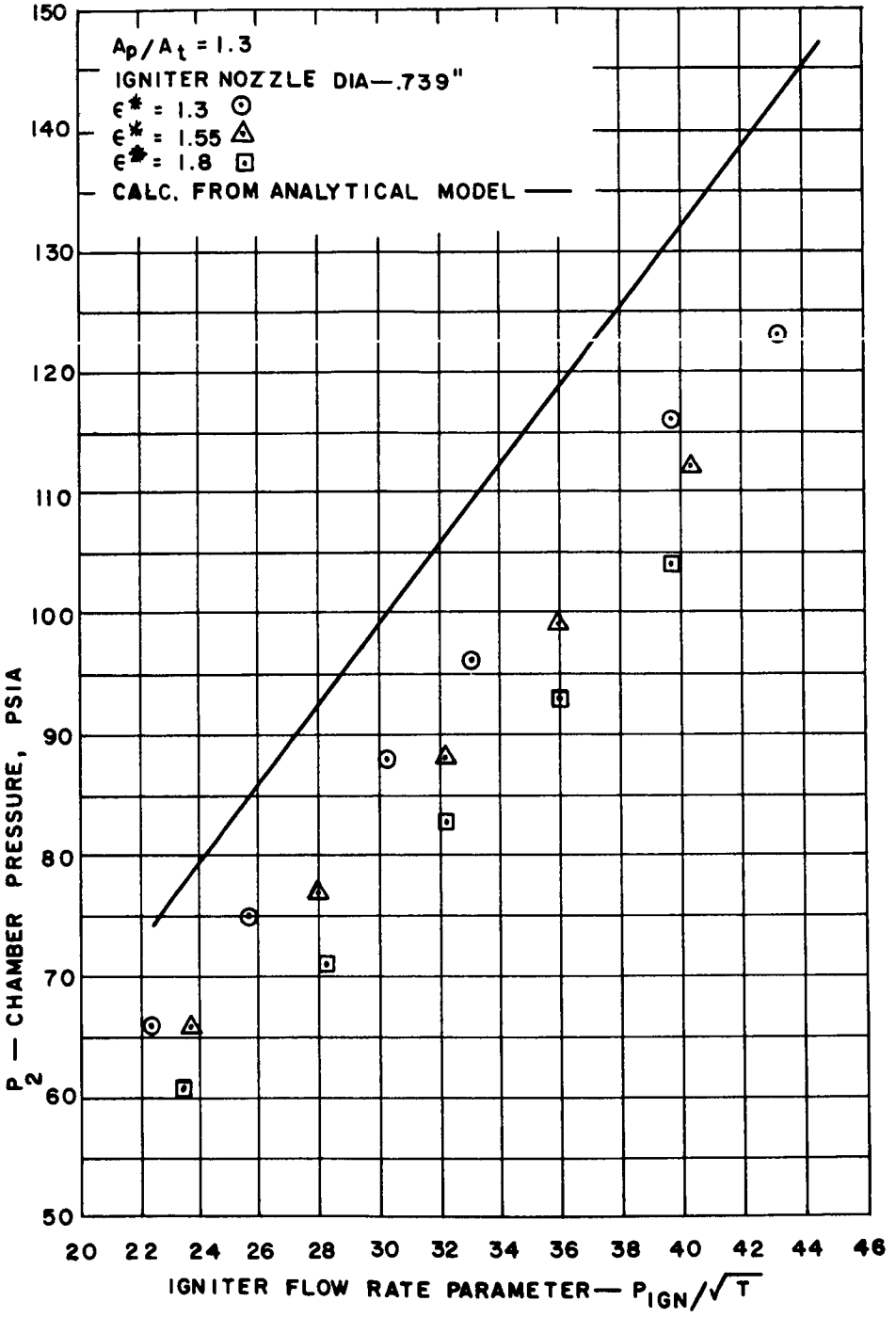

Aft-End Ignition Cold-Flow Test Data for Igniter Model: Throat Diameter of 0.739 in. and Motor-Bore Model Port-to-Throat Ratio of 1.3

Figure 31

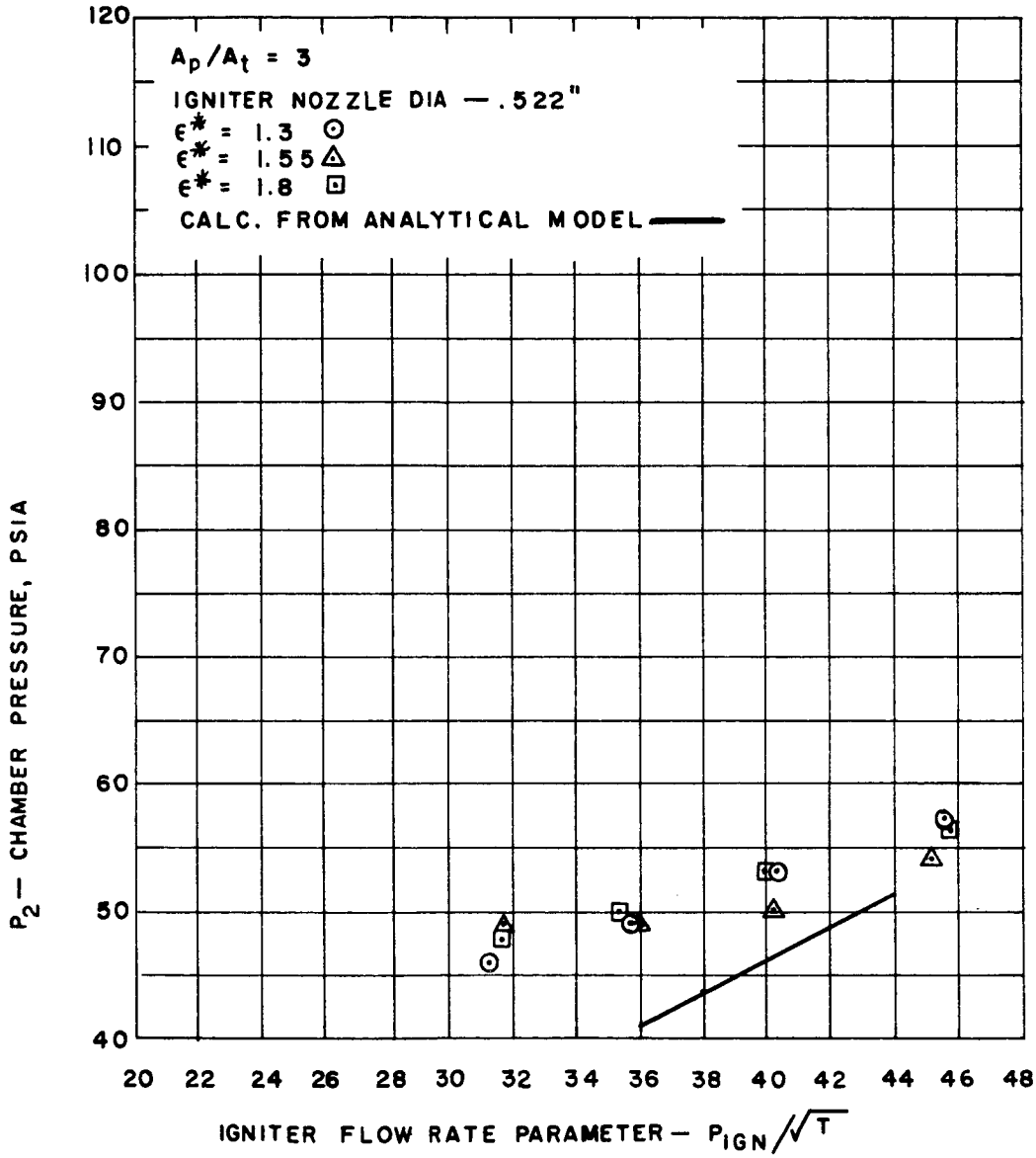

Aft-End Ignition Cold-Flow Test Data for Igniter Model:Throat Diameter of 0.522 in. and Motor-Bore Model Port-to-Throat Ratio of 3.0

Figure 32

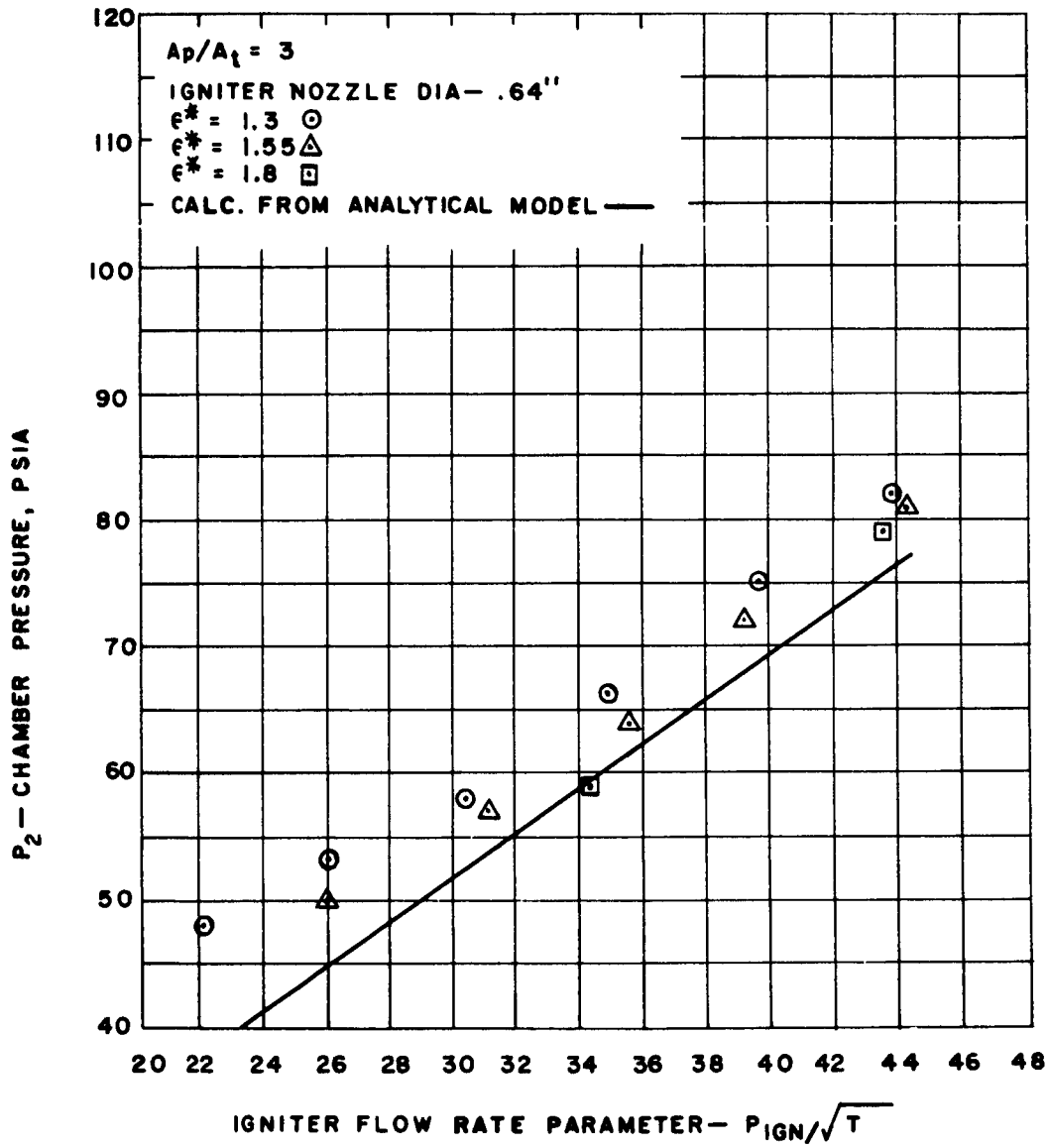

Aft-End Ignition Cold-Flow Test Data for Igniter Model: Throat Diameter of 0.64 in. and Motor-Bore Model Port-to-Throat Ratio of 3.0

Figure 33

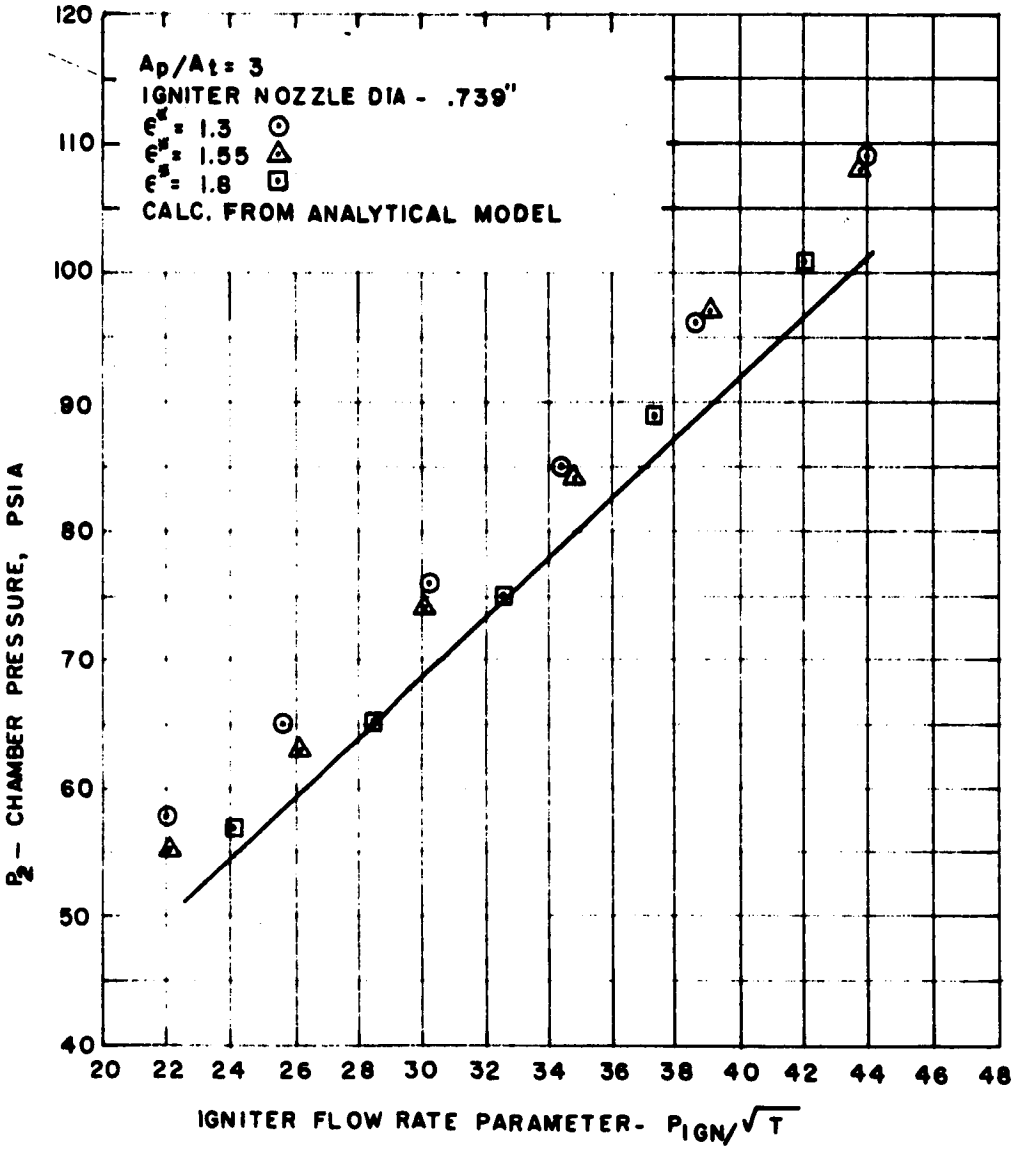

Aft-End Ignition Cold-Flow Test Data for Igniter Model:Throat Diameter of 0.739 in. and Motor-Bore Model Port-to-Throat Ratio of 3.0

Figure 34

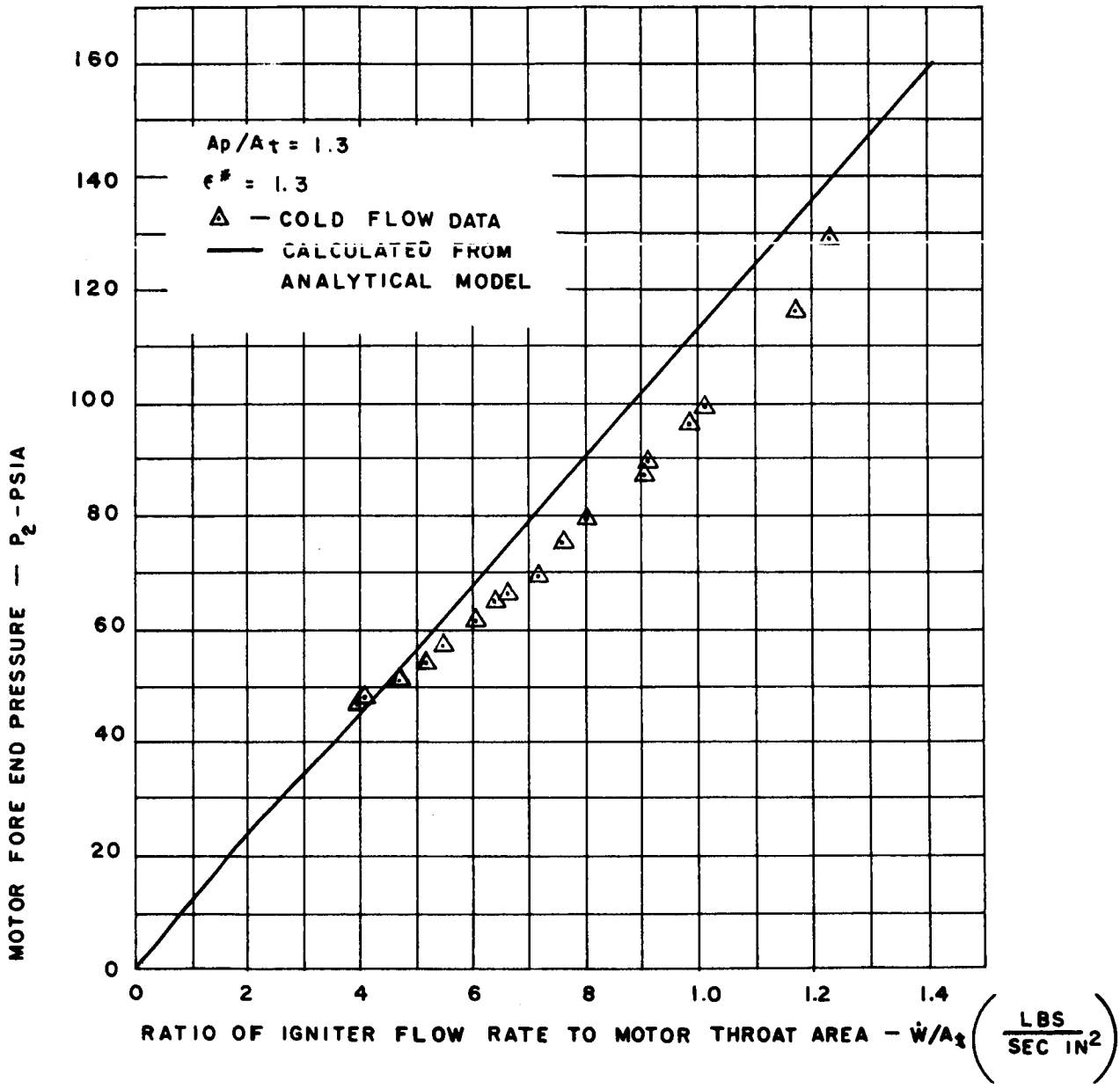

Motor-Bore Model Pressure Plotted as a Function of Igniter Model Flow Rate at Igniter Positions of 1.3 and Motor-Bore Model Port-to-Throat Ratio of 1.3

Figure 35

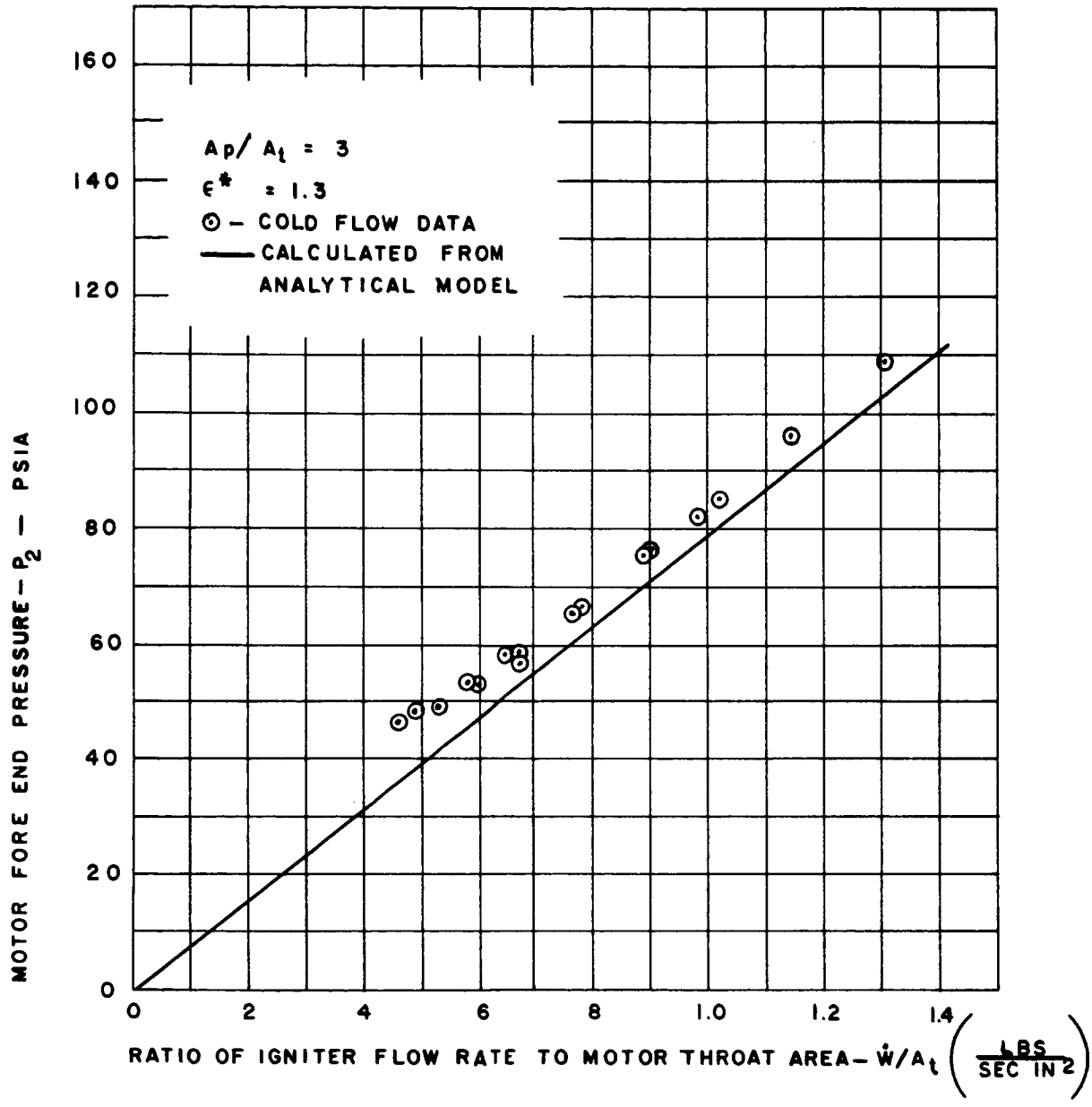

Motor-Bore Model Pressure Plotted as a Function of Igniter Model Flow-Rate at Igniter Positions of 1.3 and Motor-Bore Model Port-to-Throat Ratio of 3.0

Figure 36

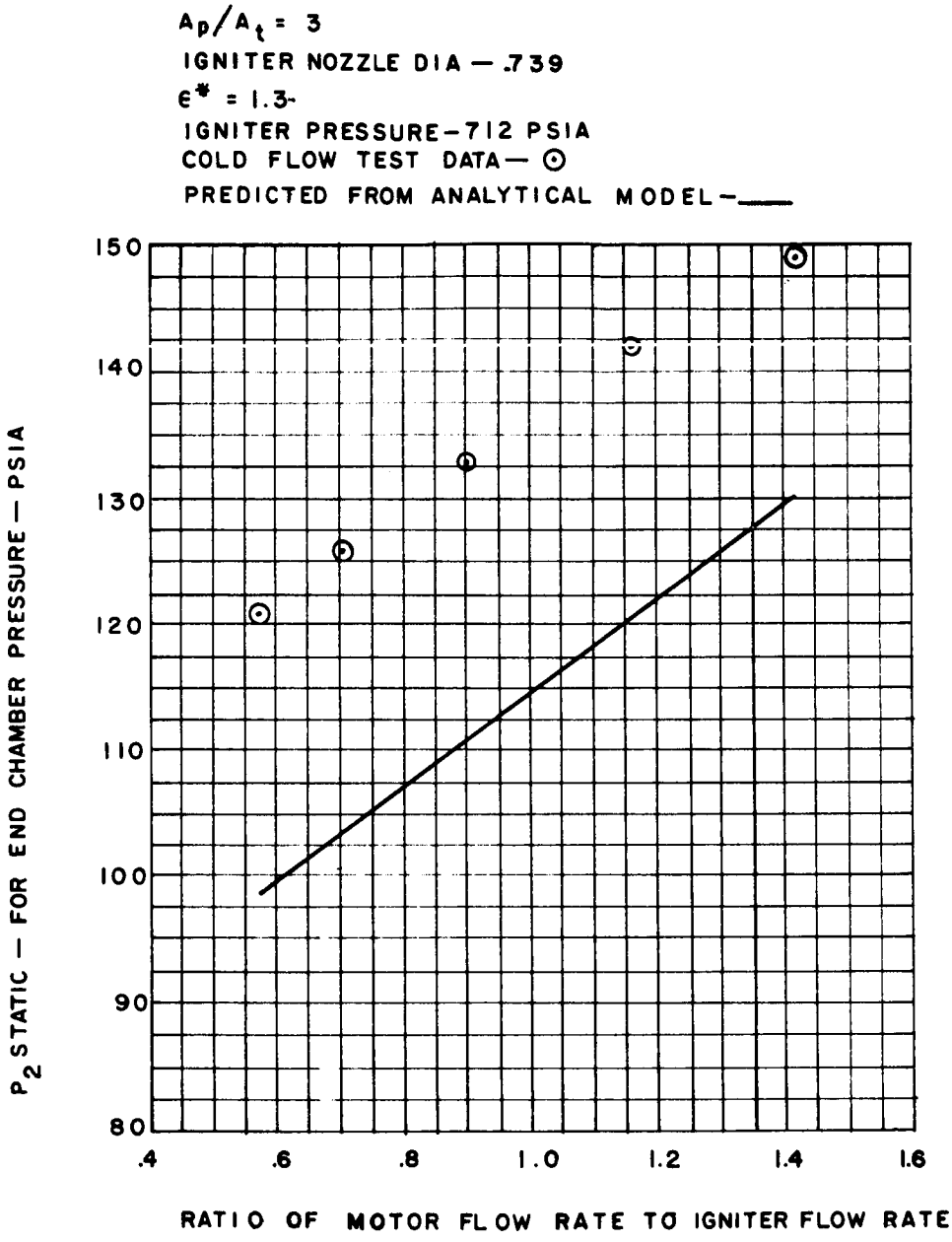

Motor-Bore Model Pressure Plotted as a Function of the Ratio of Igniter Model to Motor-Bore Model Flow Rate

Figure 37

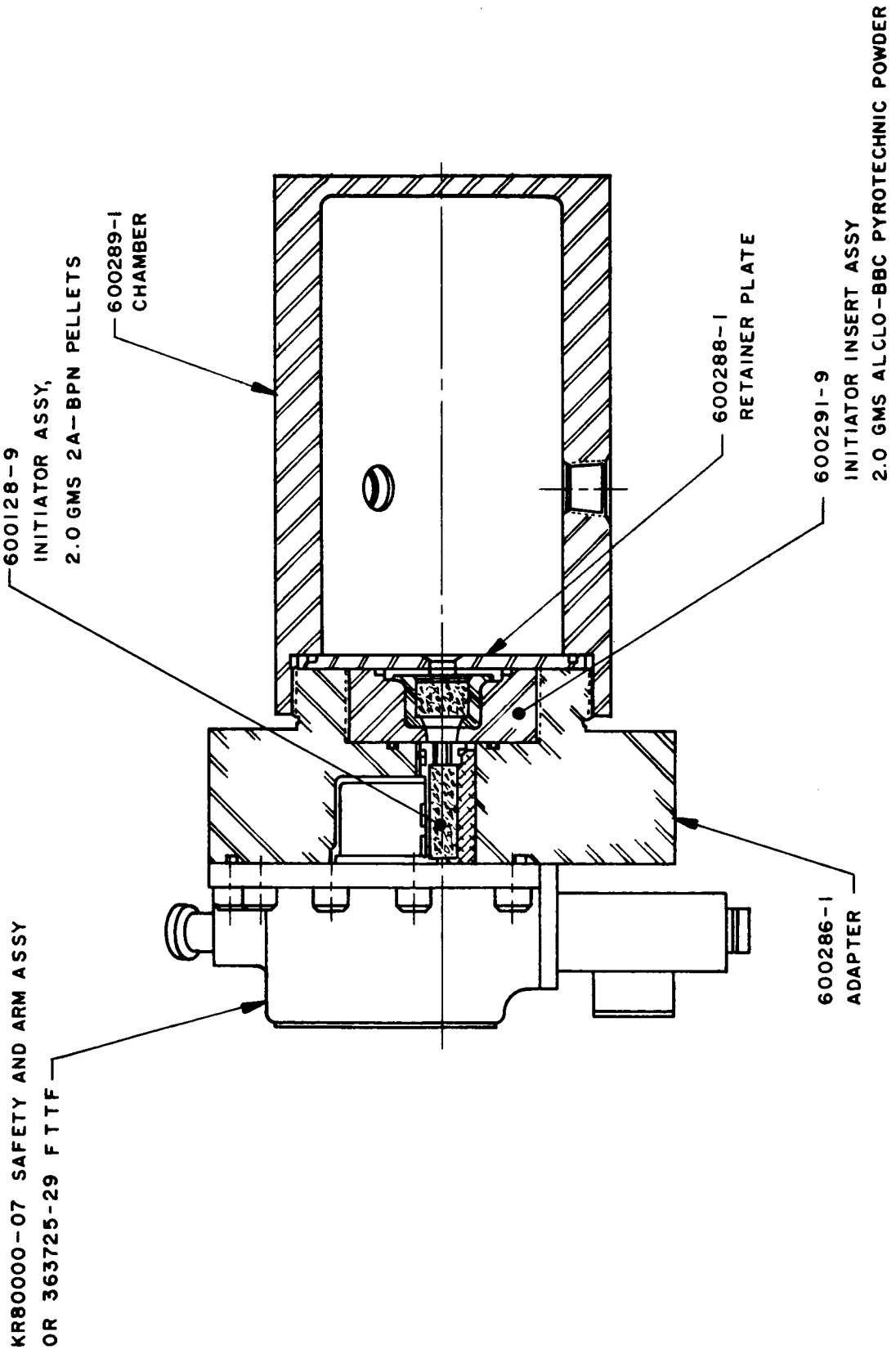

Squib-to-Initiator Test Hardware

Figure 38

Run No.	2A-BPN Initiator Serial Number	ALCLO-BBC Initiator Serial No.	No. of Squibs Actuated	Maximum Chamber Pressure, psig		Average Max Chamber Pressure, psig	Time from Fire Switch to Maximum Chamber Pressure, sec
				P_{c1}	P_{c2}		
1	-05	-09	2	Off Scale at 175 psig			
2	-01	-11	2	265	305	285	0.027
3	-12	-03	2	260	294	277	0.024
4	-04	-05	2	260	306	283	0.024
5	-06	-12	2	240	260	250	0.023
6	-09	-10	2	280	300	290	0.028
7	-10	Not Installed	2	168	192	180	0.025
8	-08	-08	2	215	235	225	0.028
9	-03	-01	2	236	256	246	0.020
10	-07	-04	1 Upper	268	273	270	0.025
11	-02	-06	1 Lower	248	264	256	0.020
12	Not Installed	-07	2	105	110	108	0.012

Figure 39

Mod 260 Ignition Motor Squib-to-Initiator Test Data

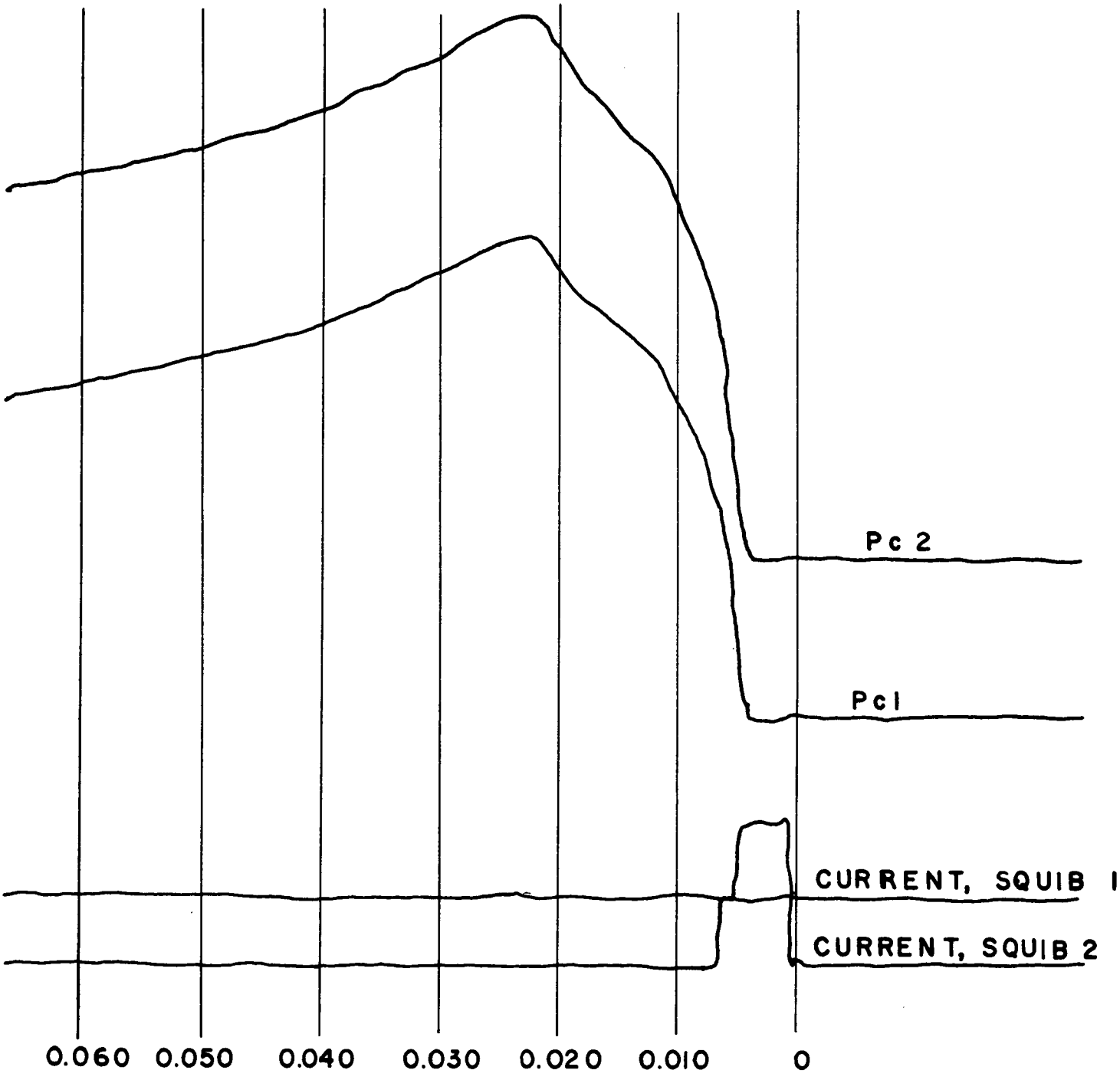

Typical Squib-to-Initiator Test Visicorder Trace

Figure 40

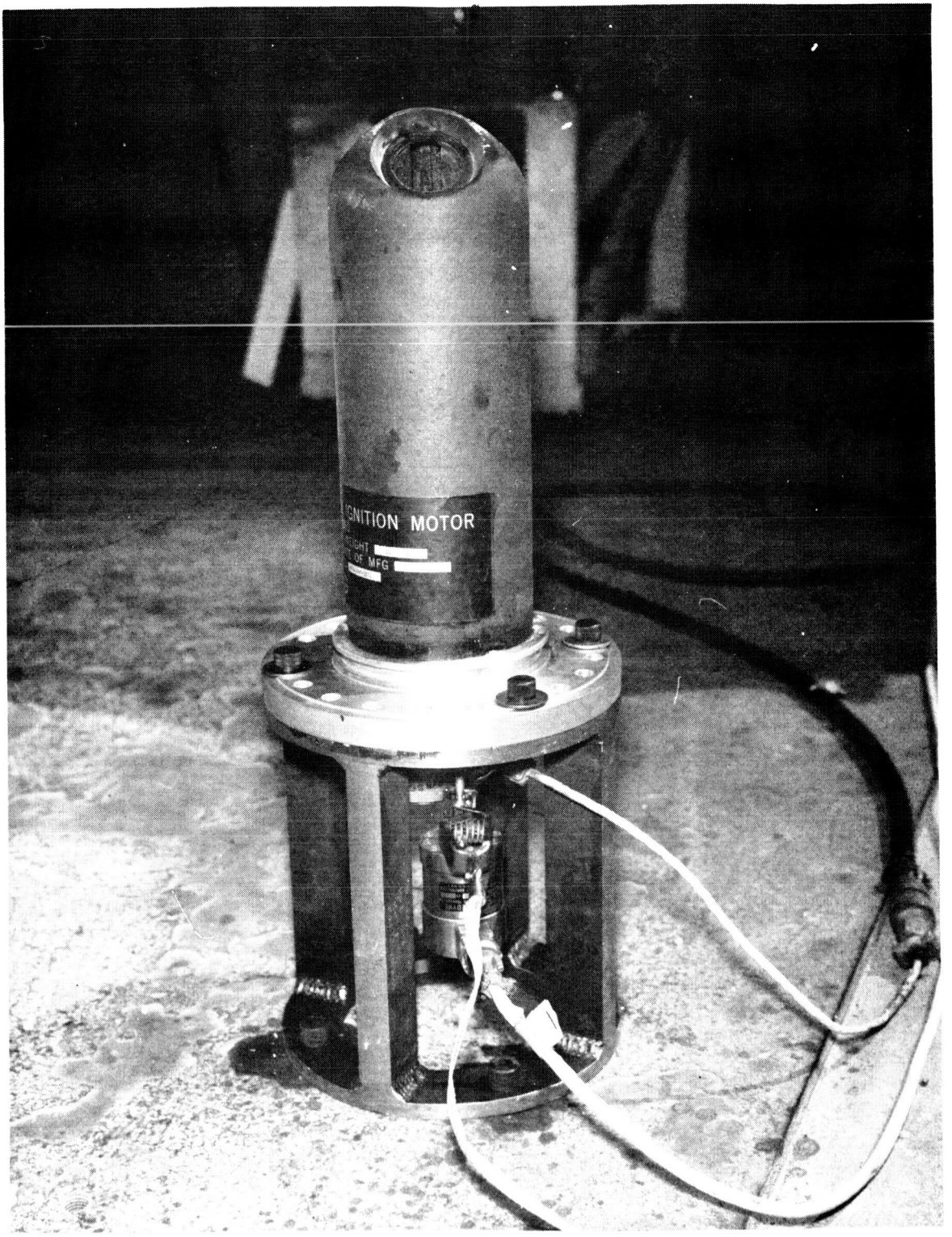

Mod 260 Ignition Motor Booster Open-Air Test Setup

Figure 41

Booster	260-IMB-01	260-IMB-02	260-IMB-03	260-IMB-04	260-IMB-05	260-IMB-06	260-IMB-10	260-IMB-11
Maximum Initiator Pressure, psia	368	385	404	429	464	450	564	465
Time to Maximum Initiator Pressure, psia	0.065	0.040	0.027	0.028	0.028	0.028	0.040	0.034
Maximum Operating Pressure, psia	585	1428	530	1041	1038	1023	636	660
Time to Maximum Operating Pressure, sec	0.11[illegible]	0.113	0.086	0.070	0.071	0.072	0.100	0.094
Ignition Motor	N/A	N/A	N/A	260-IM-01	260-IM-02	260-IM-03	260-IM-05	260-IM-04
Propellant Weight, lb	Booster	Booster	Booster	1155	1156	1170	1179	1178
Maximum Pressure, psia	Test	Test	Test	1103	1128 (1)	1002	960	960
Web Avg. Pressure, psia				988	(2)	924	900	(4)
Web Duration, psia				0.0655	(2)	0.730	0.710	(4)
Maximum Thrust, lb				272,000	2[illegible]8,000	250,000	237,000	237,000
Maximum Mass Flow Rate, lb/sec				1215	1285	1107	1058	1058
Ignition Interval (3), sec				0.125	0.125	0.115	0.135	0.140

(1) Measured pressure data lost at 0.110 sec; pressure calculated from thrust data
(2) Thrust data lost at 0.390 sec
(3) Time from fire switch to 75% of the ignition motor web average pressure
(4) Instrumentation cable lost at 0.56 sec

Summary of Mod 260 Ignition Motor and Booster Assembly Ballistic Performance Data

Figure 42

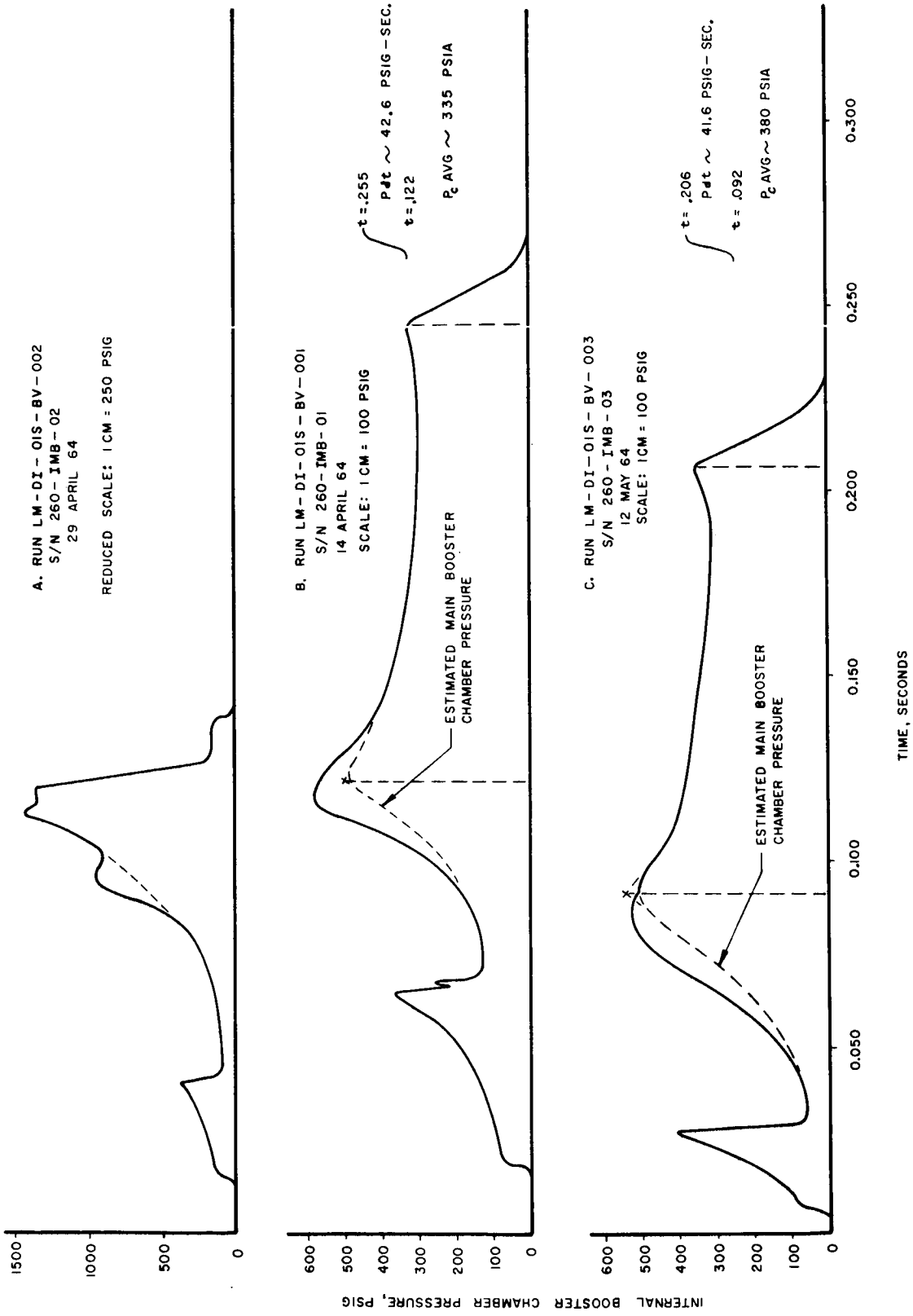

Ballistic Firing Curves, Mod 260 Ignition Motor Booster Open-Air Tests

Figure 43

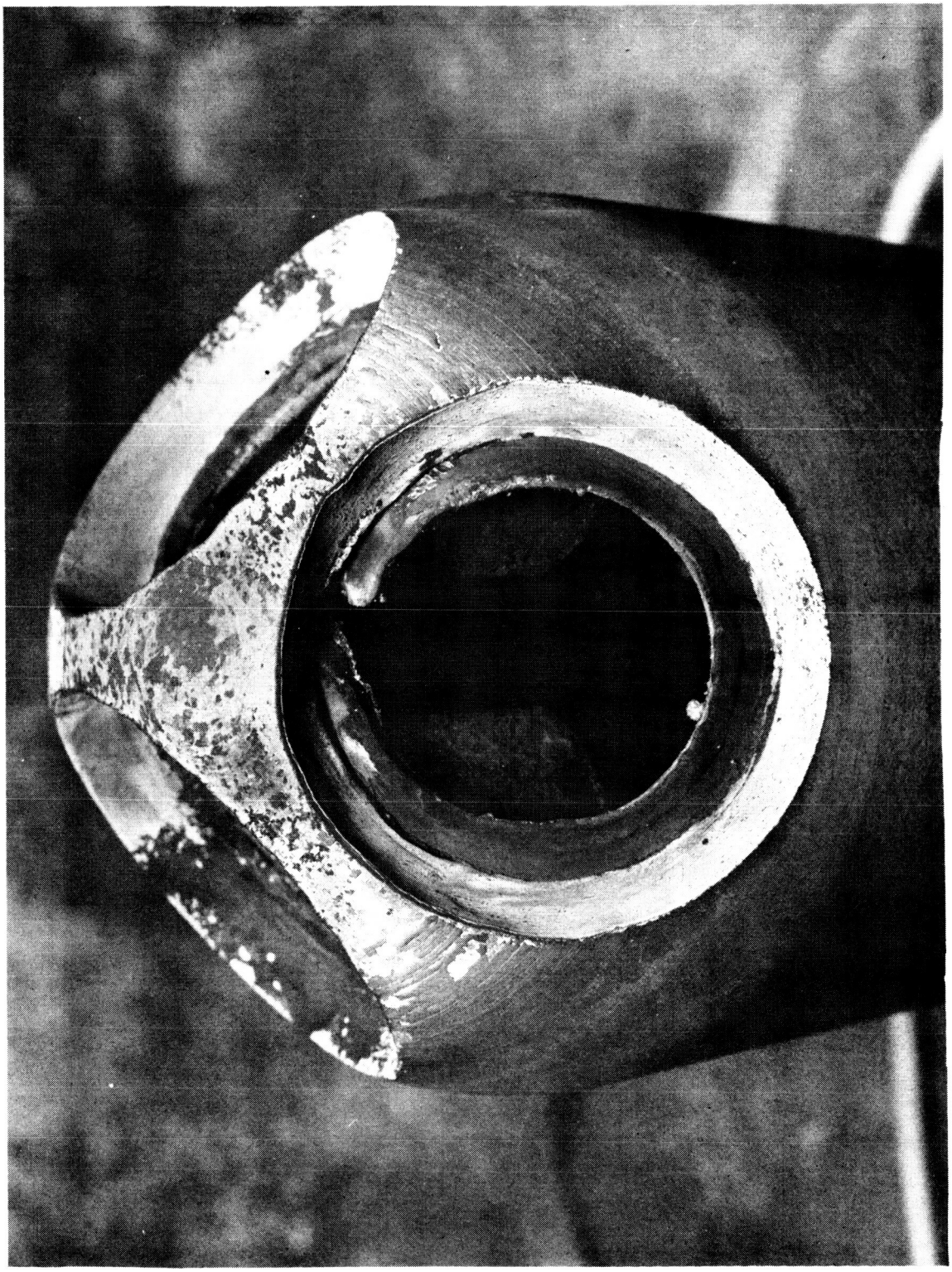

Postfiring View of Booster 260-IMB-01 Nozzle Ports

Figure 44

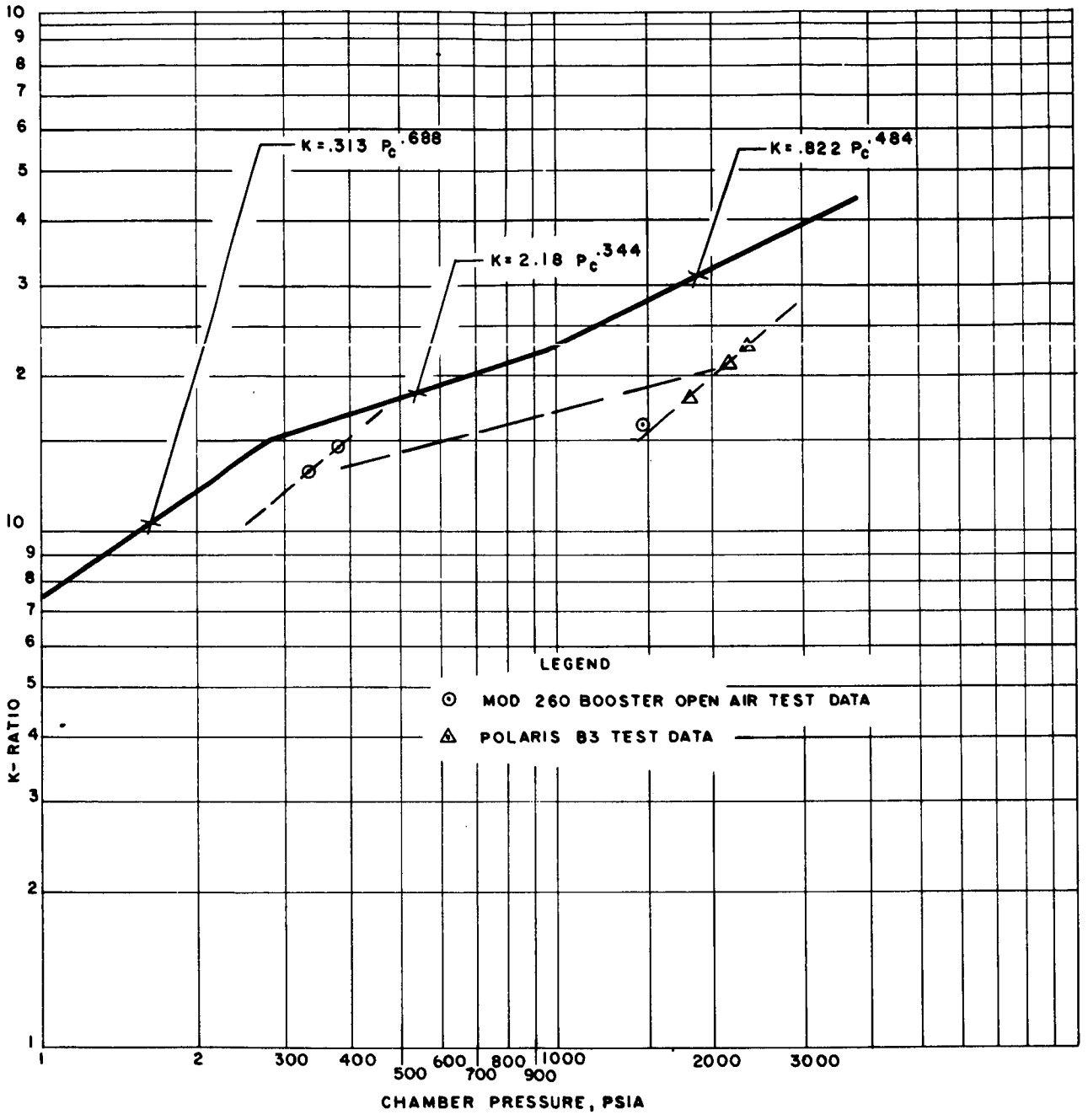

K Ratio vs Chamber Pressure for Alclo-Iron

Figure 45

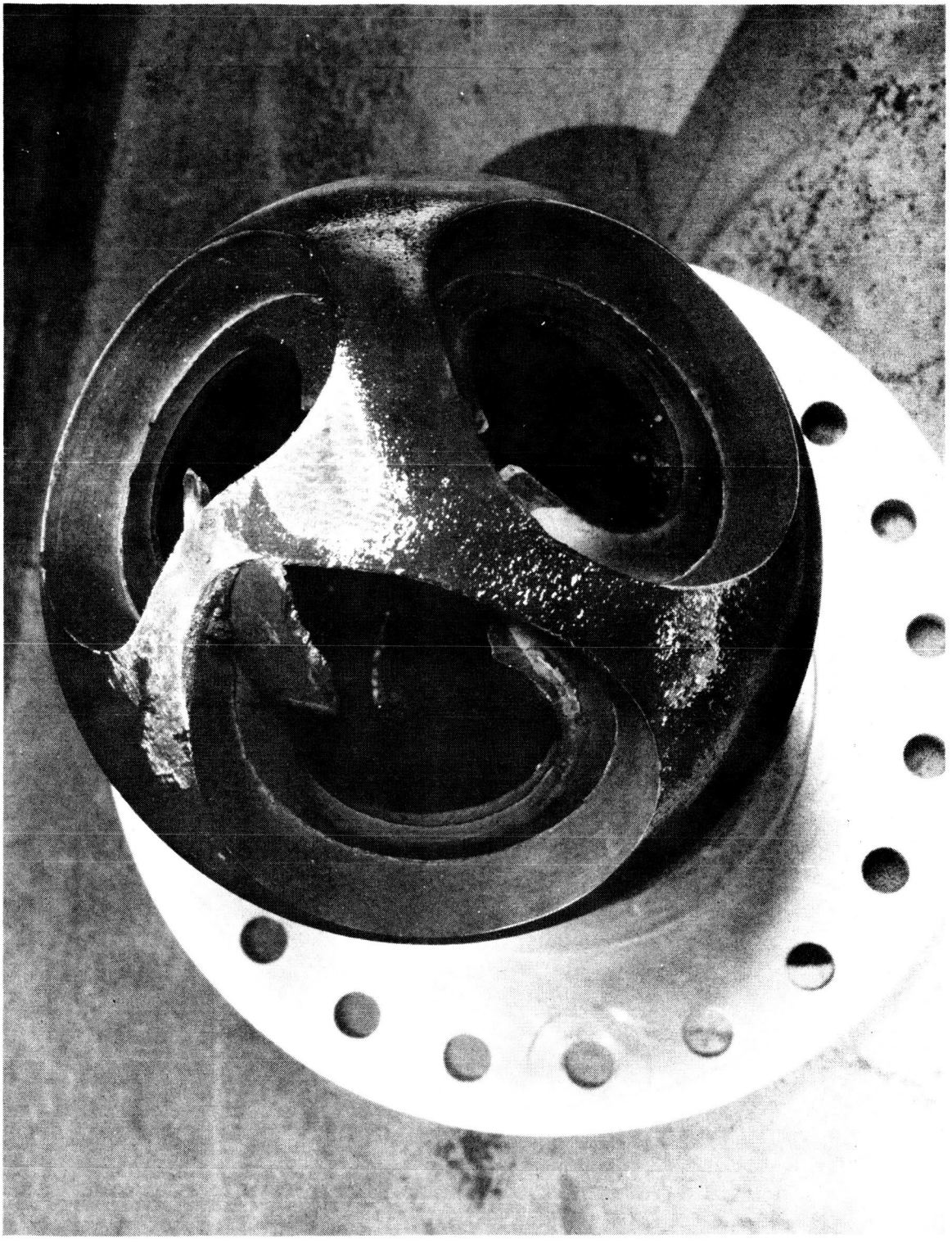

Postfiring View of Booster 260-IMB-02 Nozzle Ports

Figure 46

Postfiring View of Booster Leak Check Hole

Figure 47

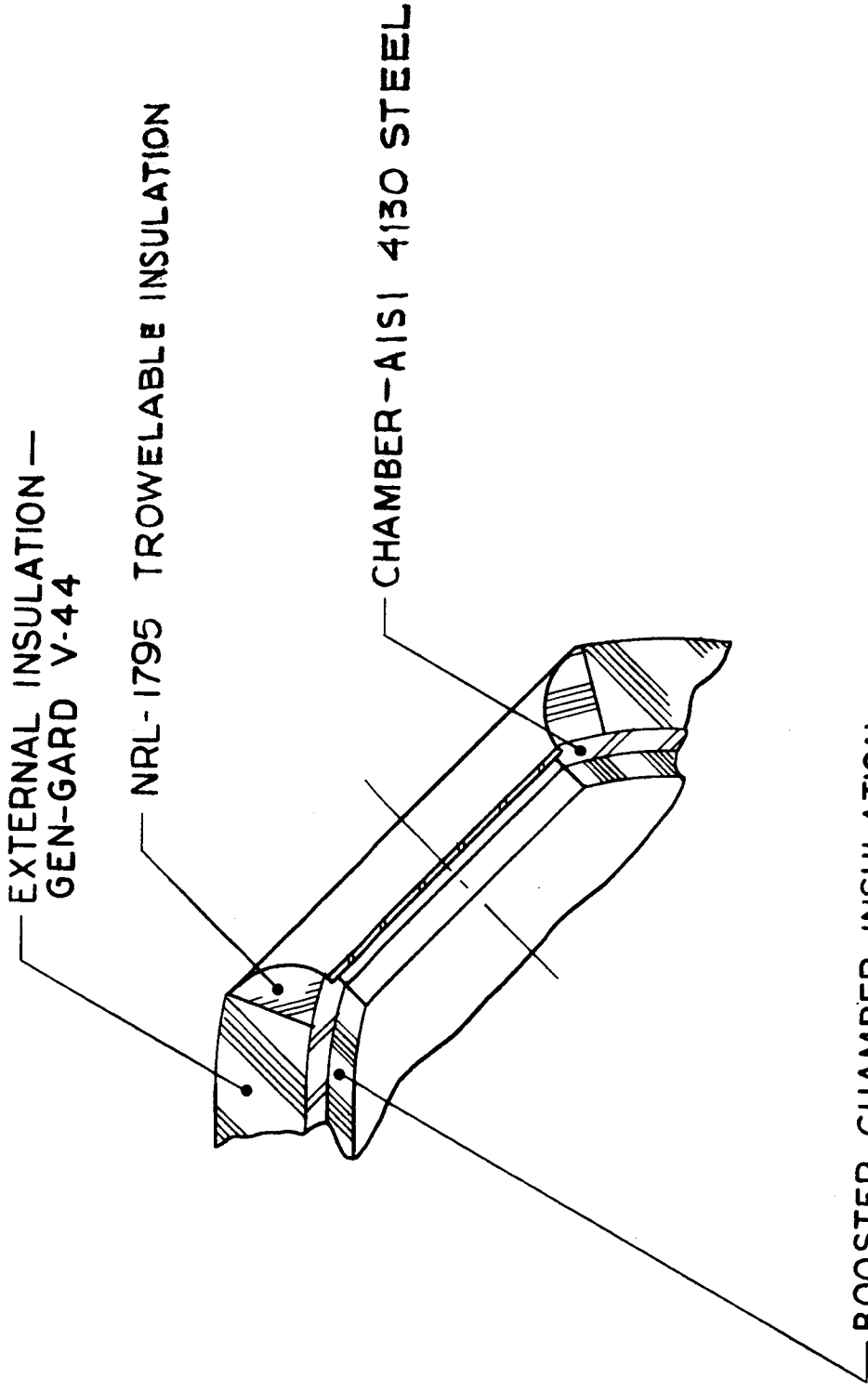

External Insulation Around Booster Chamber Nozzle Ports

Figure 48

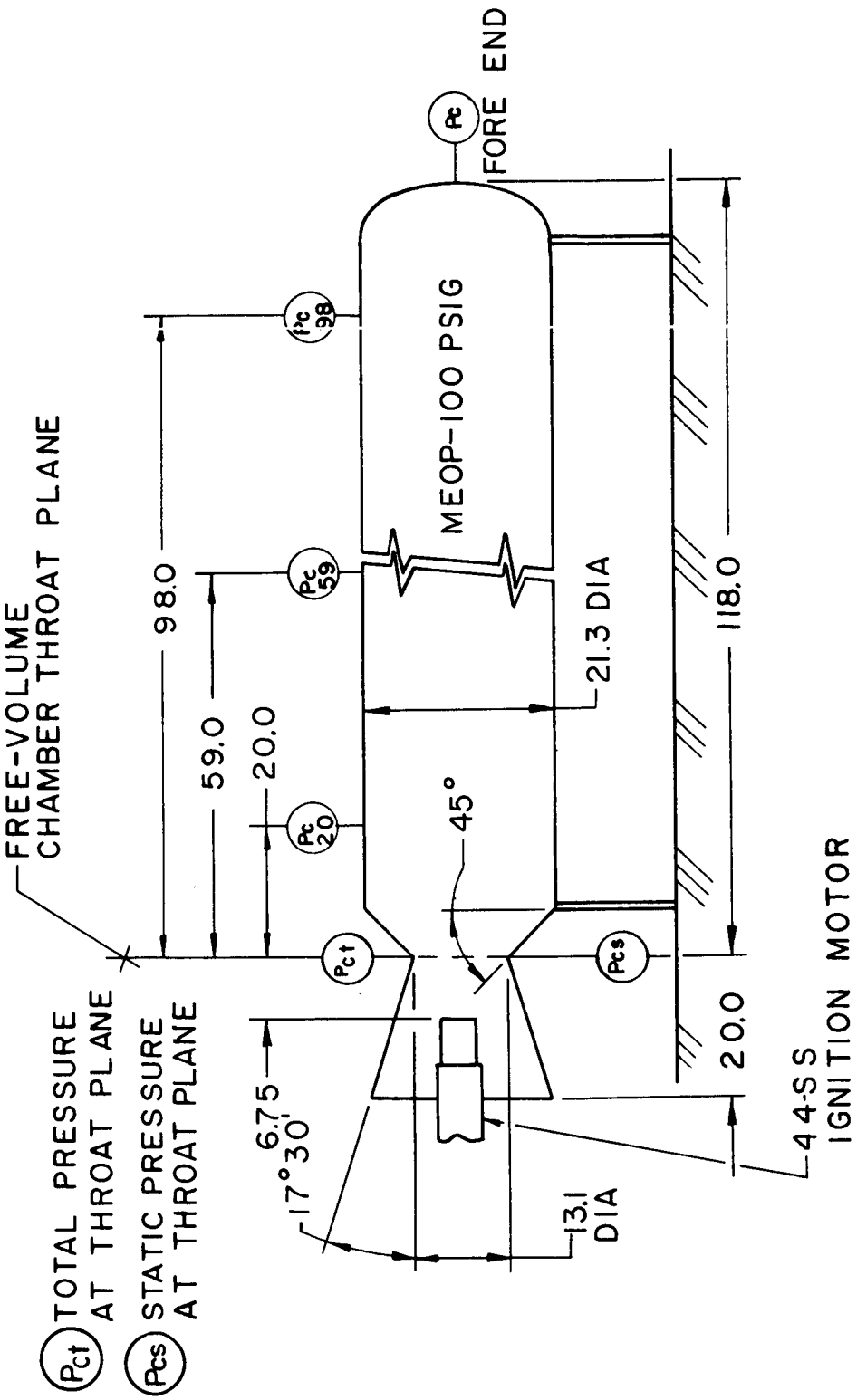

44-SS Free-Volume Simulator Test Setup

Figure 49

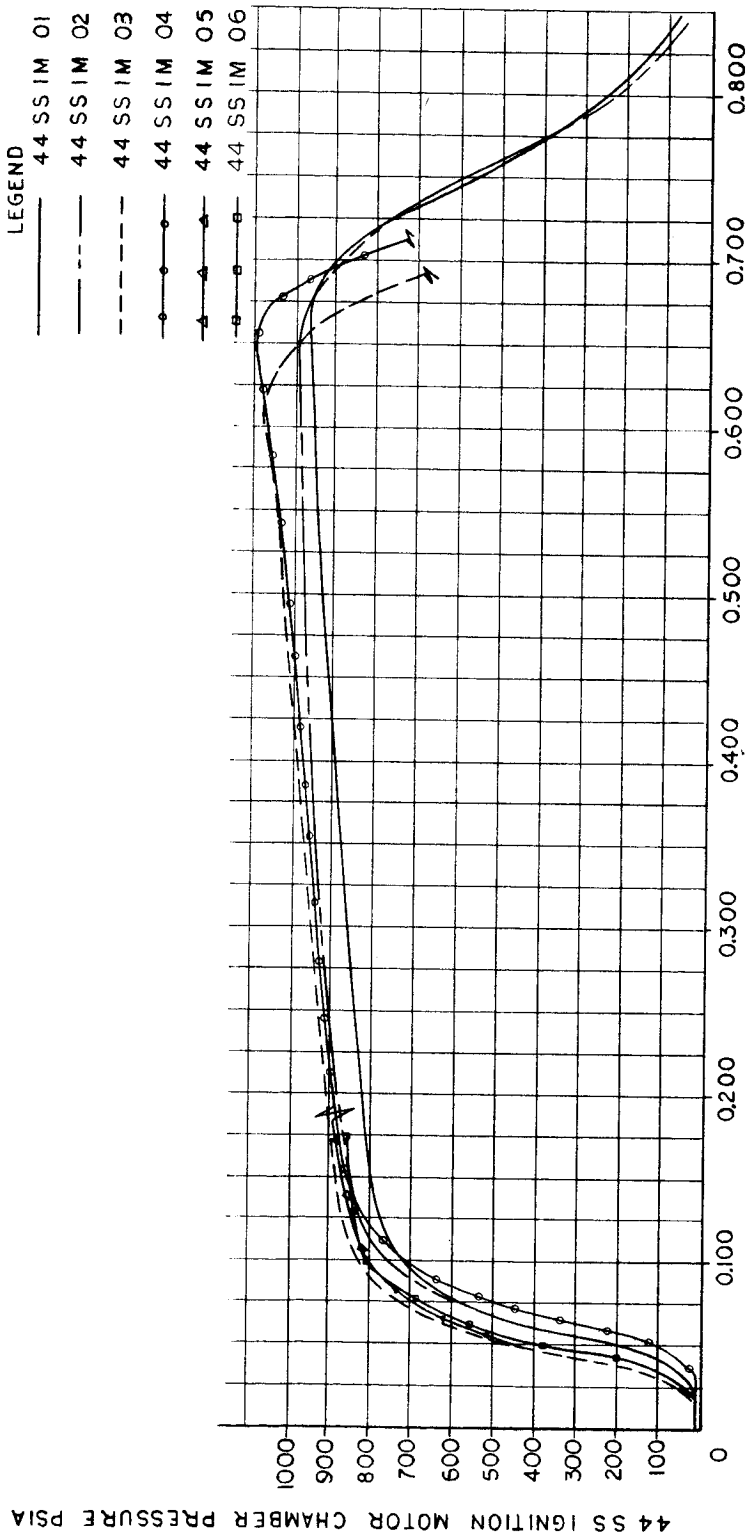

Composite Ballistic Performance Curves for 44-SS Ignition Motors

Figure 50

	44SS-IM-01	44SS-IM-02	44SS-IM-03	44SS-IM-04	44SS-IM-05	44SS-IM-06
Ignition Motor Weight, lb	140.8	137.7	137.8	141.0	139.0	141.0
Propellant Weight, lb	26.2	26.2	25.7	25.6	25.7	25.7
Ignition Interval, sec	0.083	0.082	0.073	0.095	0.072	0.071
Web Average Pressure, psia	844	880	928	920	(1)	(2)
Web Duration, sec	0.650	0.650	0.612	0.615	(1)	(2)
Maximum Pressure, psia	962	990	1073	1095	(1)	(2)
Average Throat Area, in^2	6.29	6.22	6.20	6.25	(1)	(2)
Fired In:	FVS Test	FVS Test	FVS Test	Motor 44-SS-1	Motor 44-SS-2	Motor 44-SS-3

(1) Pressure data lost at 0.186 sec; transducer cable broken.

(2) Pressure data lost at 0.170 sec; transducer cable broken.

Summary of 44-SS Ignition Motor Ballistic Performance Data

Figure 51

Time, sec	Ignition Motor 44-SS-IM-	Mass Flow Rate, lb/sec			Free-Volume Simulator Fore-End Bore Pressure, psia			Free-Volume Simulator Bore Pressure at 59.0-in., psia	
		--01	--02	--03	--01	--02	--03	--01	--02
0.100		30.3	31.6	34.4	66.2	71.3	72.2	63.7	57.7
0.200		34.5	36.2	37.8	75.2	81.2	80.0	72.6	78.9
0.300		36.2	38.1	39.6	78.4	83.5	83.9	74.8	80.2
0.400		37.5	39.3	41.4	81.0	85.0	86.7	78.3	81.9
0.500		38.8	40.2	42.3	83.1	87.7	91.4	81.8	83.9
0.600		40.0	40.7	44.4	85.3	89.2	95.6	84.3	84.7

Time, sec	Ignition Motor 44-SS-IM-	Free-Volume-Simulator Bore Pressure at 20.0-in., psia			Free-Volume-Simulator Throat Plane Static Pressure, psia		Free-Volume-Simulator Throat Plane Total Pressure, psia
		--01	--02	--03	--01	--02	--03
0.100		60.0	53.3	67.7	36.5	39.6	58.1
0.200		66.1	72.1	75.1	32.7	39.9	64.0
0.300		70.4	75.1	77.5	35.0	34.3	66.9
0.400		75.4	76.0	81.2	40.8	34.3	69.8
0.500		77.0	78.2	85.7	40.3	38.5	72.4
0.600		81.4	78.2	88.3	41.9	37.1	75.7

Summary of 44-SS Free-Volume Simulator Pressure Data

Figure 52

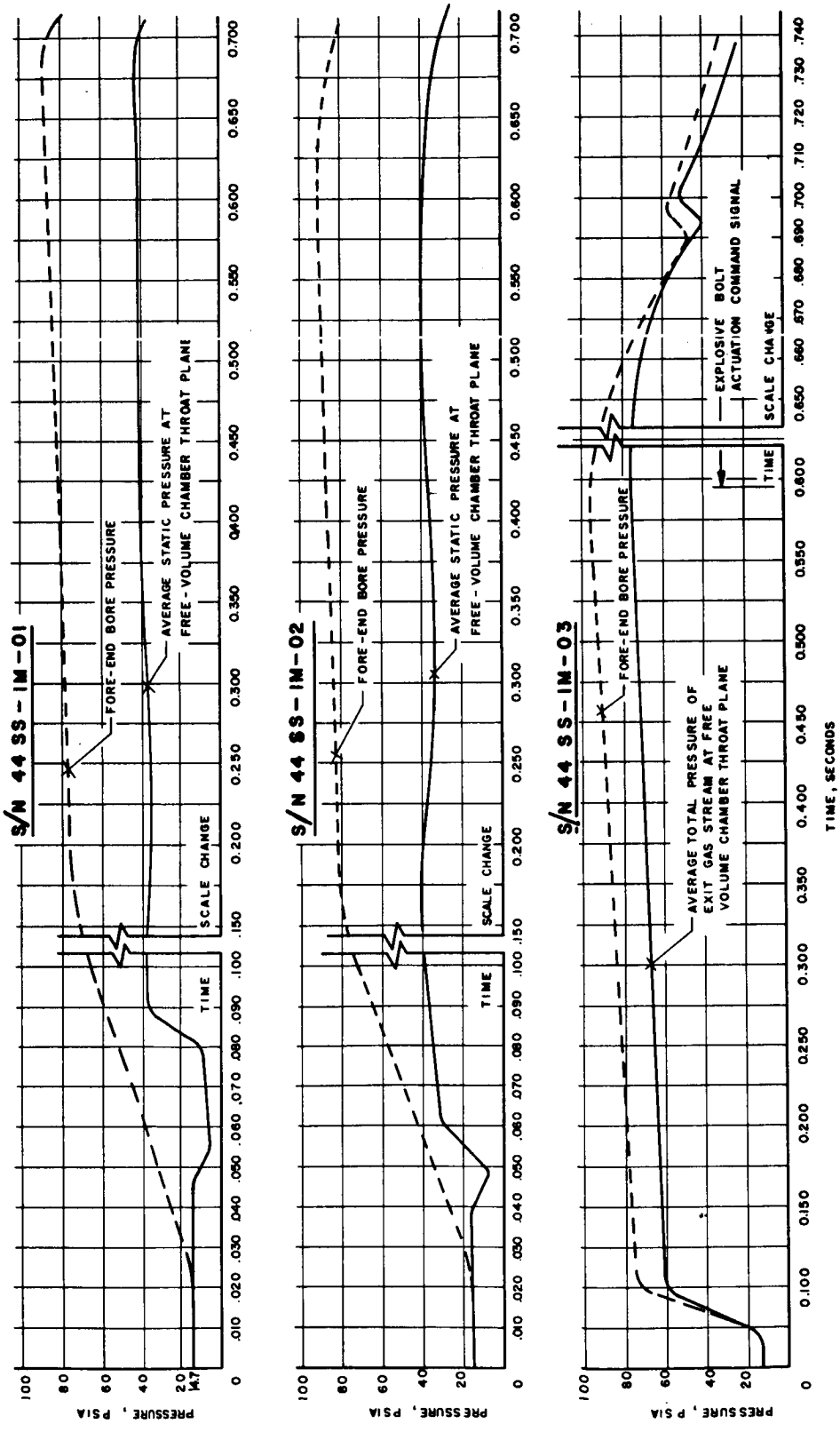

44-SS Ignition Motor Free-Volume Tests, Free-Volume Chamber Throat Plane and Fore-End Bore Pressure Data

Figure 53

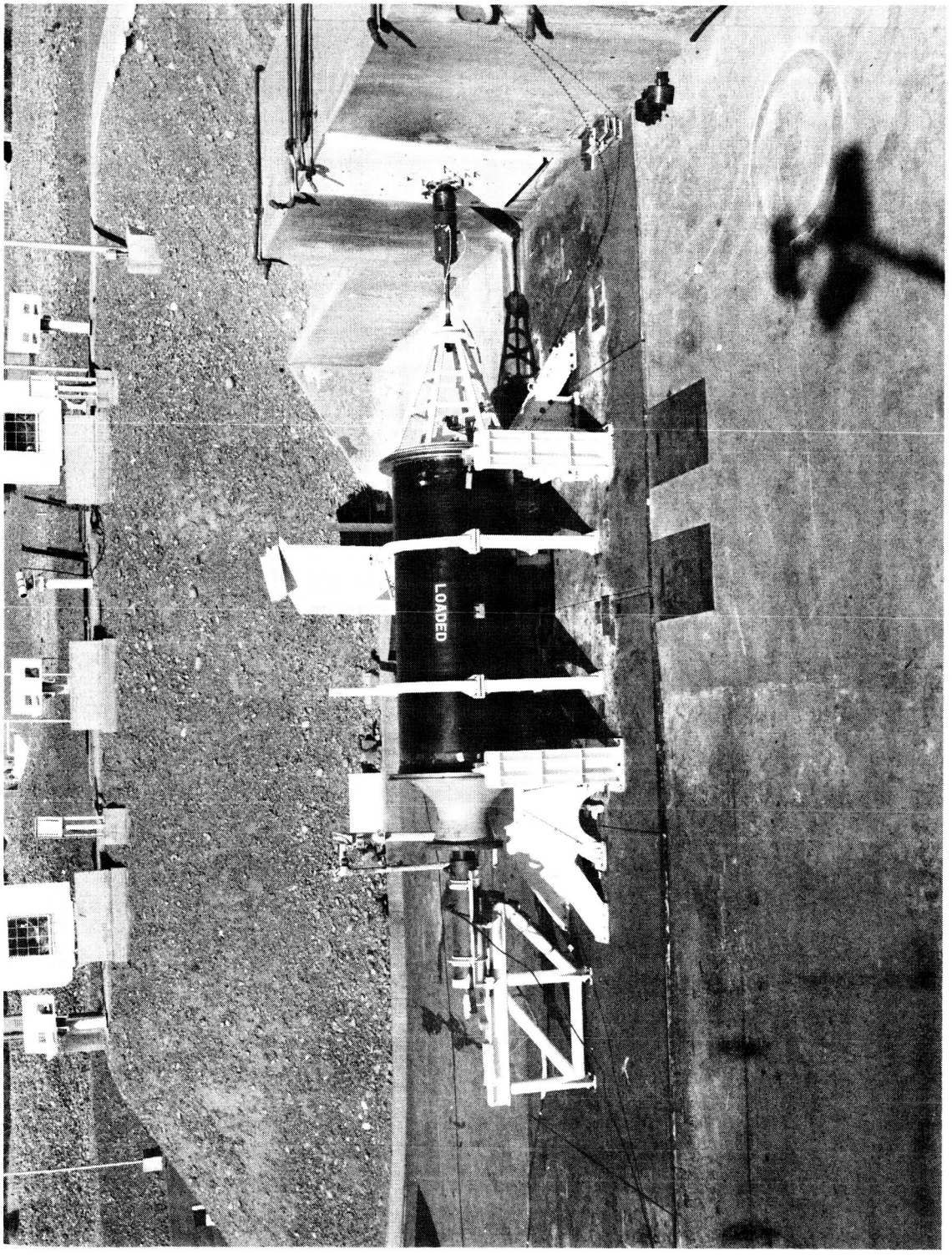

44-SS Motor Test Firing Setup

Figure 54

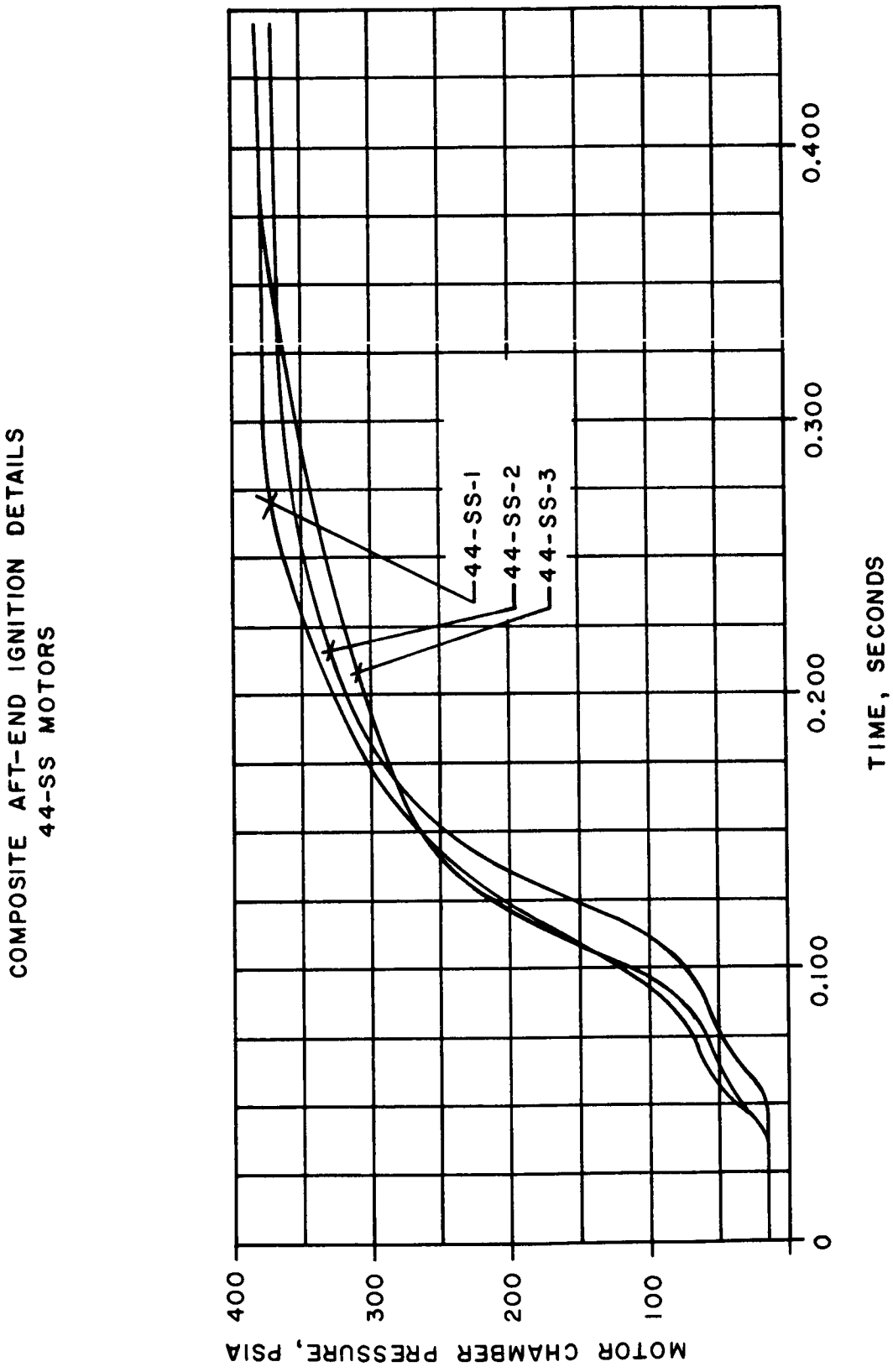

Ignition Performance Details for Motors 44-SS-1, -2, and -3

Figure 55

	44-SS-1		44-SS-2		44-SS-3	
	Time, sec	Pressure, psia	Time, sec	Pressure, psia	Time, sec	Pressure, psia
Fire Switch	0	14.7	0	14.7	0	14.7
2000 vdc Capacitor Discharge to EBW Squib	0.035	14.7	0.016	14.7	0.012	14.7
Initial Motor Bore Pressurization	0.045	-	0.026	-	0.027	-
First Indication of Motor Propellant Ignition	0.090	62	0.070	60	0.075	65
Igniter Release Control Unit Actuated	0.145(1)	234	0.140	243	0.110(5)	231
44-SS Motor Ignition Interval	0.165	275	0.160	281	0.162	285
Igniter Release Control Unit Logic Satisfied	0.177(2)	294	0.172(2)	298	0.140(5)	255
Explosive Bolts Actuated	0.220	331	0.202	328	0.174(5)	295
First Movement of Ignition Motor	Not Measured		0.210	334	0.182	297
Ignition Motor Reaches End of Support Track	0.305(3)	365	0.285(4)	376	0.258	336

Notes: (1) Not Measured; 0.145 sec time, estimated from maximum present actuator pressure of 234 psia

(2) Not Measured; the 1-shot oscillator requires 0.030 to 0.032 seconds to time out and reset

(3) Not Measured; 0.085 seconds from explosive bolt actuation to ignition motor ejection observed in 44-SS free-volume test

(4) Average velocity of ejected ignition motor was 44.5 ft/sec.

(5) A signal comparator was used in place of the igniter release control unit for motor 44-SS-3;

44-SS Ignition Motor Ejection Sequence During 44-SS Motor Test Firings

Figure 56

44-SS Ignition Motor Ejection Sequence During 44-SS Motor Test Firings

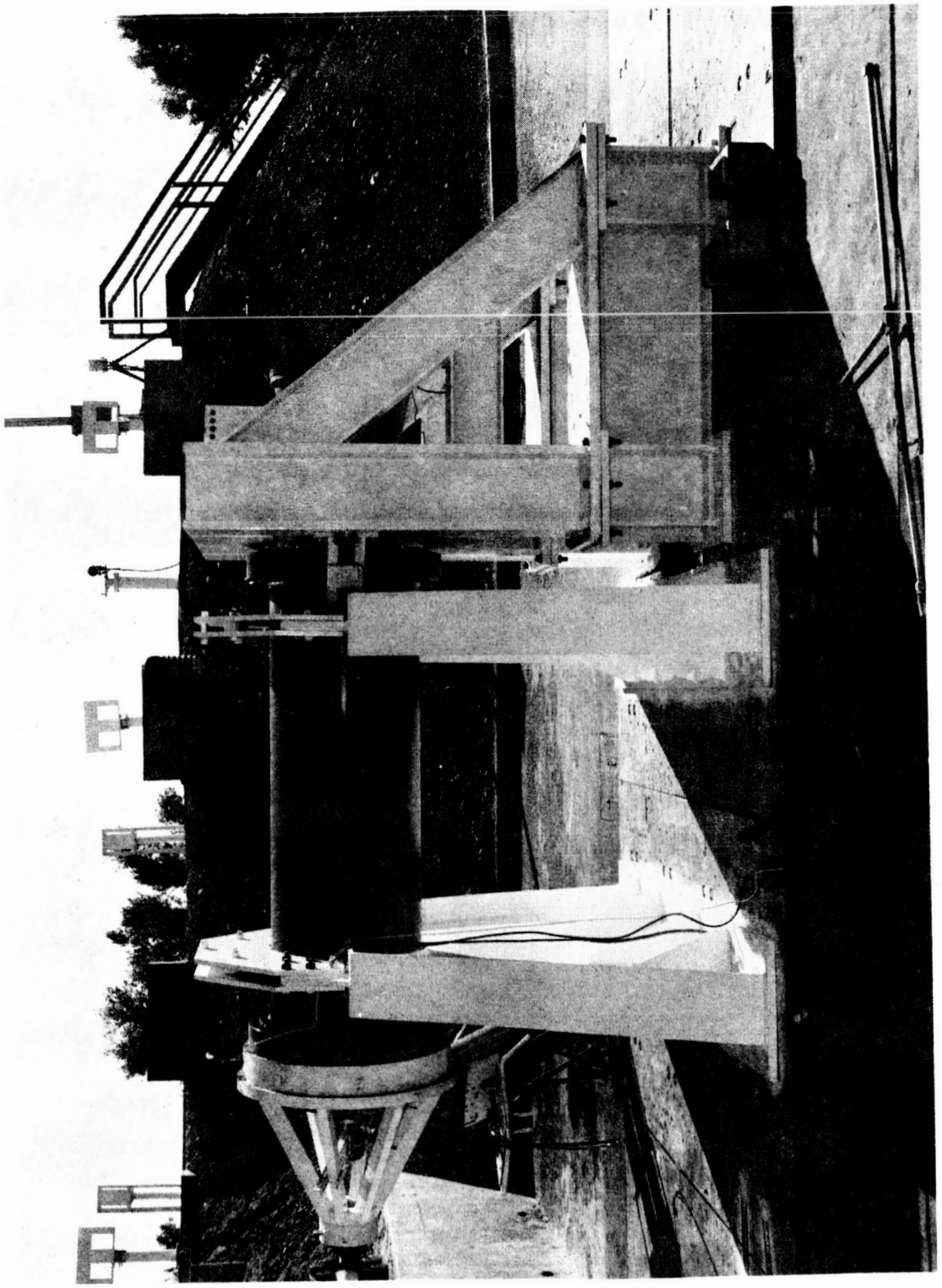

Installation and Test Equipment for Mod 260 Ignition Motor Open-Air Test

Figure 57

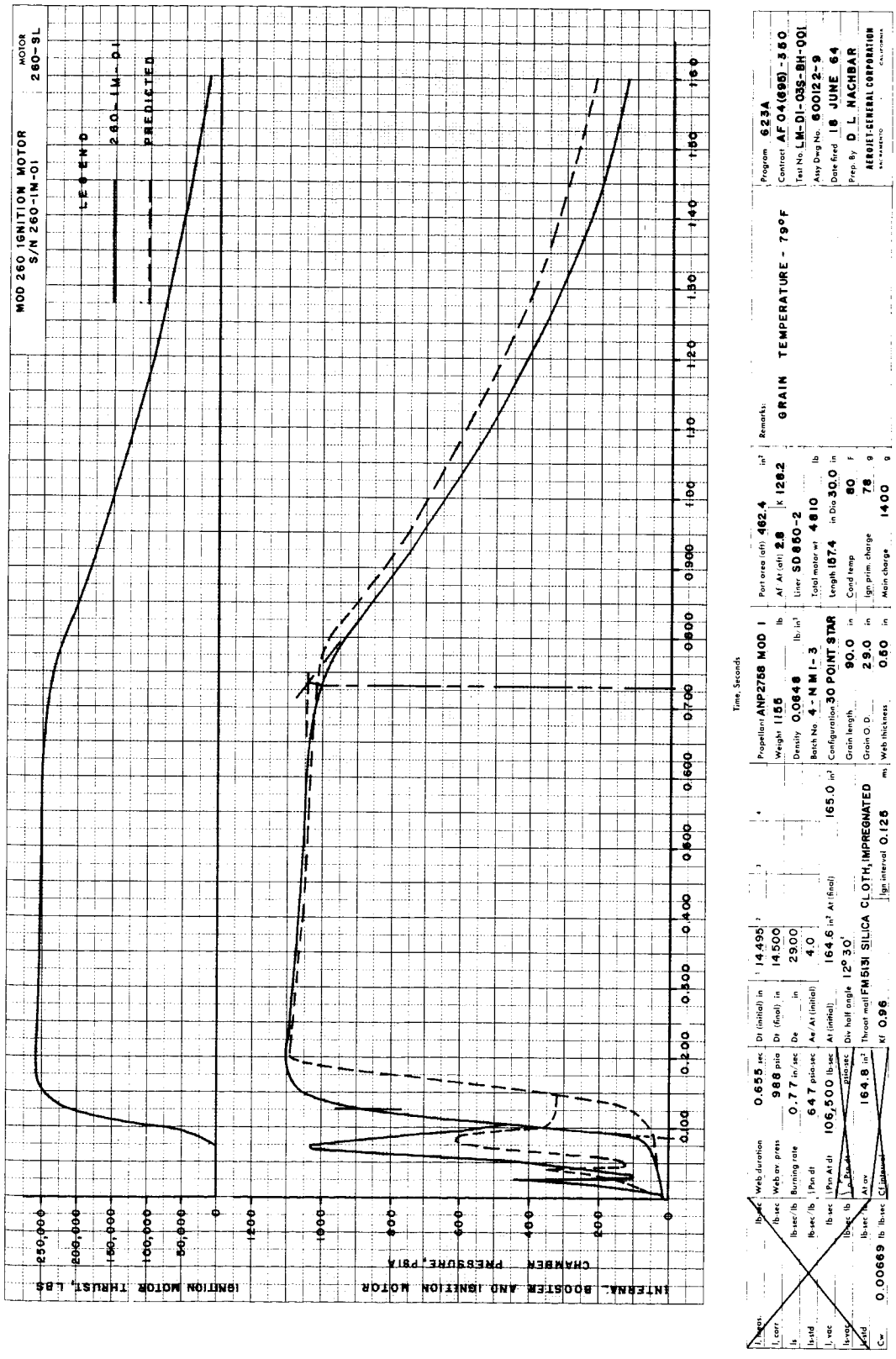

Figure 58

Ballistic Firing Data, Mod 260 Ignition Motor 260-IM-01

260-SL MOTOR IGNITION MOTOR OPEN-AIR TEST;
SUMMARY OF MEASURED AND PREDICTED BALLISTIC DATA

Computer Time, sec	Ignition Sequence Time, sec	Ignition Motor Chamber Pressure, psia		Ignition Motor Thrust, lbf x 10^{-3}	
		Predicted	Measured	Predicted	Measured
GE 225 Program					
	0.000		---	---	---
	0.080		69.8	---	14.5
	0.090		128.8	---	26.7
0.050	0.100	431.2	338.5	---	71.6
0.070	0.110	770.0	596.1	---	137.1
0.090	0.120	925.0	791.2	---	188.9
0.110	0.130	990.2	942.1	---	225.4
0.130	0.150	1016.3	1063.5	---	252.8
0.150	0.175	1033.9	1096.6	---	259.7
1103 Program					
0.00	0.200	1094.2	1100.3	258.1	259.7
0.05	0.250	1085.5	1099.3	256.3	258.9
0.10	0.300	1076.8	1081.9	254.4	257.4
0.15	0.350	1068.7	1078.2	252.6	255.1
0.20	0.400	1061.1	1074.5	251.0	254.3
0.25	0.450	1054.2	1063.5	249.5	252.8
0.30	0.500	1046.7	1055.1	247.9	252.0
0.35	0.550	1038.9	1052.5	246.1	251.3
0.40	0.600	1031.6	1045.1	244.5	249.8
0.45	0.650	1025.1	1037.7	243.1	249.0
0.50	0.700	1019.2	1018.7	241.8	243.7

Summary of Measured and Predicted Ballistic Performance, Mod 260
Ignition Motor Open-Air Test

Computer Time, sec	Ignition Sequence Time, sec	Ignition Motor Chamber Pressure, psia		Ignition Motor Thrust, lbf x 10^{-3}	
		Predicted	Measured	Predicted	Measured
0.55	0.750	1013.2	986.2	240.4	236.1
0.60	0.800	982.4	927.3	233.0	221.6
0.65	0.850	887.7	864.7	209.7	204.1
0.70	0.900	827.2	787.5	194.8	185.0
0.75	0.950	759.9	710.3	178.2	167.5
0.80	1.00	695.3	636.6	162.3	150.8
0.85	1.05	635.0	581.4	147.5	134.0
0.90	1.10	579.1	522.5	133.7	119.6
1.00	1.20	528.3	408.5	109.7	92.1
1.10	1.30	439.1	309.1	89.3	68.5
1.30	1.50	266.7	270.4	57.3	32.0
1.50	1.70	175.2	177.6	34.4	15.2
1.80	2.00	85.9	87.0	14.2	7.6
2.40	2.60	0	0	0	0

Summary of Measured and Predicted Ballistic Performance, Mod 260
Ignition Motor Open-Air Test

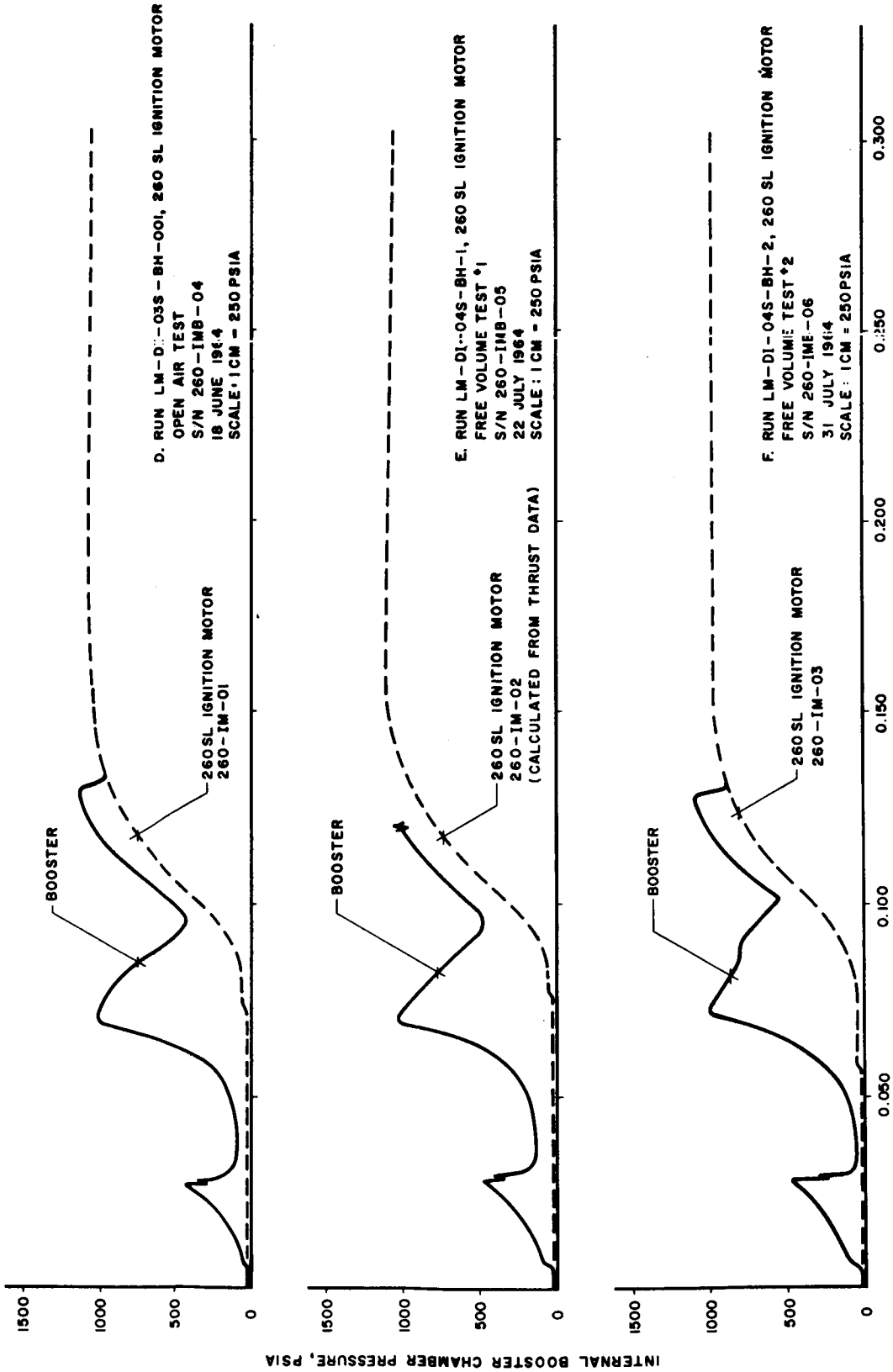

Mod 260 Ignition Motor Booster Ballistic Performance Curves,
260-IMB-04, -05 and -06

Figure 60

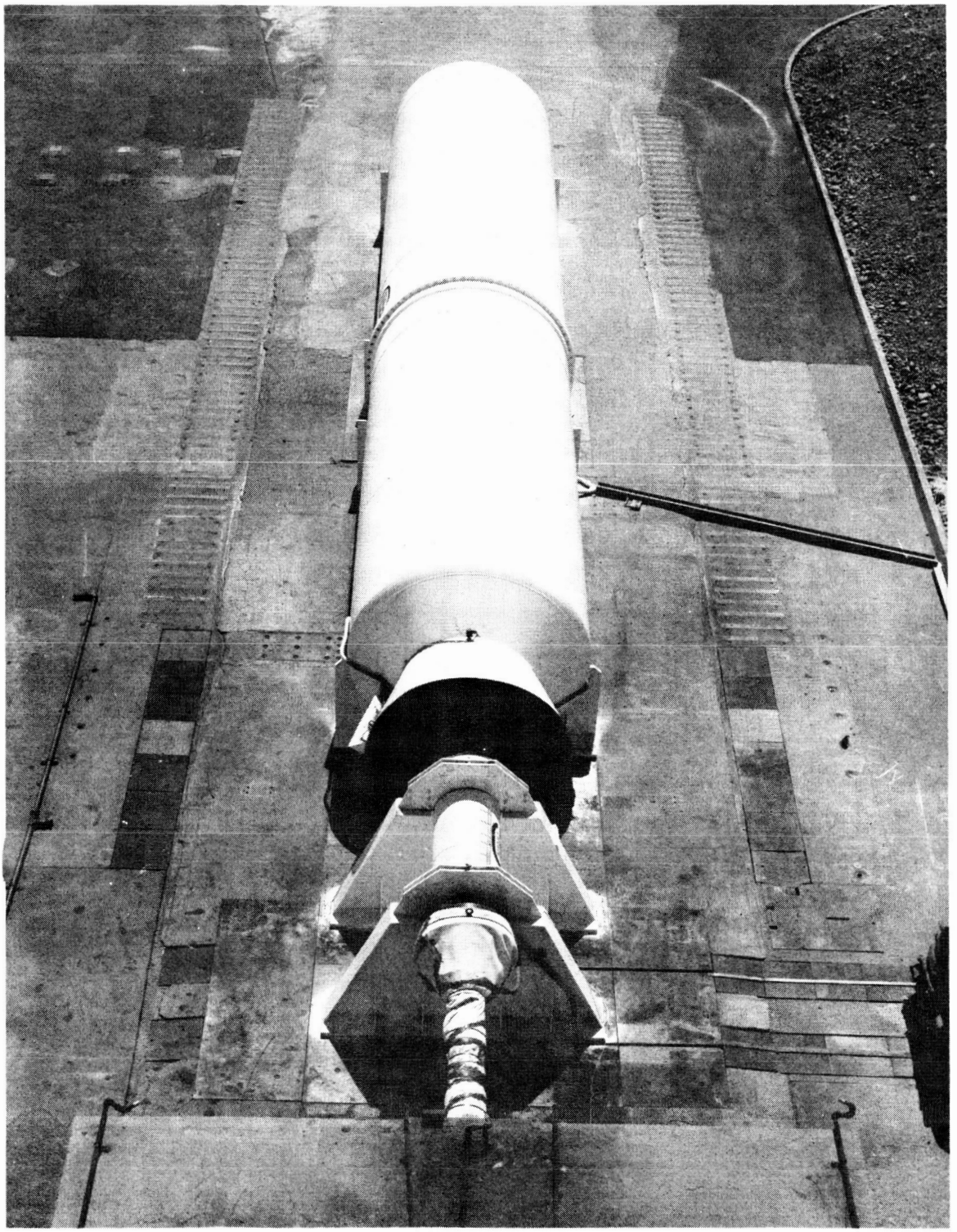

Overall View of Mod 260 Ignition Motor and Free-Volume Simulator

Figure 61

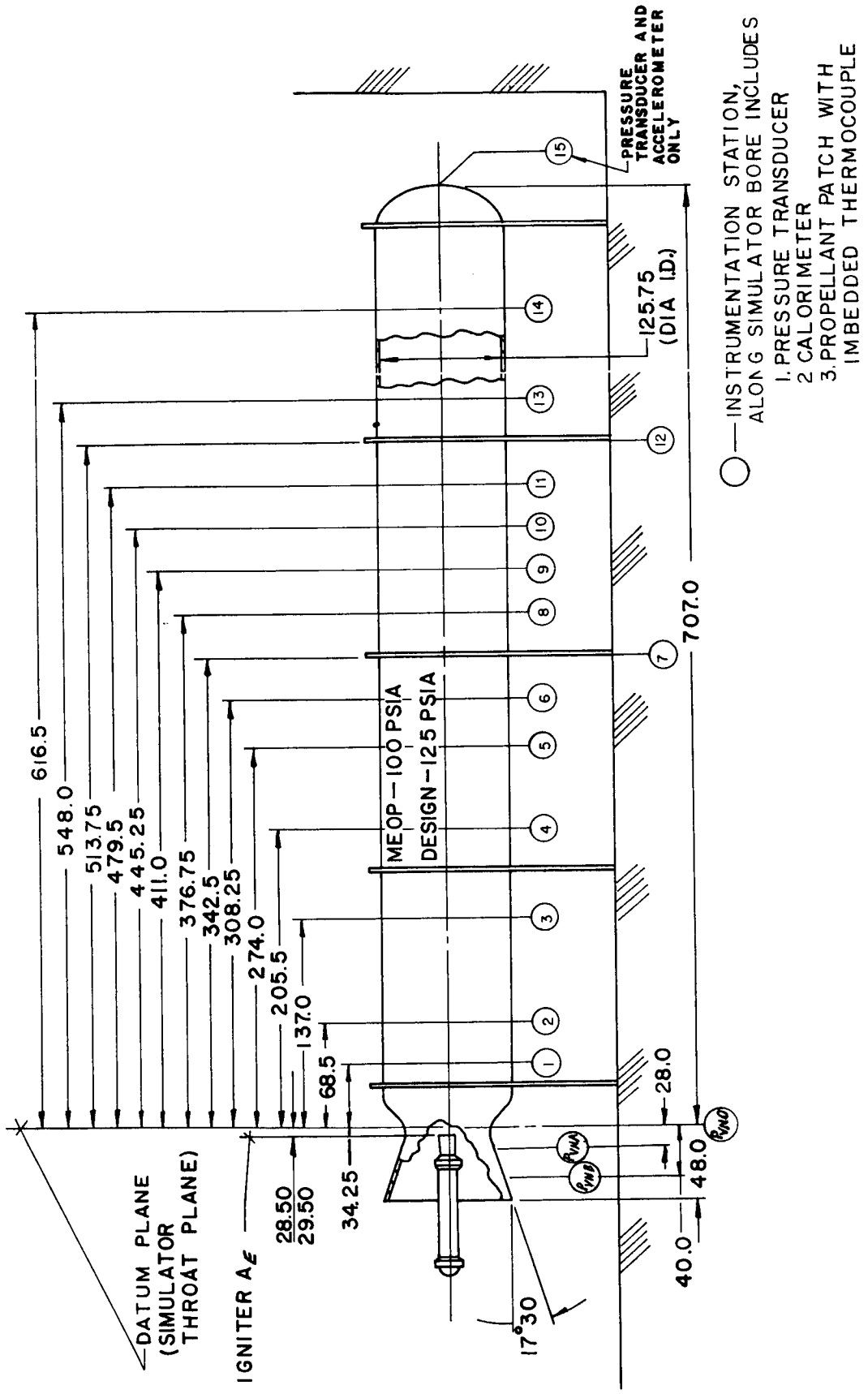

260-SL Motor Free-Volume Simulator Instrumentation Locations

Figure 62

Designation	Location*	Range	Description
Pc-1 Pc-2	Booster Adapter Ignition Motor	0 to 1500 psig	Internal ignition motor chamber pressure
Pign	Booster Adapter	0 to 1500 psig	Internal ignition motor booster chamber pressure
Fy-A Fy-B	Ignition Motor Load Cell	250K	Ignition motor thrust
Pvn-B Pvn-A	-40.0 -28.0	0 to 50 psig 0 to 50 psig	Simulator exit cone static pressure
Pvn-01	0 at 90 degrees	0 to 25 psig	Simulator throat plane static pressure
Pvn-02	0 at 0 degrees	0 to 75 psig	Simulator throat plane total pressure; 3.0-in.-long tube
Pvn-03	0 at 120 degrees	0 to 75 psig	Simulator throat plane total pressure; 6.0-in.-long tube
Pvn-04	0 at 240 degrees	0 to 75 psig	Simulator throat plane total pressure; 9.0-in.-long tube
Ifs	N/A	Trace only	Fire-switch current trace; 4.4 amp minimum per squib
FS	N/A	Trace only	Fire-switch indication for all oscillographs
Pvc-1 Pvc-2 Pvc-3 Pvc-4 Pvc-5 Pvc-6 Pvc-7 Pvc-8 Pvc-9 Pvc-10 Pvc-11 Pvc-12 Pvc-13 Pvc-14 Pvc-15	34.25 68.5 137.0 205.5 274.0 308.25 342.5 376.75 411.0 445.25 479.5 513.75 548.0 616.5 707.0 Forward Head	0 to 100 psig	Simulator bore pressure

*Reference: Free-Volume simulator throat plane: - indicates downstream.

260-SL Free-Volume Simulator Test Series, Instrumentation List

Designation	Location*	Range	Description
Tvc-1	34.25	0 to 3000°F	BHL thermocouple installed in the propellant patches located along the free-volume simulator wall
Tvc-2	68.5		
Tvc-3	137.0		
Tvc-4	205.5		
Tvc-5	274.0		
Tvc-6	308.25		
Tvc-7	342.5		
Tvc-8	376.75		
Tvc-9	411.0		
Tvc-10	445.25		
Tvc-11	479.5		
Tvc-12	513.75		
Tvc-13	548.0		
Tvc-14	616.5		
Tvcc-1	34.25	0 to 700°F	Calorimeters located along free-volume simulator wall
Tvcc-2	68.5		
Tvcc-3	137.0		
Tvcc-4	205.5		
Tvcc-5	274.0		
Tvcc-6	308.25		
Tvcc-7	342.5		
Tvcc-8	376.75		
Tvcc-9	411.0		
Tvcc-10	445.25		
Tvcc-11	479.5		
Tvcc-12	513.75		
Tvcc-13	548.0		
Tvcc-14	616.5		
Gyc-0	0	± 1000 g	Accelerometer mounted on exit cone of free-volume simulator (second test only)
Gyc-15	707.0 Forward Head	± 1000 g	Accelerometer mounted on forward dome of simulator

260-SL Free-Volume Simulator Test Series, Instrumentation List

Figure 63, Sheet 2 of 2

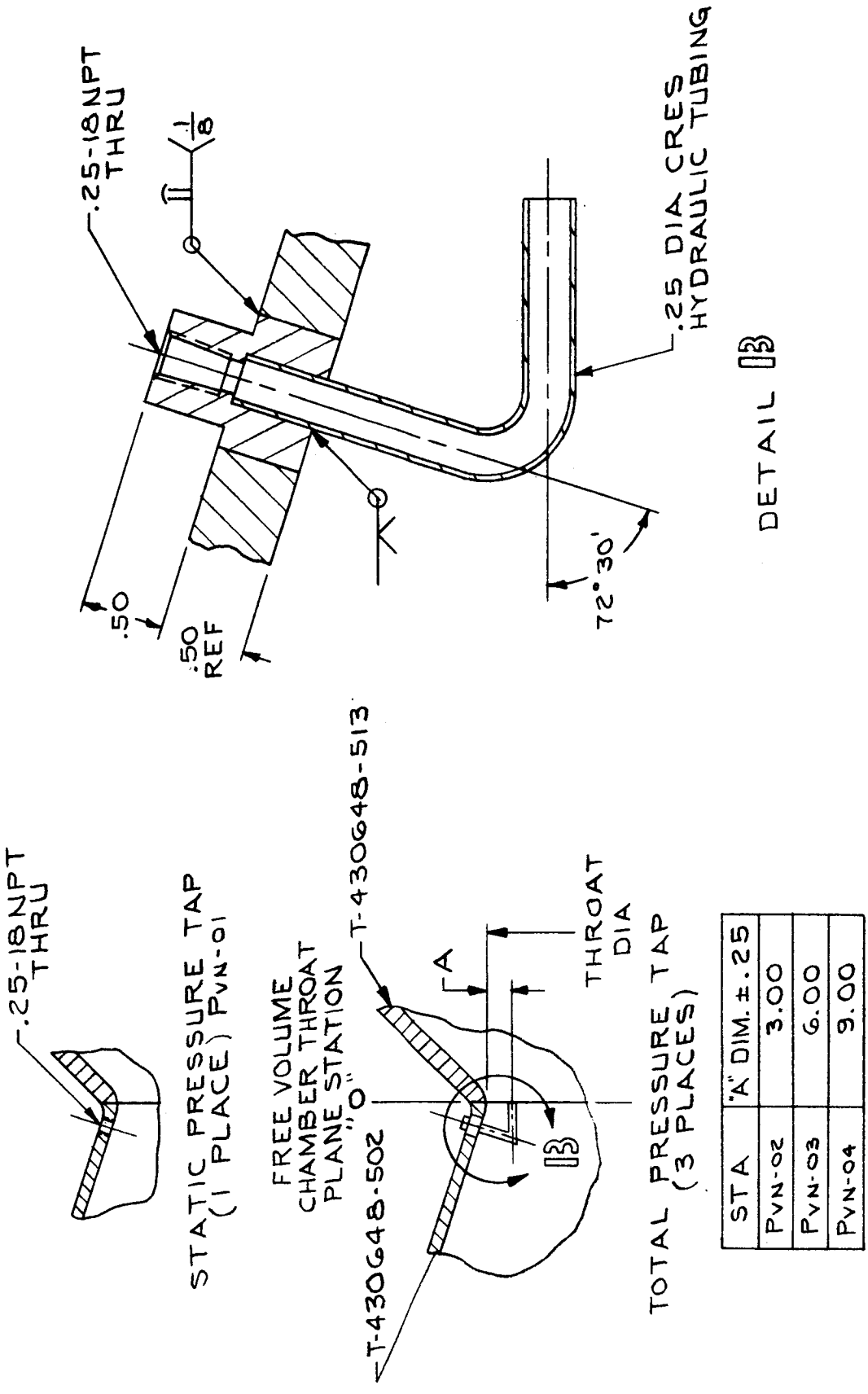

STA	"A" DIM. ±.25
PVN-02	3.00
PVN-03	6.00
PVN-04	9.00

260-SL Free-Volume Simulator Test Series, Throat Plane Pressure Measurements

Figure 64

NOTES:

1. WELD MICRO-MINIATURE THERMOCOUPLE LEADS TO EXTENSION WIRE (WELD RED TO RED).
2. INSERT THERMOCOUPLE UNTIL TC JUNCTION IS FLUSH WITH THE TOP RIM OF THE PROPELLANT CAVITY.
3. BOND THERMOCOUPLE WITH DUCO CEMENT AS SHOWN AND AIR CURE FOR 15 MINUTES.
4. AFTER INSURING SEPARATION OF BARE WIRE ELEMENTS, POT WITH BEE'S WAX.
5. CAST PROPELLANT SO THAT TC JUNCTION IS JUST BELOW THE PROPELLANT SURFACE.

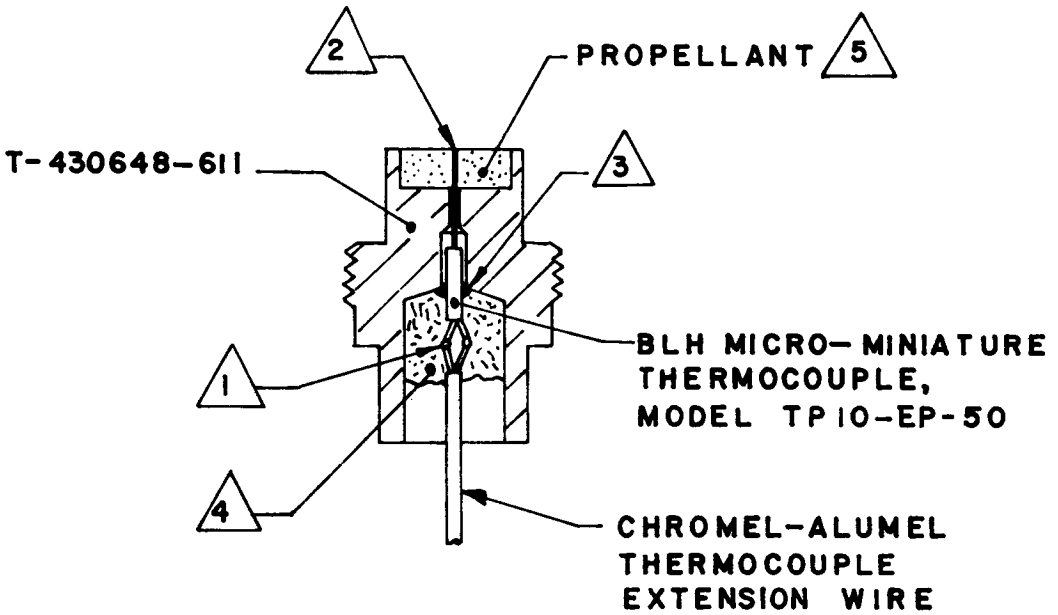

Figure 65

260-SL Free-Volume Simulator Test Series, Propellant Patch Assembly

	Test No. 1 260-IM-02	Test No. 2 260-IM-03
Station 1:		
Max Pressure; psia	77.9	79.1
Time of Propellant Patch Ignition, sec	Invalid	0.30
Total Heat Flux, cal/cm^2	Invalid	87
Heat Flux Rate, cal/cm^2-sec	Invalid	90
Station 2:		
Max Pressure, psia	77.0	77.6
Time of Propellant Patch Ignition, sec	0.24	0.34
Total Heat Flux, cal/cm^2	112	123
Heat Flux Rate, cal/cm^2-sec	120	131
Station 3:		
Max Pressure, psia	80.8	Invalid
Time of Propellant Patch Ignition, sec	0.23	.29
Total Heat Flux, cal/cm^2	123	122
Heat Flux Rate, cal/cm^2-sec	125	138
Station 4:		
Max Pressure; psia	84.2	83.7
Time of Propellant Patch Ignition, sec	0.27	Invalid
Total Heat Flux, cal/cm^2	Invalid	Invalid
Heat Flux Rate, cal/cm^2-sec	Invalid	Invalid
Station 5:		
Max Pressure, psia	87.2	Invalid
Time of Propellant Patch Ignition, sec	0.25	Invalid
Total Heat Flux, cal/cm^2	100	88
Heat Flux Rate, cal/cm^2-sec	94	94
Station 6:		
Max Pressure, psia	86.8	85.3
Time of Propellant Patch Ignition, sec	Invalid	0.34
Total Heat Flux, cal/cm^2	86	78
Heat Flux Rate, cal/cm^2-sec	85	81
Station 7:		
Max Pressure, psia	86.7	85.3
Time of Propellant Patch Ignition, sec	0.27	0.28
Total Heat Flux, cal/cm^2	70	58
Heat Flux Rate, cal/cm^2-sec	69	66

Summary of 260-SL Free-Volume Simulator Test Data

	Test No. 1 260-IM-02	Test No. 2 260-IM-03
Station 8:		
Max Pressure, psia	86.9	85.4
Time of Propellant Patch Ignition, sec	0.24	0.29
Total Heat Flux, cal/cm^2	61	42
Heat Flux Rate, cal/cm^2-sec	63	56
Station 9:		
Max Pressure, psia	86.7	85.6
Time of Propellant Patch Ignition, sec	0.38	0.35
Total Heat Flux, cal/cm^2	46	42
Heat Flux Rate, cal/cm^2-sec	47	50
Station 10:		
Max Pressure, psia	87.5	85.6
Time of Propellant Patch Ignition, sec	0.32	0.38
Total Heat Flux, cal/cm^2	35	Invalid
Heat Flux Rate, cal/cm^2-sec	34	Invalid
Station 11:		
Max Pressure, psia	87.9	85.4
Time of Propellant Patch Ignition, sec	0.48	0.43
Total Heat Flux, cal/cm^2	30	29
Heat Flux Rate, cal/cm^2-sec	28	28
Station 12:		
Max Pressure, psia	85.2	86.2
Time of Propellant Patch Ignition, sec	0.58	0.54
Total Heat Flux, cal/cm^2	23	23
Heat Flux Rate, cal/cm^2-sec	19	22
Station 13:		
Max Pressure, psia	85.5	86.5
Time of Propellant Patch Ignition, sec	0.75	Invalid
Total Heat Flux, cal/cm^2	15	11
Heat Flux Rate, cal/cm^2-sec	9	9
Station 14:		
Max Pressure, psia	88.3	86.0
Time of Propellant Patch Ignition, sec	Off Scale	0.66
Total Heat Flux, cal/cm^2	10	18
Heat Flux Rate, cal/cm^2-sec	9	16
Station 15:		
Max Pressure, psia	Invalid	84.9

Summary of 260-SL Free-Volume Simulator Test Data

Figure 66, Sheet 2 of 2

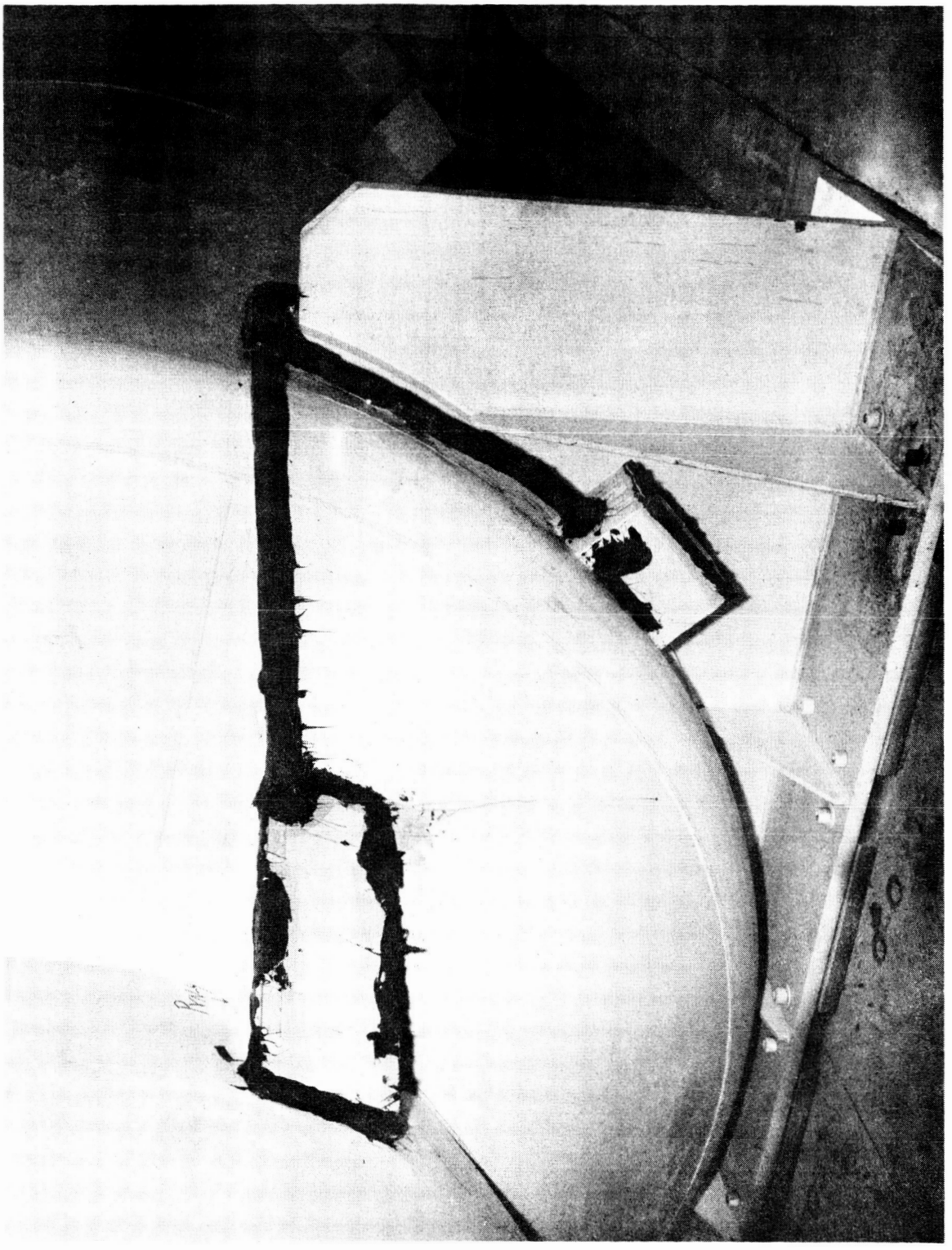

Environmental Protection for Aft- Free-Volume Simulator Instrumentation

Figure 67

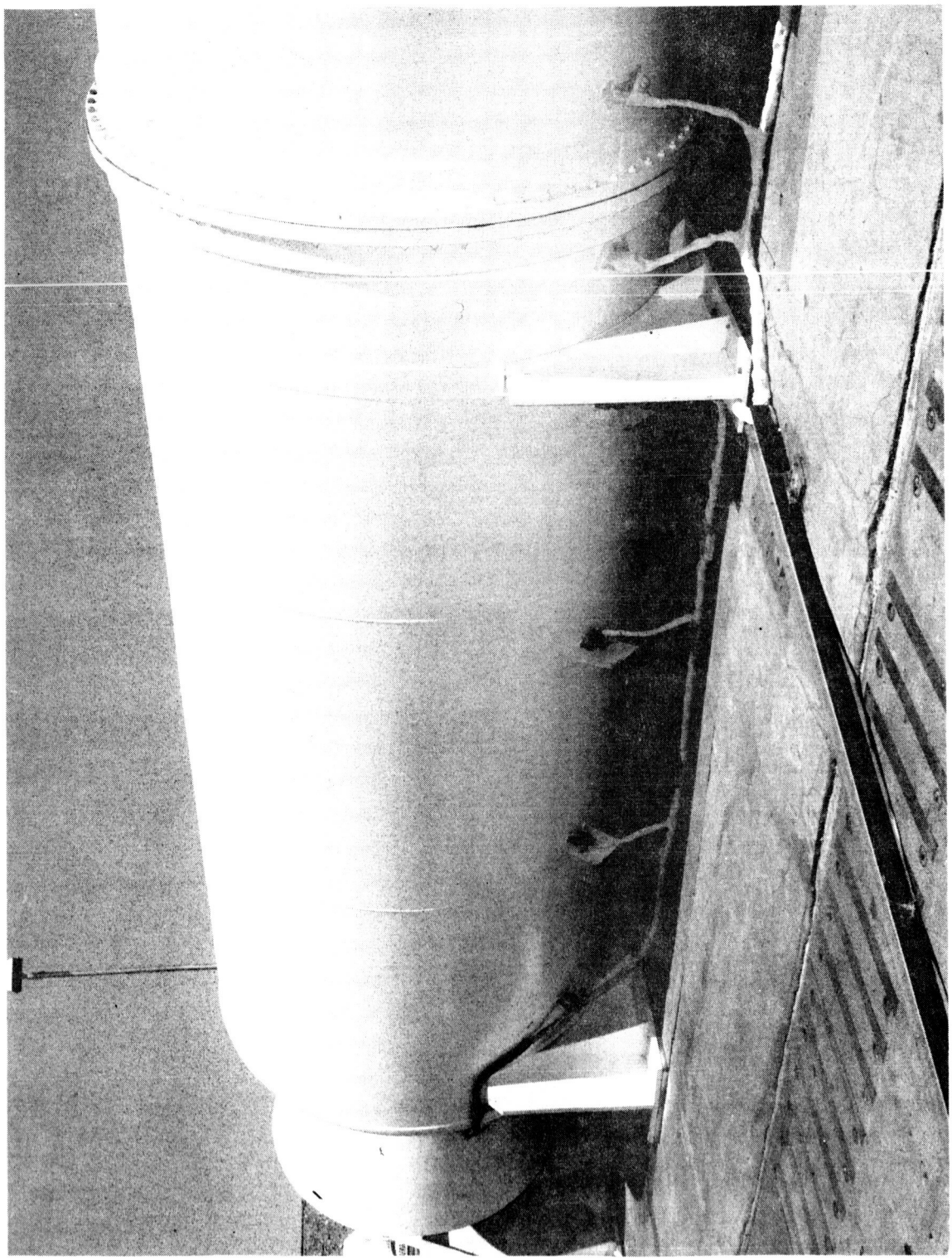

Environmental Protection for Free-Volume Simulator Bore Instrumentation

Figure 68

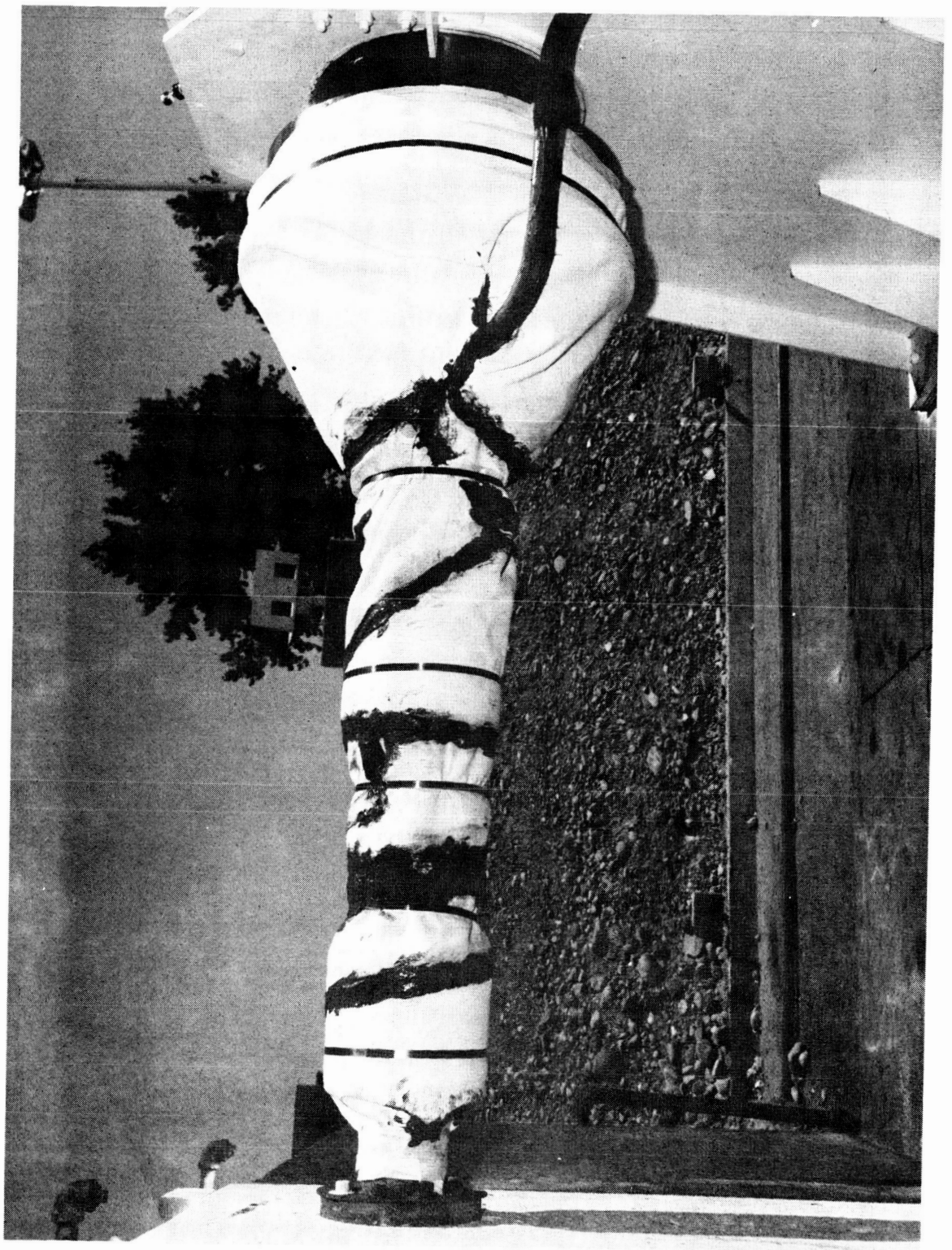

Figure 69

(Pressure, psia)

Time, sec	P_{vc-1}		P_{vc-2}		P_{vc-3}		P_{vc-4}	
	IM-02	IM-03	IM-02	IM-03	IM-02	IM-03	IM-02	IM-03
0.20	84.4	70.2	73.4	70.7	66.0	74.2	80.7	76.7
0.25	77.9	--	77.0	74.5	80.8	78.9	84.2	82.9
0.30	76.1	74.2	76.2	74.7	79.2	80.2	83.1	82.9
0.40	75.1	76.2	75.5	75.0	76.7	80.2	81.4	83.0
0.50	74.7	79.1	74.5	77.6	75.9	Data	80.7	83.7
0.60	65.3	76.2	74.2	75.2	76.5	lost	80.0	82.4
0.70	Data	74.7	75.2	73.0	77.2	at .4	80.0	81.4
0.80	becomes	72.2	75.7	71.5	77.2	sec	80.0	80.0
0.90	invalid	69.2	70.3	69.2	72.7		74.7	75.5
1.00	at .63	64.0	64.9	64.1	66.7		67.0	69.3
1.25	sec	38.5	37.8	38.5	39.2		41.1	44.0
1.50		24.7	21.5	24.5	21.7		22.6	25.9

	P_{vc-5}		P_{vc-6}		P_{vc-7}		P_{vc-8}	
0.20	84.1	Data	82.1	Unfiltered	84.4	79.7	84.3	79.1
0.25	86.1	lost	84.4	Data	86.1	83.0	86.7	82.3
0.30	87.2	at	86.8		86.7	83.5	86.9	82.8
0.40	84.6	.15 sec	83.8		84.9	84.2	85.5	84.0
0.50	84.1		82.7		84.0	85.3	84.3	85.4
0.60	83.1		81.6		83.5	84.2	83.9	83.5
0.70	83.6		80.5		83.7	82.3	84.1	82.1
0.80	83.6		81.0		84.0	80.9	84.1	79.8
0.90	78.2		75.4		77.4	76.6	78.9	76.0
1.00	69.0		67.5		68.1	69.0	68.3	68.5
1.25	43.0		--		42.8	44.0	43.0	44.7
1.50	24.1		--		24.5	27.3	24.6	28.3

	P_{vc-9}		P_{vc-10}		P_{vc-11}		P_{vc-12}	
0.20	83.7	79.5	82.7	79.7	84.6	80.4	84.0	79.7
0.25	86.6	83.7	87.0	--	85.8	83.1	85.2	83.8
0.30	86.7	84.4	87.5	82.7	87.9	83.8	85.2	84.1
0.40	85.4	84.9	85.0	84.2	84.6	84.5	84.7	84.8
0.50	84.4	85.6	84.7	85.6	83.7	85.4	84.3	86.2
0.60	83.7	84.9	84.7	84.7	83.4	84.0	84.3	84.8
0.70	84.2	82.8	83.7	72.7	83.4	82.3	84.5	82.6
0.80	84.4	80.5	83.7	80.8	83.7	80.4	84.5	80.8
0.90	78.4	76.9	76.2	76.7	76.8	76.4	77.6	77.4
1.00	68.5	69.0	68.0	69.0	67.8	61.8	68.5	69.1
1.25	43.3	45.1	45.3	45.5	43.6	45.3	43.4	46.2
1.50	24.5	28.7	23.6	29.5	24.4	28.6	24.7	28.1

Summary of 260-SL Free-Volume Simulator Bore Pressure Data

Figure 70, Sheet 1 of 2

Time, sec	P_{vc-13}		P_{vc-14}		P_{vc-15}	
	IM-02	IM-03	IM-02	IM-03	IM-02	IM-03
0.20	82.7	80.8	80.9	80.3	Data	80.1
0.25	85.5	83.5	88.3	83.5	lost	82.2
0.30	85.5	83.8	87.3	85.2	at .16	83.3
0.40	84.3	85.4	84.8	85.6	sec	84.2
0.50	83.4	86.5	83.7	86.0		84.9
0.60	83.4	86.3	84.2	85.5		84.2
0.70	83.6	82.9	Data	82.4		81.9
0.80	83.6	80.8	becomes	80.6		80.1
0.90	76.8	78.1	invalid	77.3		76.4
1.00	67.6	69.2	at .64 sec	70.0		68.3
1.25	43.0	45.9		45.9		44.3
1.50	24.6	29.3		29.7		28.1

Summary of 260-SL Free-Volume Simulator Bore Pressure Data

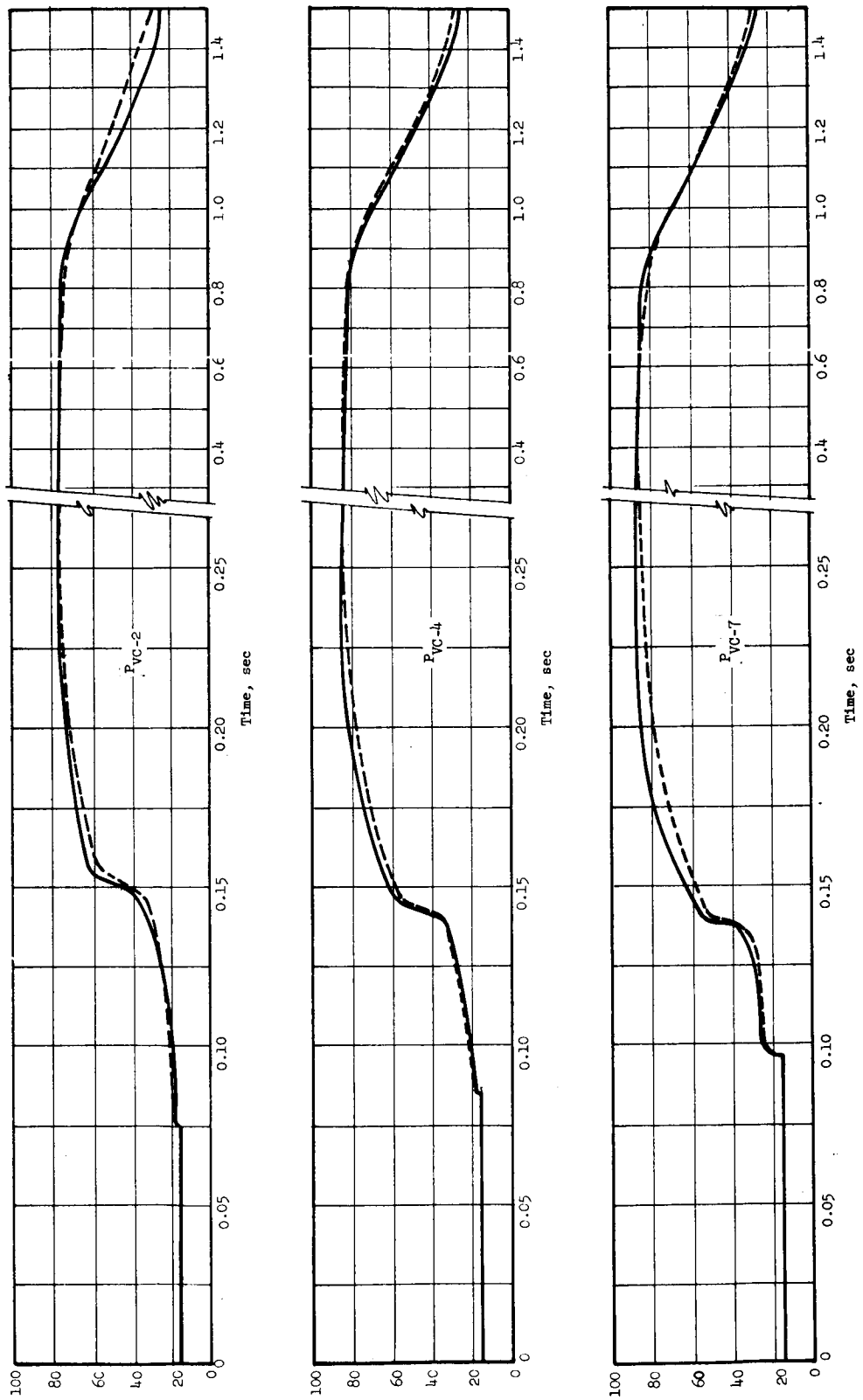

Typical Bore Pressure Curves, 260-SL Free-Volume Simulator Tests

Figure 71, Sheet 1 of 2

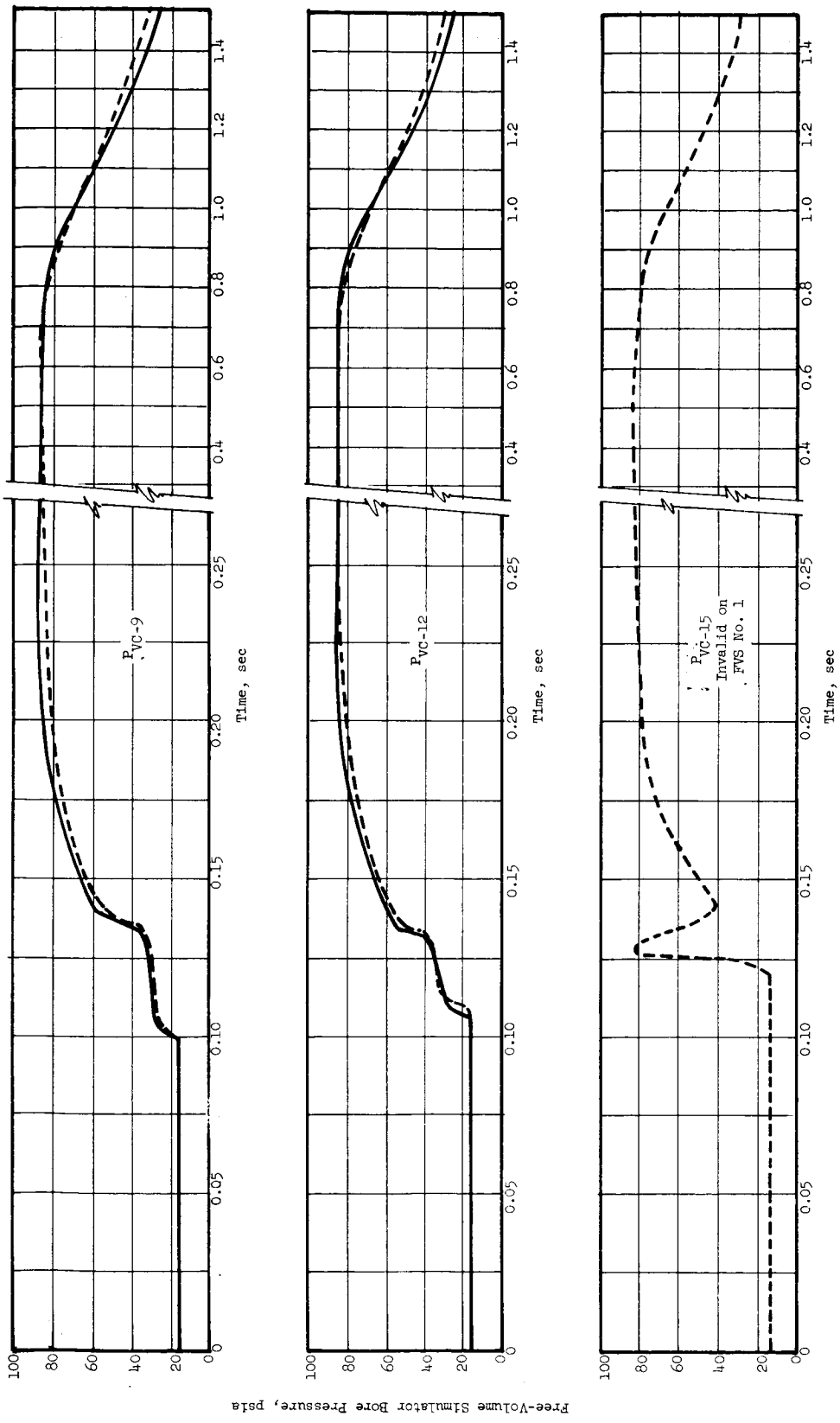

Typical Bore Pressure Curves, 260-SL Free-Volume Simulator Tests

Figure 71, Sheet 2 of 2

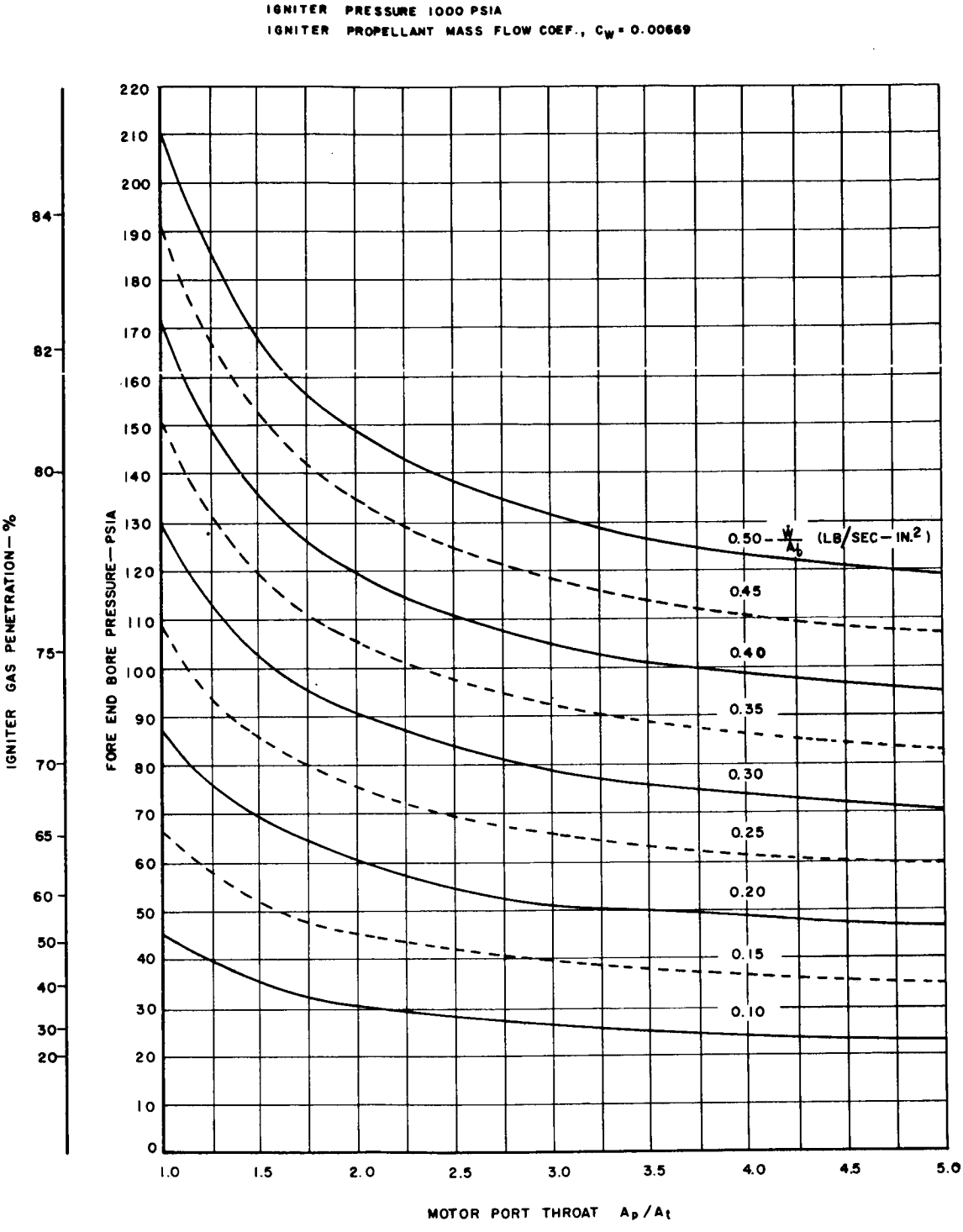

IGNITION GAS PENETRATION AND FORE END MOTOR BORE PRESSURE AS A FUNCTION OF IGNITER MASS FLOW ($\dot{W}$) MOTOR PORT AREA (A_p) AND MOTOR THROAT AREA (A_t) BETWEEN IGNITER OPERATING PRESSURES OF 800 TO 1200 PSIA

Solution of Aft-End Ignition Analytical Model Equations for C_W = 0.00669

Figure 72

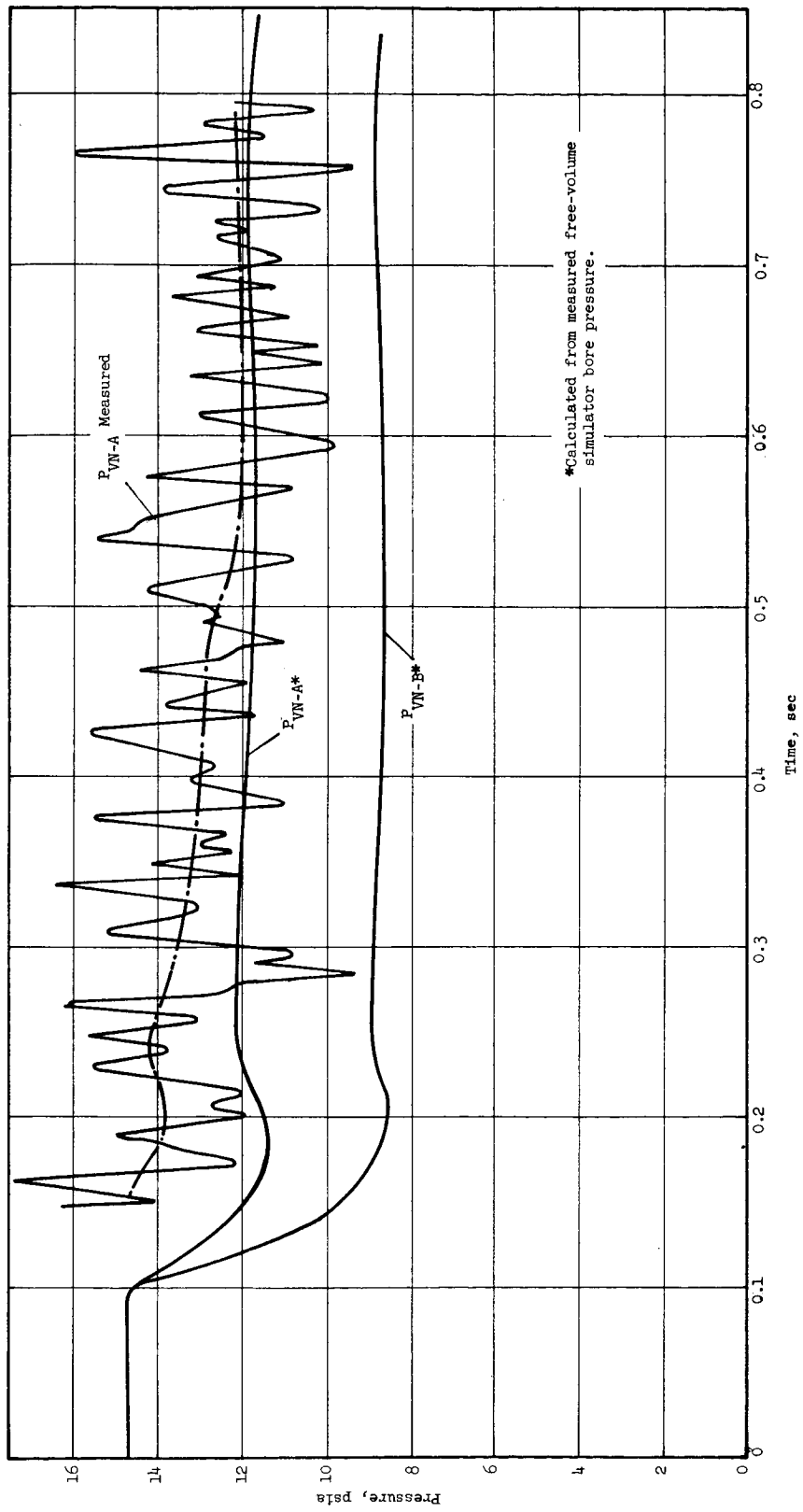

260-SL Free-Volume Simulator Exit Cone Static Pressure vs Time Curve, Test No. 1

Figure 73

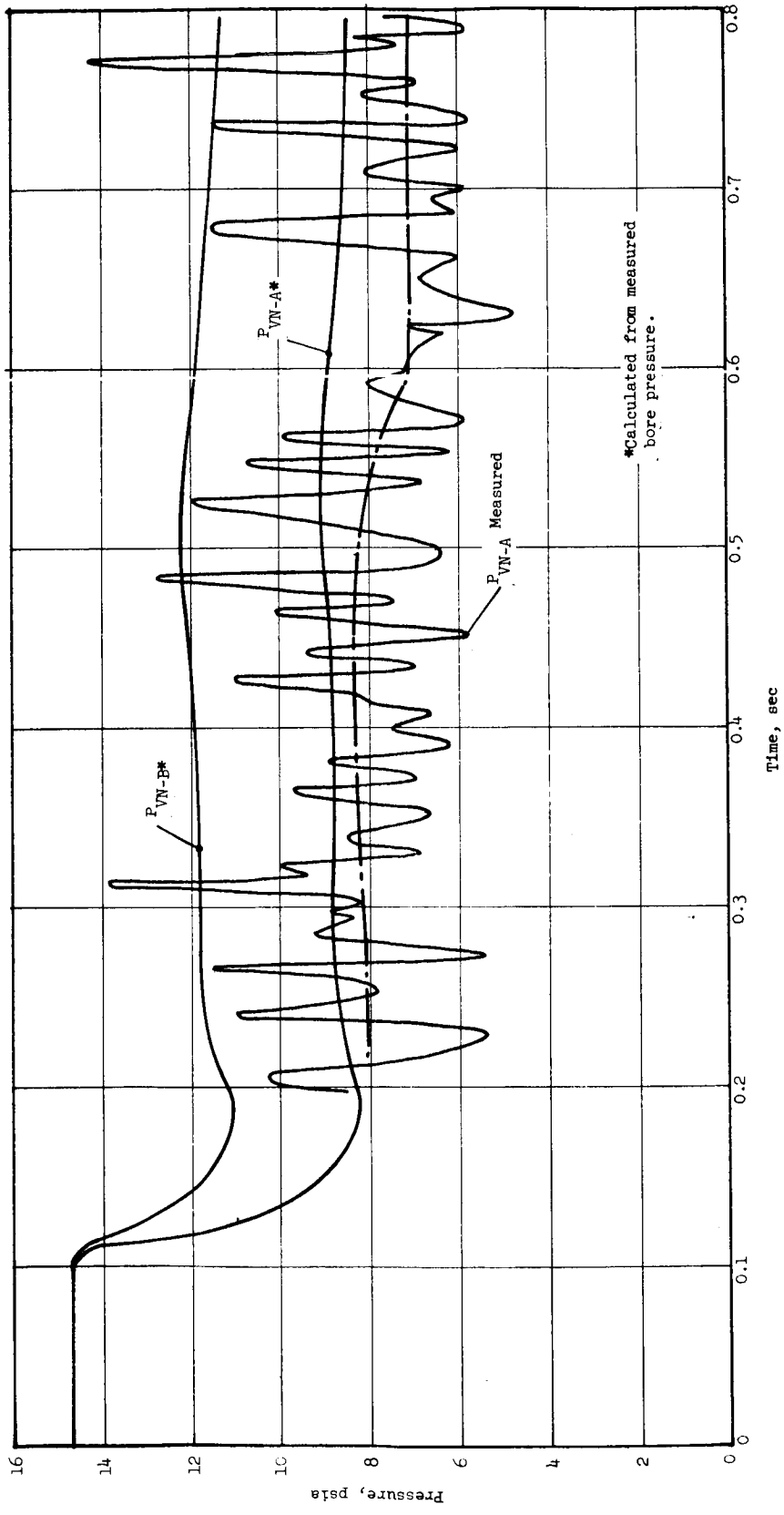

260-SL Free-Volume Simulator Exit Cone Static Pressure vs Time Curve, Test No. 2

Figure 74

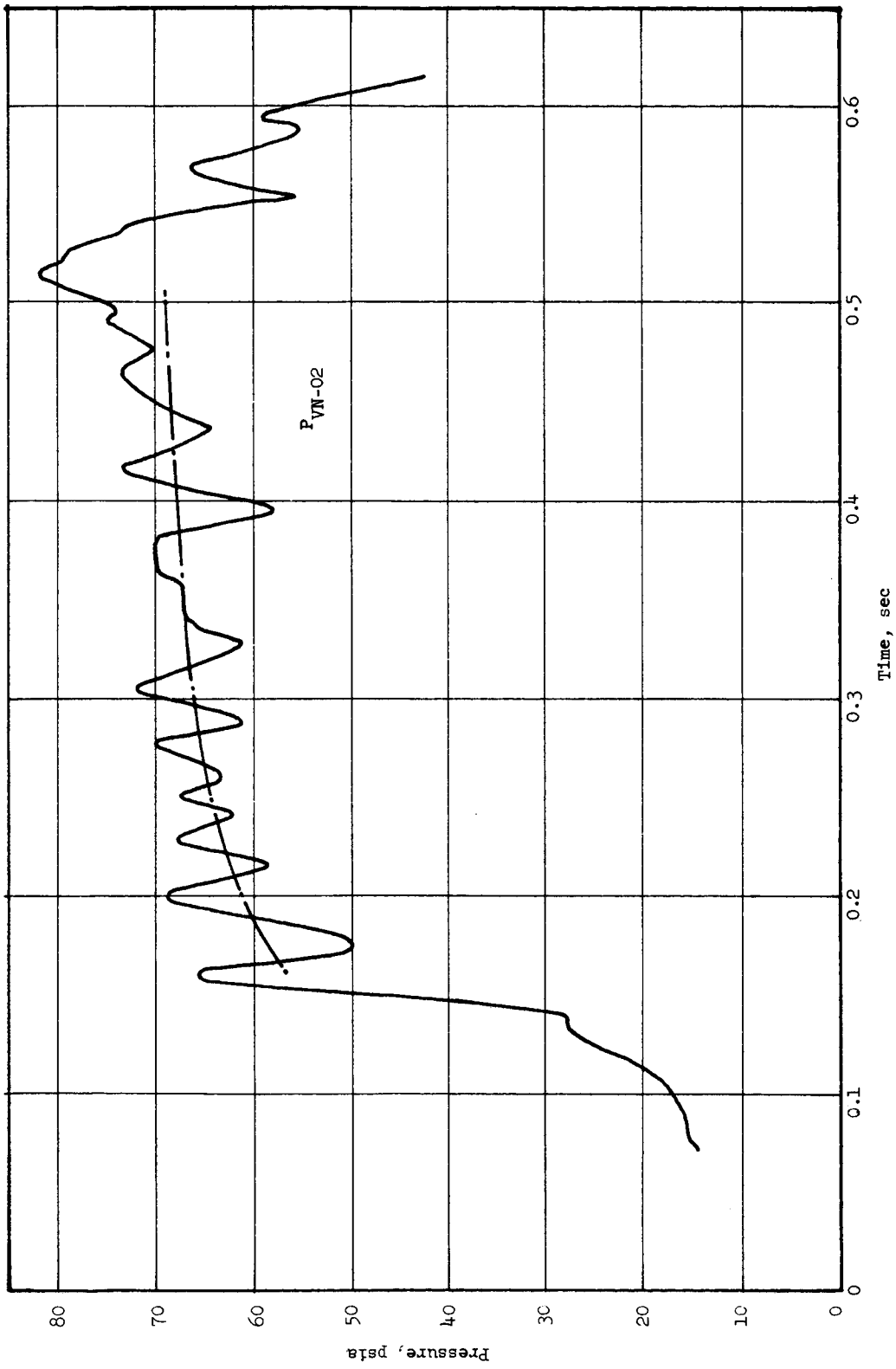

260-SL Free-Volume Simulator Throat Plane Total Pressure vs Time Curve,
3.0-in.-long Tube, Test No. 2

Figure 75

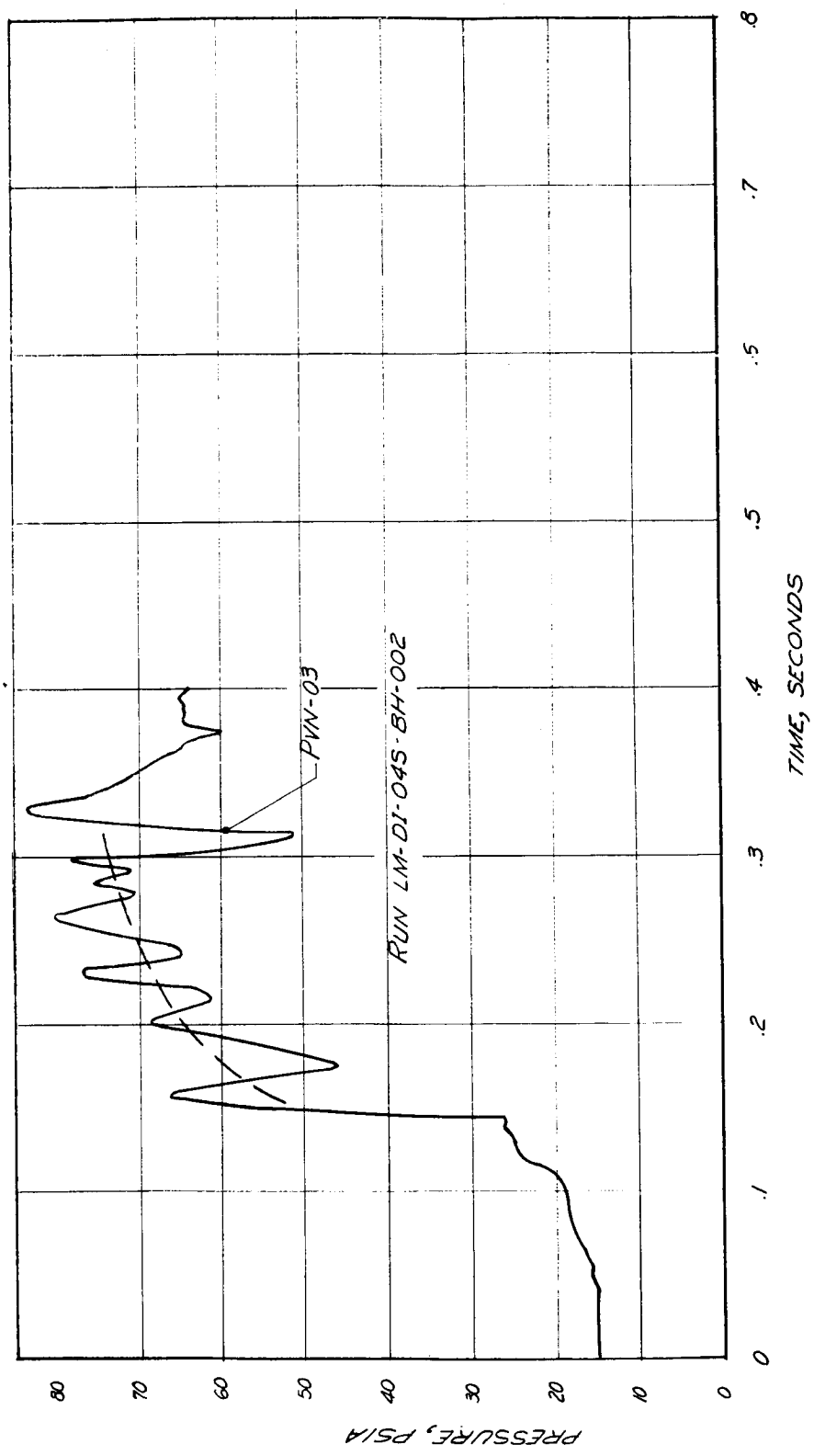

260-SL Free-Volume Simulator Throat Plane Total Pressure vs Time Curve, 6.0-in.-long Tube, Test No. 2

Figure 76

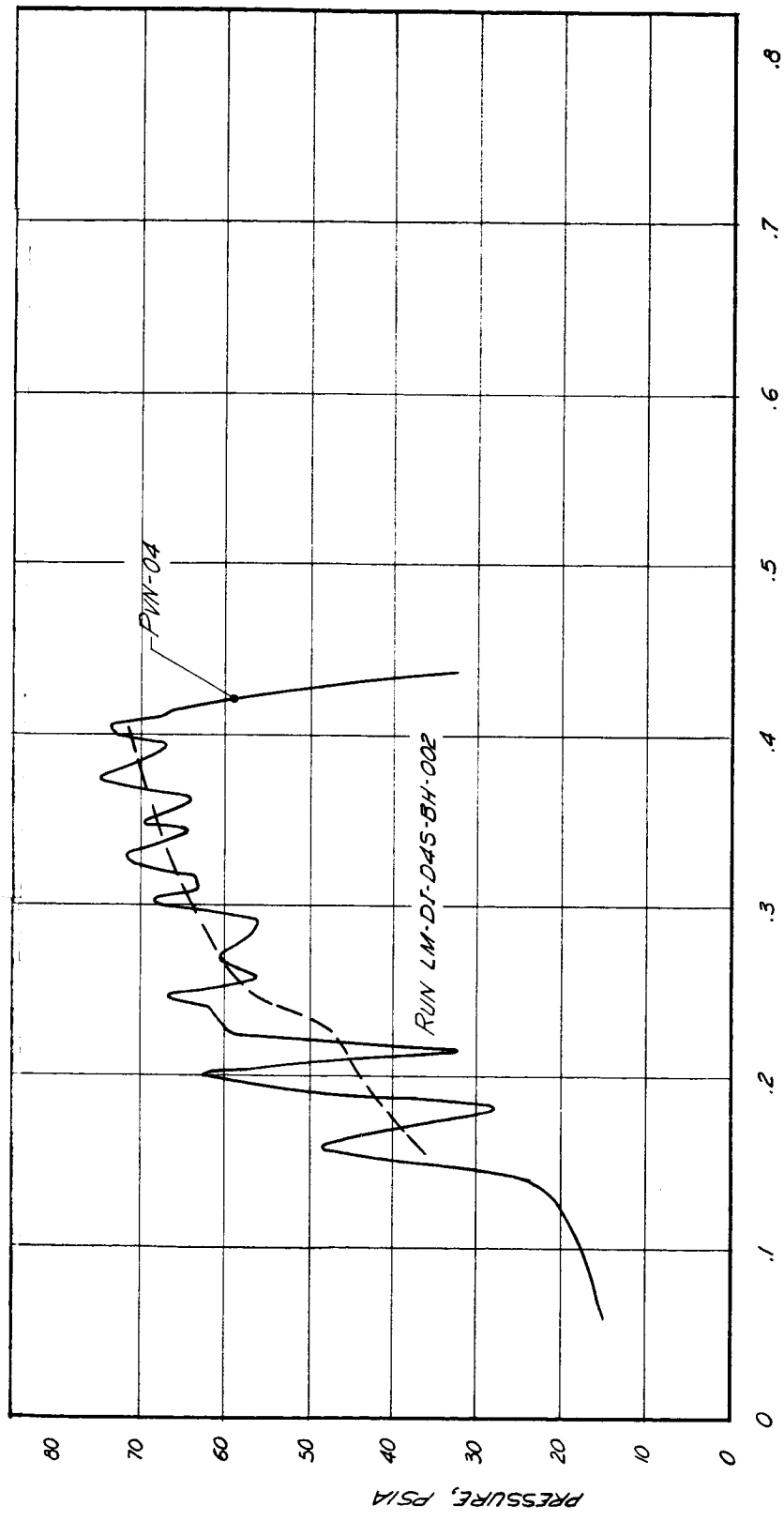

260-SL Free-Volume Simulator Throat Plane Total Pressure vs Time Curve,
9.0-in.-long Tube, Test No. 2

Figure 77

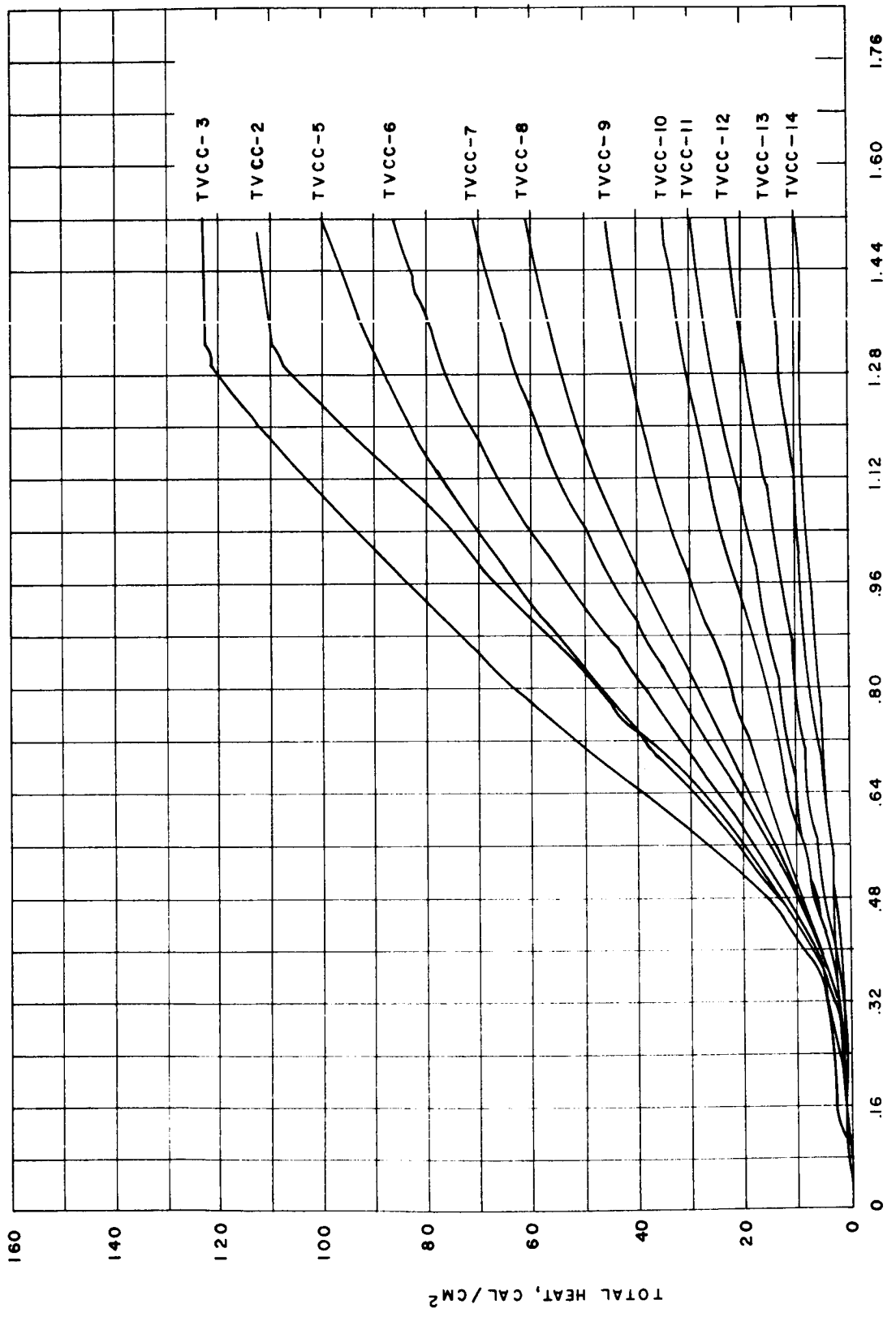

260-SL Free-Volume Simulator Calorimetry Data, Test No. 1

Figure 78

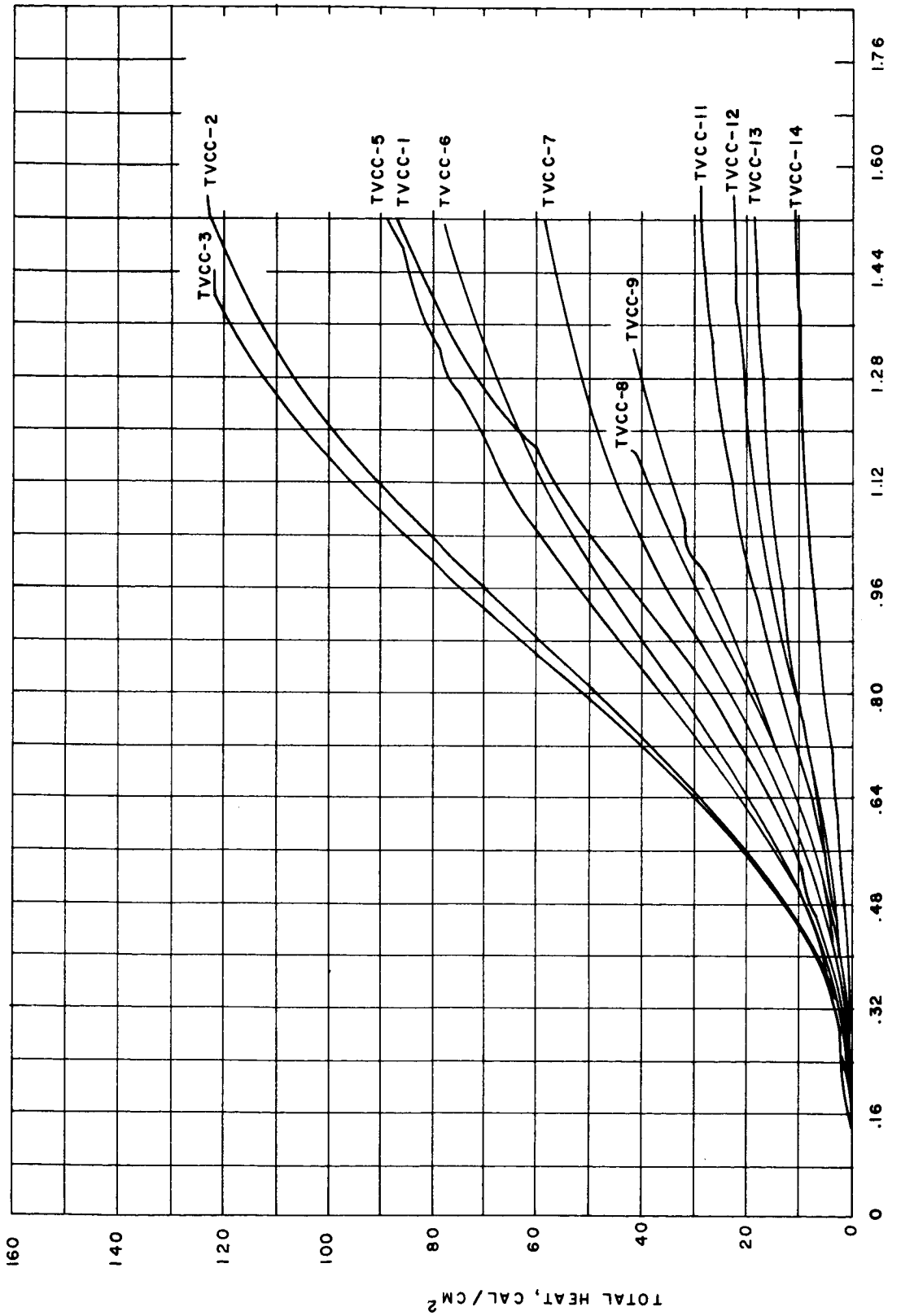

260-SL Free-Volume Simulator Calorimetry Data, Test No. 2

Figure 79

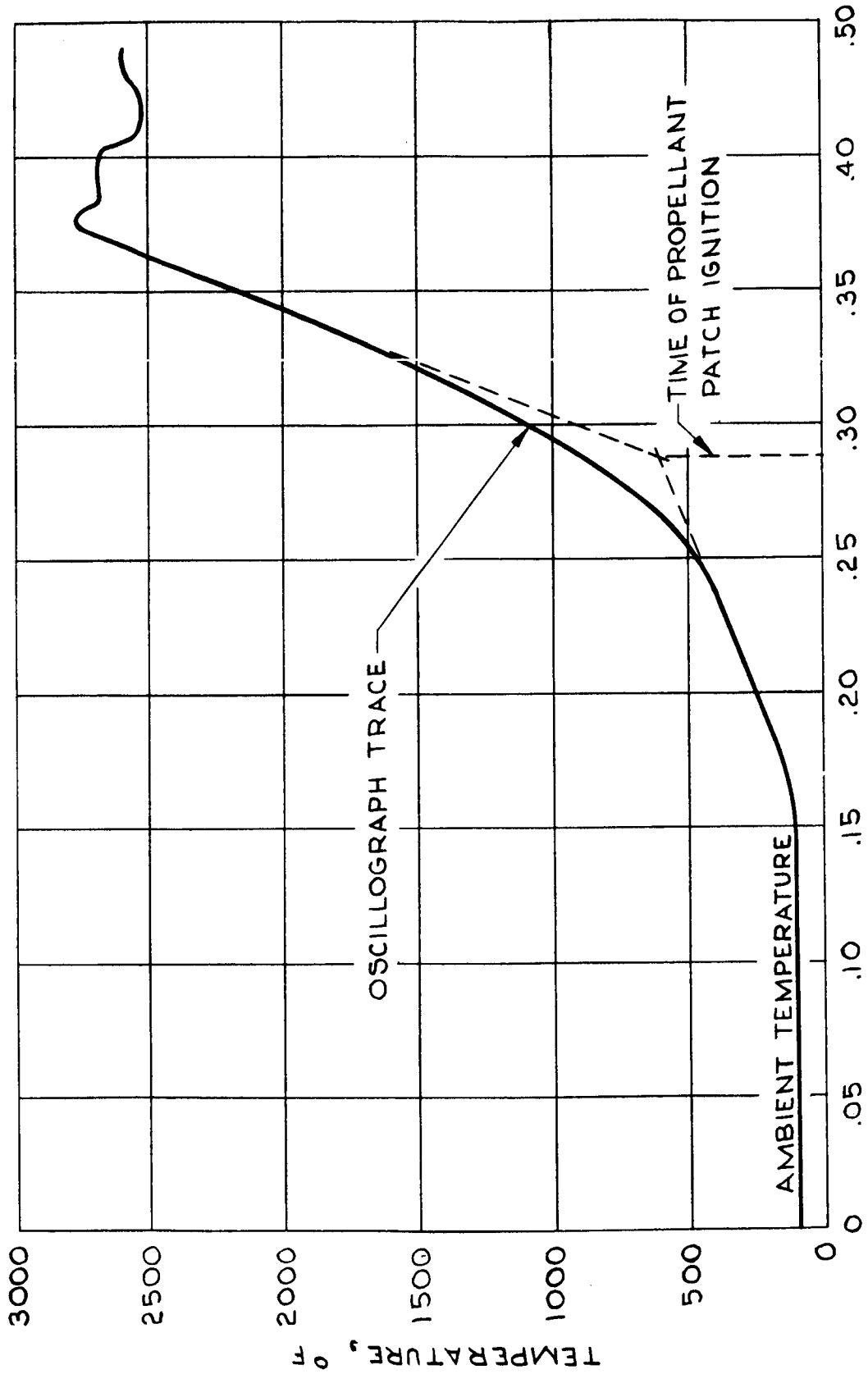

Graphical Presentation of Theoretical Time to First Propellant Ignition for 260-SL Motor

Figure 80

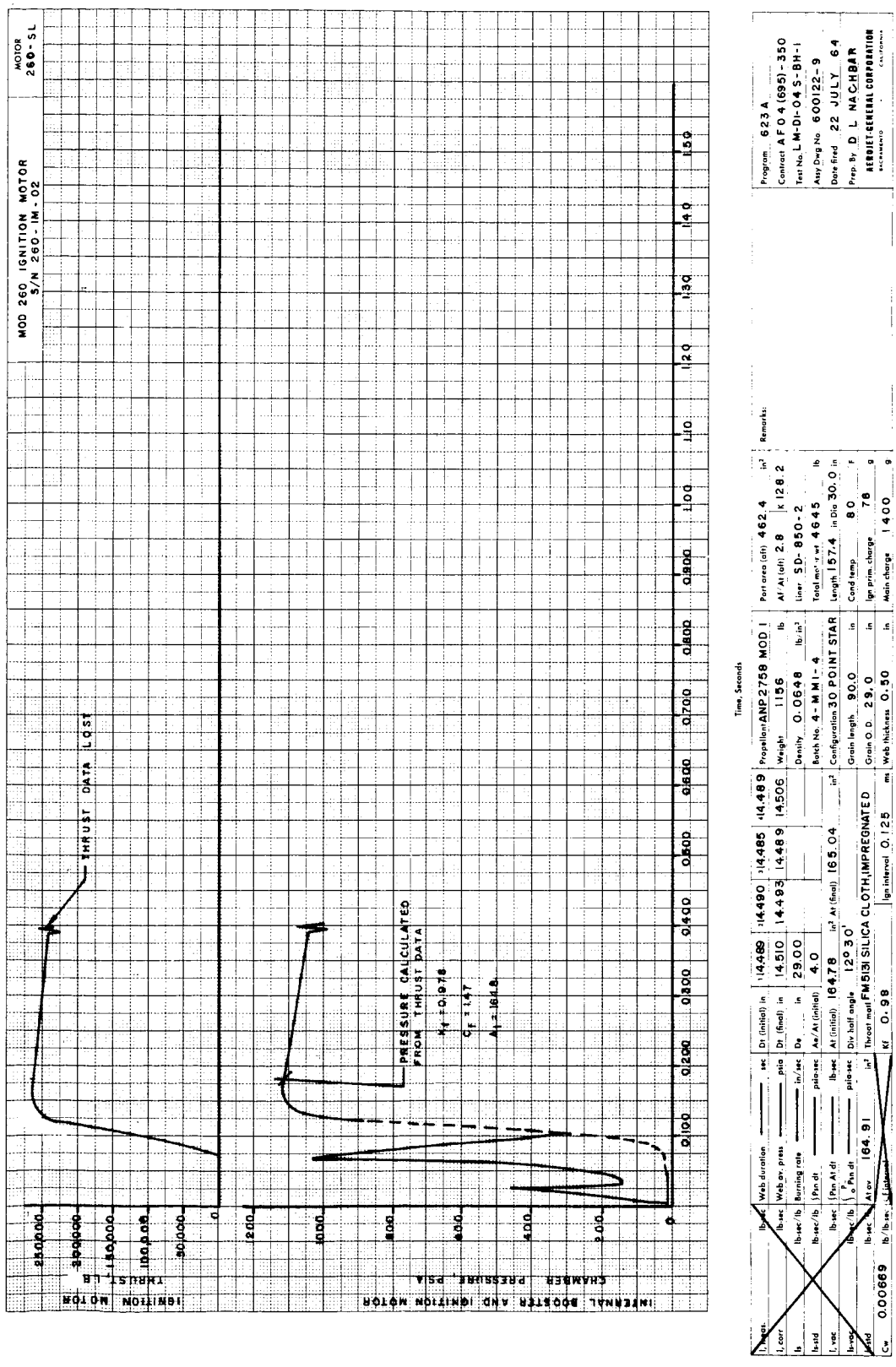

Ballistic Firing Data, Mod 260 Ignition Motor 260-IM-02

Figure 81

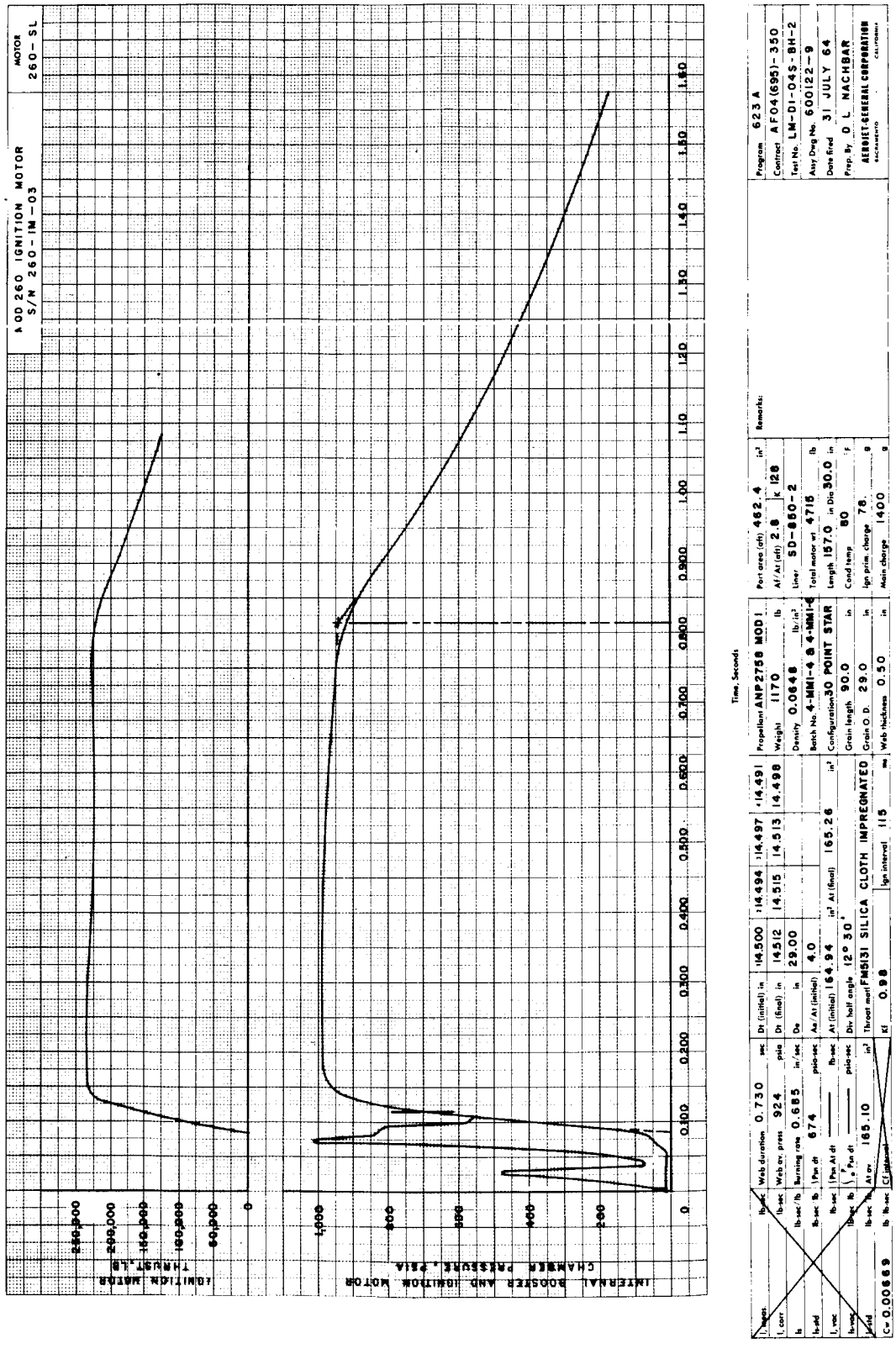

Figure 82

Ballistic Firing Data, Mod 260 Ignition Motor 260-IM-03

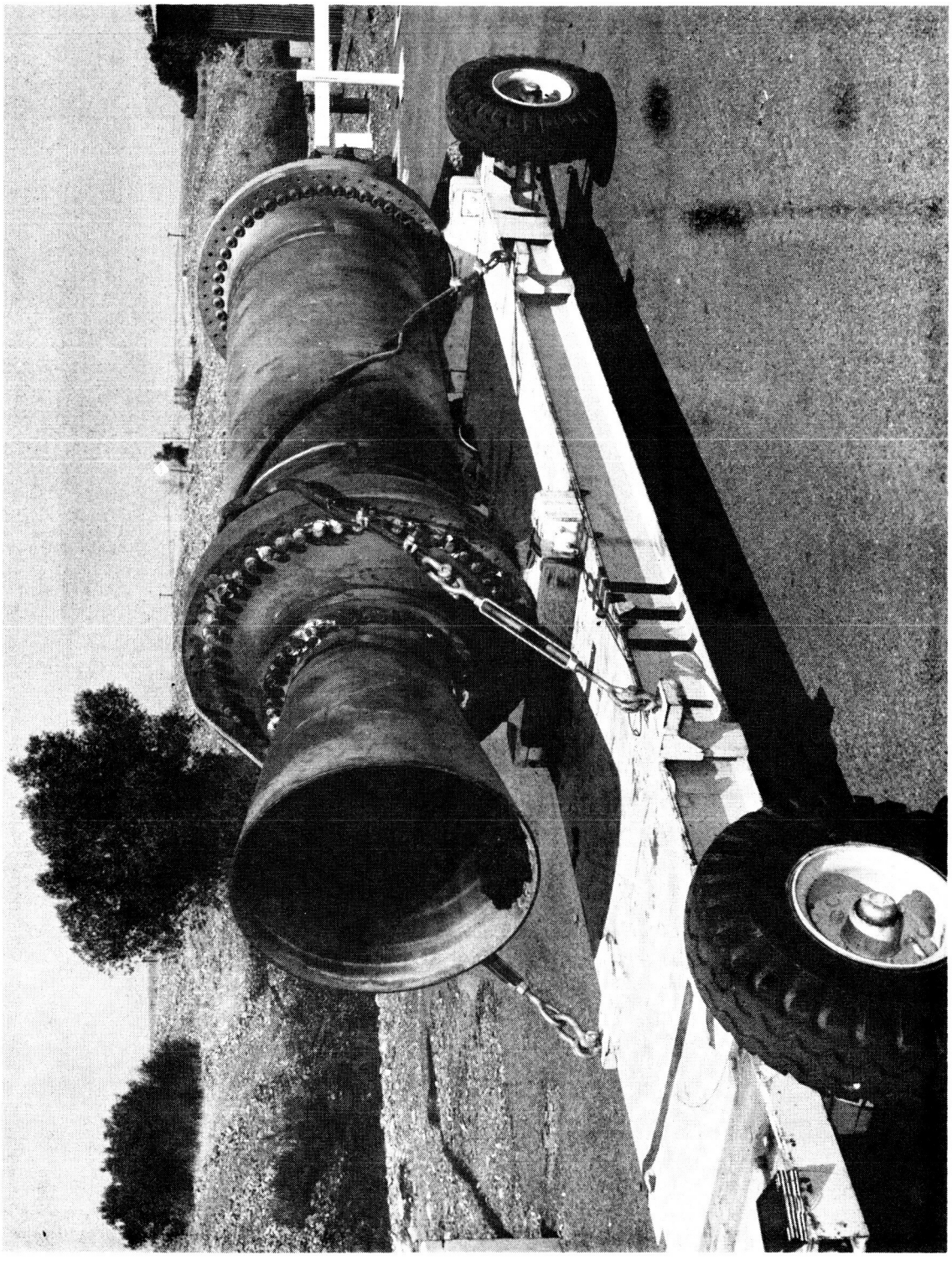

Postfiring View of Ignition Motor

Figure 83

Designation	Location*	Range	Description
P_{IGN}	Ignition Motor Booster Adapter	0-1500 psig	Ignition motor and booster chamber pressure
P_{c1}	Ignition Motor Booster Adapter	0-1500 psig	Ignition motor chamber pressure
P_{c2}	Ignition Motor Booster Adapter	0-1500 psig	Ignition motor chamber pressure
P_{VN-B}	- 40.0 in.	0-30 psia	Simulator exit cone static pressure
P_{VN-A}	- 28.0 in.	0-30 psia	Simulator exit cone static pressure
P_{VN-0}	0	0-50 psig	Simulator throat plane static pressure
P_{VC-15}	707.0 in. Fore-head	0-100 psig	Simulator fore-end bore pressure
P_{VC-8}	376.75 in.	0-100 psig	Simulator bore pressure
P_{VC-4}	205.5 in.	0-100 psig	Simulator bore pressure
E_{FS}	N/A	Trace Only	Fire-switch
I_{FS}	N/A	Trace Only	Firing current
E_{EBA}	N/A	Trace Only	Explosive bolt actuation
t_sLI-1	N/A	Trace Only	Breakwire at 1.0-in.
t_sLI-2	N/A	Trace Only	Breakwire at midpoint of track (20.75 ft)
t_sLI-3	N/A	Trace Only	Breakwire at end of track (41.5 ft)
t_sRAC	N/A	Trace Only	Igniter release control unit logic satisfied
t_sTRA	N/A	Trace Only	Tower assembly release actuation
LT	N/A	Trace Only	Tower assembly retraction motion
G-MSF-y		100 g	Acceleration of ignition motor support fixture adjacent to the ignition motor forward flange

*Free-volume-simulator throat plane: indicates downstream

Mod 260 Ignition Motor Retention-and-Release System Demonstration
Test Instrumentation List

Figure 84, Sheet 1 of 2

Description	Location*	Range	Description
G-X-090-5'	Tower	100 g	Acceleration of tower assembly at the base, midpoint and top, in two axes perpendicular to the axis of the track
G-X-090-26'	↓	↓	
G-X-090-53'			
G-Z-090-5'			
G-Z-090-26'			
G-Z-090-53'			
PN_2	Accumulator	0-500 psig	Tower retraction motor controller accumulator charge
P_hEXT	Accumulator	----	Tower retraction motor actuator hydraulic pressure, extend
P_hRET	Accumulator	----	Tower retraction motor actuator hydraulic pressure, retract
T_{VN}-090-18	Simulator Exit Cone	0-25 MV	Simulator nozzle temperature
T_{VN}-180-18	Simulator Exit Cone	0-25 MV	Simulator nozzle temperature
TVCA-090-10	Simulator Aft Closure	0-25 MV	Simulator aft closure temperature
TVCA-180-10	Simulator Aft Closure	0-25 MV	Simulator aft closure temperature
T_{VC}-2	68.5	0-25 MV	Propellant patch
T_{VC}-3	137.0	0-25 MV	Propellant patch

*Reference: Free-volume-simulator throat plane; - indicates downstream

Mod 260 Ignition Motor Retention-and-Release System Demonstration
Test Instrumentation List

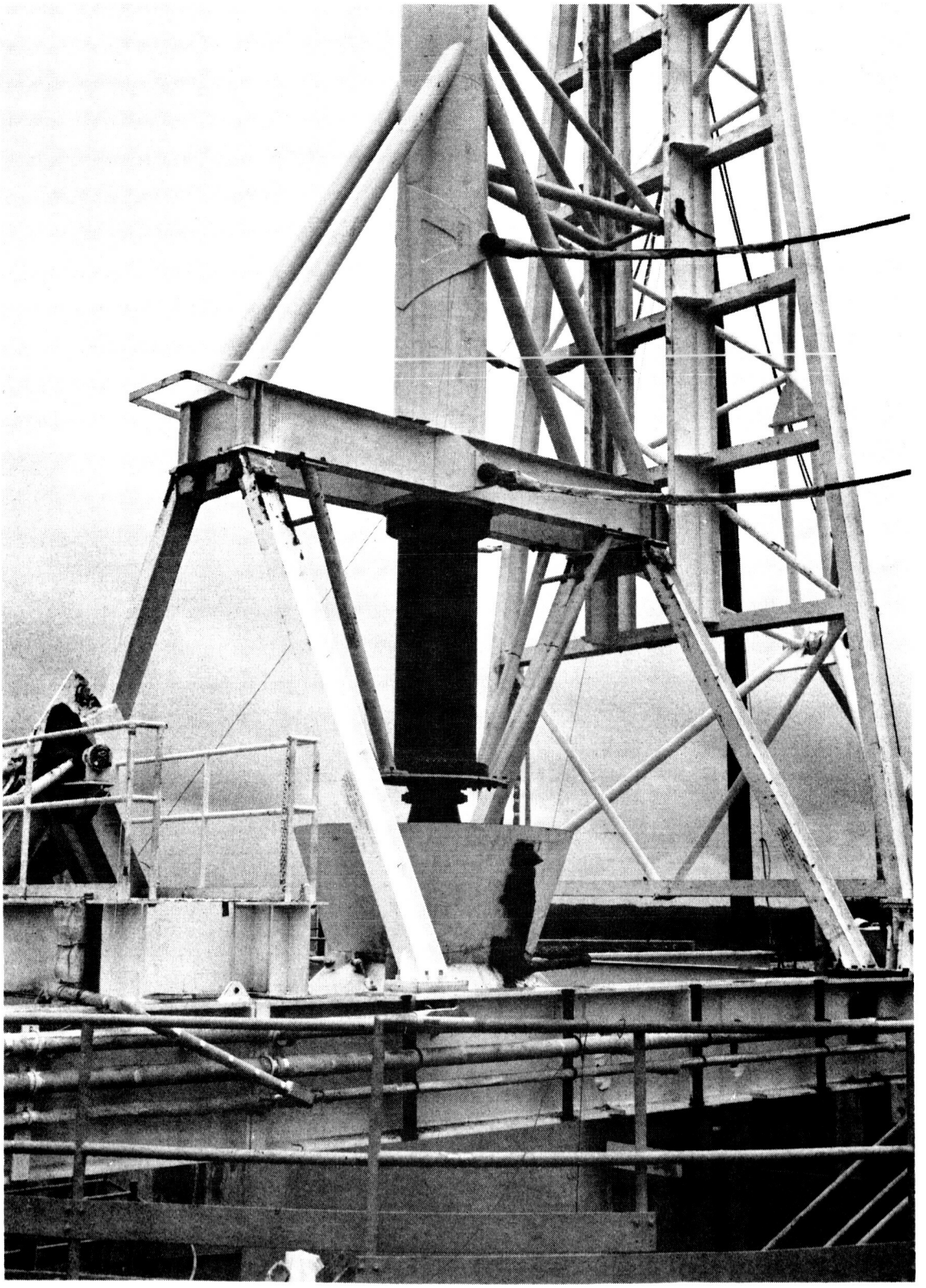

Prefiring View of Mod 260 Ignition Motor Retention-and-Release System Installation

Figure 85

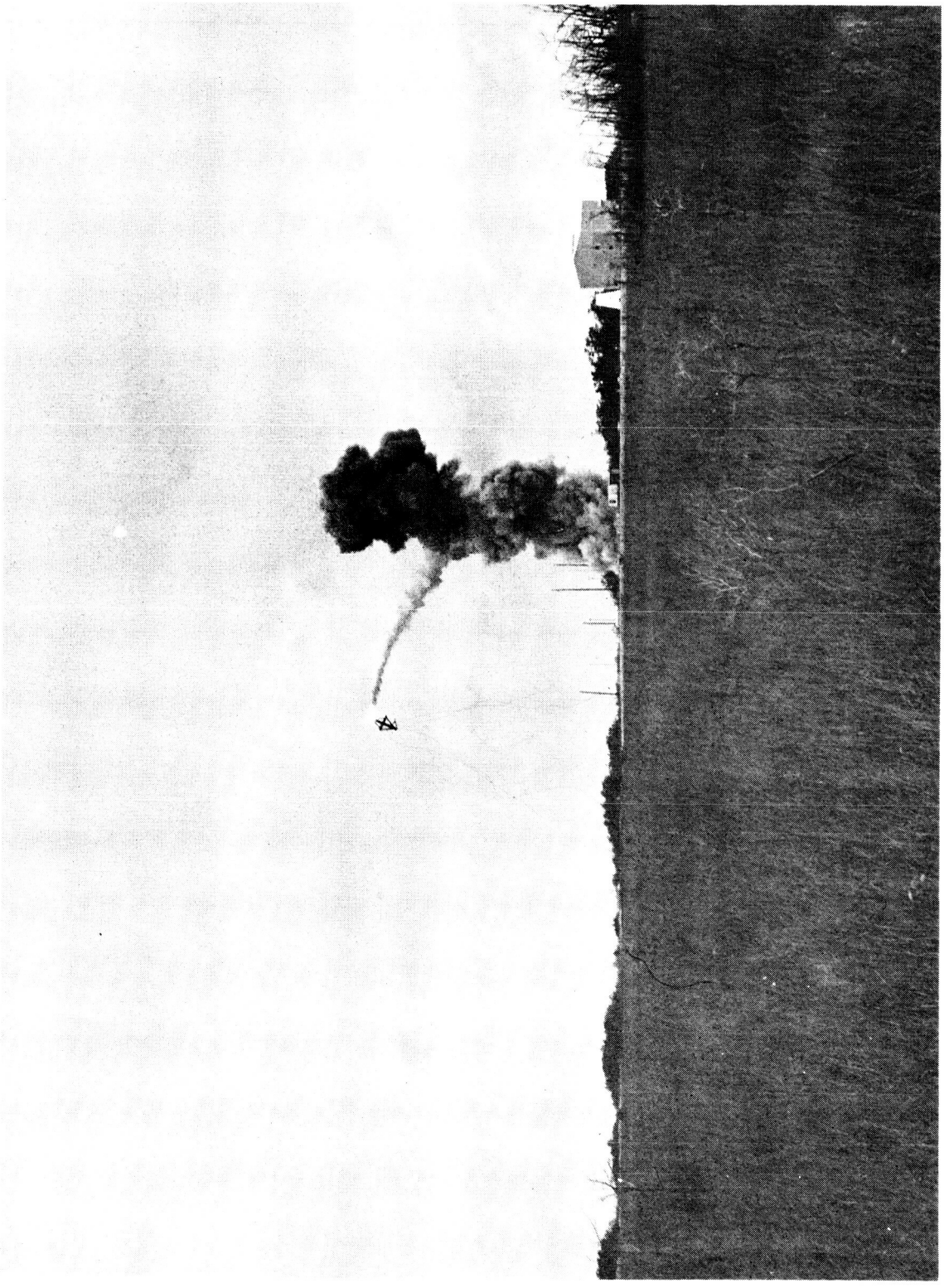

Mod 260 Ignition Motor Retention and Release System Test

Figure 86

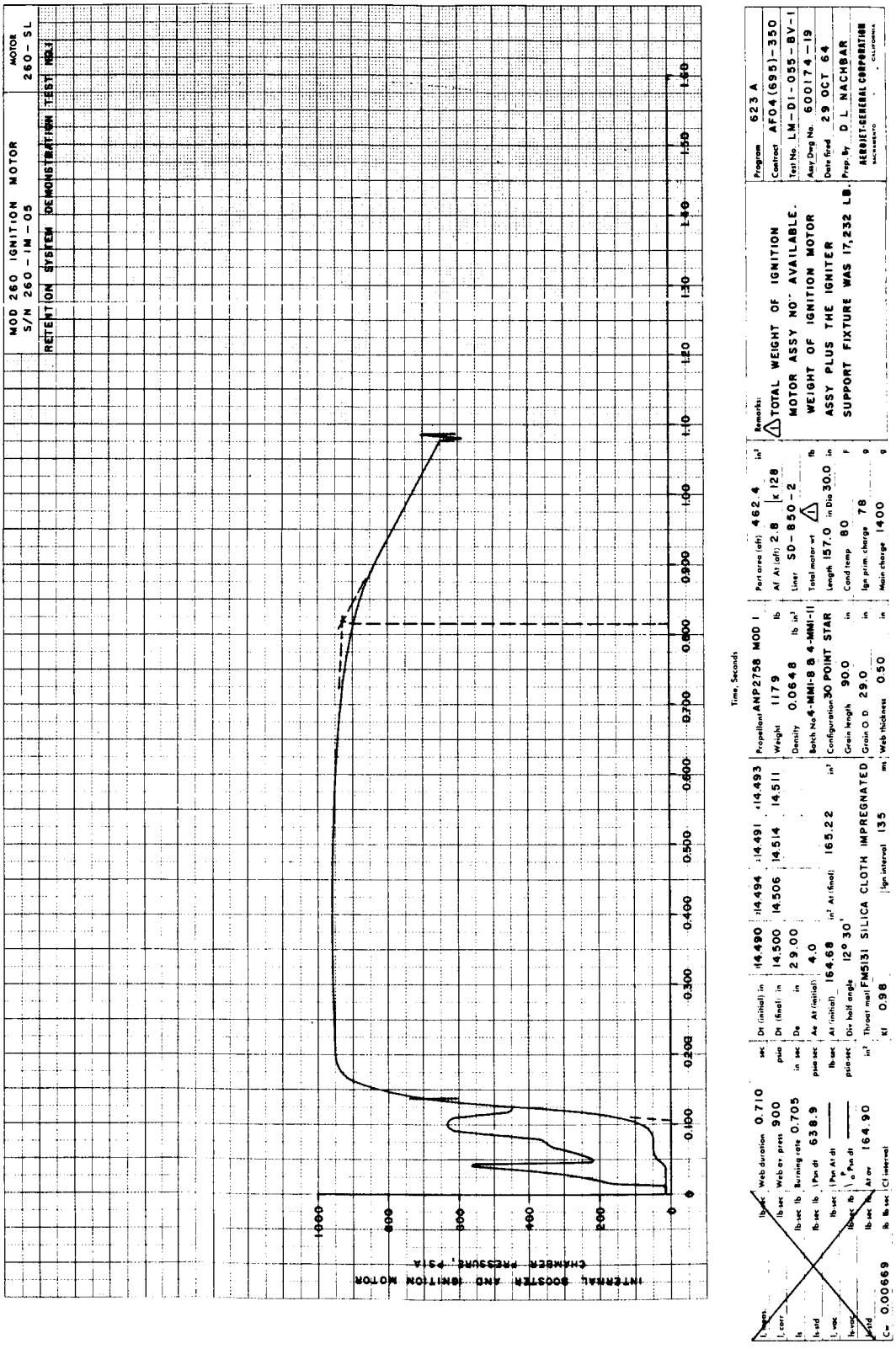

Figure 87

Ballistic Firing Data, Mod 260 Ignition Motor 260-IM-05

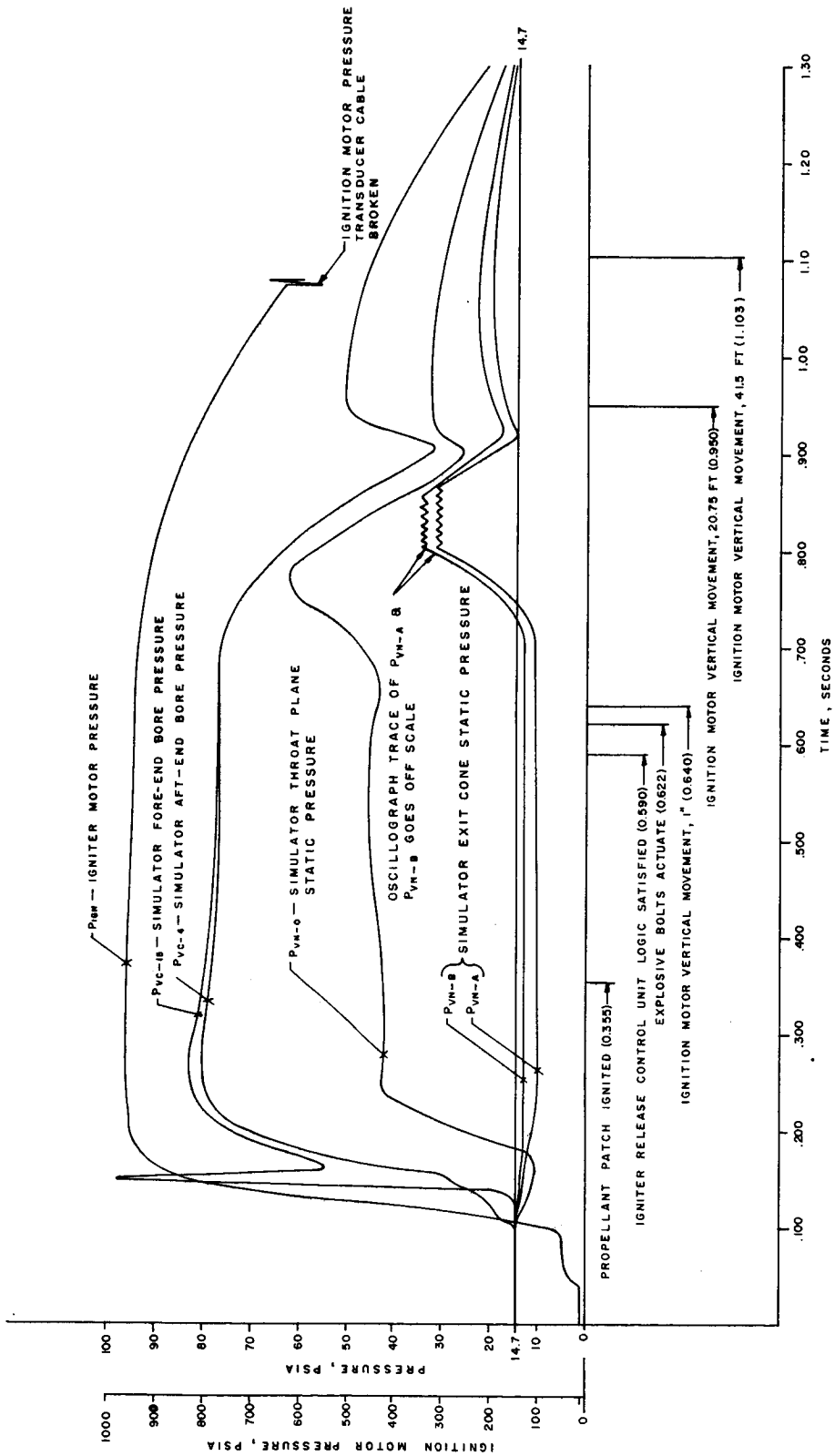

Mod 260 Ignition Motor Retention-and-Release System Demonstration Test No. 1, Free-Volume Simulator Bore and Exit Cone Pressure Data

Figure 88

RETENTION-AND-RELEASE SYSTEM DEMONSTRATION TEST NO. 1
SUMMARY OF PRESSURE AND FLOW CONDITIONS IN THE FREE-VOLUME SIMULATOR THROAT AND EXIT CONE

Time, sec	Measured Throat Plane Static Pressure, P_{VN-O}, psia	EXIT CONE STATIC PRESSURE P_{VN-B}, psia		P_{VN-A}, psia		Flow Conditions in Free-Volume Simulator Nozzle
		Measured	Calculated	Measured	Calculated	
0.125	12.6					
0.150	10.6					
0.175	11.2	13.4		13.4		Flow subsonic
0.182	14.7					
0.200	26.1					Flow choked, but separated
0.250	42.3	12.9	11.9	8.9	8.7	
0.300	42.0	13.2	11.8	9.9	8.7	
0.400	42.5	12.9	12.0	10.0	8.8	
0.500	45.4	12.7	12.8	9.9	9.4	Flow choked
0.600	45.1	12.3	12.7	9.9	9.3	
0.650	43.1	13.5	13.0	10.4	8.9	
0.700	46.6	15.9	13.1	10.9	9.6	
0.750	60.0	16.0	16.9	14.7	12.4	
0.770	62.1	Off		Off		
0.800	58.8	Scale		Scale		Flow choked in exit cone by
0.885	39.5	at 33.2		at 32.0		igniter inlet jet plume
0.900	29.6					
0.925	31.5	17.1		14.7		
0.950	31.9	19.5		16.8		Bow shock from igniter inlet
1.000	31.5	22.5		19.7		jet plume moving through
1.150	28.6	19.5		20.5		throat plane and exit cone
1.400	14.7	14.7		14.7		

Retention-and-Release System Demonstration Test No. 1, Summary of Pressure and Flow Conditions in the Free-Volume Simulator Throat Plane and Exit Cone

Figure 89

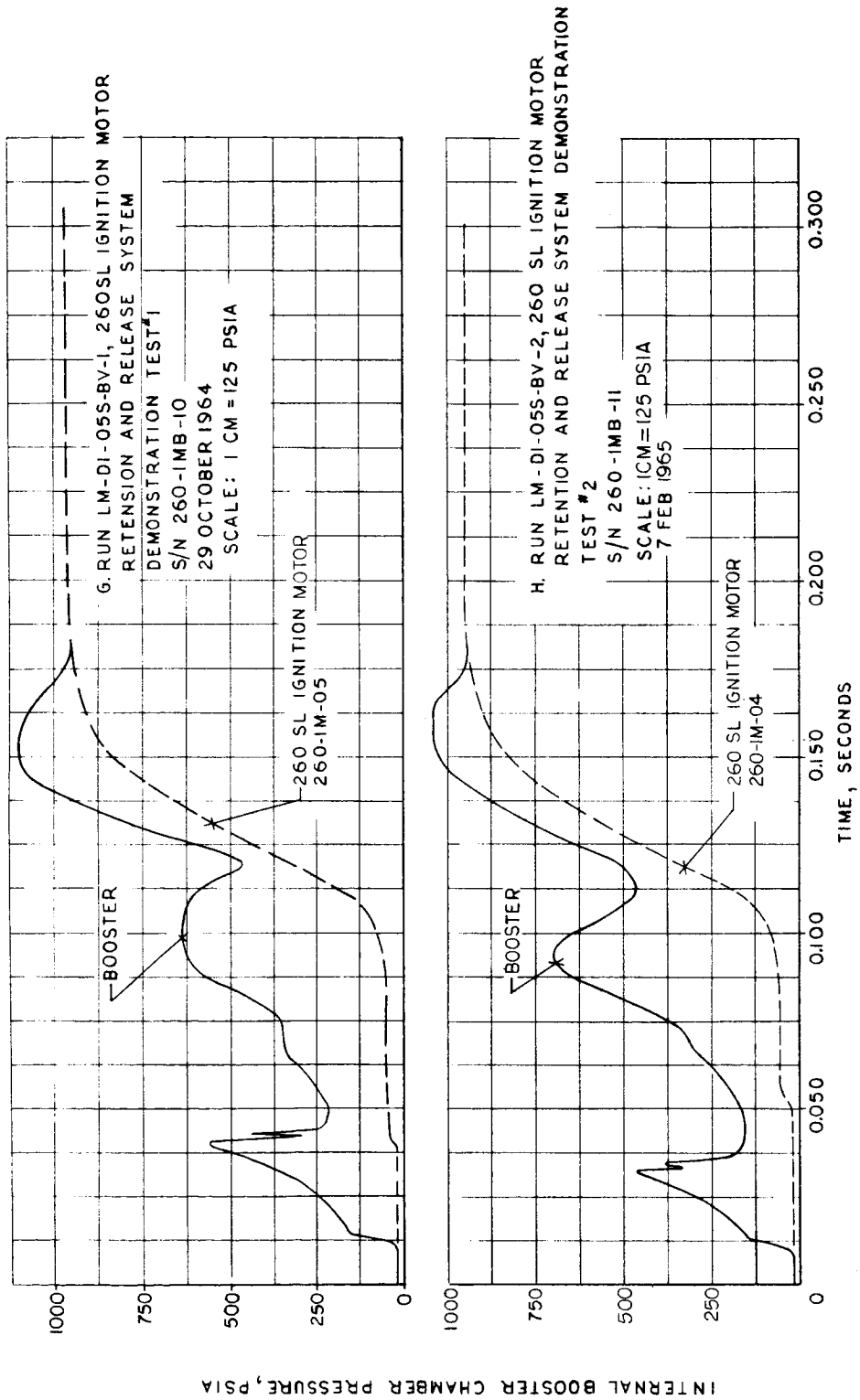

Mod 260 Ignition Motor Booster Ballistic Performance Curves, 260-IMB-10

Figure 90

Upper Attachment Bracket

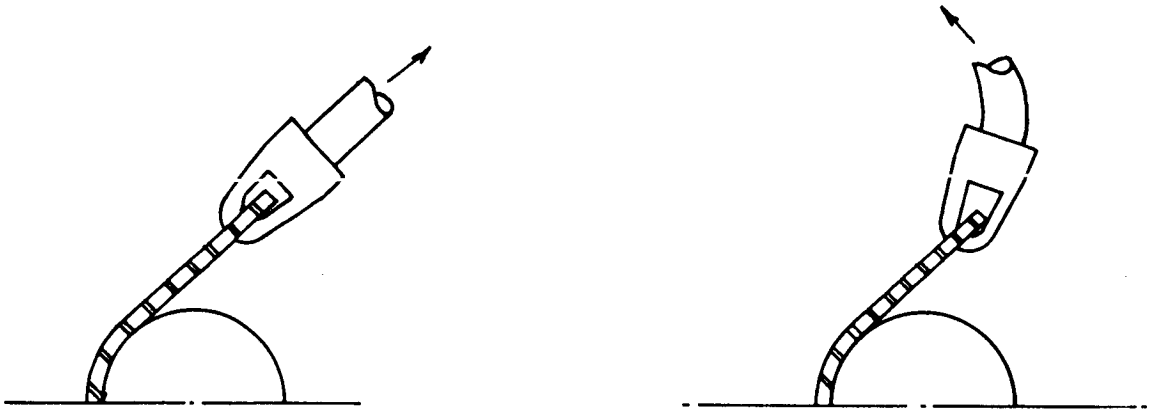

Lower Attachment Bracket

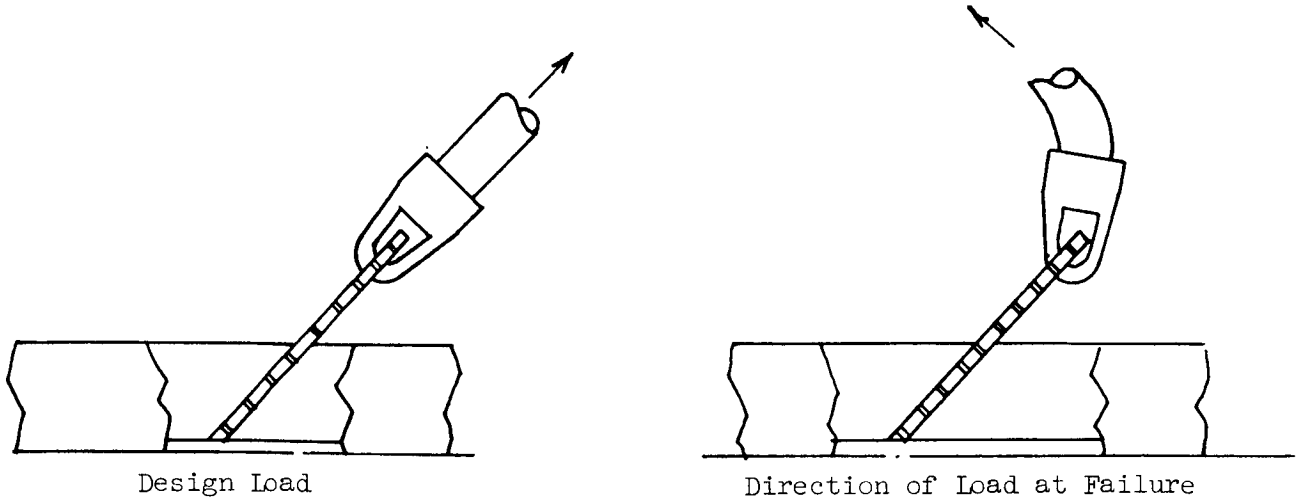

Direction of Cable Force that Occurred During the First Mod 260 Ignition Motor Retention-and-Release Demonstration Test

Figure 91

Postfiring View of Lower Cable Attachment Bracket, Retention
Test No. 1

Figure 92

Postfiring View of Upper Cable Attachment Bracket, Retention
Test No. 1

Figure 93

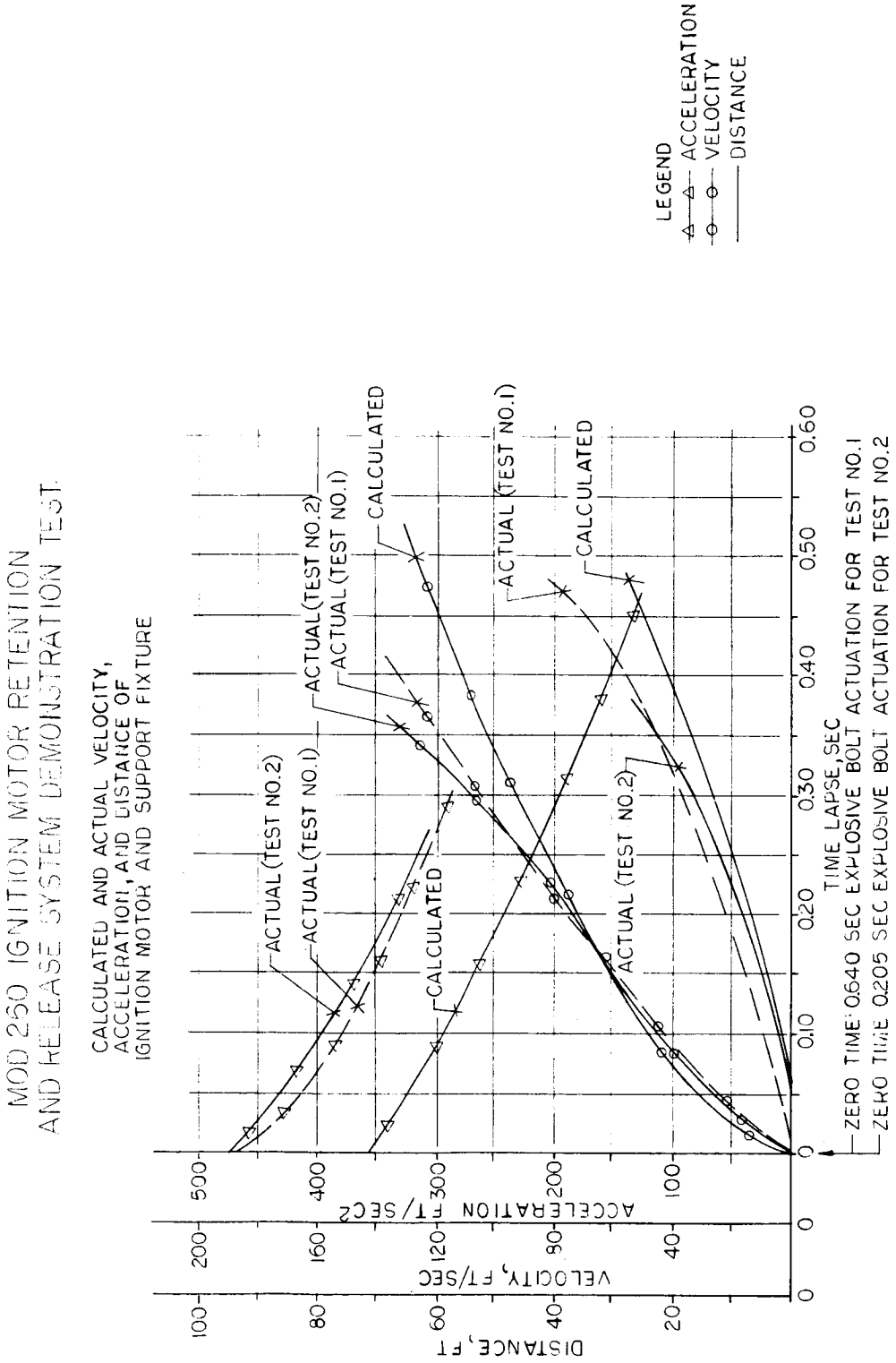

Retention Test No. 1, Calculated and Actual Velocity, Acceleration and Distance of Ignition Motor and Support Fixture

Figure 94

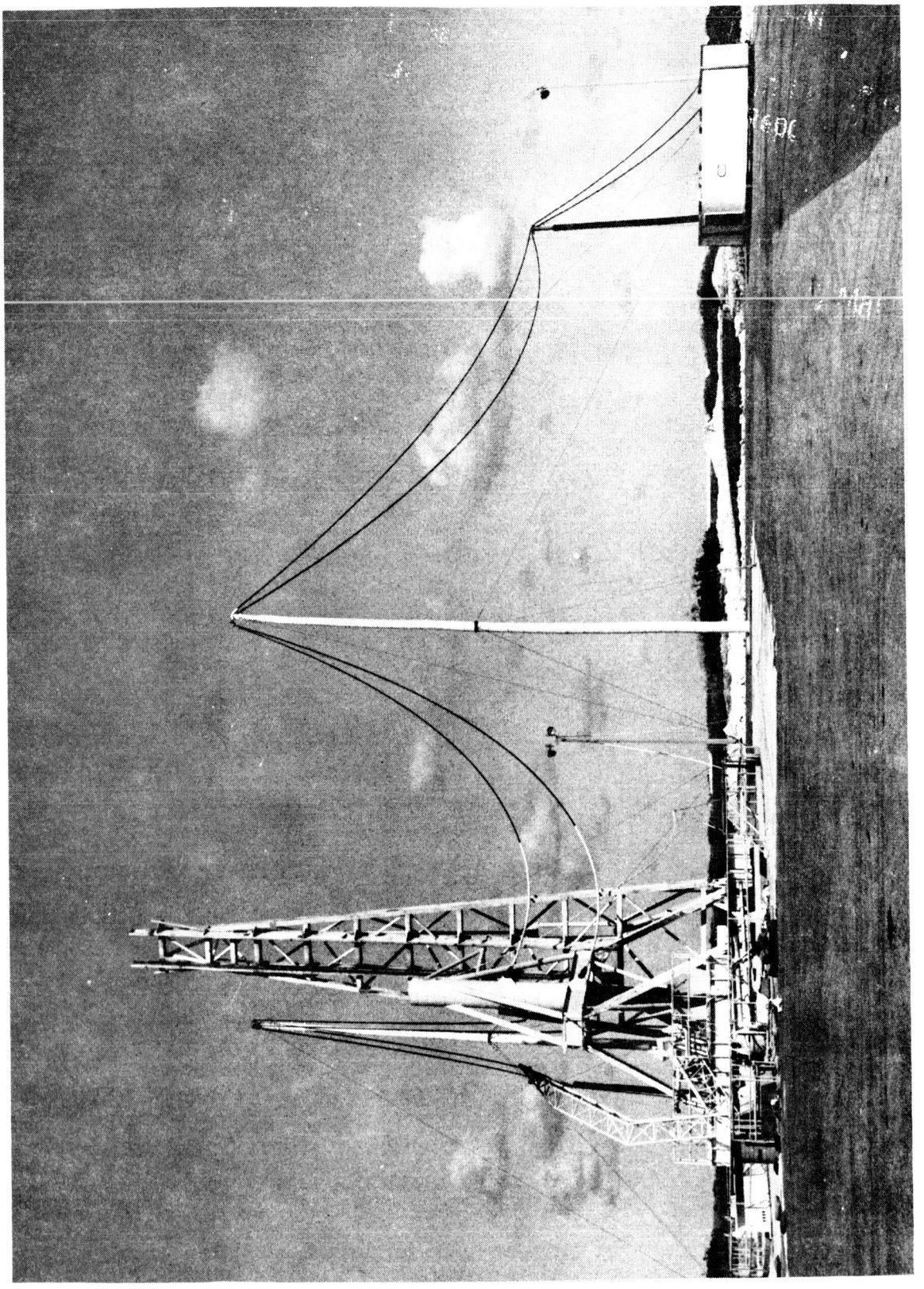

Overall View of Test Set-Up for Mod 260 Ignition Motor Retention-and-Release System Demonstration Test No. 2

Figure 95

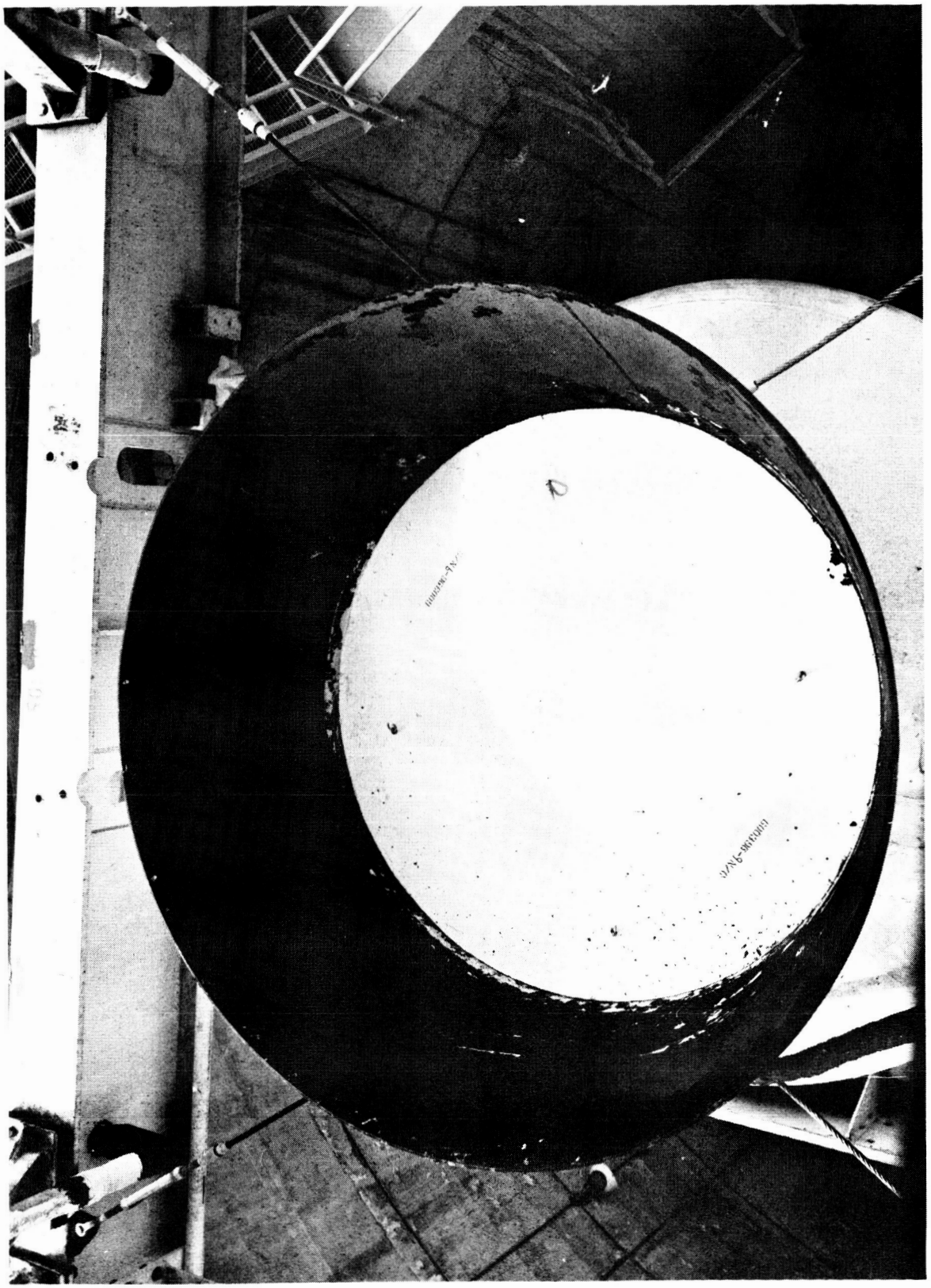

260-SL Motor Nozzle Weather Seal Installed in the Free-Volume Simulator Nozzle for the Second Retention-and-Release System Demonstration Test

Figure 96

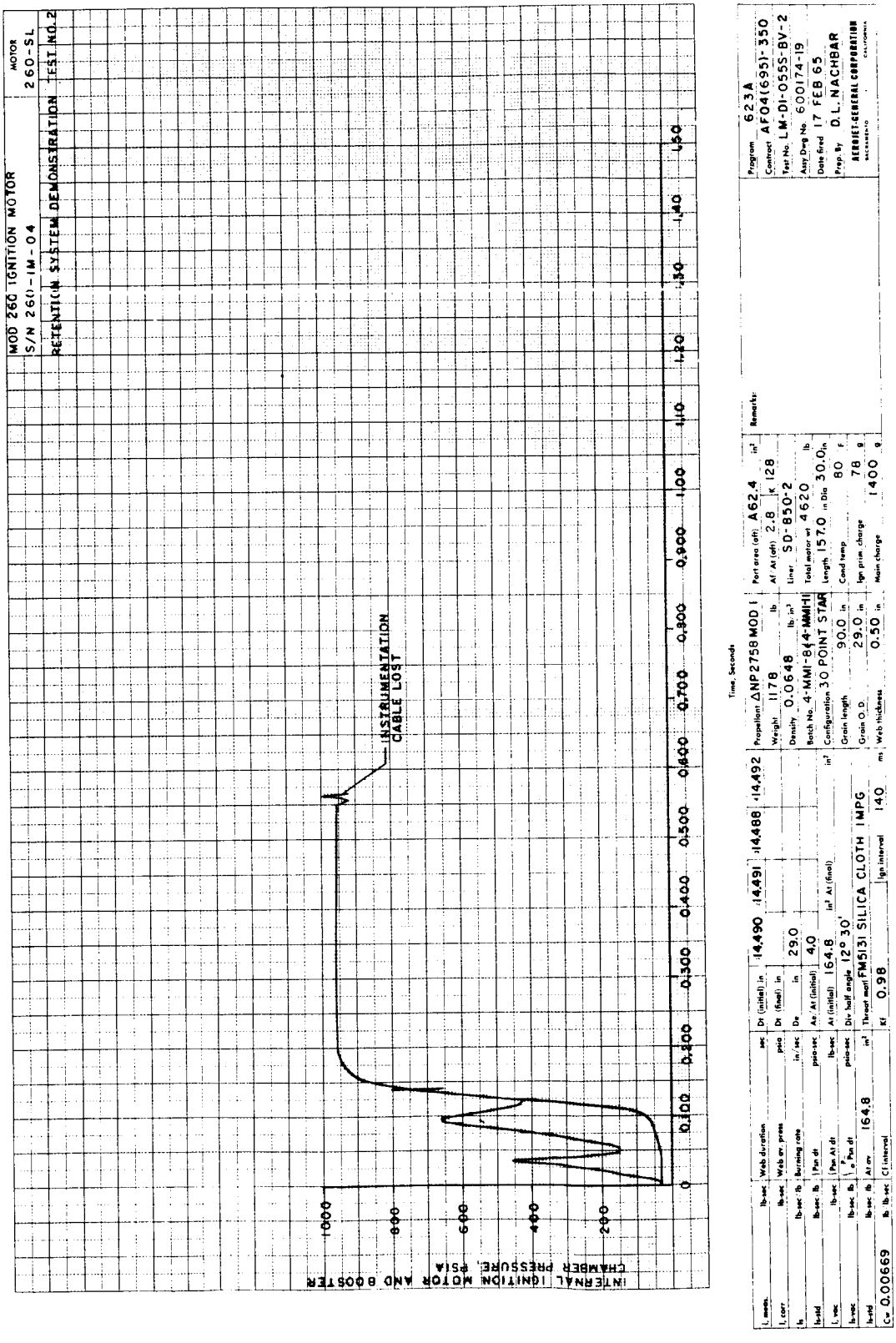

Figure 97

Mod 260 Ignition Motor Performance Curve, Retention-and-Release System Test No. 2

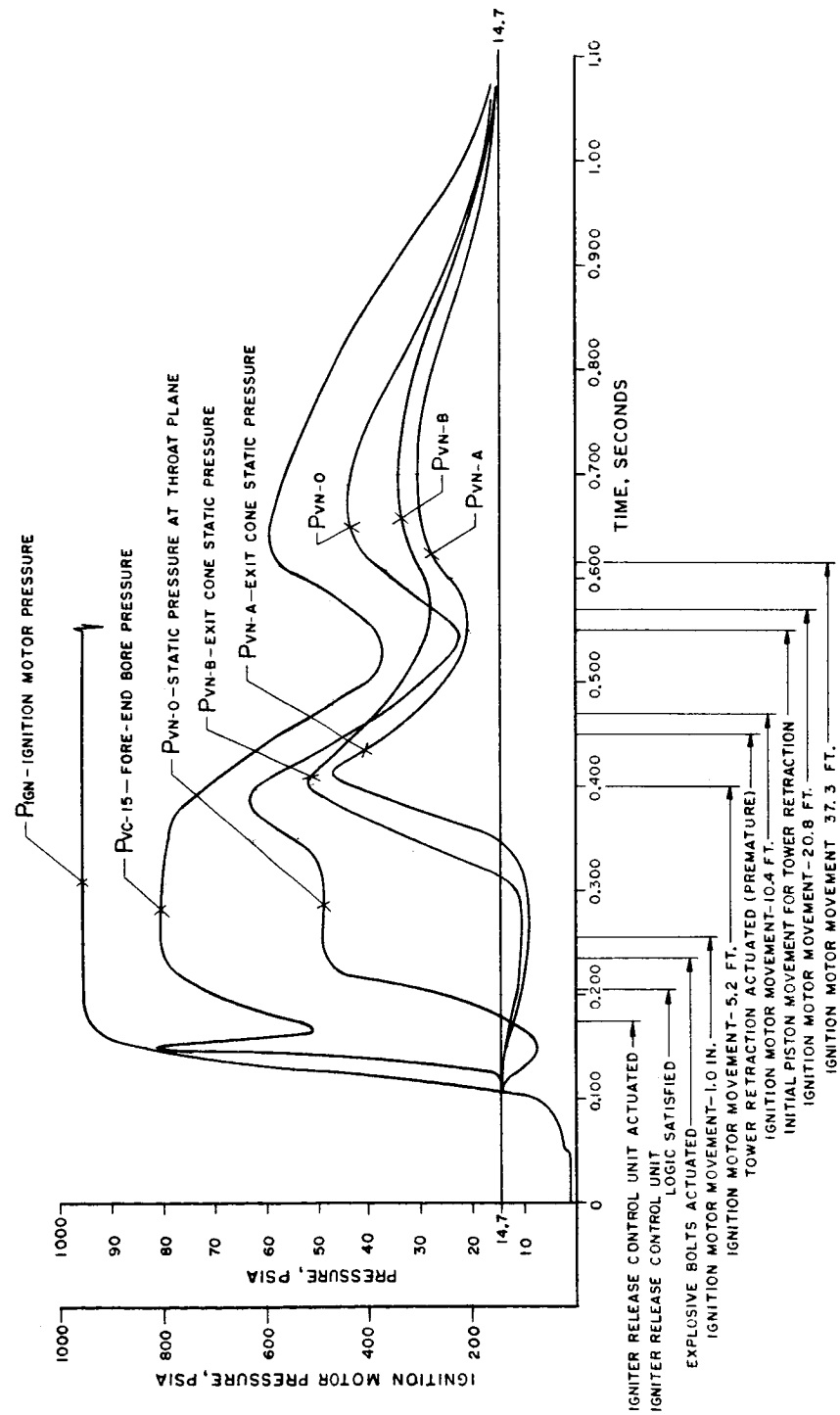

Mod 260 Ignition Motor Retention-and-Release System Demonstration
Test No. 2, Free-Volume Simulator Bore and Exit Cone Pressure Data

Figure 98

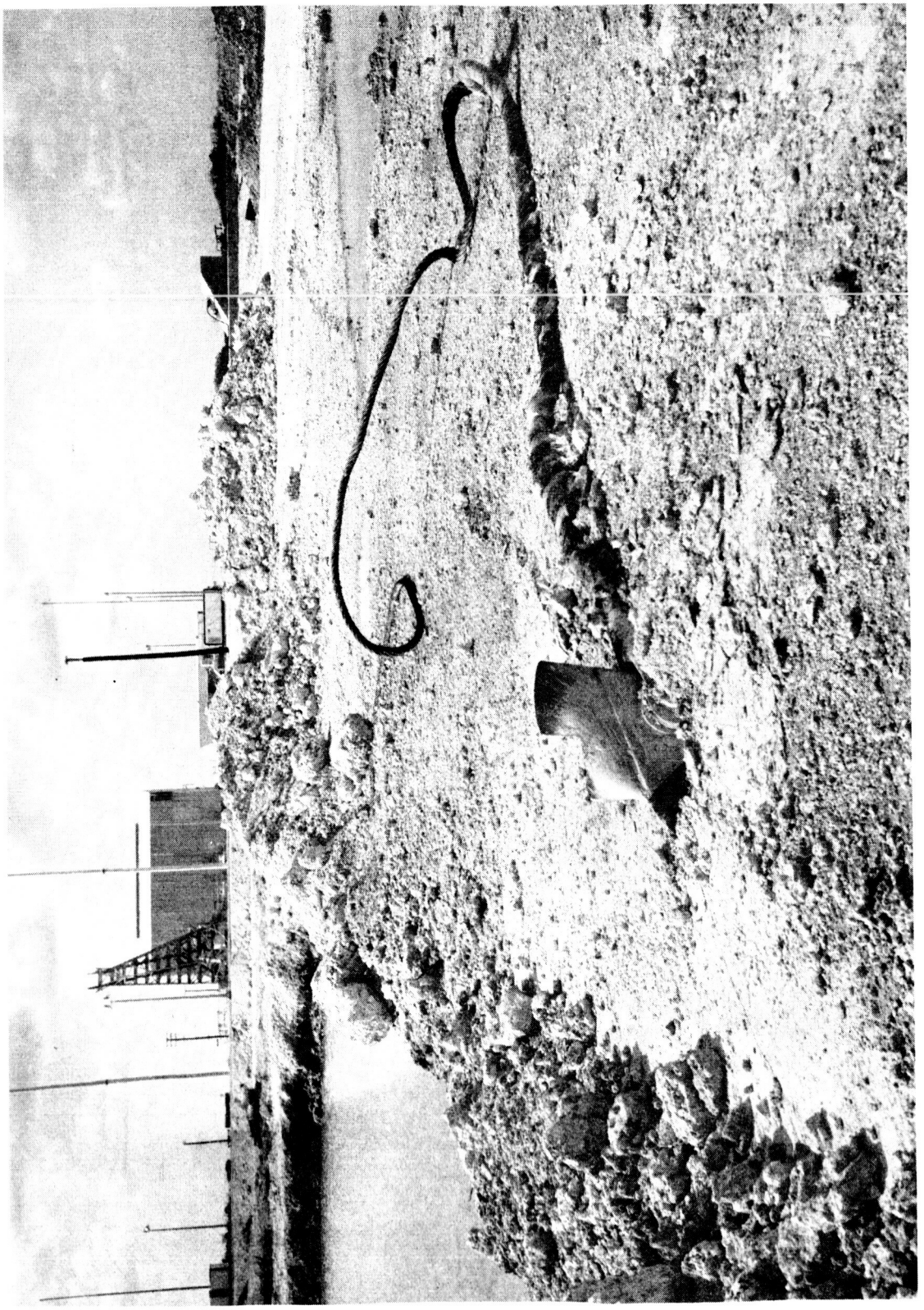

Postfiring View of Upper Cable and Attachment Bracket,
Retention Test No. 2

Figure 99

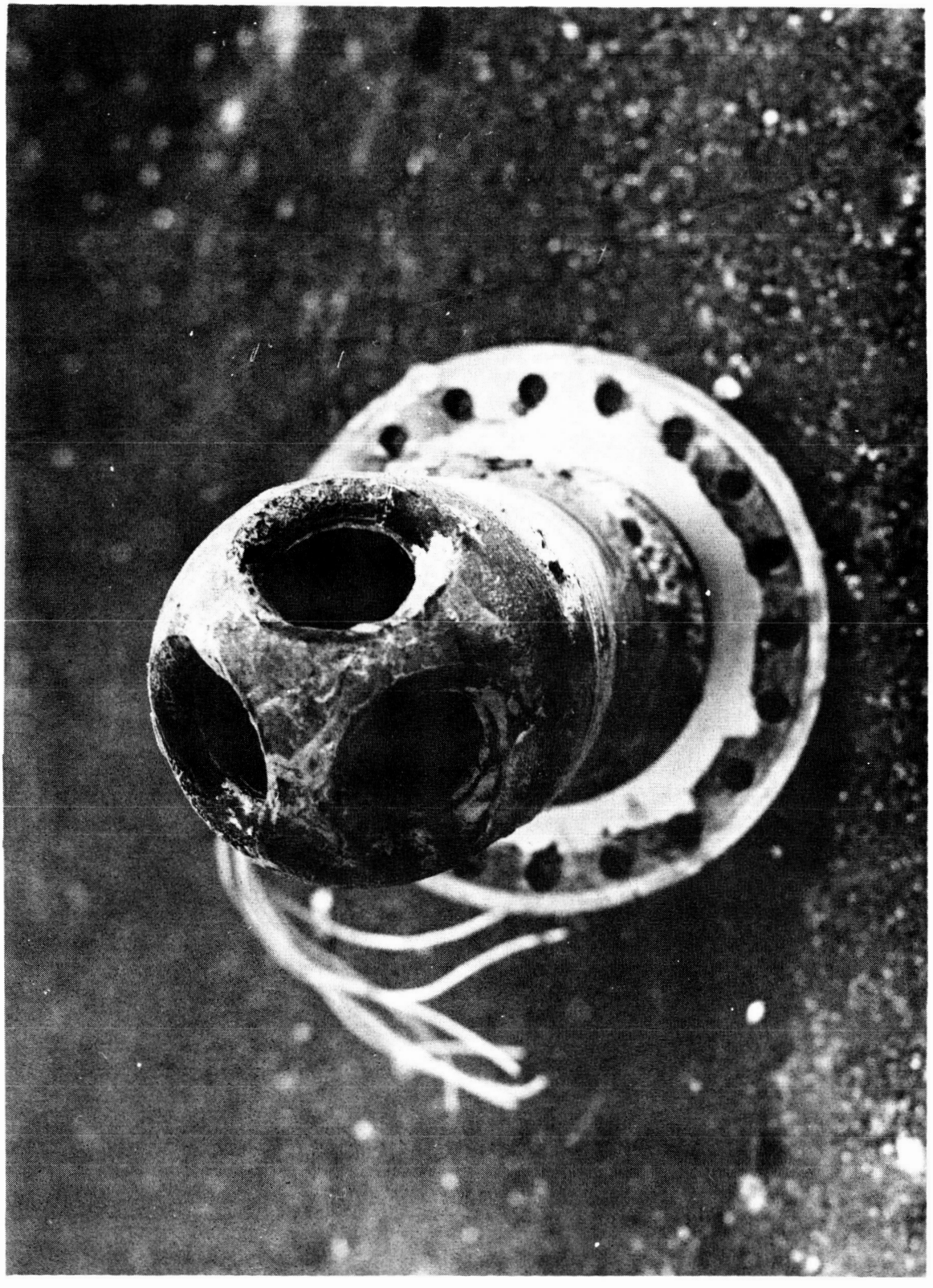

Postfiring View of Ignition Motor Booster 260-IMB-11

Figure 100

COMPARISON OF PREDICTED AND MEASURED FORE-END BORE PRESSURES
IN VARIOUS AFT-END IGNITION TESTS

Igniter Application	Motor-Port-to-Throat Ratio	Ignition Parameter, $\dot{w}/A_t$	Igniter Propellant C_w	Motor (or free-volume simulated) Fore-End Bore Pressure Predicted(1)	Measured
44-SS Free-Volume Tests					
44-SS-IM-01	2.6	0.26	0.0067	72	79
44-SS-IM-02	2.6	0.27	0.0067	74	83
44-SS-IM-03	2.6	0.28	0.0067	78	85
260-SL Free-Volume Tests					
260-IM-02	3.1	0.31	0.0067	81	89
260-IM-03	3.1	0.29	0.0067	78	86
Retention System Demonstration Tests					
260-IM-04	3.1	0.27	0.0067	73	81
260-IM-05	3.1	0.27	0.0067	73	83
UTC Aft-End Ignition Tests					
TM-3A-Segmented Motor	3.4	0.20	0.0063	55	60
Free Volume Test	1.5	0.11	0.0063	35	40
Thiokol 156-1 Motor Test					
TU-412-01	3.1	0.22	0.0063	60	60 to 70(2)

(1) Predicted fore-end bore pressures obtained from Figure 72.
(2) The accuracy of the ignition transient open grid plot in the quick-look report appears to be approximately ± 5 psi.

Comparison of Predicted and Measured Fore-End Bore Pressures in Aft-End Ignition Tests

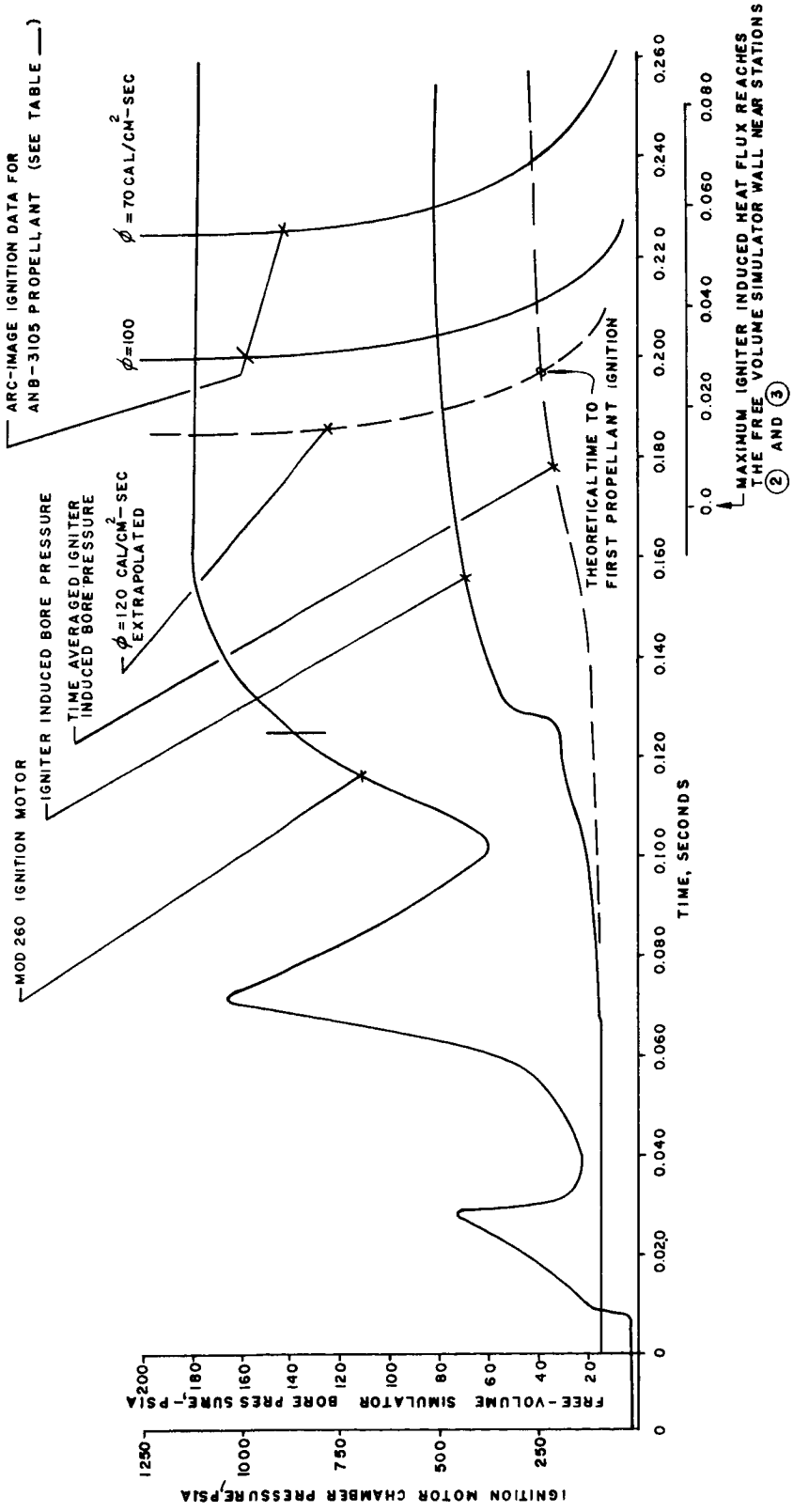

Graphical Presentation of Theoretical Time to First Propellant Ignition for 260-SL Motor

Figure 102

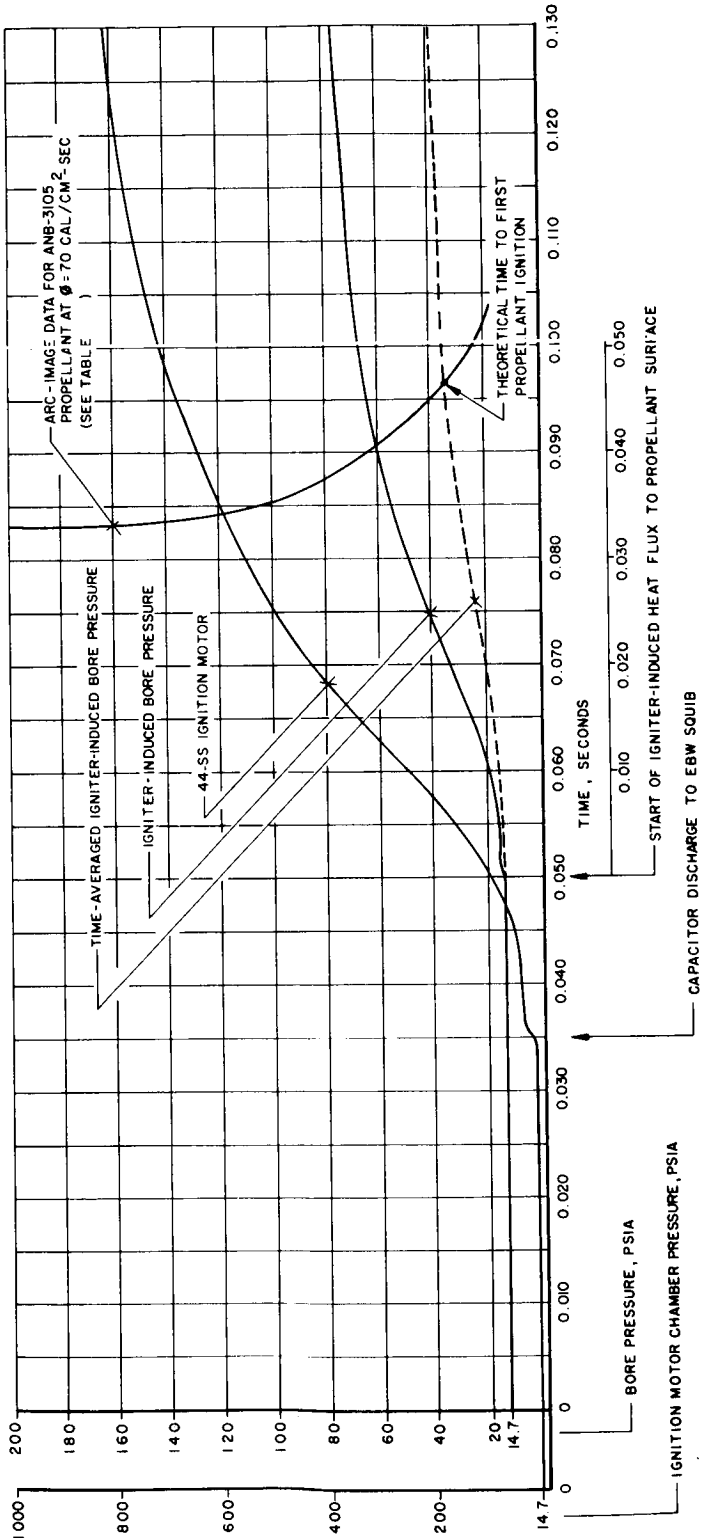

Figure 103

Graphical Presentation of Theoretical Time to First Propellant Ignition for 55-SS Motor

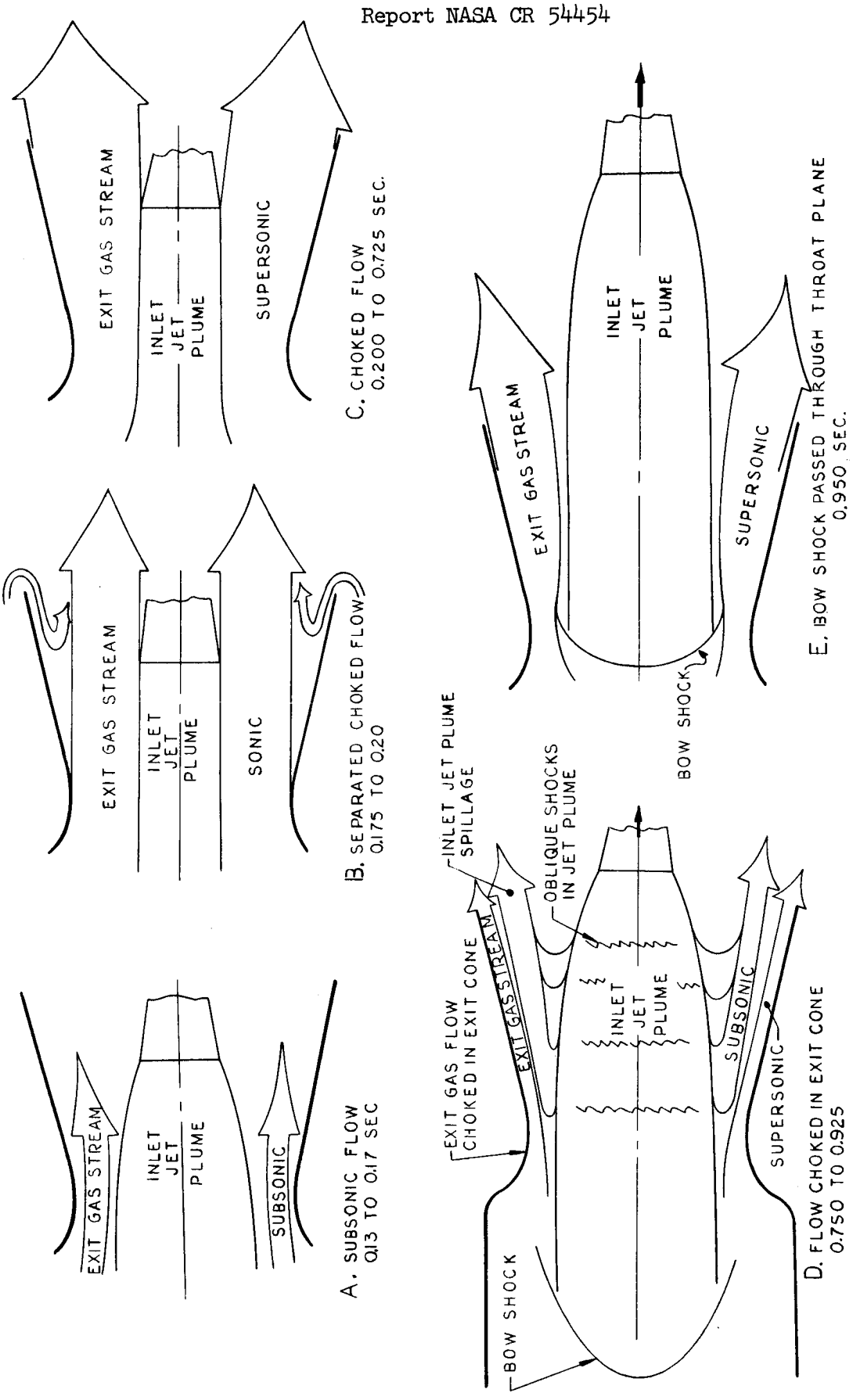

Figure 104

Flow Conditions in Motor (Simulator) Throat Plane and Exit Cone During Aft-End Ignition

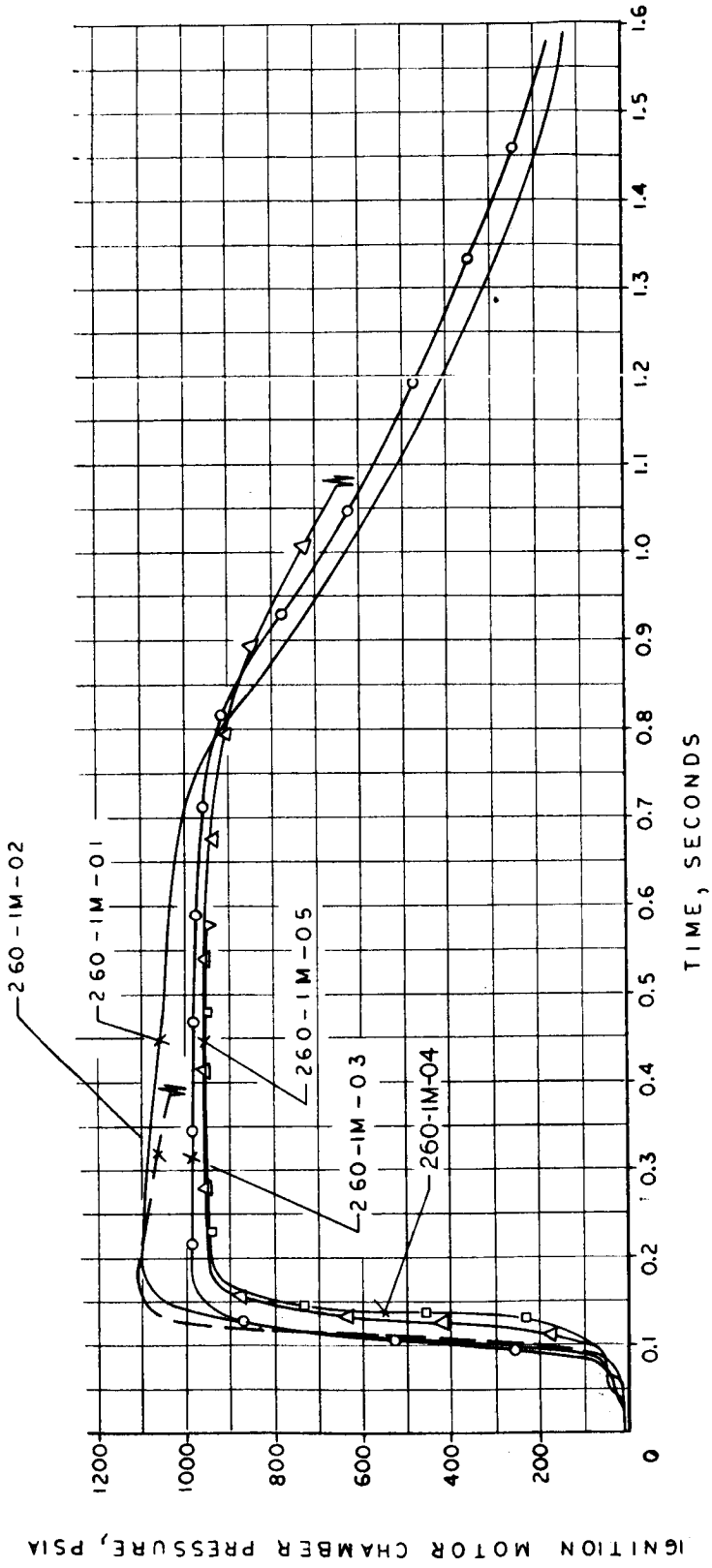

Composite of All Mod 260 Ignition Motor Ballistic Firing Curves

Figure 105

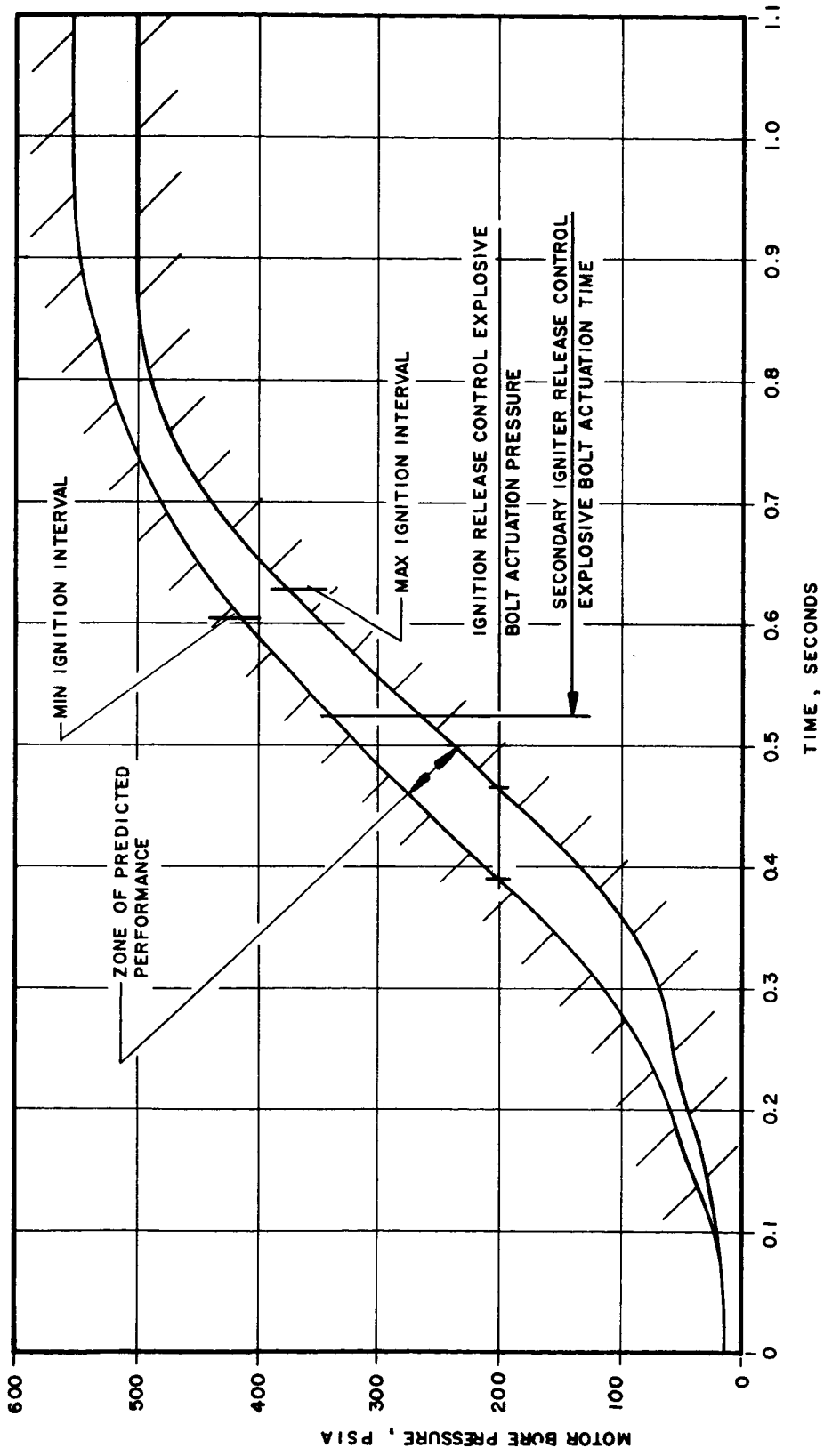

260-SL-1 Motor Final Ignition Performance Prediction

Figure 106

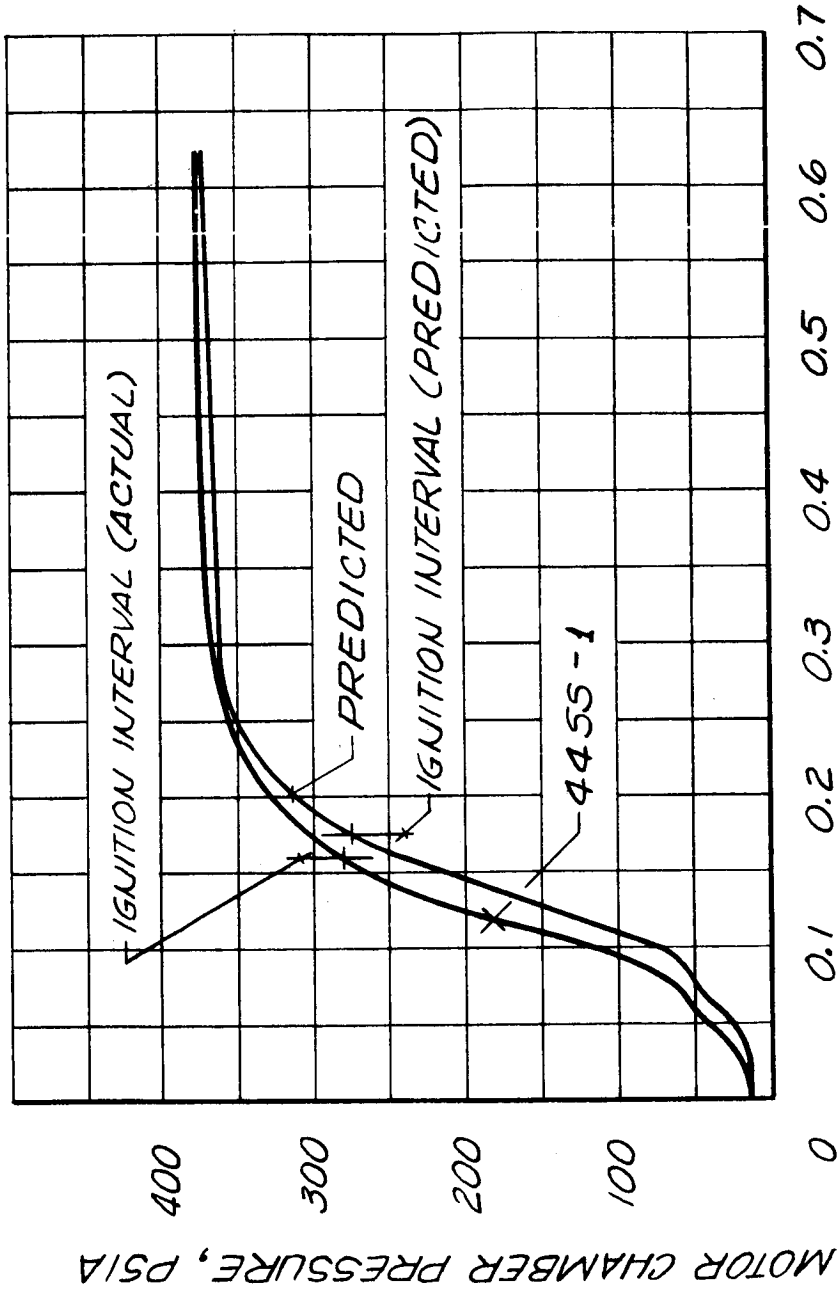

Actual and Predicted Ignition Transient for Motor 44-SS-1

Figure 107

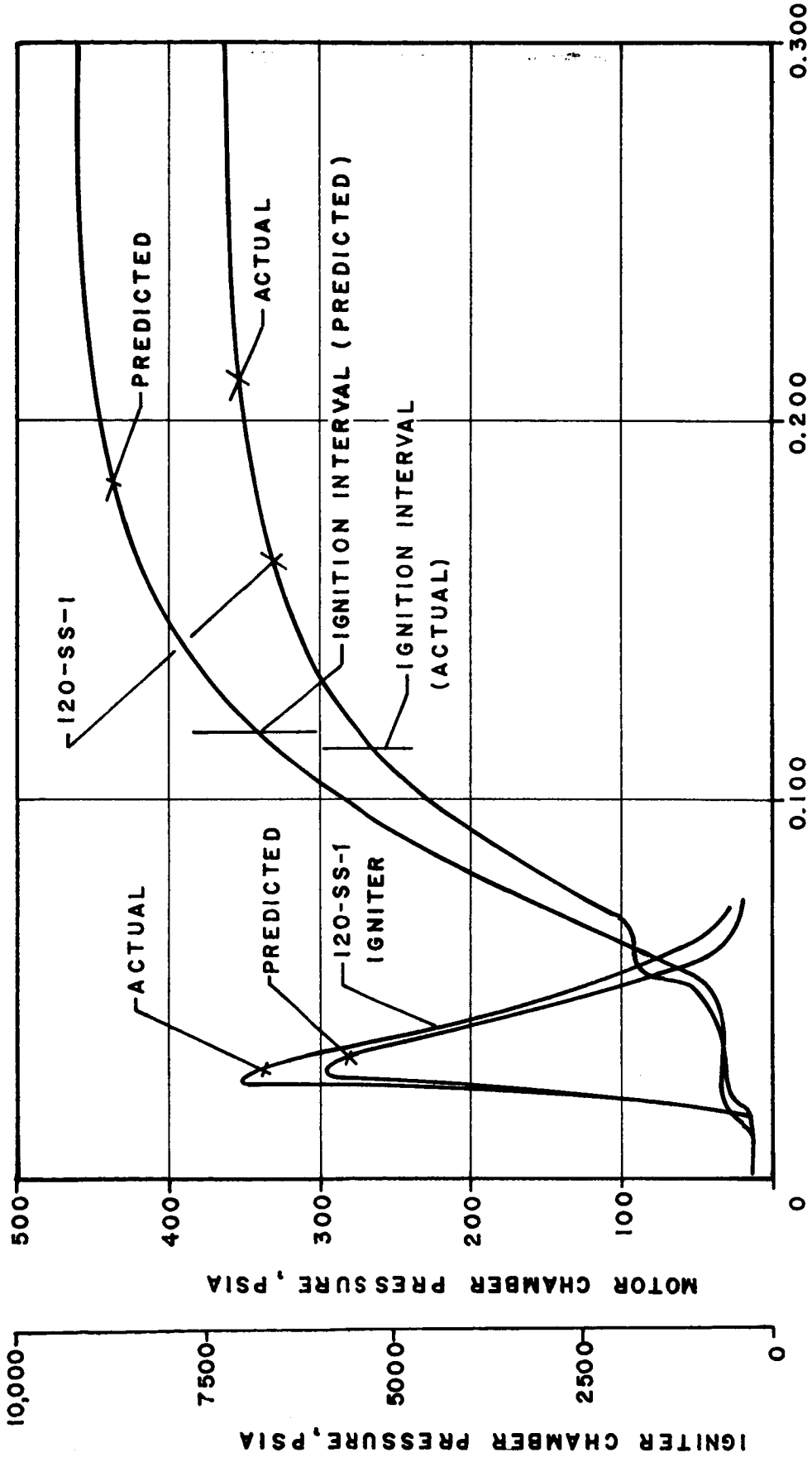

Actual and Predicted Ignition Transient for Motor 120-SS-1

Figure 108

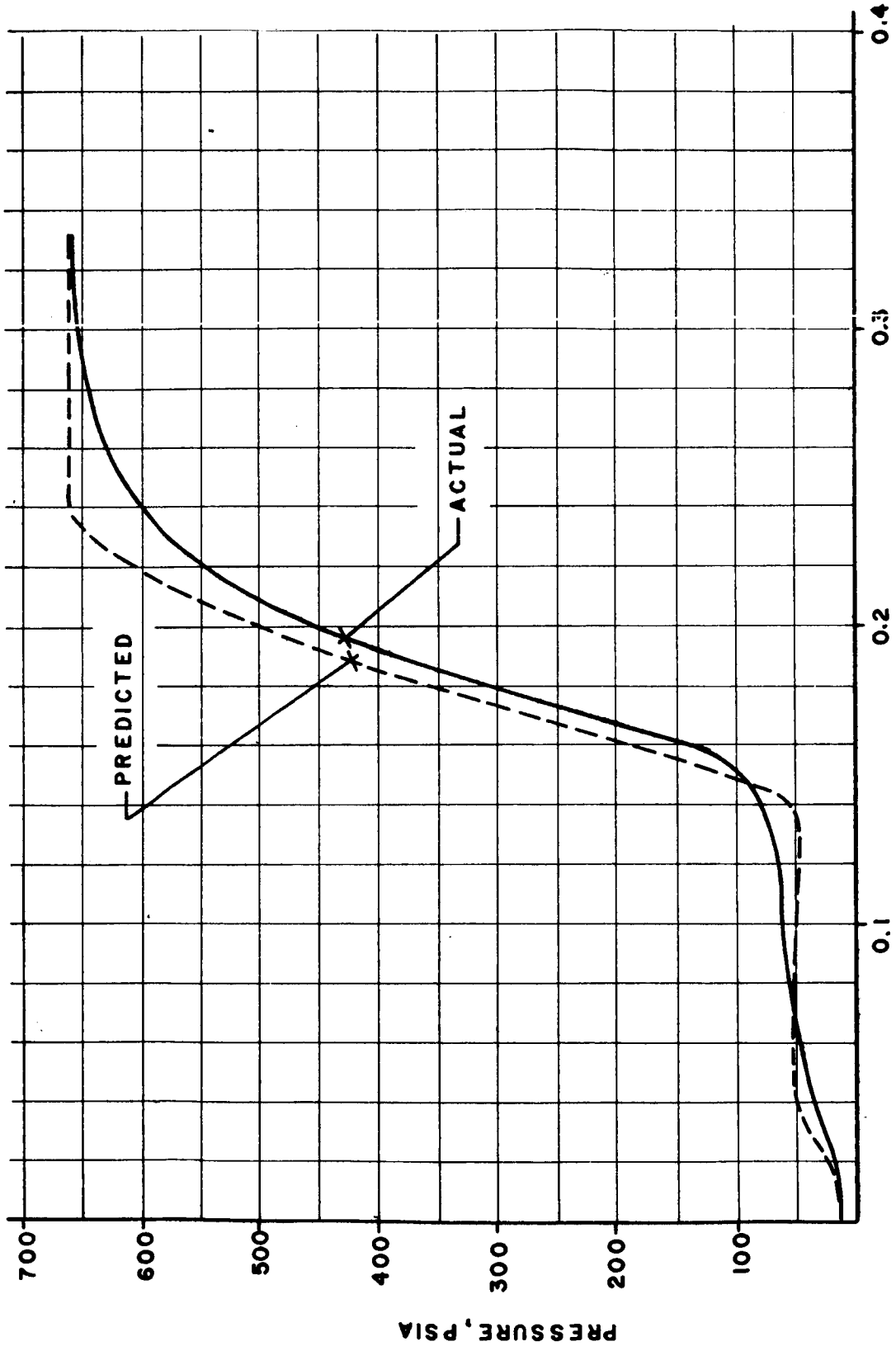

Actual and Predicted Ignition Transient for UTC Three-Segment Motor TM-3A

Figure 109

APPENDIX A

SOLID ROCKET MOTOR AFT-END IGNITION ANALYTICAL MODEL

Aft-end ignition of a solid propellant motor is accomplished by introducing hot ignition gases into the motor bore through the motor throat. The hot gases enter the motor bore and compress the air in the bore toward the forward end. When the pressure between the hot gases and the trapped air is equalized, the movement of hot gas is reversed and the gases flow out the motor throat. Motor ignition occurs by convective heat transfer from the hot gas to the motor propellant surface. Therefore, in aft-end ignition, motor ignition is a function of the energy delivered to the propellant surface, the amount of propellant surface exposed to the delivered energy, and themotor bore pressure.

The igniter energy required for motor ignition is a function of the threshold ignition energy required by the motor propellant and is a common ignition design parameter for both forward- and aft-end type igniters. However, unlike forward-end ignition when the entire propellant surface is in contact with the igniter gas, in aft-end ignition a significant percentage of the motor propellant is not directly exposed to the igniter gas, due to the volume of trapped air in the forward end of the motor bore. Thus, the depth of hot gas penetration into the motor bore and the motor bore pressure are required parameters for aft-end ignition design. To define these parameters, the mathematical relationship between aft-end igniter size, motor bore penetration depth, and pressure was required.

The aft-end ignition analytical model is based on two elementary concepts: continuity and momentum. A schematic diagram of aft-end ignition flow conditions is shown in Figure 1. The igniter is a gas generator, with a sufficiently long

burning duration to fill the motor bore and establish steady-state flow between the inlet and exit gas streams. The motor bore is assumed to be an inert free-volume so that steady-state flow between the inlet and exit gas streams is established prior to motor propellant ignition.

The continuity concept is that the constancy of flow both in and out of the motor determines the flow area required in each direction. The igniter exit area is sized and positioned so that the inlet gas stream expands to the static pressure in the motor throat and thus occupies a portion of the motor throat area. The remaining flow area must be sufficient to allow the same flow out of the motor at the same static pressure at sonic velocity. Thus, continuity determines the level of pressure at the motor throat plane.

The second concept is the momentum exchange required to reduce the inlet gas stream velocity to stagnation, reverse the direction, and flow the gas out of the motor. A detailed analysis of the complete flow field is highly complex, but is not actually required in this analysis, since the momentum in the motor bore determines the motor fore-end bore pressure.

The following assumptions are made in this analysis:

1. One-dimensional flow equations are used throughout.

2. Motor propellant ignition does not occur until steady state flow conditions between the inlet and exit gas streams are attained.

3. All gas generated by the igniter enters the motor bore and expands isentropically to the static pressure in the motor throat at steady-state flow conditions.

4. The inlet jet plume maintains the same size and velocity as determined in item 3 for a distance into the motor bore where the port area is uniform. (Station 2 in Figure 1.)

5. The igniter gases do not mix with the cool air in the motor bore, but compress the trapped air isentropically.

6. The inlet gas stream does not mix appreciably with the exit gas stream.

7. The exit gas stream is choked at the motor throat plane.

Since the trapped cool air in the bore is compressed isentropically, the relation between the original air volume and the compressed air volume is:

$$P_1 V_1^{1.4} = P_2 V_2^{1.4} \tag{1}$$

For steady flow conditions, the inlet flow rate is equal to the exit gas stream flow rate:

$$C_w P_{IGN} A_{IGN} = C_w P_t A_e \tag{2}$$

The sum of the inlet and exit gas stream flow areas is equal to the motor throat area:

$$A_i + A_e = A_t \tag{3}$$

The one-dimensional ratio between the inlet jet plume cross-sectional area at the motor throat plane and the igniter throat area is expressed by the relation:

$$\frac{A_i}{A_{IGN}} = \left(\frac{2}{\gamma+1}\right)^{\frac{\gamma+1}{2(\gamma-1)}} \frac{1}{M_i} \left(1 + \frac{\gamma-1}{2} M_i^2\right)^{\frac{\gamma+1}{2(\gamma-1)}} \tag{4}$$

The ratio of the static pressure at the motor throat plane to the igniter chamber pressure is:

$$\frac{P_s}{P_{IGN}} = \left(1 + \frac{\gamma-1}{2} M_i^2\right)^{\frac{\gamma-1}{\gamma}} \tag{5}$$

Solving for M_i:

$$M_i = \left\{ \frac{2}{\gamma - 1} \cdot \left[\left(\frac{P_s}{P_{IGN}} \right)^{\frac{\gamma - 1}{\gamma}} - 1 \right] \right\}^{0.5} \tag{6}$$

Substituting in Equation 4:

$$\frac{A_i}{A_{IGN}} = \frac{\left(\frac{2}{\gamma + 1} \right)^{\frac{\gamma + 1}{2(\gamma - 1)}}}{\left(\frac{P_s}{P_{IGN}} \right)^{\frac{1}{\gamma}} \sqrt{\left(\frac{2}{\gamma - 1} \right) 1 - \left(\frac{P_s}{P_{IGN}} \right)^{\frac{\gamma - 1}{\gamma}}}} \tag{7}$$

For the condition of choked flow of the exit gas stream out of the motor:

$$P_s = \left(\frac{2}{\gamma + 1} \right)^{\frac{\gamma}{\gamma - 1}} P_t \tag{8}$$

The momentum theorem states that the sum of the forces on a control volume is equal to the time rate-of-change of momentum leaving the control volume less the momentum entering the volume. All assumptions made for the continuity equations also apply to the momentum equations.

Considering momentum and forces as being positive when directed toward the left in Figure 1, the equation for a control volume at the motor throat plane and forward is:

$$\sum F_1 = \dot{m}_i v_i + \dot{m}_e v_e + \int P dA + P_s A_t - P_2 A_p = 0 \tag{9}$$

From Equation 2, $\dot{m}_i = \dot{m}_e$ at steady flow conditions.

Substituting Equation 3 and rearranging:

$$P_2 A_p = \dot{m} v_i + \int P dA + P_s A_i + P_s A_e = \dot{m} v_e \tag{10}$$

Similarly, a momentum equation is written for a second control volume near the motor throat plane:

$$\Sigma F_2 = \dot{m}\, v_o - \dot{m}\, v_e + P_o\,(A_p - A_i) - \int P\,dA - P_s A_e = 0 \qquad (11)$$

Substituting $\dot{m}\, v_e$ from Equation 11 in Equation 10:

$$P_2 A_p = \dot{m}\,(v_i + v_o) + P_o\,(A_p - A_i) + P_s A_i \qquad (12)$$

Substituting the relation for the pressure ratio P_t/P_o in Equation 12:

$$P_2 A_p = \dot{m}\,(v_i + v_o) + \frac{P_t\,(A_p - A_i)}{\left[1 + \left(\frac{\gamma - 1}{2}\right) M_o^{\,2}\right]^{\frac{\gamma}{\gamma - 1}}} - P_s A_i \qquad (13)$$

The isentropic relationships between the velocities, area ratios, Mach numbers and pressure ratios are written for the inlet and exit gas streams as follows:

$$v_i = a^* \sqrt{\left(\frac{\gamma + 1}{2}\right) M_i^{\,2} \left[1 + \frac{\gamma - 1}{2} M_i^{\,2}\right]^{-1}} \qquad (14)$$

$$\frac{P_{IGN}}{P_s} = \left[1 + \left(\frac{\gamma - 1}{2}\right) M_i^{\,2}\right]^{\frac{\gamma}{\gamma - 1}} \qquad (15)$$

$$v_o = a^* \sqrt{\left(\frac{\gamma - 1}{2}\right) M_o^{\,2} \left[1 + \left(\frac{\gamma - 1}{2}\right) M_o^{\,2}\right]^{-1}} \qquad (16)$$

$$\frac{A_p - A_i}{A_e} = \left(\frac{2}{\gamma + 1}\right)^{\frac{\gamma + 1}{2(\gamma - 1)}} M_o^{-1} \left[1 + \frac{\gamma - 1}{2} M_o^{\,2}\right]^{\frac{\gamma + 1}{2(\gamma - 1)}} \qquad (17)$$

$$a^* = \sqrt{\gamma g R \left(\frac{2}{\gamma + 1}\right) T} \qquad (18)$$

When the exit gas stream is choked at the motor throat, the following relationship also applies:

$$v_e = a^* \tag{19}$$

The solution of Equations 2 through 19 for the motor bore pressure, P_2, is difficult and time consuming for a given set of motor and igniter conditions. Solutions of these equations are presented in Figure 72, main text, for the Mod 260 ignition motor with the following characteristics:

P_{IGN}: 1000 psia

T: 6000°F

γ : 1.2

C_w: 0.00669 sec^{-1}

A similar solution is presented in Figure 2 ; the igniter characteristics are the same as those for the Mod 260 ignition motor, except the mass-flow coefficient was reduced to 0.0063. The two graphs do not show the igniter pressure as a variable parameter; however, for igniter pressures ranging from 800 to 1200 psia the curves are not significantly affected. The hot-gas penetration depth is presented as a second ordinate in Figures 72 and 2 for the corresponding motor bore pressures. The percent of penetration is expressed as:

$$\% \text{ Penetration} = 100\left(\frac{V_1 - V_2}{V_1}\right)$$

The aft-end ignition analytical model equations provide the ignition design parameter, $\dot{w}/A_t$, in terms of motor throat area and motor port-to-throat ratio. Thus, for any given motor size and any desired bore pressure or bore penetration depth, the required igniter mass-flow rate can be obtained.

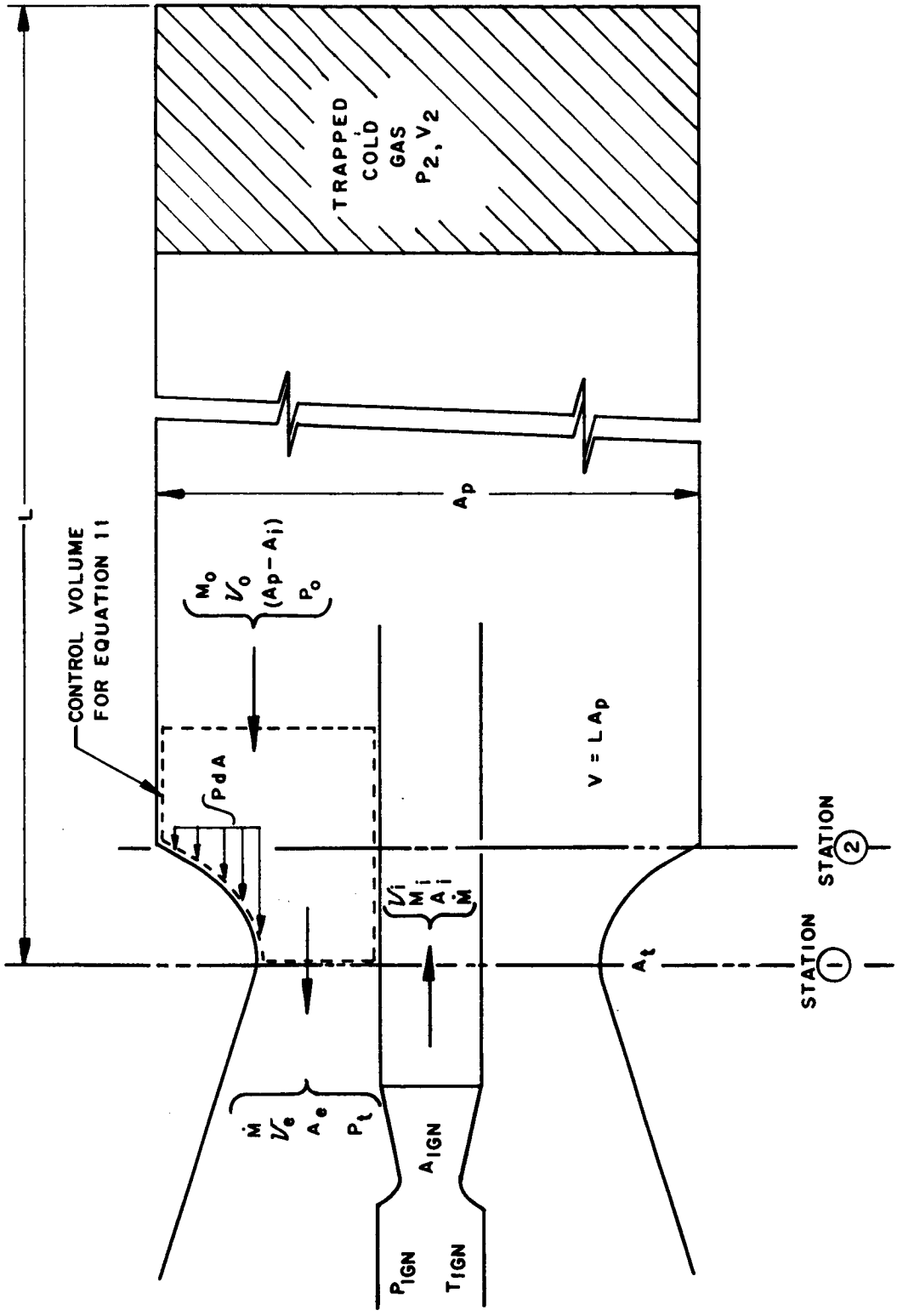

Schematic Diagram of Aft-End Ignition Flow Conditions

Figure 1

IGNITER PRESSURE: 1000 PSIA
IGNITER PROPELLANT MASS FLOW COEF., C_W=0.0063

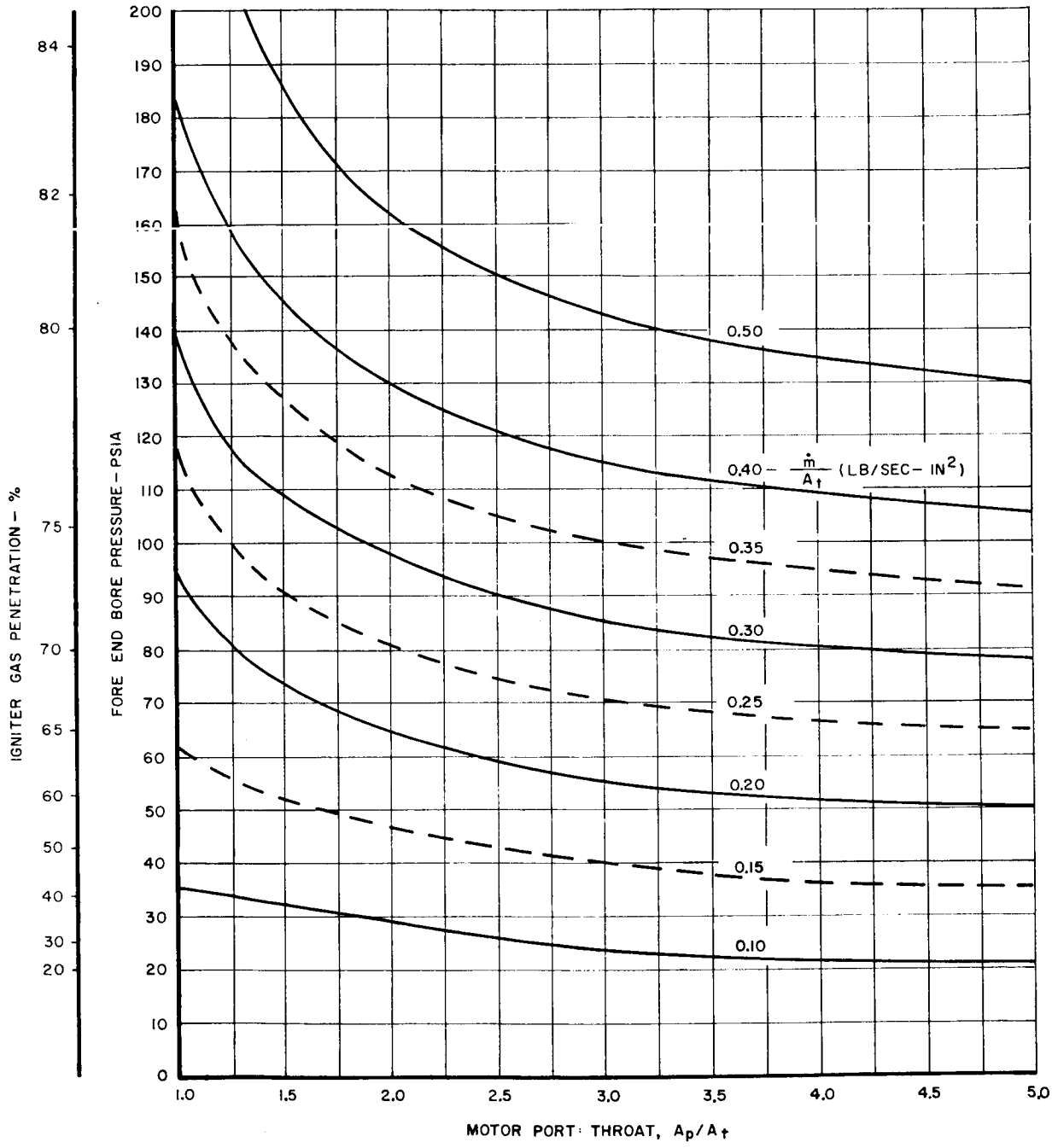

IGNITION GAS PENETRATION AND FORE-END MOTOR BORE PRESSURE AS A FUNCTION OF IGNITER MASS FLOW ($\dot{m}$), MOTOR PORT AREA (A_p) AND MOTOR THROAT AREA (A_t) BETWEEN IGNITER OPERATING PRESSURES OF 800 TO 1200 PSIA.

Graphical Solution of Aft-End Ignition Analytical Model Equations for C_W = 0.0063

Figure 2

APPENDIX B

METHOD OF SIZING ALCLO-TYPE FORWARD-END IGNITERS FOR SOLID ROCKET MOTORS

The empirical method used to determine the pyrotechnic charge weight of forward-end Alclo-type igniters is based on an igniter energy-propellant surface area relationship. This energy relationship was the result of an ignition study conducted to improve the method used to size igniters for various solid-rocket motors. This investigation led to the conclusion that good ignition was always achieved when motor propellant ignition occurred before the igniter had released all of its energy. A method was derived for determining the portion of the total igniter energy required to ignite the propellant. The amount of igniter energy released at propellant ignition was determined by assuming that propellant ignition occurs at the time the slope of the pressure-rise curve intersected the ambient pressure condition, as shown in Figure 1. A series of ignition tests was made with nine Polaris motors; the igniter energy delivered and the igniter energy delivery rate was varied in each test. The actual igniter energy required to ignite the propellant, defined as the threshold ignition energy, was determined for each test using the method shown in Figure 1. The resulting data are shown in Figure 2 (the data points for motors SS-A, TW-1, FW-1, FW-2 and FW-3 are included, but these data were not available when the initial correlation was made). Limits were established to include all the data points, also shown in Figure 2. The zone enclosed by the limits was then defined as the marginal igniter energy required for propellant ignition. Thus, the total energy available from the igniter must be greater than the marginal energy requirement, since this empirical correlation only defines energy levels and does not consider overall igniter performance on igniter heat-transfer efficiency.

This energy correlation was used to size theigniters for the 100-in.-dia motor program, as shown in Figure 3. Ignition of these large motors was very satisfactory, as shown inFigure 4. The igniters for two 65-in.-dia subscale motors, SS-A and SS-B, were designed before this correlation was available. As shown in Figure 3, the total available igniter energy in each case was in the threshold or marginal zone. Motor SS-B had a 3.0 sec hang-fire. Ignition of SS-A was satisfactory, but as indicated in Figure 4, ignition occurred after the SS-A igniter had released all of its total available energy.

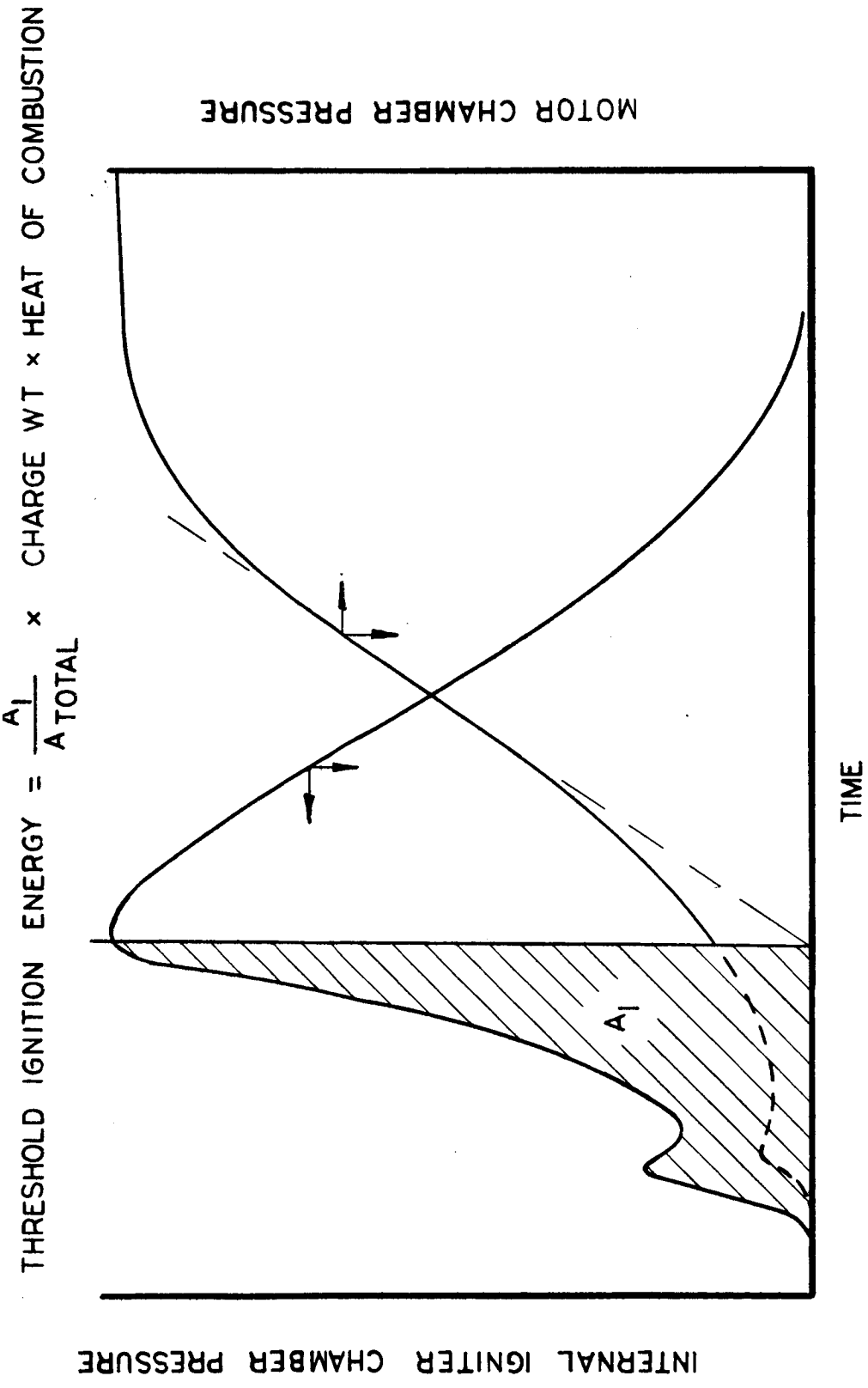

Threshold Ignition Energy Determination

Figure 1

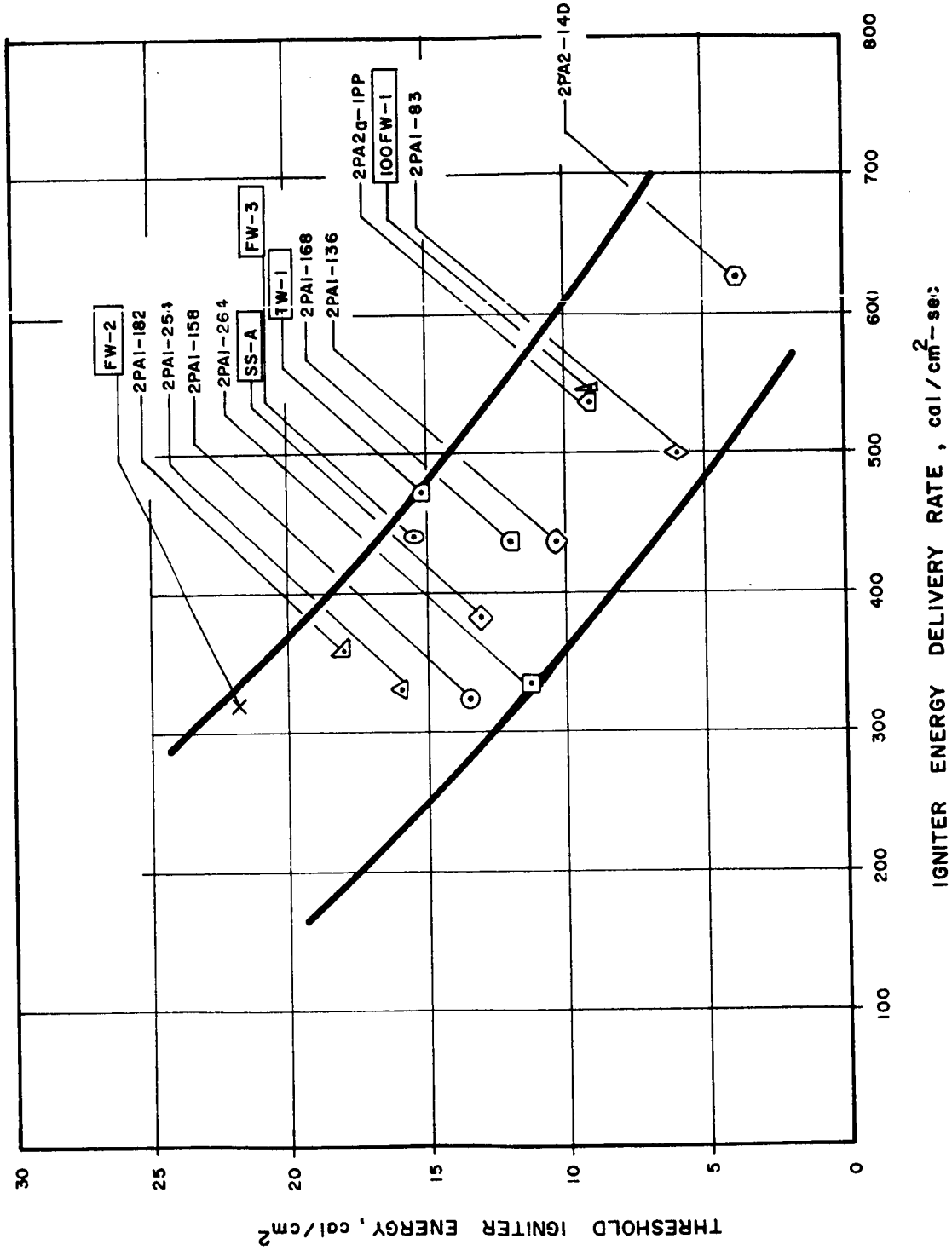

Empirical Basis for Threshold Igniter Energy vs Igniter Energy Delivery Rate Correlation Limits

Figure 2

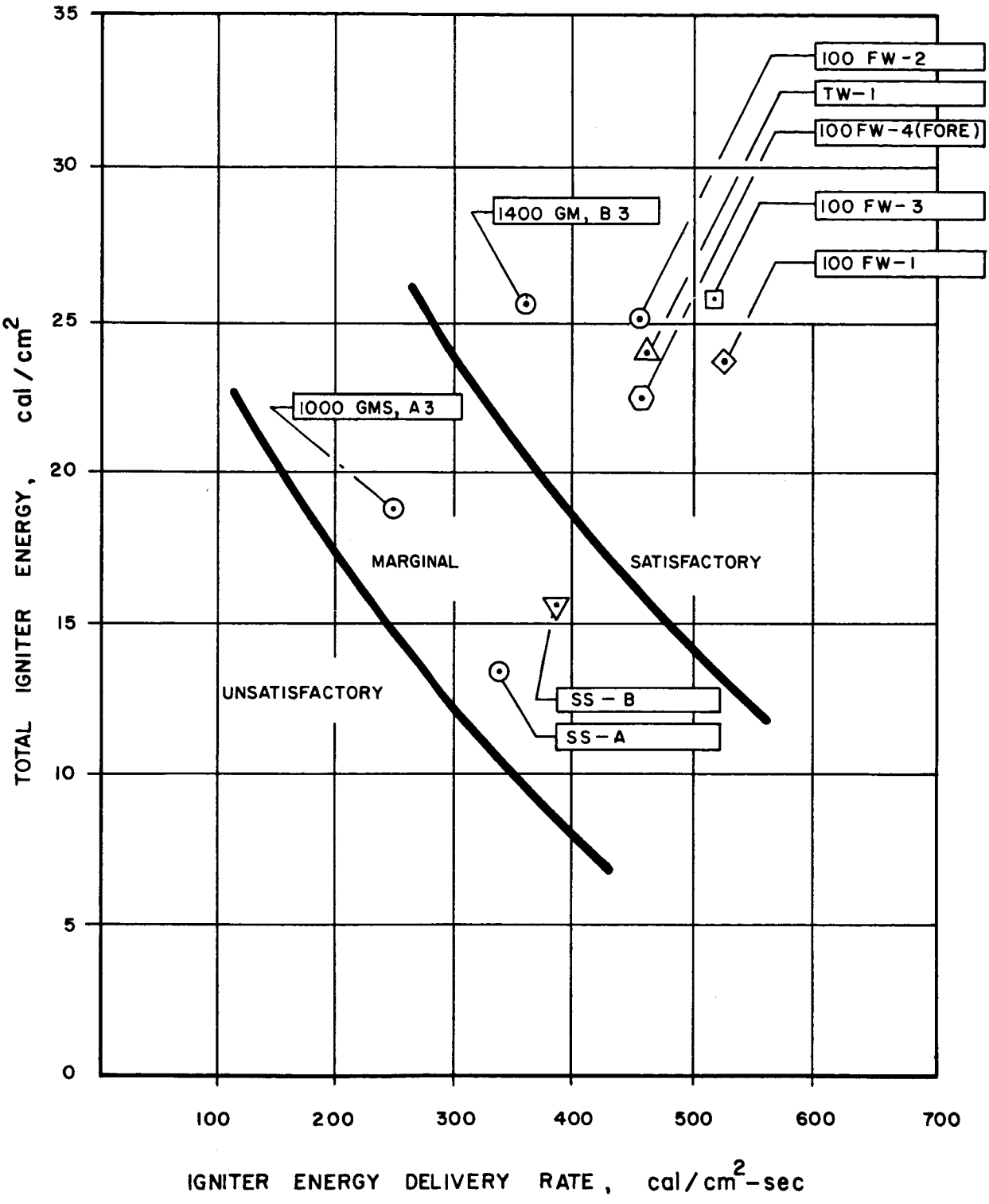

Total Igniter Energy vs Energy Delivery Rate Correlation

Figure 3

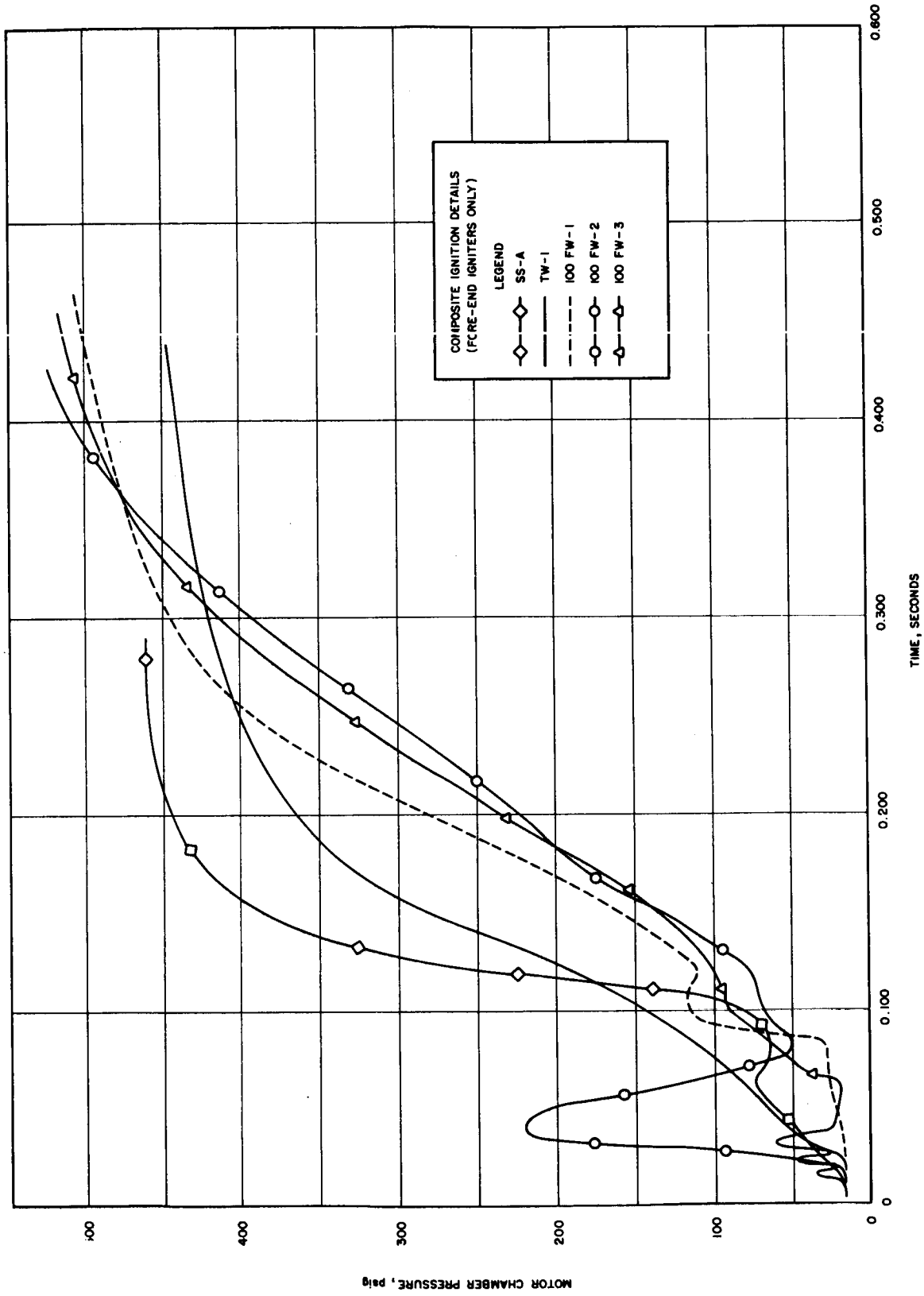

Composite Ignition Details, 100-in.-dia Motor Program

Figure 4

APPENDIX C

ESTIMATE OF PRESSURE DISTRIBUTION ON 260-SL MOTOR NOZZLE AND EXIT CONE DURING AFT-END IGNITION

Igniter in Position

Pressure distributions on the 260-SL motor nozzle and exit cone with the igniter in position were determined by assuming one-dimensional isentropic expansion of the motor exit gas stream around the igniter. Assuming that the annulus between the motor exit cone and the igniter exit plane is a sharp-edged orifice with a discharge coefficient of 0.8, a new throat is formed in this annulus and flow at the motor throat plane becomes subsonic. Based on sonic flow at the annulus and one-dimensional isentropic expansion of the exit gas stream downstream of the new throat, pressure distributions along the nozzle were determined. The formation of the new throat in the annulus causes an increase of approximately 6% in the motor steady-state operating pressure.

During Igniter Ejection

Pressure distributions on the motor nozzle and exit cone during igniter ejection were determined by assuming that the highest loads are generated when the igniter has moved downstream to a position where the free-flow area around the inlet jet plume is equal to the motor throat area, shown as follows:

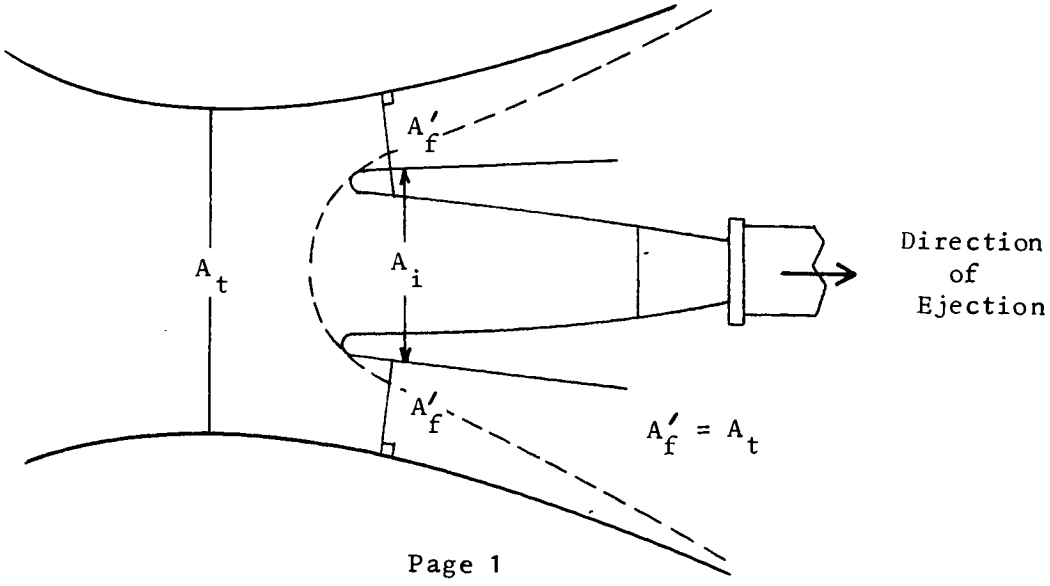

When the igniter is in the position shown, the exit gas flow is choked in the exit cone.

If the igniter is upstream of the position shown, the effective motor throat area is smaller than the design throat area, $A_f' < A_t$. In this case, the downstream effective area ratios are larger than the area ratios during normal operation; consequently, the exit cone and nozzle pressures are less than the pressures that occur during normal motor pressure rise.

When the igniter is downstream of the position shown, the exit gas flow is again choked at the motor throat, $A_f' < A_t$. As the igniter moves farther downstream, the pressure distributions approach normal operating conditions.

Assuming the igniter position previously shown ($A_f'=A_t$), subsonic flow in the motor nozzle and exit cone upstream of the effective throat, and one-dimensional isentropic flow downstream of the effective throat, the pressure distributions were determined. The area of the igniter jet plume or igniter case was subtracted from the total area for each area ratio calculated.

The effect of the bow shock in front of the igniter jet plume was not included. Rough estimation of the bow-shock shape indicated that the intersection of this shock with the nozzle wall occurs near the exit plane. Since normal operating pressures are lowest at the exit plane, the pressure increase caused by the bow-shock intersection will not be significant.

APPENDIX D

DRAG-FORCE CALCULATION FOR THE MOD 260 IGNITION MOTOR AND RETENTION SYSTEM

I. METHOD 1: CONICAL SEPARATION CRITERIA[1] (Figure 1)

All calculations are based on a 275 psia motor chamber pressure.

At P_t = 275 psia: $P_o = 0.56\ P_t$ for choked flow

$$P_s/P_{IGN} = \frac{0.56\ (275)}{1000} = 0.154 \quad A_i/A_{IGN} = 1.71$$

$$A_{IGN} = 164$$

$$A_i = 1.71\ (164) = 280 \text{ sq in.}$$

$$A^* = A_t \text{ motor} - A_i = 3960 - 280$$

$$A^* = 3680 \text{ sq in.}$$

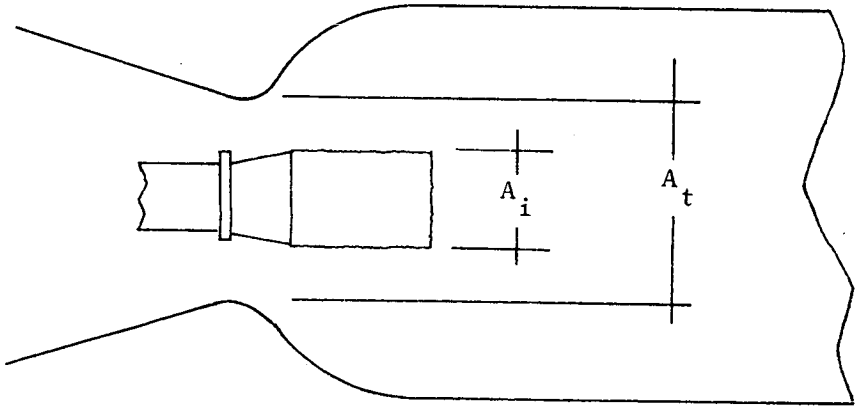

$$A'_{estm} \sim A @ \epsilon^* = 1.5 - A_{e_{IGN}} \quad \text{(Figure 1)}$$

$$A'_{estm} \sim 5940 - 0.785(30^2)$$

$$A'_{estm} \sim 5233 \text{ sq in.}$$

---

[1] Terms are described in Figures 1 and 2 and in the nomenclature.

$F_{(2)} = C_{dq} A$ Assume $C_d = 1.7$

$F_{(2)} = (1.7)\ (55.3)\ (2070)$

$F_{(2)} = 194{,}000$ lb

Total Force = $F_{(1)} + F_{(2)} = 288{,}000$ lb at 275 psia

II. METHOD 2: NORMAL SHOCK (FIGURE 2)

$A_{estm} \sim A_{(2)} = 2.5 - A_{impingement}$ (Figure 2)

$A_{estm} \sim 9900 - 1266$

$A_{estm} \sim 8634$ sq in.

$A/A^* = \frac{8634}{3680} = 2.34$

$P_o/P_t = 0.095$ $P_2/P_o = 5.1$ $P_{t2}/P_{t1} = 0.57$ from Compressible Flow Tables

$P_o = (0.095)(275) = 26.1$ psia, static pressure of gas stream

$P_2 = (5.1)\ (26.1) = 133$ psia, static pressure across normal shock

$P_{t2} = (0.57)(275) = 157$ psia, total pressure across normal shock

$\frac{P_{sonic}}{P_{total}}$ at choked flow = 0.57

Flow around corner of impingement plate reduced to sonic velocity

$P_{sonic} = (0.57)(157) = 88$ psia

Force on attachment plate:

$F_{(1)} = P_{avg} A_{impingement}$

$F_{(1)} = \left[\frac{P_2 - P_{sonic}}{2} - P_o\right]$ (1266)

$$F_{(1)} = \left[\frac{133 - 88}{2} - 26.1\right] \quad (1266)$$

$$F_{(1)} = (84.4)\ (1266)$$

$$F_{(1)} = 110{,}000 \text{ lb}$$

$$A/A^* = \frac{5233}{3680} = 1.42$$

$M_o' = 1.71\ P_o'/P_t = 0.215\ \bar{P}_s/P_o' = 1.70$ From Compressible Flow Table

$P_o' = (0.215)\ (275) = 59.2$ psia, static pressure at exit plane of ignition motor

$\bar{P}_s = (59.2)(1.7) = 100.1$ psia, static pressure on front surface of ignition motor attachment plate

$$A''_{estm} \sim A\ @\ \epsilon = 2.5 - A_{IGN\ motor}$$

$$A''_{estm} \sim 9900 - 0.785(40)^2$$

$$A''_{estm} \sim 8645 \text{ sq in.}$$

$$A''/A^* = \frac{8645}{3680} = 2.35$$

$$M_o'' = 2.20\ P_o''/P_t = 0.094$$

$P_o'' = (0.094)(275) = 25.8$ psia, static pressure behind the attachment plate

Force on attachment plate:

$$F_{(1)} = (\bar{P}_s - P_o'')\ (A_{impingement})$$

$$F_{(1)} = (100.1 - 25.8)\ (1266)$$

$$F_{(1)} = 94{,}000 \text{ lb}$$

Force on retention system crossbeams at motor exit plane:

$$A_{impingement\ on\ fixture\ crossbeams} \sim 2070 \text{ sq in.}$$

$$P_o/P_t = \frac{14.7}{275} = 0.054$$

q/P_t = 0.202 from Compressible Flow Table

$q = (0.202)(275) = 55.3$

Force on retention system crossbeams at motor exit plane, $F_{(2)}$ = 194,000 lb (Method 1)

Total Force = $F_{(1)} + F_{(2)}$ = 304,000 lb at 275 psia

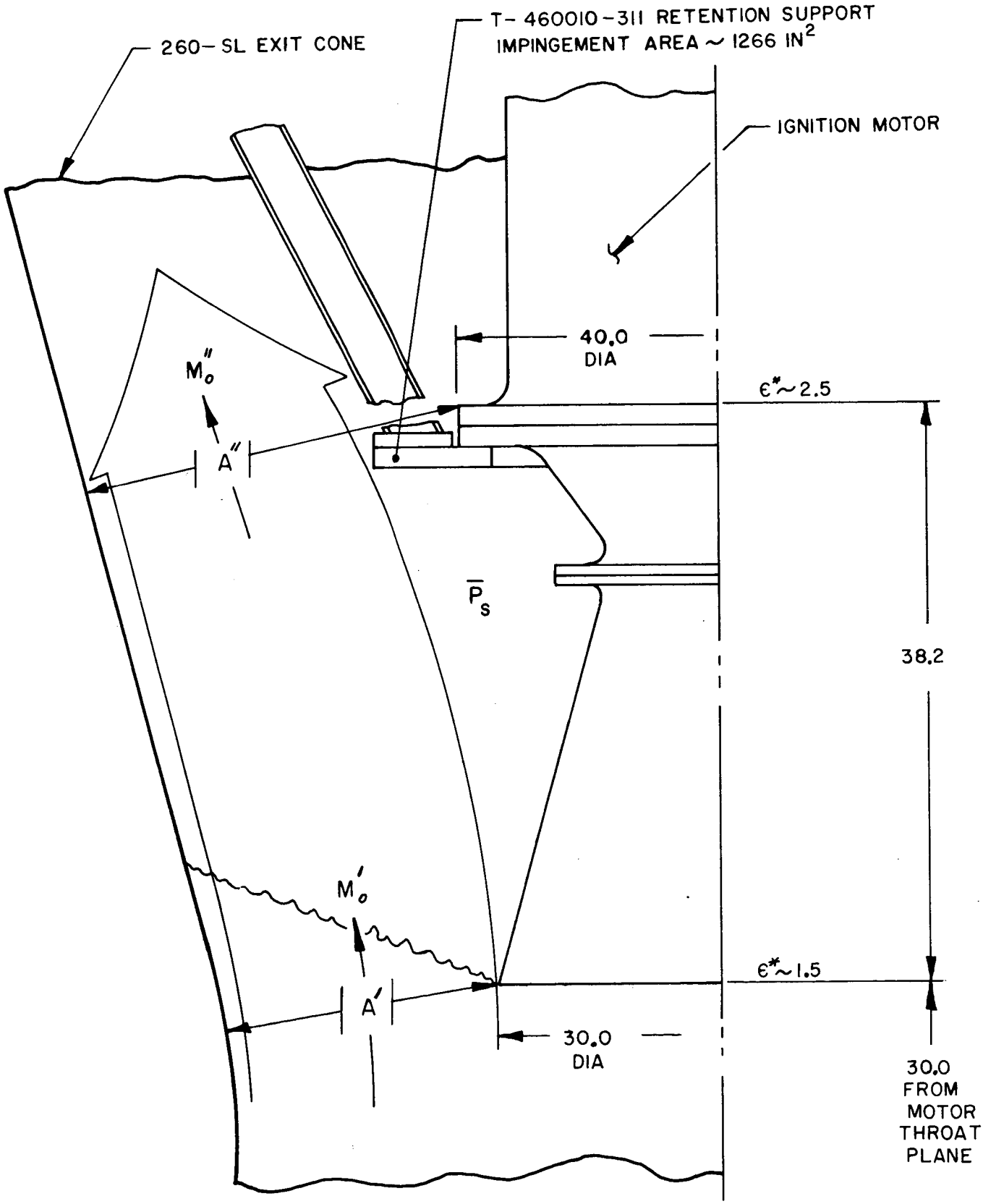

Schematic Diagram of Flow Conditions for Conical Separation Method for Estimating Impingement Force

Figure 1

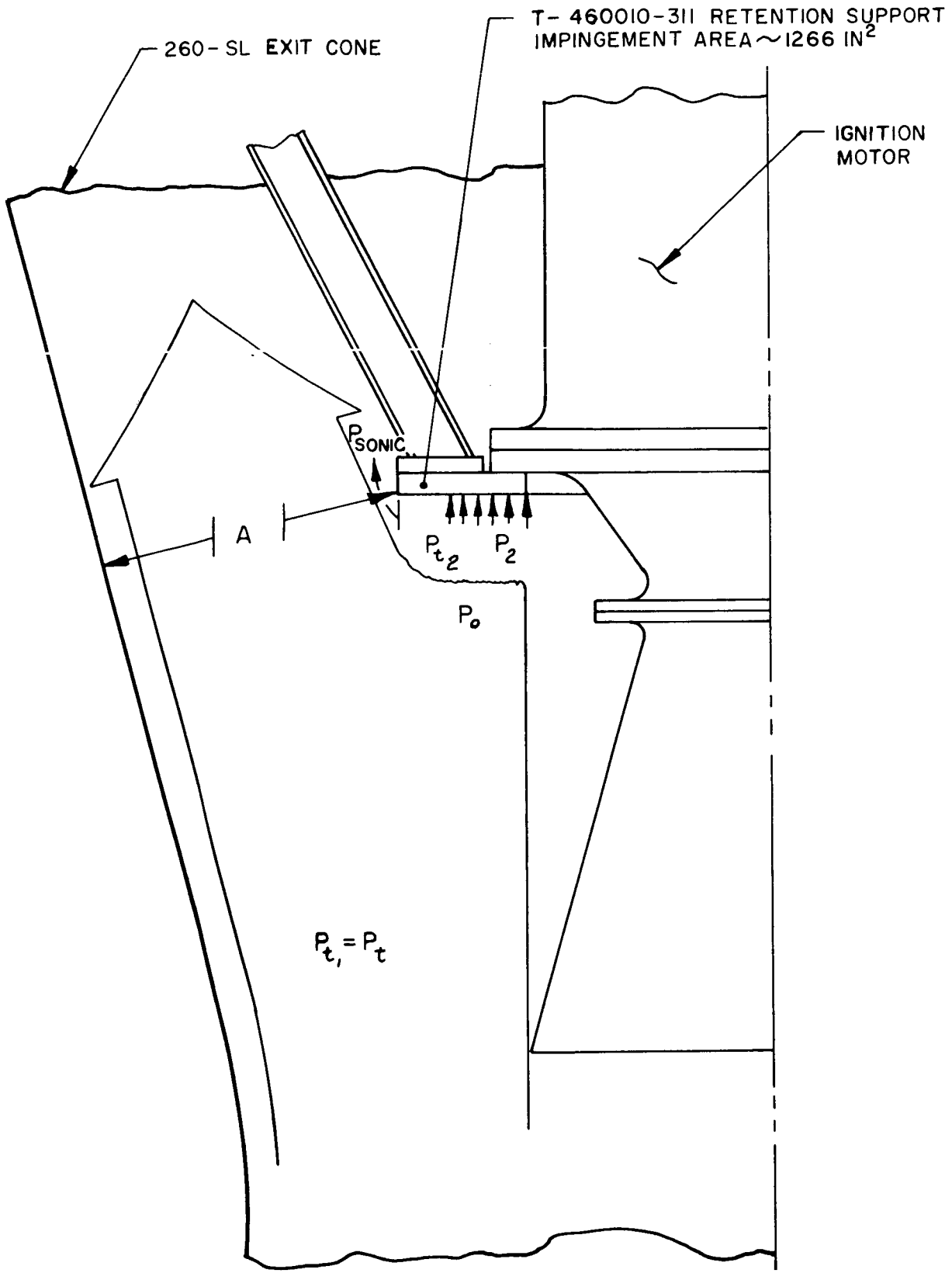

Schematic Diagram of Flow Conditions for Normal Shock Method for Estimating Impingement Force

Figure 2

APPENDIX E

COMPUTER PROGRAM FOR FLOW ANALYSIS OF AFT-END IGNITION

The computer program for aft-end ignition flow analysis is an extension to the computer solution of the aft-end ignition analytical model equations derived in Appendix A. The analytical model equations relate the motor bore pressure (and bore-penetration depth) to igniter mass-flow rate, motor throat area and motor port-to-throat ratio. However, the analytical model treats the motor only as an inert free-volume and does not account for the mass flow generated by the motor propellant upon ignition.

This computer program includes the analytical model equations combined with semiempirical equations for predicting the transient pressure rise in solid propellant motors.[7] All of the assumptions made for the analytical model described in Appendix A apply. For this computer program, the following assumptions are added:

1. During the time when the igniter motor is being ejected from the motor nozzle, no additional blockage of the motor throat by igniter gases occurs.

2. Air in the chamber when ignition starts is assumed to be compressed isentropically and without mixing in the forward end of the chamber. By the time the motor is completely ignited, this air will have mixed with propellant gas, and some of this mixing will undoubtedly take place during the ignition transient. However, the error introduced by excluding this mixing is small, and the assumption eliminates the need for considering mixing of gases in the motor chamber.

3. Gases generated by the igniter and by the motor propellant are assumed to have the same specific heat ratio.

The laws of conservation of mass, energy, and momentum and the perfect gas law are applied to obtain equations for the pressure in the chamber as a function of time. Gas enters the motor chamber through the throat plane from the igniter. Some of this gas is brought to stagnation in the bore; the remainder is turned around and flows out of the bore through an exit orifice equal to the difference between the motor throat area and the area of the igniter jet in the throat plane. Application of the laws of conservation of mass and energy under these conditions yields 12 equations for the 14 unknowns involved in the problem. The additional two equations that are required are obtained by application of the momentum equations described in Appendix A. Ten of the unknowns in these equations are eliminated by substitution, and the remaining four are obtained for each time point through an iterative procedure. The values obtained are integrated numerically to obtain chamber pressure as a function of time. Separate equations for subsonic and sonic flow at the motor throat are derived.

The cold air that is entrapped in the chamber during the ignition transient is assumed to be at the motor-bore stagnation pressure, P_2, at all times. However, in order to make the equations converge for each time point, some fraction, V*, of the propellant gas in the chamber is assumed to be at the chamber pressure, P_2, and the remainder at the total pressure at the motor throat plane. This is equivalent to the assumption that a pressure gradient exists in the motor bore near the aft end of the motor. The value currently being used for V* is 90%; this value was suggested by cold-flow data from the test program.

Equations to predict the shape of the ignition-transient portion of the pressure-time curve for aft-end ignition are programed on a GE 225 Computer, specifically for the prediction of the ignition transient of the 260-SL motor. The equations are based on a quasisteady flow analysis of the phenomena occuring

in the motor bore subsequent to initiation of the aft-end igniter. The derivation of these equations follows.

The propellant gas in the chamber at any time, W_c, is divided into two parts. Some fraction, V*, of this gas is assumed to be at the stagnation pressure at the fore end of the chamber, P_2.

The remainder, 1-V*. is assumed to be at the total pressure at the nozzle throat, P_t. The total volume occupied by this gas is, from the perfect gas law,

$$V = V_1 - V_2 = \left[\frac{V^* W_c RT}{P_2} + \frac{(1-V^*)W_c RT}{P_t}\right]$$

This equation may be solved for V_2, the volume occupied by the air entrapped in the chamber:

$$V_2 = V_1 - \left[\frac{V^* W_c RT}{P_2} + \frac{(1-V^*)W_c RT}{P_t}\right]$$

The air entrapped in the chamber is compressed isentropically. Since the mass of this gas is constant.

$$PV^{\gamma} = \text{constant}$$

$$\text{or } P_2 V_2^{\gamma} = P_a V_1^{\gamma}$$

or, substituting for V_2 from the equation above:

$$P_2 \left[V_1 - \frac{V^* W_c RT}{P_2} - \frac{(1-V^*)W_c RT}{P_t} \right]^{1.4} = P_a V_1^{1.4}$$

The igniter and motor mass flow rates are given by the following:

$$C_w = \frac{\sqrt{\gamma g}\left(\frac{2}{\gamma+1}\right)^{\frac{\gamma+1}{2(\gamma-1)}}}{\sqrt{RT}} \tag{1}$$

$$\dot{w}_i = C_w P_{IGN} A_{IGN} \tag{2}$$

$$\dot{w}_e = C_w P_t (A_t - A_i) \tag{3}$$

and

$$\dot{w}_e = \frac{P_t(A_t - A_i) M_e \sqrt{\gamma g}}{\sqrt{RT}\left(1 + \frac{\gamma-1}{2} M_e^2\right)^{\frac{\gamma}{\gamma-1}}} \tag{3a}$$

$$\frac{P_t}{P_a} = \left(1 + \frac{\gamma-1}{2} M_e^2\right)^{\frac{\gamma}{\gamma-1}} \tag{3b}$$

for subsonic flow at the motor throat.

The static pressure at the motor throat is given by:

$$P_s = P_t \left(\frac{2}{\gamma+1}\right)^{\frac{\gamma}{\gamma-1}} \tag{4}$$

for sonic flow, and

$$P_s = P_a \tag{4a}$$

for subsonic flow.

Isentropic one-dimensional expansion of the igniter jet to the throat static pressure at the throat plane of the motor yields the following expression for the cross-sectional area of the igniter jet plume at the motor throat plane:

$$A_i = \frac{A_{IGN}\left(\frac{2}{\gamma+1}\right)^{\frac{\gamma+1}{2(\gamma-1)}}}{\left(\frac{P_s}{P_{IGN}}\right)^{\frac{1}{\gamma}}\sqrt{\frac{2}{\gamma-1}\left[1 - \left(\frac{P_s}{P_{IGN}}\right)^{\frac{\gamma-1}{\gamma}}\right]}} \tag{5}$$

The Mach number of the igniter jet at this point may be expressed in terms of the igniter total pressure and the throat static pressure:

$$\frac{P_{IGN}}{P_s} = \left(1 + \frac{\gamma-1}{2} M_i^2\right)^{\frac{\gamma}{\gamma-1}} \tag{6}$$

The velocity of this flow is therefore:

$$v_i = a^* \sqrt{\frac{\gamma+1}{2} M_i^2 \left(1 + \frac{\gamma-1}{2} M_i^2\right)^{-1}} \tag{7}$$

where

$$a^* = \sqrt{\gamma g RT \left(\frac{2}{\gamma+1}\right)} \tag{8}$$

The Mach number of the exit gas stream in the motor port just forward of the throat plane is related to the motor port area, the area of the igniter jet at the throat, and the motor throat area:

$$\frac{A_p - A_i}{A_t - A_i} = \frac{1}{M_o} \left(\frac{2}{\gamma+1} + \frac{\gamma-1}{\gamma+1} M_o^2\right)^{\frac{\gamma+1}{2(\gamma-1)}} \tag{9}$$

The velocity of this flow is then given by:

$$v_o = a^* \sqrt{\frac{\gamma+1}{2} M_o^2 \left(1 + \frac{\gamma-1}{2} M_o^2\right)^{-1}} \tag{10}$$

The velocity of the exit gas stream at the motor throat is given by:

$$v_e = a^* \tag{11}$$

for choked flow, and

$$v_e = a^* \sqrt{\frac{\gamma+1}{2} M_e^2 \left(1 + \frac{\gamma-1}{2} M_e^2\right)^{-1}} \tag{11a}$$

for subsonic flow.

The momentum equation is applied at the motor throat plane and to the flow in the vicinity of the motor throat as described in Appendix A:

$$\dot{m}_i v_i + \dot{m}_e v_e = P_2 A_p - P_s A_t - \int P dA \tag{12}$$

$$\dot{m}_e v_e = \frac{P_t (A_p - A_i)}{\left(1 + \frac{\gamma - 1}{2} M_o^2\right)^{\frac{\gamma}{\gamma - 1}}} + \dot{m}_e v_o - P_s (A_t - A_i) - \int P dA \tag{13}$$

The rate of accumulation of mass in the bore is given by:

$$\frac{dw_e}{dt} = \dot{w}_i + c\rho A_b P_2^{\,n} - \dot{w}_e \tag{14}$$

The burning area, A_b, is obtained from the expression:

$$A_b = K_2 \left(1 - e^{-\frac{t - t_i}{\mathcal{T}}}\right) \text{ for } t > t_1 \tag{14a}$$

and

$$A_b = 0 \text{ for } t \leq t_1$$

t_1 is the time of first propellant ignition in the motor, and is arbitrary in the solution of these equations.

The problem thus is represented by a system of 13 simultaneous algebraic equations, and one ordinary differential equation in 14 unknowns. The differential equation (14) is expressed in finite difference form for solution on the computer:

$$W_{c_{(t)}} - W_{c_{(t - \Delta t)}} = (\dot{w}_i + c\rho A_b P_2^{\,n} - \dot{w}_e)\, \Delta t \tag{14b}$$

Equations 1 through 14 are solved separately for the cases of subsonic flow and sonic flow at the motor throat. In each case, 10 of the unknowns are eliminated by substitution, resulting in the following equations:

Subsonic case

$$P_2\left\{V_1 - \frac{V^*W_{c_{(t-\Delta t)}}RT}{144\,P_2} - \frac{(1-V^*)W_{c_{(t-\Delta t)}} + C_w P_{IGN} A_{IGN}\Delta t}{\frac{144\,P_a}{RT}} - P_t\sqrt{\gamma g}\,\Delta t\left\{\frac{2}{\gamma-1}\left[\left(\frac{P_t}{P_a}\right)^{\frac{\gamma-1}{\gamma}}-1\right]\right\}^{.5}\left\{A_t - \frac{A_{IGN}\left(\frac{2}{\gamma+1}\right)^{\frac{\gamma+1}{2(\gamma-1)}}}{\left(\frac{P_a}{P_{IGN}}\right)^{\frac{1}{\gamma}}\sqrt{\frac{2}{\gamma-1}-\frac{P_a}{P_{IGN}}^{\frac{\gamma-1}{\gamma}}}}\right\}\sqrt{\frac{144\,P_a}{RT}} - \frac{c\rho A_b P_2^{n-1}RT}{144}\right\}^{1.4} = P_a V_1^{1.4} \quad (15)$$

$$W_{c_{(t)}} = W_{c_{(t-\Delta t)}} + C_w P_{IGN} A_{IGN}\Delta t + c\rho A_b P_2^{n}\Delta t$$

$$- P_t\sqrt{\gamma g}\,\Delta t\left\{\frac{2}{\gamma-1}\left[\left(\frac{P_t}{P_a}\right)^{\frac{\gamma-1}{\gamma}}-1\right]\right\}^{.5}\left\{A_t - \frac{A_{IGN}\left(\frac{2}{\gamma+1}\right)^{\frac{\gamma+1}{2(\gamma-1)}}}{\left(\frac{P_a}{P_{IGN}}\right)^{\frac{1}{\gamma}}\sqrt{\frac{2}{\gamma-1}\left[1-\left(\frac{P_a}{P_{IGN}}\right)^{\frac{\gamma-1}{\gamma}}\right]}}\right\} \quad (16)$$

$$A_p = \frac{A_{IGN}\left(\frac{2}{\gamma+1}\right)^{\frac{\gamma+1}{2(\gamma-1)}}}{\left(\frac{P_a}{P_{IGN}}\right)^{\frac{1}{\gamma}}\sqrt{\frac{2}{\gamma-1}\left[1-\left(\frac{P_a}{P_{IGN}}\right)^{\frac{\gamma-1}{\gamma}}\right]}}$$

$$A_t = \frac{A_{IGN}\left(\frac{2}{\gamma+1}\right)^{\frac{\gamma+1}{2(\gamma-1)}}}{\left(\frac{P_a}{P_{IGN}}\right)^{\frac{1}{\gamma}}\sqrt{\frac{2}{\gamma-1}\left[1-\left(\frac{P_a}{P_{IGN}}\right)^{\frac{\gamma-1}{\gamma}}\right]}} = \frac{\left(1+\frac{\gamma-1}{2}M_o^2\right)^{\frac{\gamma+1}{2(\gamma-1)}}\left[\sqrt{\frac{2}{\gamma-1}\left[1-\left(\frac{P_a}{P_{IGN}}\right)^{\frac{\gamma-1}{\gamma}}\right]}\right]^{\frac{\gamma+1}{2\gamma}}}{M_o\left[\left(\frac{P_t}{P_a}\right)\right]} \quad (17)$$

$$P_2 A_p = \frac{P_2\sqrt{\gamma\frac{2}{\gamma+1}\left[\left(\frac{P_t}{P_a}\right)^{\frac{\gamma-1}{\gamma}}-1\right]}\sqrt{\frac{\gamma+1}{\gamma-1}M_o^2\left(1+\frac{\gamma-1}{2}M_o^2\right)}^{-1}\left\{A_t-\frac{A_{IGN}\left(\frac{2}{\gamma+1}\right)^{\frac{\gamma+1}{2(\gamma-1)}}}{\left(\frac{P_a}{P_{IGN}}\right)^{\frac{1}{\gamma}}\sqrt{\frac{2}{\gamma-1}\left[1-\left(\frac{P_a}{P_{IGN}}\right)^{\frac{\gamma-1}{\gamma}}\right]}}\right\}}{\left(\frac{P_t}{P_a}\right)^{\frac{\gamma+1}{2\gamma}}}$$

$$+\frac{C_w}{g}P_{IGN}A_{IGN}\sqrt{\left(\frac{2}{\gamma+1}\right)\gamma gRT}\sqrt{\frac{\gamma+1}{\gamma-1}\left[1-\left(\frac{P_a}{P_{IGN}}\right)^{\frac{\gamma-1}{\gamma}}\right]}+\frac{P_t\left[A_p-\left\{\frac{A_{IGN}\left(\frac{2}{\gamma+1}\right)^{\frac{+1}{2(-1)}}}{\left(\frac{P_a}{P_{IGN}}\right)^{\frac{1}{\gamma}}\sqrt{\frac{2}{\gamma-1}\left[1-\left(\frac{P_a}{P_{IGN}}\right)^{\frac{\gamma-1}{\gamma}}\right]}}\right\}\right]}{\left(1+\frac{\gamma-1}{2}M_o^2\right)^{\frac{\gamma}{\gamma-1}}}$$

$$+\frac{P_a A_{IGN}\left(\frac{2}{\gamma+1}\right)^{\frac{\gamma+1}{2(\gamma-1)}}}{\left(\frac{P_a}{P_{IGN}}\right)^{\frac{1}{\gamma}}\frac{2}{\gamma-1}\left[1-\left(\frac{P_a}{P_{IGN}}\right)^{\frac{\gamma-1}{\gamma}}\right]} \quad (18)$$

Sonic Case

$$P_2\left\{V_1 - \frac{V^*W_{c_{(t-\Delta t)}}RT}{144\,P_2} - \frac{(1-V^*)\,W_{c_{(t-\Delta t)}}RT}{144\,P_t} - \frac{c\rho\,A_b\,RT\,P_2^{n-1}\,\Delta t}{144} - \frac{C_w P_{IGN} A_{IGN}\Delta t - C_w P_t \Delta t\left[A_t - \frac{A_{IGN}\left(\frac{2}{\gamma+1}\right)^{\frac{\gamma+1}{2(\gamma-1)}}}{\left(\frac{2}{\gamma+1}\right)^{\frac{1}{\gamma-1}}\left(\frac{P_t}{P_{IGN}}\right)^{\frac{1}{\gamma}}\sqrt{\frac{2}{\gamma-1}\left[1-\frac{2}{\gamma+1}\left(\frac{P_t}{P_{IGN}}\right)^{\frac{\gamma-1}{\gamma}}\right]}}\right]^{1.4}}{\frac{144\,P_t}{RT}\left(\frac{2}{\gamma+1}\right)^{\frac{\gamma}{\gamma-1}}}\right\} = P_a V_1^{1.4} \quad (19)$$

$$W_{c_{(t)}} = W_{c_{(t-\Delta t)}} + C_w P_{IGN} A_{IGN}\Delta t + c\rho A_b P_2^{n}\Delta t$$

$$- C_w P_t \Delta t\left\{A_t\left(-\frac{A_{IGN}\left(\frac{2}{\gamma+1}\right)^{\frac{\gamma+1}{2(\gamma-1)}}}{\left(\frac{2}{\gamma+1}\right)^{\frac{1}{\gamma-1}}\left(\frac{P_t}{P_{IGN}}\right)^{\frac{1}{\gamma}}\sqrt{\frac{2}{\gamma-1}\left[1-\frac{2}{\gamma+1}\left(\frac{P_t}{P_{IGN}}\right)^{\frac{\gamma-1}{\gamma}}\right]}}\right)\right\} \quad (20)$$

$$A_p - \left\{\frac{A_{IGN}\left(\frac{2}{\gamma+1}\right)^{\frac{\gamma+1}{2(\gamma-1)}}}{\left(\frac{2}{\gamma+1}\right)^{\frac{1}{\gamma-1}}\left(\frac{P_t}{P_{IGN}}\right)^{\frac{1}{\gamma}}\sqrt{\frac{2}{\gamma-1}\left[1-\frac{2}{\gamma+1}\left(\frac{P_t}{P_{IGN}}\right)^{\frac{\gamma-1}{\gamma}}\right]}}\right\} = \frac{\left(\frac{2}{\gamma+1}\right)^{\frac{\gamma+1}{2(\gamma-1)}}\left(1+\frac{\gamma-1}{2}M_o^2\right)^{\frac{\gamma+1}{2(\gamma-1)}}}{M_o}$$

$$A_t - \left\{\frac{A_{IGN}\left(\frac{2}{\gamma+1}\right)^{\frac{\gamma+1}{2(\gamma-1)}}}{\left(\frac{2}{\gamma+1}\right)^{\frac{1}{\gamma-1}}\left(\frac{P_t}{P_{IGN}}\right)^{\frac{1}{\gamma}}\sqrt{\frac{2}{\gamma-1}\left[1-\frac{2}{\gamma+1}\left(\frac{P_t}{P_{IGN}}\right)^{\frac{\gamma-1}{\gamma}}\right]}}\right\} \quad (21)$$

$$P_2 A_p = \frac{C_w}{g} P_t \sqrt{\gamma g RT} \sqrt{M_o^2 \left(1 + \frac{\gamma-1}{2} M_o^2\right)^{-1}} \left\{ A_t - \frac{A_{IGN}\left(\frac{2}{\gamma+1}\right)^{\frac{\gamma+1}{2(\gamma-1)}}}{\left(\frac{2}{\gamma+1}\right)^{\frac{1}{\gamma-1}} \left(\frac{P_t}{P_{IGN}}\right)^{\frac{1}{\gamma}} \sqrt{\frac{2}{\gamma-1}\left[1 - \frac{2}{\gamma+1}\left(\frac{P_t}{P_{IGN}}\right)^{\frac{\gamma-1}{\gamma}}\right]}} \right\}$$

$$+ \frac{C_w}{g} P_{IGN} A_{IGN} \sqrt{\gamma g RT} \sqrt{\frac{2}{\gamma-1}\left[1 - \frac{2}{\gamma+1}\left(\frac{P_t}{P_{IGN}}\right)^{\frac{\gamma-1}{\gamma}}\right]}$$

$$+ \frac{P_t A_{IGN}\left(\frac{2}{\gamma+1}\right)^{\frac{\gamma+1}{2(\gamma-1)}+1}}{\left(\frac{P_t}{P_{IGN}}\right)^{\frac{1}{\gamma}} \sqrt{\frac{2}{\gamma-1}\left[1 - \frac{2}{\gamma+1}\left(\frac{P_t}{P_{IGN}}\right)^{\frac{\gamma-1}{\gamma}}\right]}}$$

$$+ \frac{P_t \left[A_p - \left(\frac{A_{IGN}\left(\frac{2}{\gamma+1}\right)^{\frac{\gamma+1}{2(\gamma-1)}}}{\left(\frac{2}{\gamma+1}\right)^{\frac{1}{\gamma-1}} \left(\frac{P_t}{P_{IGN}}\right)^{\frac{1}{\gamma}} \sqrt{\frac{2}{\gamma-1}\left[1 - \left(\frac{2}{\gamma+1}\right)\left(\frac{P_t}{P_{IGN}}\right)^{\frac{\gamma-1}{\gamma}}\right]}} \right) \right]}{\left(1 + \frac{\gamma-1}{2} M_o^2\right)^{\frac{\gamma}{\gamma-1}}} \qquad (22)$$

Because of the complexity of these equations, further reduction is not possible. The equations are solved by an iterative procedure.

Two events occur during the ignition transient that require modification of the preceding equations. The first of these is ignition of the propellant surface surrounding the volume that contains the air compressed into the forward end of the chamber. Propellant surface ignition is assumed to begin at the aft end of the motor and to proceed toward the forward end in accordance with equation 14a. When the propellant surface surrounding the air begins to burn, the air

obviously will mix with the propellant exit gas stream, thus making Equation 19 invalid. Equation 19 is then replaced by the following equation, which is obtained by differentiating the perfect gas law:

$$\Delta P_2 = \frac{RT\Delta t}{144V_1}\left[C_w P_{IGN} A_{IGN} + c\rho A_b P_2^{\,n} - C_w P_2 \left\{ A_t - \frac{A_{IGN}\left(\frac{2}{\gamma+1}\right)^{\frac{\gamma+1}{2(\gamma-1)}}}{\left(\frac{2}{\gamma+1}\right)^{\frac{1}{\gamma-1}}\left(\frac{P_t}{P_{IGN}}\right)^{\frac{1}{\gamma}}\sqrt{\frac{2}{\gamma-1}\left[1-\left(\frac{P_t}{P_{IGN}}\right)^{\frac{\gamma-1}{\gamma}}\right]}} \right\}\right] \quad (19a)$$

The other event which occurs is removal of the igniter motor from the main motor exit cone. Two values are required to fix the time of this event: the pressure level in the main motor bore when the igniter is released, and the time required after release for the ignition motor to reach a point where it no longer has an effect on flow from the main motor. When this point is reached in the calculation, the igniter throat area, A_{IGN}, is set equal to zero and the total pressure at the nozzle throat, P_t, is set equal to the total pressure in the chamber, P_2. Equation 22 is then eliminated in the integration procedure.

The input for the computer program is shown in Figure 1. The data on the 260-SL-1 motor ignition performance prediction is included in Figure 1. Three quantities required as input for the computer program are not easily obtained for any given motor configuration. These quantities are: t_1, the time of first propellant ignition; $\mathcal{T}$, the time constant that describes the rate of flame spread over the propellant surface; and, t_{ex}, the time required for the igniter to reach a position during ejection where it no longer affects flow through the motor nozzle. Fortunately, values of t_1 and t_{ex} for motor 260-SL-1 were obtained from the igniter test program. The time constant, $\mathcal{T}$, in Equation 14a, is the time required to

reach the maximum propellant burning surface not directly exposed to the igniter hot gases.[9] The time constant may thus be considered as a function of the bore configuration and characteristic grain dimensions. The grain geometry, igniter placement, and bore-penetration depth that determines the amount of propellant not directly exposed to the igniter gases can be expressed in τ as follows:

$$\tau \sim f\left(\frac{A_{h1}}{K} \times L_1\right) \quad \text{for fore-end ignition}$$

and

$$\tau \sim f\left[\left(\frac{A_{h1}}{K} \times L_1\right) + \left(\frac{A_{h2}}{K} \times L_2\right)\right] \quad \text{for aft-end ignition}$$

After the time-constant function is determined, the value of τ is obtained from the empirical correlation shown in Figure 2.

The most serious limitation of the present analytical program is the omission of the effect of throat blockage during the time the igniter is being ejected from the motor throat. Data from the cold-flow tests indicate that such blockage will take place and will result in a short period of increased pressurization during the ignition transient.

CASE 2

FLOW ANALYSIS OF AFT-END IGNITION
COMPUTER INPUT DATA SHEET

MOTOR 260-SL-1

1. Igniter pressure-time curve:

Time, sec	Pressure, psia	Time, sec	Pressure, psia
0.0	Fire-Switch	0.400	950
0.125	400	0.500	940
0.150	750	0.600	940
0.175	940	0.700	920
0.200	950	0.750	850
0.250	960	0.800	800
0.300	950		

2. Throat Area: Igniter, A_{IGN} 164.6 $in.^2$

   Motor A_t 3960 $in.^2$

3. Motor Free-Volume, V_f: 4950 ft^3

4. Motor Free-Flow (Port) Area, Ap: 12,500 $in.^2$

5. Motor Propellant Surface Area, K: 467,000 $in.^2$

6. Motor Propellant Data:

   Specific Heat Ratio, γ : 1.2

   Combustion Temperature, T: 5300 °R

   Density, ρ : 0.0633 $lb/in.^3$

   Mass Flow Coefficient, C_w: 0.00628 sec^{-1}

7. Motor Propellant Burning Rate Data:

   $r = cP^n$

   Burning Rate Constant, c: 0.0417

   Burning Rate Exponent, n: 0.38

8. Ambient Pressure: 14.7 psia

Flow Analysis of Aft-End Ignition, Computer Input Data Sheet

Figure 1, Sheet 1 of 4

CASE 1

FLOW ANALYSIS OF AFT-END IGNITION
COMPUTER INPUT DATA SHEET

MOTOR 260-SL-1

1. Igniter pressure-time curve:

Time, sec	Pressure, psia	Time, sec	Pressure, psia
0.0	Fire-Switch	0.500	1055
0.100	340	0.600	1045
0.125	825	0.700	1020
0.150	1065	0.750	980
0.175	1095	0.800	930
0.200	1100		
0.300	1085		
0.400	1075		

2. Throat Area: Igniter, A_{IGN} 164.6 in.^{2}

Motor, A_t 3960 in.^{2}

3. Motor Free-Volume, V_i: 4950 ft^3

4. Motor Free-Flow (Port) Area, Ap: 12,500 in.^{2}

5. Motor Propellant Surface Area, K: 467,000 in.^{2}

6. Motor Propellant Data:

Specific Heat Ratio, γ : 1.2

Combustion Temperature, T: 5300 °R

Density, ρ : 0.0633 lb/in.^{3}

Mass Flow Coefficient, C_w: 0.00628 sec^{-1}

7. Motor Propellant Burning Rate Data:

$r = cP^n$

Burning Rate Constant, c: 0.0417

Burning Rate Exponent, n: 0.38

8. Ambient Pressure: 14.7 psia

Flow Analysis of Aft-End Ignition, Computer Input Data Sheet

Figure 1, Sheet 2 of 4

9. Motor Initial Steady-State Operating Pressure:

   P_{equi}: 550 psia

10. Time Constant, τ, in $K_2(1-e^{-\frac{t}{\tau}})$

    : 0.22 1 sec

11. Time of First Propellant Ignition, t_1: 0.200 sec

12. Pressure When Ignition Motor Release Control Is Actuated:

    P_{ex}: 200 $\pm$ 2 psia

13. Time Required for Complete Igniter Ejection, t_{ex}: 0.250 sec (2)

(1) $\tau \sim f\left[\left(\frac{A_{h1}}{K} \times L_1\right) + \left(\frac{A_{h2}}{K} \times L_2\right)\right]$

$A_{h1} = 0$

$A_{h2} = 0.30\ (K)$

$L1 = 0$

$L2 = (0.3)(730) \simeq 220$

$\tau \sim f\left[\left(\frac{.3K}{K}\right)(220)\right]$

$\tau \sim f\ (66.0)$

$\tau = 0.22$ sec from Figure 2

(2) t_{ex} includes:

0.075 sec for igniter release control unit function

0.175 sec ejection time

Flow Analysis of Aft-End Ignition, Computer Input Data Sheet

9. Motor Initial Steady-State Operating Pressure:

   P_{equi}: 500 psia

10. Time Constant, τ, in $K_2(1-e^{-\frac{t}{\tau}})$

    τ: 0.22 sec (1)

11. Time of First Propellant Ignition, t_1: 0.275 sec

12. Pressure When Ignition Motor Release Control Is Actuated:

    P_{ex}: 200 $\pm$ 2 psia

13. Time Required for Complete Igniter Ejection, t_{ex}: 0.250 sec (2)

Flow Analysis of Aft-End Ignition, Computer Input Data Sheet

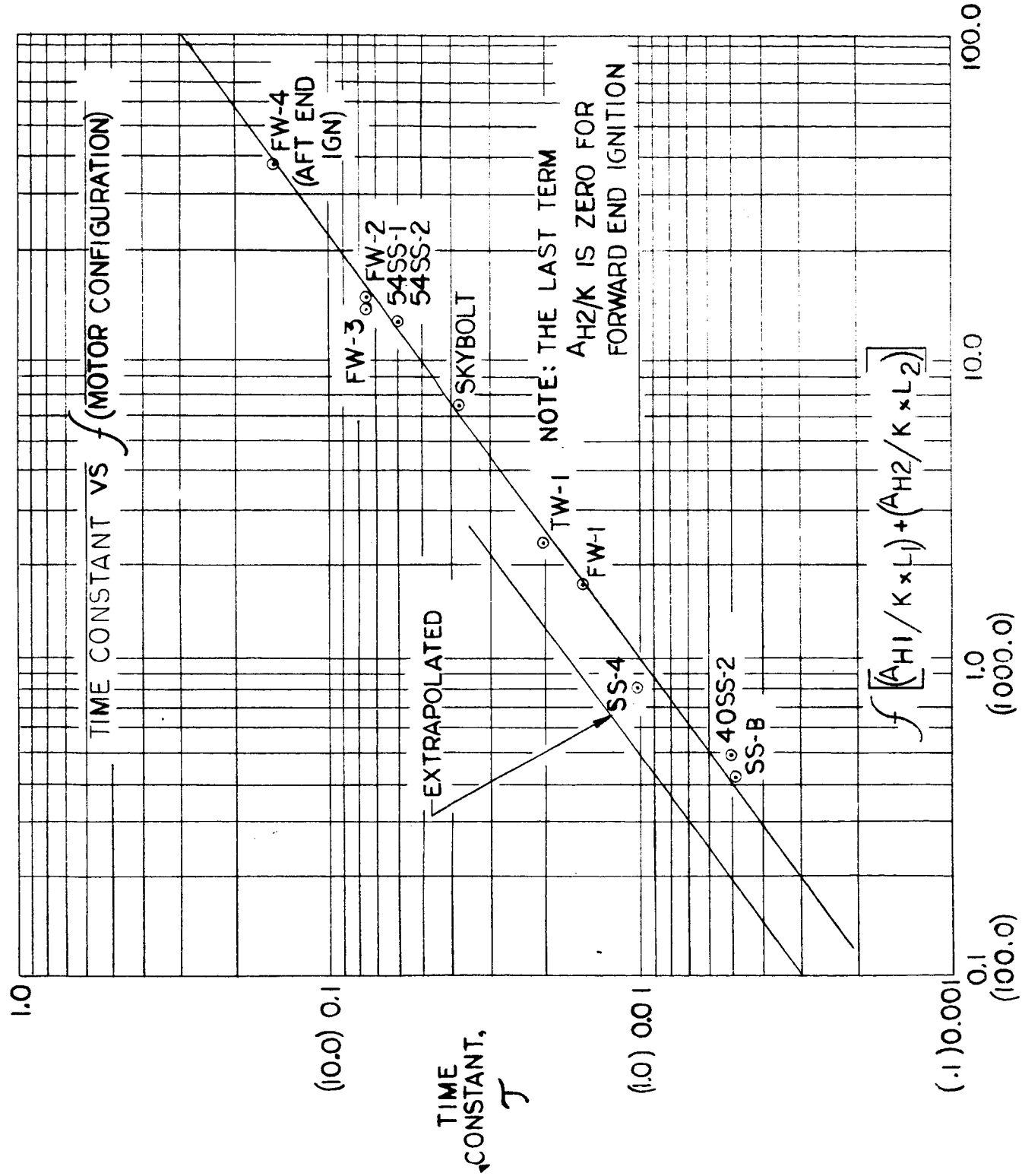

Empirical Correlation of the Time Constant as a Function of Motor Configuration

Figure 2

APPENDIX F

AFT-END IGNITER DESIGN

Motor Parameters Required:

Throat Area, A_t

Free-Volume, V_1

Port Area, A_p

Initial Burning Surface Area, K

Exit Cone Half-Angle

Motor Propellant Properties Required:

Ratio of Specific Heats

Burning Rate Constant

Burning Rate Exponent

Mass Flow Coefficient

Igniter Pyrotechnic Material Properties Required:

Burning Rate Constant

Burning Rate Exponent

Mass Flow Coefficient

Ratio of Specific Heats

Density

Igniter Design Criteria:

Induced Heat Flux:

$$q = 70 \text{ cal/cm}^2\text{-sec}$$

Motor Ignition Pressure:

Equal to or less than 1.0 times the motor initial steady-state operating pressure

Igniter Position:

No Jet Plume Impingement on Motor Throat; $\epsilon^* \geq 1.1$

Port-To-Throat Area Ratio:

$$\frac{A_{P_{IGN}}}{A_{IGN}} \geq 2.5$$

Igniter Design Parameters to be Selected on the Basis of the Specific Ignition Requirements:

Depth of Igniter Gas Penetration or Motor Bore Pressure

Operating Pressure

Duration of Web Burning

Expansion Ratio

Igniter Mass Flow:

$\dot{w}_i$ Calculated in Accordance with Equations in Appendix A

Igniter Throat Area:

$$A_{IGN} = \frac{\dot{w}_i}{C_w P_{IGN}}$$

Igniter Burning Surface Area:

$$K_{IGN} = \frac{Cw\ (1000)\ A_{IGN}\ (P_{IGN/1000})^n}{c'\rho}$$

$$\text{Where } c' = \frac{\sqrt{\Gamma}}{(P_{IGN/1000})^n}$$

Igniter Grain Configuration:

Factors Affecting Igniter Grain Design:

Ease of Propellant Installation

Igniter Size

Grain Stress

Igniter Ballistic Performance:

Obtain from Input to 1103 Interior Ballistics Computer Program

Igniter-Induced Motor Bore Pressure:

P_2 Calculated from Equations in Appendix A

Time Averaged Igniter-Induced Motor Bore Pressure:

$$\bar{P}_c = \frac{\int_o^t P_2 dt}{t}$$

Igniter-Induced Heat-Flux:

$$\bar{q} = \left[0.0296 \frac{\gamma Q}{T_o} \left(\frac{\mu g}{x} \right)^{0.2} \left(\frac{\dot{w}_i}{A_{p/144}} \right)^{0.8} \right]^{.27}$$

Time to First Motor Propellant Ignition:

Determined Graphically as Follows:

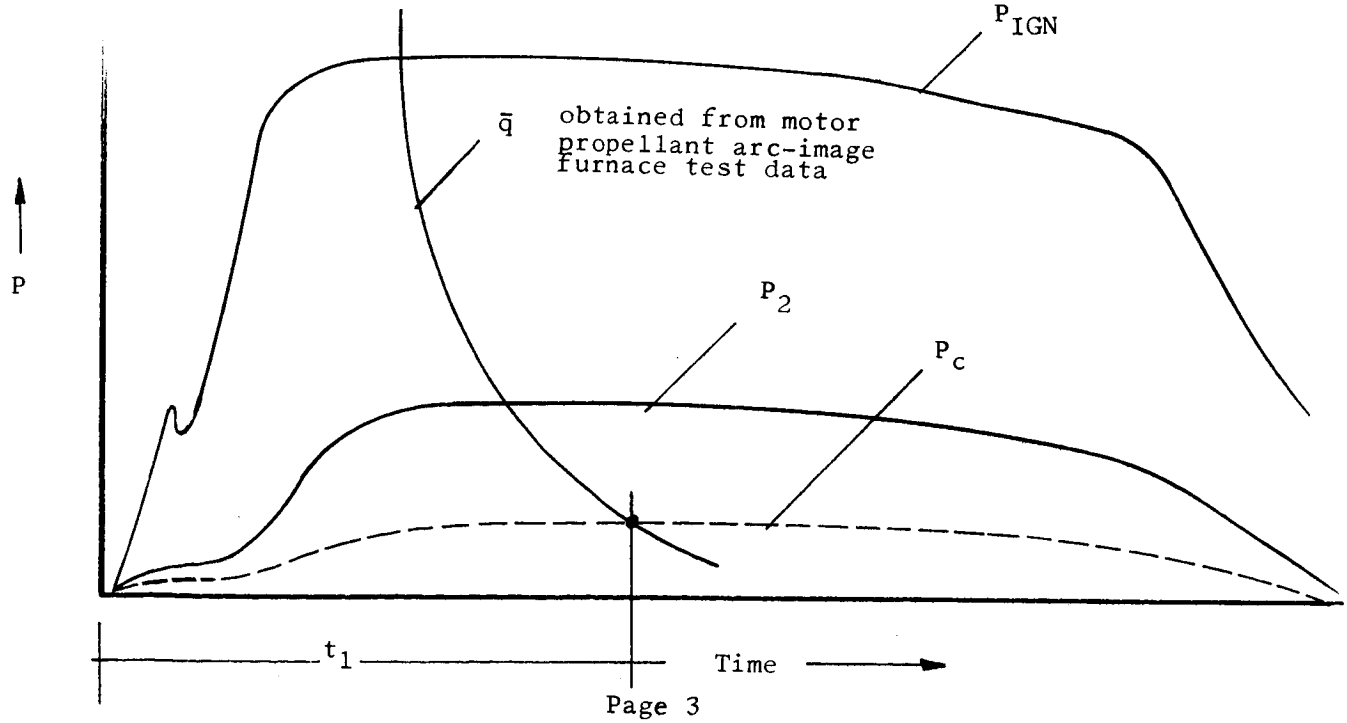

Igniter Position:

Igniter Inlet Jet Plume Boundary:

$P_{IGN}^{(Max)}$ = Nozzle Pressure Ratio

P_a

From Figure 1, Determine Prandtl-Meyer Angle, V_i, at Selected Igniter Nozzle Expansion

From Figure 2, Determine Jet Boundary Radius Ratio, $\acute{R}/r_j$, at Selected Igniter Nozzle Expansion Ratio and Igniter Propellant Specific Heat Ratio

Determine Jet Boundary Radius, $\acute{R}$, Using Selected Igniter Exit Plane Radius

Lay out Igniter Exit Cone Along Motor Center Line

Move the Igniter Exit Cone Toward Motor Throat Plane until the Jet Boundary Clears the Motor Throat

Calculate ϵ^* at This Position

$$\epsilon^* = \frac{A_f}{A_t}$$

If ϵ^* is less than 1.2, Revise Selected Expansion Ratio or Igniter Exit Cone Half-Angle

Predicted Motor Ignition Performance:

Predicted Performance Obtain from Computer Program Described in Appendix C

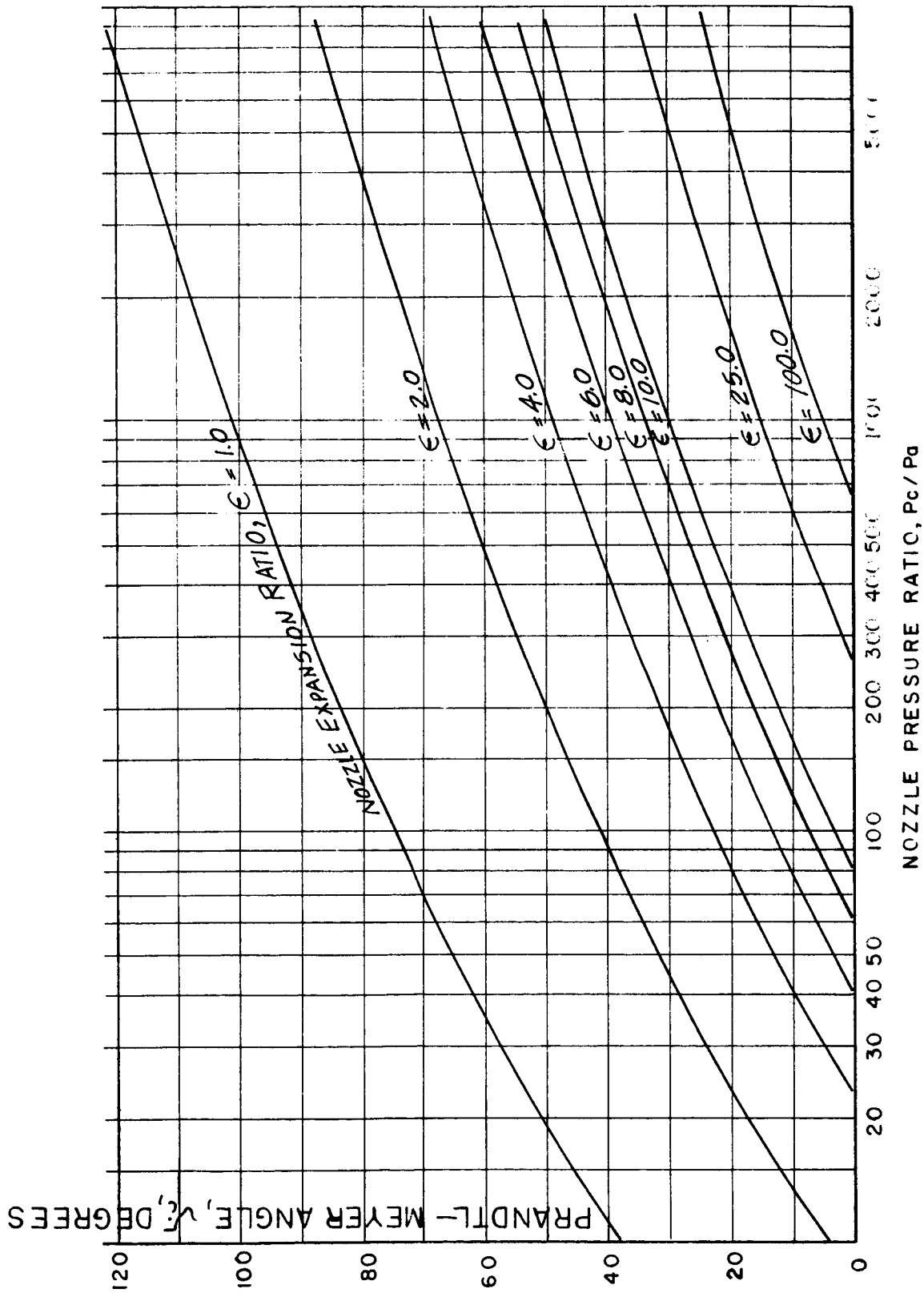

Prandtl-Meyer Angle as a Function of Pressure Ratio and Expansion Ratio at a Specific Heat Ratio of 1.2

Figure 1

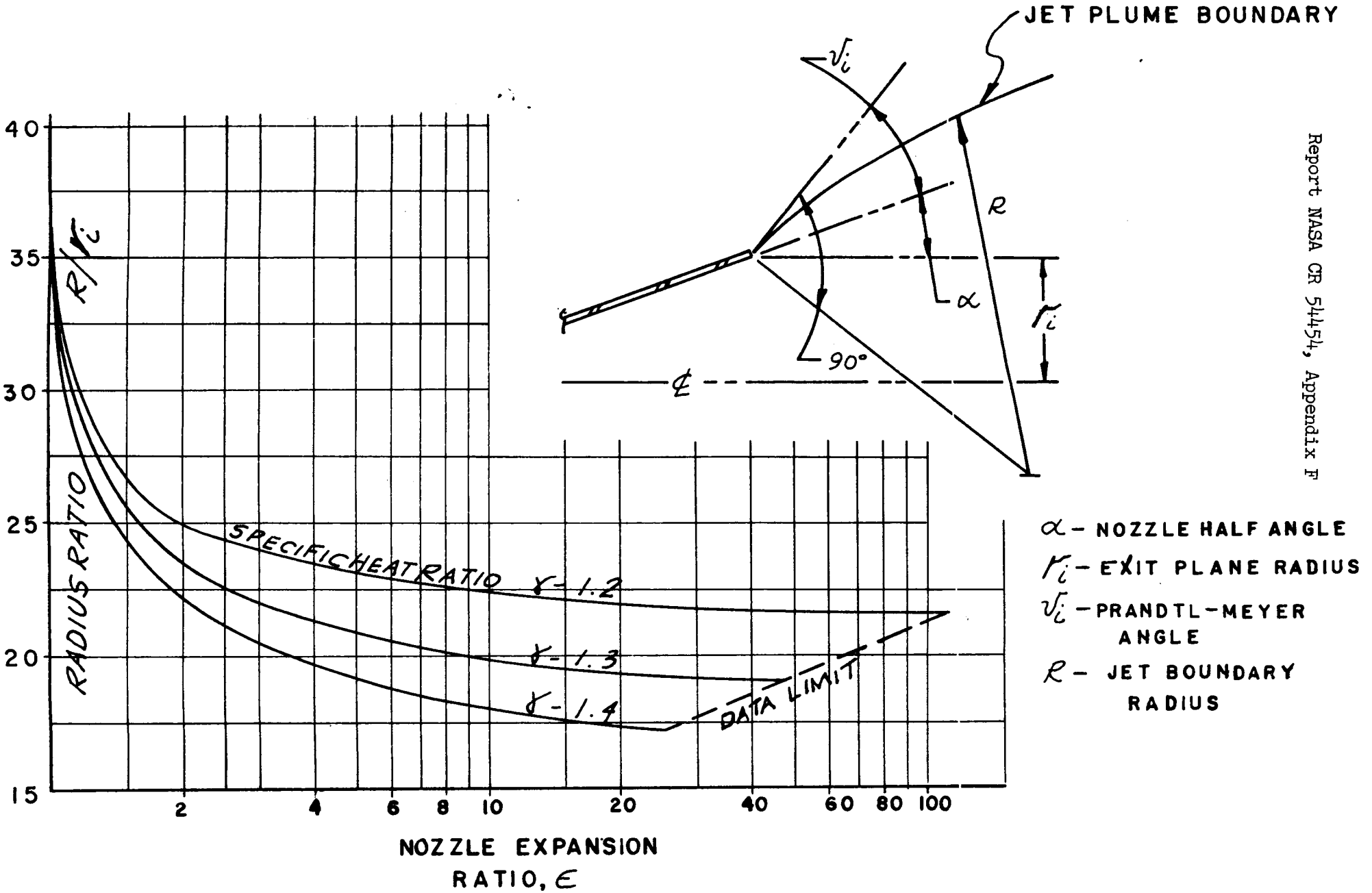

Report NASA CR 54454, Appendix F

Figure 2

Jet Boundary Radius Ratio as a Function of Specific Heat Ratio and Nozzle Expansion Ratio